Cdc42 isoforms : localization, functions and regulation

Yamini Ravichandran

Doctoral Thesis of Sorbonne Université

École doctorale Complexité du Vivant

Cell Polarity, Migration and Cancer Laboratory (Institut Pasteur)
Molecular Mechanisms of Intracellular Transport Laboratory (Institut Curie)

Cdc42 isoforms: Functions, Localization and Regulation

Presented by

Yamini RAVICHANDRAN

Ph.D. in Cell Biology

Under the supervision of Dr. Jean-Baptiste MANNEVILLE

& Co-supervision of Dr. Sandrine ETIENNE-MANNEVILLE

Presented on 15th October 2020

In front of a jury composed by:

Patricia Bassereau Directrice de Recherche CNRS, Institut Curie, Paris	*President/Examiner*
Pekka Lappalainen Professor, University of Helsinki, Finland	*Referee*
Cathy Jackson Directrice de Recherche CNRS, Institut Jacques Monod, Paris	*Referee*
Jérôme Delon Chargés de Recherche, Institut Cochin, Paris	*Examiner*
Jean-Baptiste Manneville Directeur de Recherche, Institut Curie, Paris	*Thesis director*
Sandrine Etienne-Manneville Directrice de Recherche, Institut Pasteur, Paris	*Co-thesis director*
Batiste BOEDA Chargés de Recherche, Institut Pasteur, Paris	*Invitee*

Doctoral Thesis of Sorbonne Université

École doctorale Complexité du Vivant

Cell Polarity, Migration and Cancer Laboratory (Institut Pasteur)
Molecular Mechanisms of Intracellular Transport Laboratory (Institut Curie)

Cdc42 isoforms: Functions, Localization and Regulation

Presented by

Yamini RAVICHANDRAN

Ph.D. in Cell Biology

Under the supervision of Dr. Jean-Baptiste MANNEVILLE

& Co-supervision of Dr. Sandrine ETIENNE-MANNEVILLE

Presented on 15th October 2020

In front of a jury composed by:

Patricia Bassereau Directrice de Recherche CNRS, Institut Curie, Paris	*President/Examiner*
Pekka Lappalainen Professor, University of Helsinki, Finland	*Referee*
Cathy Jackson Directrice de Recherche CNRS, Institut Jacques Monod, Paris	*Referee*
Jérôme Delon Chargés de Recherche, Institut Cochin, Paris	*Examiner*
Jean-Baptiste Manneville Directeur de Recherche, Institut Curie, Paris	*Thesis director*
Sandrine Etienne-Manneville Directrice de Recherche, Institut Pasteur, Paris	*Co-thesis director*
Batiste BOEDA Chargés de Recherche, Institut Pasteur, Paris	*Invitee*

'karmanyeva-adhikaraste ma phalesu kadachana'

"Be active, never be inactive, and do not react to the outcome of the work."

-The Bhagavad Gita

Acknowledgement

Doing a PhD in Paris was never my plan, I had applied to 10 different German institutes and 1 application to the Institut Curie-iC3i PhD program. Fortunately, I was invited for the iC3i interview to Paris. I finished second in the PhD interview and did not secure the iC3i PhD. Luckily though, during the course of my interview program, I encountered Jean-Baptiste Manneville (JB) from Bruno Goud's lab. I distinctly remember JB giving a talk regarding a 'Golgi-localized Cdc42 project' and advertising an existing vacancy for the same, in collaboration with the lab of Sandrine Etienne-Manneville at Institut Pasteur. The thought of obtaining a Marie-Curie fellowship and working in a collaborative project between renowned labs intrigued me. I wrote up my application and sent it to JB. The next thing, I recall is being in an interview with Sandrine before heading back to India. Followed by which within a week's time I received an email from Sandrine, letting me know I got the position. For giving me the opportunity to work on this project, I am extremely grateful to both Sandrine and JB to date. Starting from my initial journey from India to the final days of writing my thesis, they have both been extremely motivating, optimistic and encouraging.

They have both been a great influence in moulding me as a researcher during the past four years. Sandrine has taught me how to be a focused researcher and be my own critic. While JB has been an example of an ever-enthusiastic researcher. His attention to details, his energy and discipline when it comes to completing tasks, has left me continuously attempting to be more like him. They have both let me explore several aspects of my project enabling me to be an independent researcher, yet always being within reach if I needed to lean in. Most importantly, they have inspired me to maintain work-life balance and I am always amazed by how they achieve it effortlessly.

I also take great pleasure in thanking Bruno Goud, first for accepting me to be a part of his lab and thereafter supporting me in every way possible to make my collaboration between both institutes smoother. He took great interest in my PhD project and also generously accepted to participate in the review article we wrote with JB. Given his hectic schedule, I am extremely glad that he took out the time to read my thesis manuscript and share his valuable comments. Lastly, 'Thank you Bruno for patiently entertaining me when I came to you for trivial queries and even more when I came seeking career advice'.

My guru Batiste Boeda! I cannot thank him enough for being my mentor in the lab from day one. He has taught me a great deal of techniques, especially sharing his personalized tips and tricks. His guidance has played an immense role in making me more of an independent researcher. I am forever grateful to him for taking me under his wing and sharing his knowledge and expertise, with great patience like a true guru would. 'Batiste, I will surely remember to get better souvenirs from India, the next time I will be allowed to go!'

Vanessa Roca has been a valuable addition to my PhD project. She joined the Etienne-Manneville lab right in the middle of my PhD and hopped on my project initially to help me with molecular biology experiment. Yet, soon she grew to become an essential part of several

experimental aspects of my project. Having her on my project, let me travel for all the coursework, conferences and most importantly during my academic secondment to Switzerland. She has also been my French teacher, an emotional support and a cheerleader for even the tiniest of my triumphs during the PhD. 'Merci beaucoup Vanessa!'

During the course of this PhD, I am glad Sandrine gave me the opportunity to co-supervise three different Masters students in the Etienne-Manneville Lab, and this has been a transformational experience. Grégoire Mathonnet, it was a pleasure to initiate the project titled "A role for Cdc42 in the nucleus" with you. Your scientific curiosity, your energy and your determination made my work experience with you delightful. Followed by Astrid Boström who continued to work on this project. Astrid continued with equal enthusiasm and made several interesting findings in the project. She also managed to collaborate with external members to probe different aspects of the project. Lastly, Dylan Ramage another excellent intern picked up the project upon Astrid's departure. Dylan has been a pleasure to work with. Especially his report has served as a comprehensive summary of the project so far. I have really been fortunate to supervise such talented Masters students and I would like to thank Sandrine and Batiste for guiding me through this process.

From the Etienne-Manneville Lab Cecile Leduc, thank you for taking the time to share your expertise on microscopes, every time I came seeking for help. You have kindly shared your experience as a permanent scientist and we have had several insightful discussions. Franck Commailleau, you have been an integral part of the initial days of my PhD. Thank you for being my hands-on molecular biology mentor and for teaching me the need to be disciplined. Gaëlle Dutour-Provenzano, your cheerfulness and positivity are much needed to lighten the ambience in the lab. You love to help others and thank you for helping me too. You have eagerly volunteered for common tasks in the lab, which has not gone unnoticed. It was an enjoyable experience to work with you. Florent Peglion, thank you for pushing me to my limits, it has made me strive harder. Isabelle Perfetinni, Duc-Quang Tran, Emmanuel Terriac and Emma van Bodegraven, it was a pleasure to share lab space with you. 'Quang thank you for your motivation while I wrote my thesis and Emma thanks for letting me know which series to watch to lighten my mood!'

From the Goud Lab, Guillaume Kulakowski has been instrumental for setting up GUV assays during the initial stages of my PhD. He very kindly shared his expertise. Sabine Bardin, thank you for always being proactive whenever I approached you for help. Kristine Schauer and Stephanie Miserey-Lenkei, I am glad I met you both in the Goud lab. It was a pleasure to receive your constructive comments and suggestions during every lab meeting and for engaging several discussions both scientific and non-scientific. 'Kristine, I will remember you every time I look at my phone screen!'

Hugo Lachuer (PK), we have both grown fond of each other over the past two years, especially as we were the recurring night owls of the Goud Lab. Thank you for keeping this 'senior' PhD company both on good and bad days. A farewell note, 'Eat those greens Hugo!'

David Pereira, thank you for being a 'nice' colleague. For being a moral support in the lab especially during days when things went bad. I learnt a great deal from your sarcasm! Surya Cayre and Pallavi Mathur, thank you for contributing to the social activities of the Goud lab and lifting the spirits of everyone around you. Nathan Lardier and Samuel Mathieu, thank you for kindly considering my alternating schedules between two institutes and being generous with the microscope slots, you have both been such considerate colleagues.

In addition to the Etienne-Manneville Lab and the Goud Lab, I would like to thank the Bassereau lab. First, I am thankful to Patricia Bassereau for initially inviting me to Paris as part of the iC3i PhD program. Furthermore, all the GUV synthesis demonstrated in this thesis were performed in her laboratory. Therefore, I am glad that she kindly allowed me to work in her laboratory and I would also like to thank her for accepting to be a part of my PhD jury. It goes without saying that I am grateful to the entire Bassereau team for being cooperative and sharing their lab space with me for the past four years. I would specifically like to thank Julien Pernier, for teaching me several aspects associated with GUV synthesis and Feng-Ching Tsai for sharing her critical comments and suggestions with regard to my results during the Goud lab meetings. 'Thank you Feng, for also taking the time to read my thesis.'

The first three years of this PhD project were funded by the Horizon 2020-PolarNet-ITN (Innovative Training network) funded by the Marie-Sklodowska-Curie Actions. Obtaining this prestigious H2020 ITN fellowship made this PhD experience extremely unique. The network consisted of 15 PhD candidates and 14 supervisors spread across various countries in Europe. As part of the training program, meetings across European institutes were held and also participation in conferences was highly encouraged. I would specifically like to thank the network co-ordinator Mike Boxem for being receptive throughout the program. Victoria Yan, Eider Valle-Encinas, Amalia Riga, Victoria Garcia Castiglioni and Filippo Ioannou, I am glad we met through the PolarNet-ITN. We have all witnessed each other's journey as a PhD student, during these past four years, and have supported one another immensely. It was a pleasure to meet wonderful scientists and friends like you. Thank you for your good-heartedness and presence.

As part of the PolarNet-ITN we were asked to complete an academic secondment, where we were required to visit another laboratory outside of our host country to complement our PhD project. For this, I opted to work in the lab of Gisou van der Goot situated in EPFL, Switzerland. Especially, since the van der Goot Lab specializes in the field of protein palmitoylation. Gisou very kindly agreed to let me work in her lab and showed interest in my study. In addition, on both the occasions that I was working in her lab, I was invited to their lab activities (a wonderful lab dinner and of course they took me for a hiking trip!) which made me feel even more welcomed. I would specifically like to thank Laurence Gouzi Abrami, for her patience and guidance. She has performed the radioblots demonstrated in this work and initiated the PAT screen for Cdc42. She also showed great interest in my project and followed up on my progress even after I returned to Paris. I would like to thank other members specifically; Numa Piot, Giorgia Pisoni, Slyvia Ho, Franciso Mesquita, Olha

Novokhatska, Oksana Andrei Segeeva, and Genevieve Rossier for assisting in several ways and making my stay even more pleasant in the van der Goot Lab.

In this interdisciplinary project, all the mass spectrometry analysis was performed at the Institut Curie Mass Spectrometry and Proteomics facility. I would like to thank Damarys Loew for collaborating with us on this project. Florent Dingli thank you for performing the mass spec experiments. Guillaume Arras the bioinformatician who initially trained me on using the myProMS software. Followed by which Valentin Sebatet was assigned as the bioinformatician on this project. Valentin has eagerly assisted me with every query I had and has patiently trained me on several aspects with regard to the mass spec data analysis. Spinning disk experiments performed in this work were conducted in the Pasteur Imaging facility, Imagopole. I would specifically like to thank Jean-Yves Tinevez for my initial training and Ioanna Theodorou for her helping me every time I reached out.

Marie Lemesle and Aurelie Lima, thank you for tirelessly helping me with the mountain of bureaucratic tasks during the past four years. Never had I ever imagined how much paperwork was involved in a PhD. Both of you ensured the setting up of necessary formalities to enable my collaborative PhD between both institutes.

I would like to thank Fondation pour la recherche médicale (FRM) Fin de thèse de sciences program, for funding the 4th year of my PhD.

During the course of this PhD, I also joined the ASAPbio community. Being a part of the ASAPbio fellows program 2020 has shown me an alternative side to science being that of scientific publishing. Interacting with like-minded early career researchers has been a great support system towards the end of this PhD. I would especially like to thank Iratxe Peubla who has stepped in on my behalf for the ASAPbio fellows program, considering my demands for the completion of my PhD.

My motivation to pursue a PhD in the first place came from my Masters internship supervisor Indranil Banerjee. He has been my scientific mentor and friend. I would especially like to thank him for coaching me for my PhD interview in Paris and for handling associated bureaucratic tasks. In his lab, not only did I discover the fascinating world of biological research but I also met my partner Gautham. For this I am forever indebted to him.

My sincere thanks to the rats for their co-operation and I strongly apologize to them for their sacrifice.

Friends are said to be the family we choose. I discovered the true essence of this saying, during these past four years. Lavinia Capuana, my dearest friend! From being just another lab mate, to becoming inseparable friends, you have become the elder sister I never had. For spoiling me, for guiding me, for cheering me up and for loving me, I am forever grateful. I cannot thank you enough for taking me to Como and introducing me to your warm parents Enzo and Christina Capuana. They have been even kinder and warmer. These past four years your family and you have made me feel at home, here in Europe. *'Te voglio bene, Lavi!'*

Naveen Velmurugan, you were a piece of Tamil Nadu here in Paris. Your family and you have been a constant sight of happiness over the past 4 years. Thank you for cheering me up on every occasion. Roy uncle and aunty, thank you for being supportive on every visit I made to Calcutta, for the initial steps involved with this PhD. Thank you for not just helping me but for all the love you have shown me. Priya Singh and Brinda Roy, my girl squad! We have all come a long way from SRM. You ladies never cease to give me power and strength! Nausheen Mulani, I am glad we met in Pasteur and created a bond of our own and of course, thank you for proofreading my thesis! Agrim Prakash, thank you for reassuring that good times are just a phone call away!

Gautham, thank you for always sticking by my side. As a scientist, as a friend, as an advisor and as a partner you have supported, cheered and encouraged me all along. Especially when it came to writing my thesis, thank you for patiently bearing with me. You have been my pillar of strength! I am forever grateful to have found you *kuttimi*.

Dharuna, I know have been absent for the past 6 years. Yet, you have respected my decision and been there for me when I needed you. Thank you for being so considerate! I couldn't be prouder of you my not-so little brother.

Maa and Dad, thank you for trusting every decision I made. You have been very patient and understanding over the past four years. Thank you for all the sacrifices you have made and for prioritizing my needs above yours. You have constantly put up with all my tantrums and seen my problems as yours. You even adopted Dundu! I cannot love you both enough!

Lastly, I apologize to those whom I have failed to mention here and I thank everyone dearly.

List of abbreviations

AC	Alternating current
AJs	Adherens junctions
APC	Adenomatous polyposis coli protein
aPKC	atypical protein kinase C
APT1/2	Acyl protein thioesterase
Arf	Adenosine diphosphate-Ribosylation Factor
Arp2/3	Actin-related protein 2/3
BrainPS	L-α-phosphatidylserine (Brain, Porcine)
BSM	Sphingomyelin (Brain, Porcine)
CA	Constitutively active
CaaX	C = cysteine, A = any aliphatic amino acid, and X = any amino acid
Cdc42	Cell division control protein 42 homolog
Cdc42b	Brain Cdc42
Cdc42u	Ubiquitous Cdc42
Cer	Ceramide
Chol	Cholesterol
CI	Clathrin Independent
CLIC	CI tubulovesicular carriers
COP	Coat protein
COPI	Coat protein I
Crb	Crumbs
CRIB	Cdc42- and Rac-interactive binding
DAG	Diacylglycerol
Dbl	Diffuse B-cell lymphoma
DHPE	1,2-Dihexadecanoyl-sn-glycero-3-phosphoethanolamine (triethylammonium salt)
DHR2	DOCK homology region 2
DIC	Differential interference contrast
Dlg	Discs-large
DOCK180	Dedicator of cytokinesis
DOG	1-2-dioleoyl-sn-glycerol
DOPC	1,2-dioleoyl-sn-glycero-3-phosphocholine
ECM	Extra-cellular matrix
EEA1	Early Endosome Antigen 1
EggPC	1,2-dioleoyl-sn-glycero-3-phosphocholine

ER	Endoplasmic Reticulum
ESCRT	Endosomal sorting complexes required for transport
FRAP	Fluorescence recovery after photobleaching
GAP	GTPase-activating proteins
GDI	GDP dissociation inhibitor
GDP	Guanosie-5'-diphosphate
GEEC	GPI-AP enriched early endosomal compartments
GEF	Guanine nucleotide exchange factors
GFP	Green Fluorescent protein
GGTase1	Geranylgeranyl transferase type I
GlcCer	Glucosylceramide
GM	Golgi apparatus-like lipid mix
GM130	Golgi matrix protein 130
GPMV	Giant plasma membrane vesicles
GSK3β	Glycogen synthase kinase 3β
GSL	Glycophospholipid
GST	Glutathione S-Transferase
GTP	Guanosie-5'-triphosphate
GUV	Giant unilamellar vesicles
HEK	Human Embryonic kidney
IPTG	Isopropyl β-D-1-thiogalactopyranoside
IQGAP1	IQ motif containing GTPase-activating protein 1
ITO	Indium tin oxide
LB	Lysogeny broth
Ld	Liquid disordered
Lgl	Lethal (2) giant larvae
LiverPE	L-α-phosphatidylethanolamine (Liver,Bovine)
LiverPI	L-α-phosphatidylinositol (Liver, Bovine)
Lo	Liquid ordered
LUV	Large unilamellar vesicle
MDCKII	Madin-Darby Canine Kidney
mDia	mammalian Diaphanous–related
MLV	Multilamellar vesicle
MT	Microtubules
MTOC	Microtubule organizing center
mTOR	Mammalian target of rapamycin or mechanistic target of rapamycin
mTORC1	Mammalian target of rapamycin complex 1
N-WASP	Neural Wiskott–Aldrich-syndrome protein

NLS	Nuclear localization sequence
NMD	Neural Migration Disorders
NPCs	Neural Precursor Cells
PA	Phosphatidic acid
PAK	p21-activated kinase
Pals1	Protein Associated with Caenorhabditis elegans Lin-7 protein 1
Paltj	Pals1-associated tight junction protein
PAR6	Partitioning defective 6
PAT	Protein S-acyltransferase
PC	Phosphatidylcholine
PCP	Planar cell polarity
PDMS	Polydimethylsiloxane
PE	Phosphatidylethanolamine
PFA	Paraformaldehyde
PH	Pleckstrin homology
PI	Phosphatidylinositols
PI(3,4,5)P3	Phosphatidylinositol(3,4,5)- trisphosphate
PI(4,5)P2	Phosphatidylinositol 4, 5-biphosphate
PIX	PAK-interacting exchange factor
PM	Plasma membrane like lipid mix
PRIDE	Protein Identification database
PS	Phosphatidylserine
PTEN	Phosphatase and tensin homolog
Rab	Ras-associated binding
Rac	RAS-related C3 botulinum toxin substrate
Ras	Rat sarcoma
RGCs	Radial glial cells
Rho	Ras homology
RT	Room Temperature
Scrib	Scribble
So	Solid-ordered
SUV	Small unilamellar vesicles
TGN	Trans-Golgi network
Tiam1	T-lymphoma invasion and metastasis-inducing protein
WASp	Wiskott–Aldrich Syndrome protein
WAVE	WASP-family verprolin-homologous protein
α-PIX	α-PAK-interacting exchange factor
β-PIX	β-PAK-interacting exchange factor

Abstract

The small G-protein Cdc42 is an evolutionary conserved polarity protein and a key regulator of the cytoskeleton as well as membrane traffic. In vertebrates, alternative splicing gives rise to two Cdc42 proteins; the ubiquitously expressed isoform (Cdc42u), and the brain isoform (Cdc42b). The two isoforms only differ in their carboxy-terminal Rho GTPase hypervariable region, which includes the CaaX box bearing lipid anchors and the polybasic region (PBR). Here we show that these divergent sequences do not directly affect the interaction of Cdc42 and its panel of binding partners (effectors), but rather contribute to the distinct subcellular localization and function of the two proteins. In contrast to the essentially cytosolic and plasma membrane-associated Cdc42u, Cdc42b localizes to intracellular membrane compartments. In astrocytes and neural precursors, which both express the two variants, we show that Cdc42u alone fulfills the polarity function required for directed persistent migration whereas Cdc42b is the major isoform regulating endocytosis. Both Cdc42 isoforms act in concert by contributing their specific functions to elucidate the complex process of chemotaxis of neural precursors, demonstrating that the expression pattern of the two isoforms is decisive for the specific behavior of cells. With *in vitro* giant unilamellar vesicles we show that Cdc42u interacts specifically with plasma membrane associated PI(4,5)P2 via its PBR di-arginine motif while Cdc42b does not. Contrarily, the C-terminal hypervariable region of Cdc42b is itself sufficient to preferentially bind to vesicles mimicking the Golgi apparatus membrane compared to vesicles mimicking the plasma membrane while the hypervariable region of Cdc42u does not distinguish between both membranes. Both Cdc42u and Cdc42b isoforms however specifically segregate to lipid disordered domains. These *in vitro* findings show the ability of Cdc42 variants to differently interact with specific membranes and could explain their differential subcellular localization *in cellulo.*

Table of Contents

Summary

Cdc42 is an evolutionary conserved small GTPase of the Rho family which acts as a key polarity regulator responsible for establishing polarity in various cell and cellular contexts (Sandrine Etienne-Manneville 2004). As such, Cdc42 is essential for controlling many cellular processes, such as cell division, cell migration and immunological synapse formation. In humans, functional dysregulation of Cdc42 has been shown to give rise to various phenotypes which include facial dysmorphism, neurodevelopmental anomalies, immunological anomalies, hematological anomalies and even phenotypes resembling Noonan syndrome (Martinelli et al. 2018). Cdc42 achieves its functions by influencing cytoskeletal dynamics, membrane trafficking and gene expression in response to a wide variety of extracellular signals (Sandrine Etienne-Manneville 2004). Interestingly a significant pool of Cdc42 localizes at the Golgi apparatus where its regulation and functions remain elusive (Farhan and Hsu 2016).

Like other small G proteins, Cdc42 acts as a molecular switch which cycles between an inactive GDP-bound state and an active GTP-bound state, which can interact with a wide variety of effectors. Cdc42 activity is controlled by Guanine nucleotide exchange factors (GEF) and GTPase activating proteins (GAPs). Most Cdc42 regulators and effectors are membrane-associated and Cdc42 activity has been associated with its ability to interact with membranes. Association of Cdc42 with plasma membrane or intracellular membrane compartments is a key factor that controls the activity and function of this protein. The goal of my PhD is to better understand how Cdc42 association with distinct cellular membranes is regulated and how this affects Cdc42 functions.

Cdc42 can insert into intracellular membranes (Mitin et al. 2012) owing to the geranylgeranylation of its C-terminal. GTP dissociation inhibitor RhoGDI1 can extract Cdc42 from the plasma membrane and thus control an inactive pool of Cdc42 which localizes in the cytosol where it cannot interact with GEFs or effectors. Interestingly, in vertebrates, two isoforms of Cdc42 arise from alternative splicing, namely: the ubiquitously expressed canonical Cdc42 (Cdc42u) and the brain-specifically expressed non-canonical Cdc42 (Cdc42b) (Marks and Kwiatkowski 1996).These isoforms share 95% identity and vary only in their last exons, exon 7 and exon 6 corresponding to Cdc42u and Cdc42b respectively. This last exon encoding the C-terminus of Cdc42u includes a di-arginine motif (-KKSRR-) which is absent in Cdc42b. Moreover, the C-terminus of Cdc42b gives rise to an alternative CaaX

box which bears a reversible palmitoylation, in addition to the geranylgeranyl group (A. Nishimura and Linder 2013).

The specific aims of my PhD project were to determine how alternative splicing could affect Cdc42 association with membranes and GDIs, influence Cdc42 interaction with its effectors and impact on Cdc42 activity. Primary rat astrocytes were used since they provide an ideal model to study front-to-rear polarization and most importantly express both isoforms of Cdc42. Moreover, previous work done in the lab highlighted that, in contrast to Cdc42u, Cdc42b mainly localizes to intracellular membranes, including the Golgi apparatus in primary rat astrocytes.

- I first participated in a study showing that Cdc42u is solely responsible for establishing polarity in migrating astrocytes whereas Cdc42b is mainly responsible for endocytosis (Hanisch et al. in revision).
- I then performed mass spectrometry analysis of the interactome of Cdc42 isoforms and their constitutively active mutants. This study showed that, while C-ter lipid modifications are required for Cdc42 association with GDI1, the alternative splicing does not significantly modify the panel of potential interactors involved in Rho GTPase signal transduction. Working in collaboration with Jerome Delon, I also used R186C Cdc42u a de novo human Cdc42u mutant in the di-arginine motif in which the additional cysteine residue is highly palmitoylated and, as a consequence, exclusively associates with the Golgi apparatus. This strongly affects its binding to GDI1 and to various effectors (Bekhouche et al. 2020). Together these results further strengthen the hypothesis that subcellular localization of the isoforms could be instrumental in their distinct functions.
- To determine the impact of alternative splicing on Cdc42 ability to interact with membranes, I used purified lipid-modified Cdc42 bound to Giant Unilamellar Vesicles (GUVs) as an *in vitro* reconstituted assay. This technique allowed us to determine how the composition, charge, lipid order and packing defects of the lipid bilayer could differentially affect the binding of each isoforms. Using point mutants, I first showed that geranyl-geranylation is absolutely required for membrane association, but that palmitoylation is not. Both isoforms preferentially bind to liquid disordered phases of the membrane and have enhanced binding upon introduction of lipid packing defects. In parallel, in a collaborative effort with the lab of Gisou van der Goot (EPFL), the protein acyltransferase (PAT) responsible for palmitoylating Cdc42b was identified to be Golgi localized.
- Finally, we showed that the di-arginine motif of Cdc42u is crucial for its interaction with $PI(4,5)P_2$ enriched membranes representative of the plasma membrane and is likely to be essential in the preferential recruitment of Cdc42u at the plasma membrane. This result was confirmed using R186C Cdc42u which, because of the mutation, lacks the di-arginine motif and fails to bind preferentially to PIP2 enriched

membranes. In contrast, Cdc42b would rely on palmitoylation governed by Golgi-localized PATs to be released from the Golgi apparatus.

Altogether, the results obtained during my PhD give a better understanding of the isoforms of Cdc42 and demonstrate that their subcellular localization plays a crucial role in their regulation. Our mass spectrometry data indicates that both isoforms interact with similar binding partners, reinforcing further the relevance of subcellular localization. The importance of the di-arginine motif has been elucidated in the GUV assays and can be extrapolated to cells to explain why Cdc42u is more associated to the plasma membrane. Lastly, our findings could be instrumental in understanding isoform specific de novo Cdc42 mutations at the C-ter hotspot, which cause rare disease-associated phenotypes in humans.

Part I
Introduction

Chapter I

Cell Polarity

1.1 Fundamentals of cell polarity

This Chapter delves into the phenomenon of cell polarity, which is a fundamental characteristic of living organisms. It arises due to the need for cells to closely regulate cellular shape and architecture with respect to their microenvironment. Maintenance of a polarized cell state enables cells to perform their functions in a given spatial confinement and make appropriate connections with one another to eventually form a multicellular organism. Some cells polarise only transiently, such as migrating cells that establish a front-to-rear polarity axis with response to polarity cues, which determines the direction of their movement (Figure 1a). Another example being, transiently polarized T-lymphocytes, which exhibit polarized secretion directed towards the immunological synapse, in order to kill their target cells and then repolarize in search of their next target (Figure 1c). As opposed to transiently polarized cells, certain cell types establish and maintain a stable polarity axis; these include epithelial cells displaying apico-basal polarity or neuronal cell types displaying neuronal polarity. The aforementioned cell polarity types and their corresponding typical phenotypes are depicted in Figure 1, with an emphasis on their intracellular organisation such as positioning of the Golgi apparatus, centrosome and polarised vesicular trafficking (Ravichandran, Goud, and Manneville 2020).

Cell polarization itself is a multi-step process. The first step in regulating cellular shape and architecture is the formation of a primary axis of polarity within cells in response to local polarity cues. This polarity cue then propagates to the rest of the cell by regulating the organization of the cytoskeleton and the direction of intracellular trafficking pathways. On a molecular level, the spatial arrangement and protein composition of specialized polarity driven domains facilitates this process. This can also be referred to as polarity signal transduction. Polarity transduction can result in diverse intracellular changes ranging from polarized vesicular transport of target molecules, localized membrane growth, directional cell migration, cell differentiation and even activation of an immune response (Johnston 2018). The master regulator of polarity signal transduction within the cell are polarity determinants. Several evolutionarily conserved polarity determinants have been identified

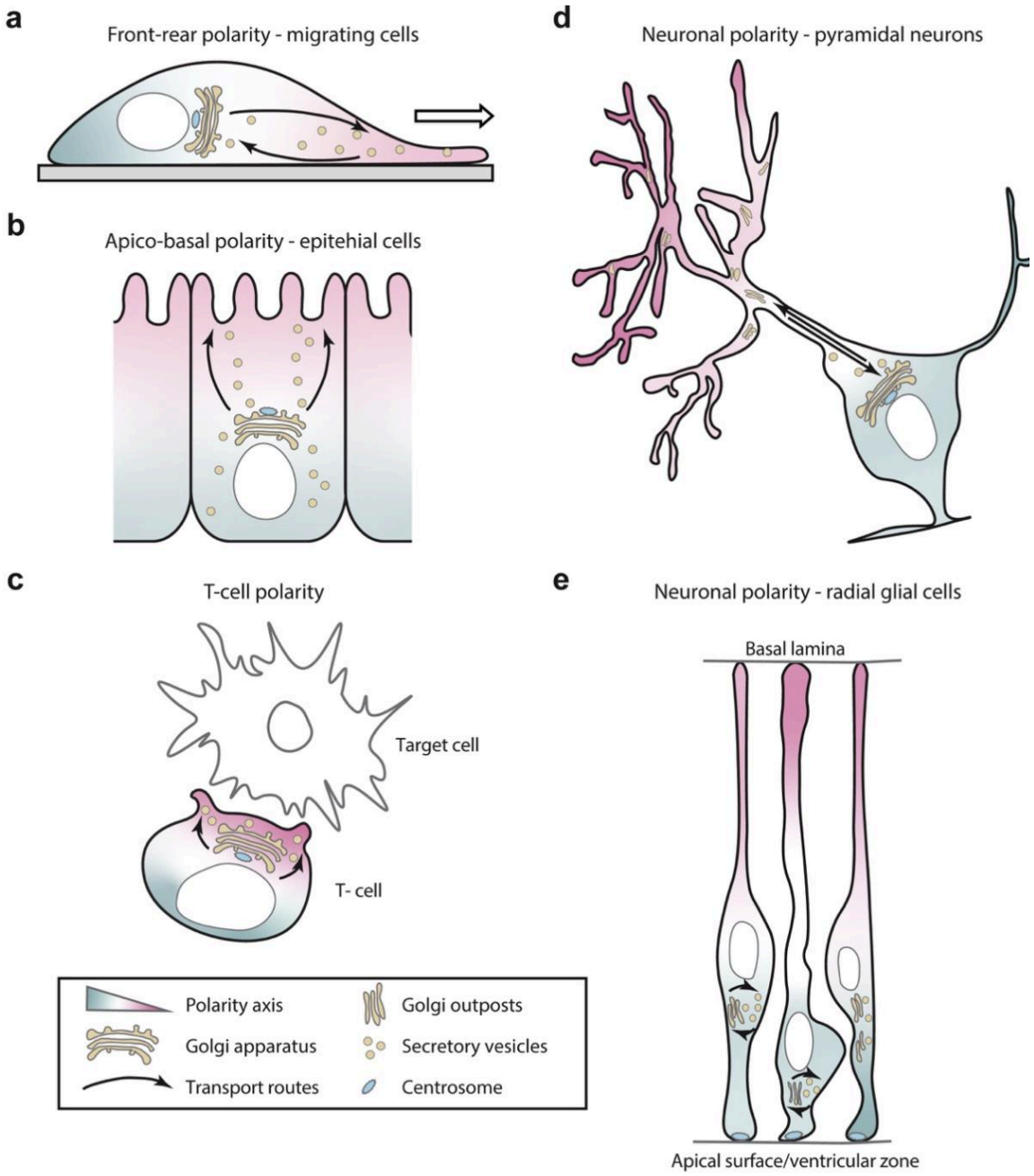

Figure 1 Polarized cell types. a). Migrating cells: the Golgi apparatus is positioned with the centrosome in front of the nucleus aligned along the direction of migration. b). Epithelial cells display apico-basal polarity which is dependent on polarized membrane trafficking. The Golgi apparatus is located between the nucleus and the apical surface in these cells. c). During the immune response process between a T-cell and a target antigen-presenting cell, the T-cell polarizes, and its Golgi apparatus reorients along the synapse to maintain polarized membrane trafficking toward setting-up a cell-cell contact.

d) Transport in the axon from the cell body to the growth cone is crucial to maintain the polarized organization of neuronal cells. In pyramidal neurons, the position of the Golgi apparatus in the cell body correlates with the position of the main axon. e) Radial glial cells display apico-basal polarity. Their centrosome localizes close to the ventricular zone, while the Golgi apparatus is detached and close to the nucleus. Vesicular trafficking is mostly oriented in a perpendicular manner to the polarity axis in these cells. (From Ravichandran, Goud, and Manneville 2020).

and shown to play key and dynamic roles in establishing and maintaining a polarized cell state (Drubin and Nelson 1996; Johnston 2018).

These molecular determinants of cell polarity have been discovered through pioneering genetic screens in diverse model organisms which include the yeast species *Saccharomyces cerevisiae* and *Saccharomyces pombe*, the worm *Caenorhabditis elegans*, and the fruit fly *Drosophila melanogaster* (Sandrine Etienne-Manneville 2004; Sandrine Etienne-Manneville and Hall 2003b; Thompson 2013). Initial studies including those conducted in yeast gave rise to the discovery of the small GTPase protein Cdc42, a fundamental determinant of cell polarity localizing to one pole of the cell via a positive feedback loop of self-recruitment (Drubin and Nelson 1996). Simultaneously Par polarity proteins were discovered in *C. elegans* embryos. This gave rise to the identification of the Par polarity complex and its associated functions (Izumi et al. 1998; Tabuse et al. 1998; Goldstein and Macara 2007). Other functional polarity complexes include the Scribble complex and the Crumbs complex which play critical roles in establishing and maintaining epithelial cell polarity (St Johnston and Ahringer 2010). Several other proteins and protein complexes have been discovered over the past four decades in the field of cell polarity. Numerous polarity determinants have also been implicated in varying pathologies, from congenital birth defects to cancer (Motokawa et al. 2018; Martinelli et al. 2018; Schwarz, Stichel, and Luhmann 2000; Butler and Wallingford 2017; S. Etienne-Manneville 2008). Therefore, a better understanding of the mechanisms controlling the function of polarity proteins is needed to obtain a complete mechanistic understanding of cell development and disease biology.

1.1.1 Epithelial cell polarity

Cells establish and maintain functionally specialized domains in the plasma membrane and in the cytoplasm to display a polarized cell state (Johnston 2018). Epithelial cells are one example of a stably polarized cell type (Figure 1b). They can simultaneously display two key forms of polarity: apico-basal polarity and planar polarity. Apico–basal polarity refers to the polarized segregation of cellular components and tailored functions between the distinct

'apical', 'lateral' and 'basal' plasma membrane domains (Johnston 2018). Once established, mutually exclusive apical and basal domains are maintained and enhanced by recruitment or competition between apical and basolateral polarity complexes. This process displays remarkable conservation across various species, though sometimes the key players act in different combinations yet eventually attain a polarized cell type.

Cells establish and maintain functionally specialized domains in the plasma membrane and in the cytoplasm to display a polarized cell state (Johnston, 2018; Johnston & Ahringer, 2010). Epithelial cells are one example of a stably polarized cell type with specialized domains (Figure 1b). They can simultaneously display two key forms of polarity: apico-basal polarity and planar polarity. Apico–basal polarity refers to the polarized segregation of cellular components and tailored functions between the distinct 'apical', 'lateral' and 'basal' plasma membrane domains (Johnston 2018; Pichaud, Walther, and Nunes de Almeida 2019). Once established, mutually exclusive apical and basal domains are maintained and enhanced by recruitment or competition between apical and basolateral polarity complexes. This process displays remarkable conservation across various species, though sometimes the key players act in different combinations yet eventually attain a polarized cell type.

A key feature of apico-basal polarized cell types are cell-cell adherens junctions (AJs). AJs are located at the border between apical and basolateral domains. AJs are responsible for maintaining the size of the apical and basolateral domains which in turn is key for tissue integrity (Aguilar-Aragon, Tournier, and Thompson 2019; Izumi et al. 1998). The distinct distribution and maintenance of domains is required for epithelial cells to carry out specialized physiological functions, for example intestinal cells position their glucose importers apically and glucose exporters basally.

1.1.2 Planar cell polarity

Planar cell polarity (PCP) is the second form of polarity displayed by epithelial cell types and corresponds to the collective polarization within a given plane of a cell sheet. PCP is involved in a wide range of cellular mechanisms, from the organization of the mammalian hair follicle or the fly eye, to the directional movements of motile cells across developing vertebrate embryos (Figure 2). PCP is governed by two major signalling pathways: the ‘core’ PCP module and the Fat–Dachsous–Four-jointed module. These signalling pathways were initially identified in screens conducted in *Drosophila melanogaster* aiming at identifying regulators of the coordinated orientation of external bristles and hairs (Davey and Moens 2017). PCP pathways give rise to complementary and mutually exclusive distribution of the signalling complexes that result in their asymmetric enrichment in distinct cell compartments within each cell of a patterned tissue. Such an asymmetric tissue patterning

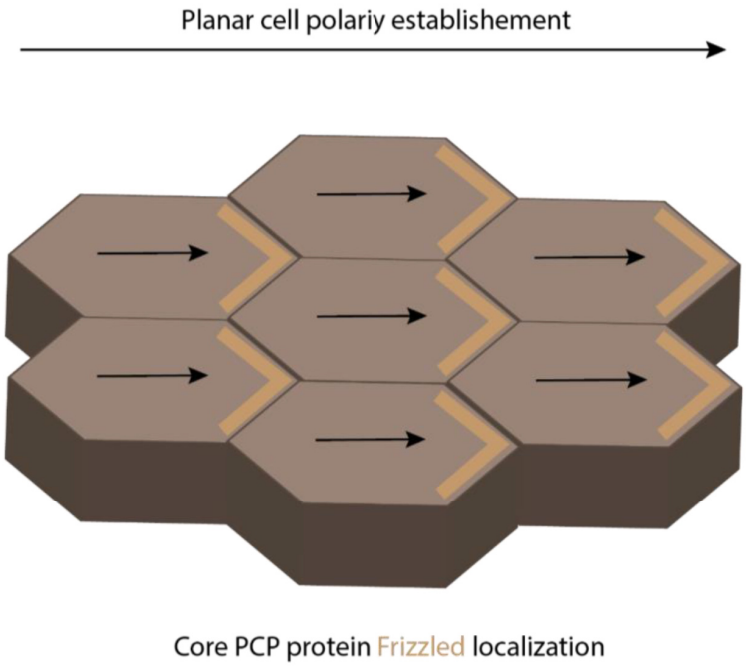

Figure 2 Planar cell polarity. PCP is observed at the multicellular level as shown in this image of hexagonal organization and aligned distribution of the polarity determinant Frizzled. This determines large scale tissue organization such as ciliogenesis.

influences the orientation of intracellular structures and cell behaviour via the regulation of cytoskeletal elements and cell-cell adhesions. The proper establishment and maintenance of PCP is essential during development, for example during convergent extension, and are involved in tissue homeostasis and repair in vertebrates. It has been reported that defects in PCP establishment are associated with human pathologies such as neural tube defects (Butler and Wallingford 2017).

1.1.3 Neuronal cell polarity

Neurons are intrinsically polarized cells. They have multiple dendrites and a single axon that play different roles in electrochemical signalling. Axons and dendrites contain distinct groups of membrane proteins, which include neurotransmitter receptors, guidance receptors and ion channels (Figure 3). The molecular makeup of cytosolic and cytoskeletal elements is also different for axons and dendrites. Shuttling a protein to either the dendrites or the axon is the crucial step in establishing and maintaining the various distinct subcellular

domains that make up a neuron, which also marks the initial steps of establishing neuronal polarity (Bentley and Banker 2016). Not surprisingly, almost every cellular process ranging from neuronal development, to neuronal signalling and neuronal plasticity is dependent on the precise localization of these proteins to their appropriate domains.

In neurons, the rough endoplasmic reticulum and the Golgi apparatus, the organelles where membrane proteins are synthesized and post translationally modified, are positioned at dendrites and in the cell body. In addition, a large amount of cytosolic protein synthesis and packaging occurs in the rough endoplasmic reticulum regions and Golgi apparatus. (Ori-McKenney, Jan, and Jan 2012) These simple observations give rise to the most fundamental question in neuronal polarized protein trafficking: how are axonal and dendritic proteins, which are synthesized collectively in organelles, differentially distributed to distinct destinations within the cell? Hippocampal and cortical cell cultures are predominant model systems used to address these problems.

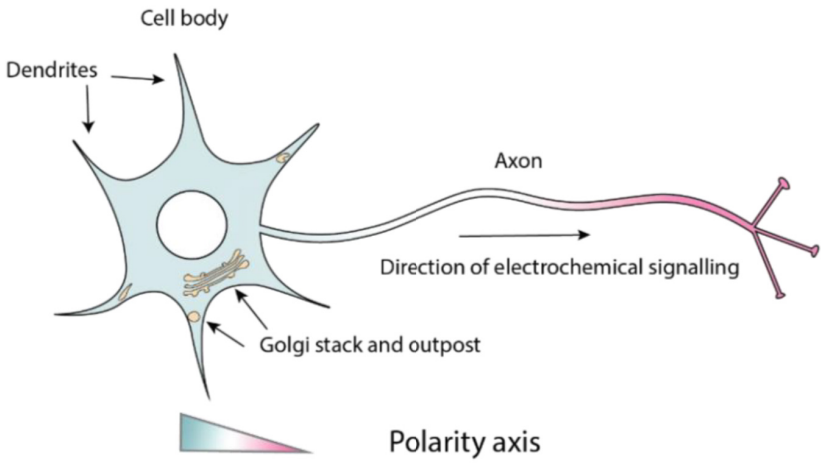

Figure 3. Neuronal polarity. Organelle distribution within a neuron with the Golgi apparatus and Golgi outposts localized at the dendrites, while being also responsible for the trafficking towards the axon. This polarized trafficking plays a key role in distribution of polarity proteins. The direction of transmission of the electrochemical signal from the dendrites to the axon is also depicted.

Another example of polarized cells from the neuronal lineage include the radial glial cells (RGCs) (Figure 1e). Originating from the ectodermal epithelium, RGCs display apico-basal polarity and make up a pseudostratified epithelial layer in the developing cerebral cortex of most mammals. RGCs are responsible for producing certain lineages of glia, including astrocytes and oligodendrocytes. In addition to their role as neural stem cells supplying specialized cells in the three neural lineages, RGCs also behave as scaffolds for neuronal migration. In this role, the basal processes of RGCs at the basal lamina serve as substrates for

the post-mitotic migrating cortical neurons (Chou, Li, and Wang 2018). The apical domain of the RGCs associates with the ventricular surface of the cerebral cortex. Overall, RGCs perform two fundamental functions during cortical development, cell division and scaffolding. Their polarized apico-basal phenotype plays a key role in the latter function (R. Mayor and Theveneau 2012; Chou, Li, and Wang 2018).

1.1.4 Cell migration

Cell migration is cell polarization driven process essential for the development of multicellular organisms. During development, certain cell populations migrate long distances, for example neural crest cells migrate throughout the embryo to form different kinds of cells such as melanocytes, vascular smooth muscle and Schwann cells (R. Mayor and Theveneau 2012). Cell migration also contributes to the progression of most human diseases. Cancer cells migrate from their primary site of initiation into lymph nodes or blood vessels to undergo metastasis (Spano et al. 2012), while immune cell migration is central to autoimmune diseases and chronic inflammation (Griffith and Luster 2013).

For cells to migrate, their polarization along the direction of migration is first required. During single cell migration this involves the establishment of a front-to-rear polarity axis, which includes molecular, structural polarization (polarized cytoskeletal rearrangements) and functional polarization (protruding front/retracting rear). In order to achieve this, an array of front-to-rear polarizing intracellular signaling cascades are set up, driven mainly by the small GTPase proteins of the Rho family (Ridley 2015). In the migrating leading edge of single cells, engagement of integrins with the extracellular matrix (ECM) triggers activation of Rho GTPases (Price et al. 1998). Sequentially, cytoskeletal rearrangements which includes rapid actin polymerization are observed (R. Mayor and Etienne-Manneville 2016). For instance, in migrating fibroblasts, the following intracellular changes are observed. The actin cytoskeleton promotes extension of the leading edge and retraction of the rear end.

Followed by reorganization of the microtubule network associated with the centrosome along the direction of migration, the Golgi apparatus reorients to face the front of the cell and vesicular trafficking is directed towards the leading edge (Figure 1a). Further, the activation of Rho GTPases at the cell front and cytoskeletal rearrangements drives the formation of membrane protrusions such as filopodia (pointed cytoplasmic projections) and lamellipodia (slender sheet like cytoplasmic projections) (Figure 4a) (Capuana, Boström, and Etienne-Manneville 2020; Sandrine Etienne-Manneville 2004). Notably, at the rear end a distinct signalling pathway promotes acto-myosin contraction characteristic of force transmission from the front to the rear of the cell. The sustained activation of Rho GTPases at the front and the sequential cytoskeletal rearrangements is necessary for persistent and directed migration.

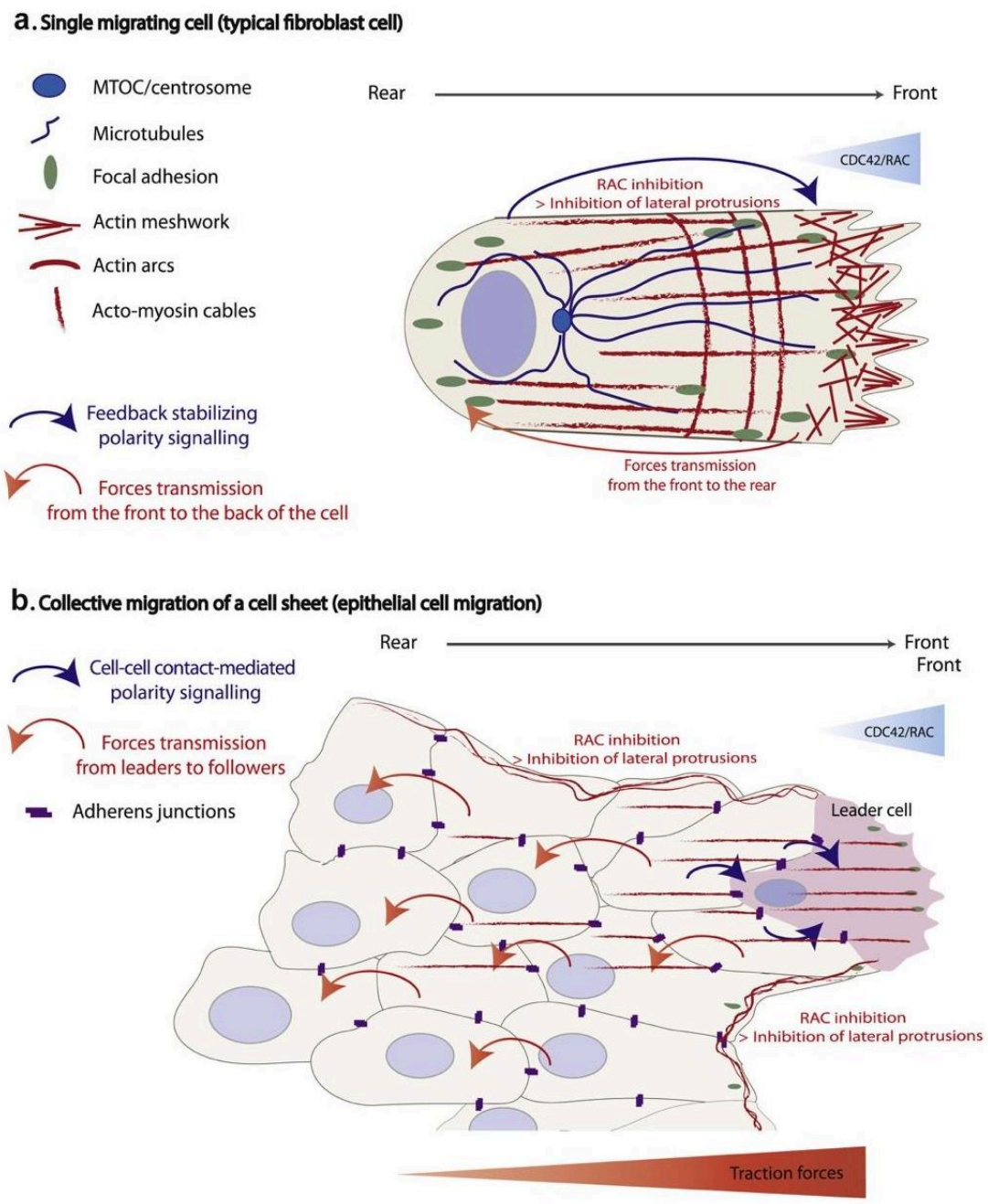

Figure 4 Single cell migration and collective cell migration. a) Intracellular organization of cytoskeletal elements and Rho GTPase gradients in a single migrating cell. The orientation of forces is also represented. b) In a collective migration scenario, the leader cells represent the migrating front of the cell collective group. Emphasis has been given to adherens junctions which give rise to differences in collective migration with respect to cytoskeletal arrangements in comparison to individually migrating cells. Adapted from Capuana, Boström, and Etienne-Manneville 2020.

1.1.4.1 Collective cell migration

Similar mechanisms are observed in individual cells during collective cell migration. Collective cell migration plays an important role during development of multicellular organisms, which involves morphogenetic movements driven by large groups of cells migrating in a coordinated manner to contribute towards the formation of tissues (Fig. 4b). In addition to morphogenetic processes during development, other examples where collective cell migration can be observed in adult organisms is during wound healing, tissue renewal, and angiogenesis (R. Mayor and Etienne-Manneville 2016). With regard to a pathological context, collective cell migration has been identified to play a significant role in tumour spreading and eventually metastasis (Capuana, Boström, and Etienne-Manneville 2020). This has driven a number of studies focusing on understanding the mechanistic players involved in collective cell migration. In a cell collective, not only does the cell front migrate towards external polarity cues but it is also affected by cell-cell contact mediated polarity signalling. Intercellular contacts established between neighbouring cells in a cohesive cell group modify the distribution of classical features observed in front-to-rear polarized single cells. The maintenance of adherens junctions between actively migrating cells is crucial for their collective behaviour. Adherens junctions (AJs) located on lateral contacts dynamically flow backward during collective migration (Peglion et al., 2014). This ensures that cells keep stable yet malleable interactions as they migrate through a complex environment (Figure 4b). The cells migrating at the front are referred to as 'leader cells' distinct from cells trailing behind called "followers". Therefore, generally a front and rear are established within a migrating collective and define a polarity axis with similarities to that of individually migrating cells (Figure 4). In terms of force amplitude, higher forces are observed at the front compared to the rear of the cell collective (Capuana, Boström, and Etienne-Manneville 2020).

Migrating astrocytes are an excellent model for studying front-to-rear polarization under collective cell migration (Figure 5). Astrocytes are the main glial cells of the central nervous system which participate in the regulation of brain homeostasis and in the formation of the blood-brain barrier (Kimelberg and Nedergaard 2010) and migrate collectively during development (Gnanaguru et al. 2013). In the adult brain, they have been shown to undergo astrogliosis in response to inflammation or trauma. Here they are able to elongate, polarise and eventually migrate toward the site of interest in order to create a glial scar (Sofroniew 2015). *In vitro* wound healing assays have been shown to mimic most of astrocytes' responses observed *in vivo* (Faber-Elman et al. 1996). In particular, they induce the morphological and structural polarisation of the cells and their directed collective migration (Sandrine Etienne-Manneville and Hall 2001; Sandrine Etienne-Manneville 2006). Astrocytes are seeded *in vitro* and allowed to reach a confluent monolayer. Astrocyte migration is then stimulated using a scratch-wound healing assay. Four to six hours after

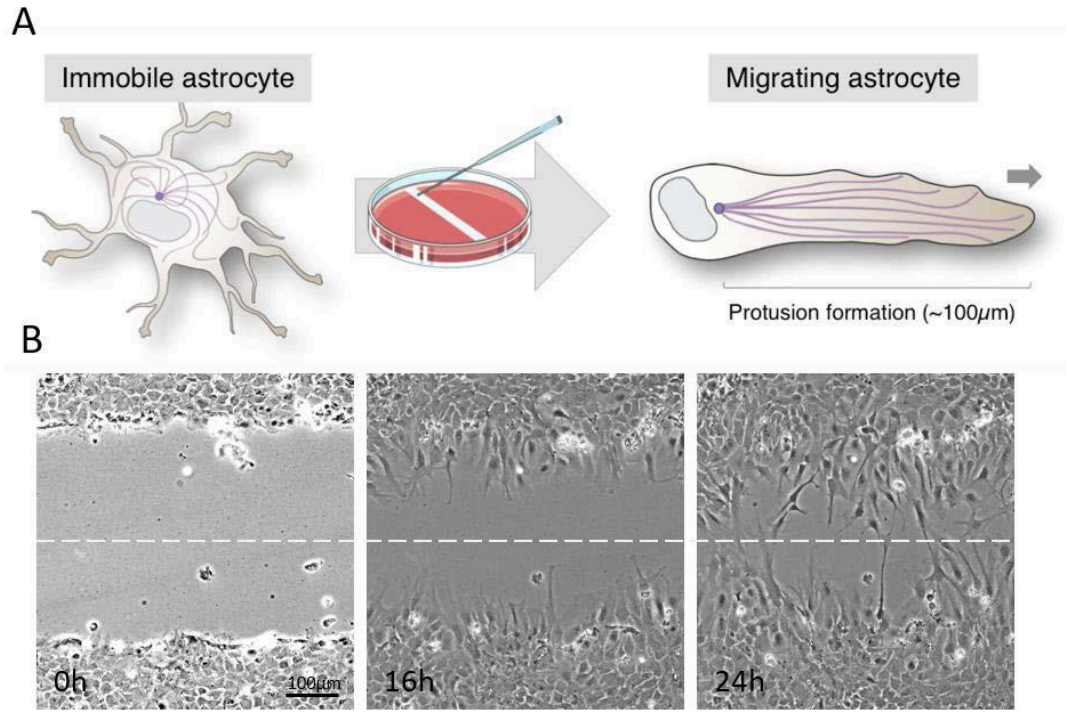

Figure 5 Astrocytes as a model for collective migration A) Schematic representation of the morphological changes that astrocytes undergo in response to scratch. When confluent, astrocytes are quiescent and are characterised by a star shape. The scratch assay induces morphological changes and astrocytes start polarising to finally migrate perpendicularly to the wound until they meet the other edge. B) Phase contrast images of astrocytes 0h, 16h and 24h after wounding.

wounding, they develop a polarised morphology, characterised by an elongated shape, establishment of long protrusions filled with microtubules (approximately 100 μm in length) perpendicular to the scratch, nuclei localization at the cell rear, and centrosome and Golgi apparatus reoriented in front of the nuclei towards the direction of migration (Figure 5). Cells do not move individually but rather migrate as a sheet toward the other edge of the scratch, until the two edges of the scratch meet. This assay has proven to be an excellent model to study the molecular changes upon cell polarisation and collective cell migration (Sandrine Etienne-Manneville and Hall 2001; 2003a).

1.2 Polarity cues, determinants and associated elements

A polarity cue refers to an extracellular signal either from neighbouring cells or the cellular environment that orients the direction of polarity (Devreotes et al. 2017; Ladoux, Mège, and Trepat 2016; Johnston 2018). However, it is polarity determinants that are essential for establishing and maintaining a polarised cell state. Polarity determinants are certain intracellular or transmembrane molecules, which are localized in a skewed manner. The key feature of polarity determinants is their ability to respond to extracellular polarity cues. In return, these cues can play a role in the localization of polarity determinants. However, in certain cases polarity determinants can polarise in the absence of any external cues, indicating that their localisation can be determined simply by an intrinsic ability to polarise spontaneously(Adams et al. 1990). Pivotal molecular determinants of cell polarity have been revealed through pioneering genetic screens in yeast, *C elegans*, and *Drosophila* (St Johnston and Ahringer 2010; Thompson 2013). The discovery of the Rho GTPase Cdc42 to be a fundamental determinant of cell polarity in budding yeast was revolutionary for the field of cell polarity. Cdc42 was identified to localize to one pole of the cell through a positive feedback loop of self-recruitment (Thompson, 2013, Adams et al., 1990). Consequently studies, in the *C elegans* zygote has been used to extensively study PAR proteins involved in the first asymmetric division of the zygote. Similarly, other key polarity protein complexes that have been instrumental in understanding polarised cell types include the Scribble module - Scrib, Lgl and Dlg and the Crumbs complex - Crb, Paltj and Pals1.

1.2.1 Rho GTPases

Mammalian cells contain several hundred GTPases. GTPases are molecular switches that employ a simple biochemical reaction to regulate complex cellular processes. They cycle between two conformational states: the ‘active’ GTP bound state and the ‘inactive’ GDP bound state. In the ‘on’ GTP bound state, GTPases recognize target proteins also known as effectors and induce a response until inactivation upon GTP hydrolysis. This biochemical strategy is evolutionarily conserved. The discovery of the Ras superfamily of GTPases and its members over the past few decades has been revolutionary, given that they are master regulators of cell behaviour (Nobes and Hall 1999; Sandrine Etienne-Manneville and Hall 2002; Wennerberg, Rossman, and Der 2005).

The Ras GTPases are classified into five major groups: Ras, Rho, Rab, Arf and Ran. The Rho (Ras homology) family of GTPases precisely has been extensively studied over the past few decades due to their complex role in regulating cell behaviour. The human genome contains over 60 activators (guanine nucleotide exchange factors, GEFs) and over 70 inactivators

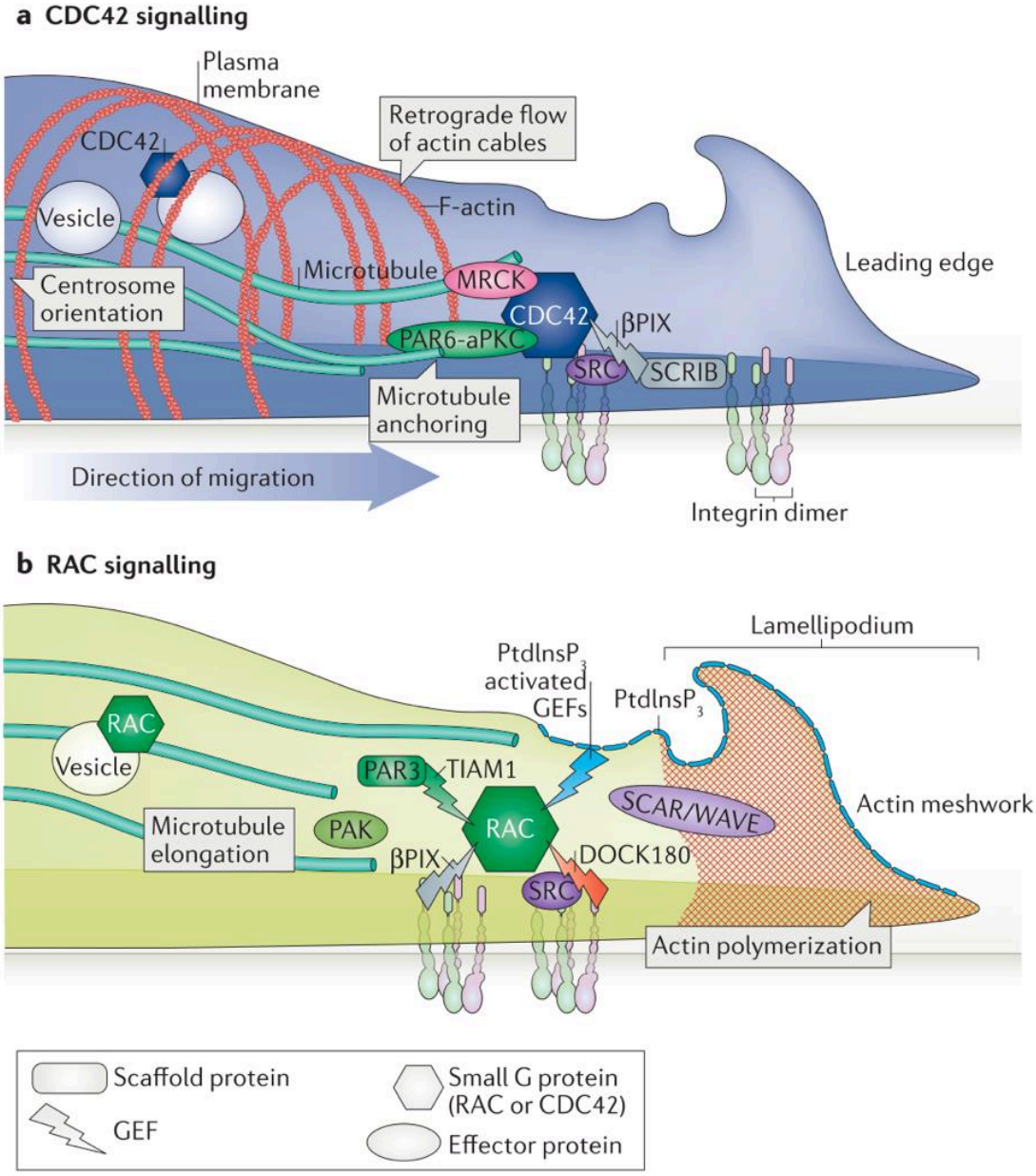

Figure 6 Single migrating cell leading edge. a) Cdc42 module dependent microtubule anchoring plays a role in organelle reorientation towards the leading edge. b)Rac dependent actin polymerization drives lamellipodium formation. Rac activation driven by its GEFs is depicted. Adapted from Mayor and Etienne-Manneville 2016.

(GTPase-activating proteins, GAPs) for the Rho GTPase family. Their effectors however do not contain a universal sequence motif. To date Rho, Rac and Cdc42 remain the three best-characterized members of the family (Sandrine Etienne-Manneville and Hall 2002). In addition to GEFs and GAPs, Rho GTPases can also be negatively regulated upon binding to GDIs (GDP dissociation inhibitors). Depending upon the Rho GTPases GDIs can either bind to the GTP bound form of GTPases or both GDP/GTP-bound. When bound to GDIs Rho GTPases are unable to bind to their effectors (Müller and Goody 2018; Sasaki and Takai 1998; Garcia-Mata, Boulter, and Burridge 2011).

Cdc42 was first discovered in yeast as a fundamental determinant of cell polarity, in 1990. Subsequent revolutionary mammalian cell studies in the Rho GTPase field demonstrated that constitutively activated mutants of Rho and Rac induced the assembly of contractile actin and myosin filaments (stress fibres) and actin-rich surface ruffles (lamellipodia), respectively (Ridley et al. 1992). Soon after Cdc42 was shown to promote the formation of actin-rich, finger-like membrane protrusions (filopodia) (Nobes and Hall 1995) (Figure 6).

This characteristic of Cdc42, Rac and Rho to modulate cytoskeletal elements was identified to be one amongst the several intracellular processes regulated by these polarity determinants (Ridley 2006)(Figure 6). Lamellipodium-driven migration requires active Rac proteins (Rac1, Rac2 and/or Rac3 depending on the cell type and conditions). Several Rac GEFs are involved in activating Rac to induce lamellipodia, including Tiam1(T-lymphoma invasion and metastasis-inducing protein), β-PIX, and DOCK180 (Lawson and Burridge 2014; Ridley 2015; Marei and Malliri 2017). Active Rac proteins interact with WAVE (WASP-family verprolin-homologous protein)-associated complex of proteins (Figures 6b), which in turn activate actin nucleation by the Arp2/3 complex. The actin polymerization in lamellipodia also involves formins and VASP (Cotteret and Chernoff 2002). Not only does active Rac control actin-driven protrusion through PAK but also microtubule elongation (Ridley 2015; Bokoch 2003)

Lamellipodia are not essential for migration, and indeed melanoblasts and fibroblasts can migrate without Rac or the Arp2/3 complex, albeit more slowly. In the absence of Arp2/3 complex, fibroblasts predominantly use filopodia to migrate (Ridley 2006). Cdc42 is the best characterized Rho GTPase involved in filopodium formation (Figure 6a), acting predominantly through formins (Mattila and Lappalainen 2008). Several other Rho GTPases can induce filopodia under different contexts. RhoF induces filopodia through the formins mDia1 and mDia2 (Ridley 2006).

Cdc42 also contributes to the reorganization of the microtubule network (Sandrine Etienne-Manneville 2013; 2004), by activating the PAR polarity complex formed by partitioning defective 6 (PAR6) and atypical protein kinase C (aPKC), which in turn induces microtubule anchoring and centrosome and Golgi positioning in front of the nucleus (Sandrine Etienne-Manneville and Hall 2003b; Palazzo et al. 2001). This results in

reorganization of membrane traffic towards the leading edge, which is likely to participate in the formation of membrane protrusions, the development of new adhesions and the reinforcement of polarity signalling (Figure 6a) (Osmani et al. 2010; Watson, Rossi, and Brennwald 2014)

1.2.2 PAR Proteins

PAR6 belonging to the PAR protein family is a key effector of Cdc42 and Rac participating in polarity signal transduction. Initially, the roles of PAR proteins in cell polarity were known almost exclusively in *C. elegans*. *C. elegans* Par6 was first identified in 1996, during a screen for embryo mutants with a partitioning-defective phenotype (par) (Lang and Munro 2017). The Par6 localises to the anterior periphery of asymmetrically dividing cells in the *C. elegans* zygote, along with Par3, another Par gene product, and PKC3, the single aPKC in worms (Johnston 2018). This observation led to the subsequent identification of these two molecules as binding partners for Par6. A key step towards understanding how cell polarity is regulated came with the observation, that Par6 is a direct target for two small GTPases, Cdc42 and Rac (Figure 6). Confirmation that Cdc42, Par6 and aPKC are all required for asymmetric cell division in the *C. elegans* zygote marked the discovery of the par polarity complex which describes the association of PAR-6, and aPKC with Cdc42. (D. Lin et al. 2000). To date the most complete understanding of how PAR proteins mediate the establishment and maintenance of cortical polarity comes from studies conducted on asymmetrical cell division of the *C. elegans* zygote and *Drosophila* bristle. The overview of polarization giving rise to the first asymmetric cell division in the *C. elegans* zygote, with respect to the roles of the anterior and posterior PARs has been extensively researched (Lang and Munro 2017).

The contribution of PAR proteins to polarity is not only restricted to asymmetrical cell division. Par6 for example is required for the maintenance of cell morphology; and in the absence of Par6, epithelial cells of embryonic *Drosophila* ectoderm lose their apical-basal polarity (Goldstein and Macara 2007). Similarly, in mammalian epithelial cells, Par6 is necessary for the asymmetric distribution of membrane proteins between the basolateral and apical surfaces (St Johnston and Ahringer 2010). Par6 is also essential for establishing cell polarity in migrating astrocytes. Cdc42 recruits PKCξ at the leading edge and together with Par6 forming the Par polarity complex (Figure 6a). Here, Par6 and PKCξ are required for the reorientation of the microtubule organising centre in the direction of migration (Sandrine Etienne-Manneville and Hall 2001). PAR proteins along with Cdc42 and Rac constitute a signalling pathway that intersect with numerous other pathways to organize the cytoskeleton, membrane traffic, and other cellular components so as to polarize cells during oriented migration (Figure 6) (Goldstein and Macara 2007).

1.2.3 The Golgi apparatus and polarized trafficking

Several studies have identified membrane trafficking itself to play a crucial role in cell polarity, by directing lipids and proteins to specific subcellular locations in the cell and maintaining a polarized state. The Golgi apparatus being the master organizer of membrane trafficking, receives de novo synthesized molecules from the endoplasmic reticulum (ER), post-translationally processes lipids and proteins, and sorts cargoes to their ultimate destination (Boncompain and Weigel 2018; Guo, Sirkis, and Schekman 2014). Conversely, the position of the Golgi apparatus inside the cell can dictate the directionality of membrane trafficking and the proper localization of polarity cues. This "chicken- and-egg" problem is typical of feedback loops involved in symmetry breaking during establishment of cell polarity. In the case of Golgi-dependent membrane trafficking, the reorientation of the Golgi apparatus along the direction of the polarity axis targets transport toward a given region of the cell, for example, toward the leading-edge plasma membrane during cell migration, in the apical process of neural stem cells, toward the apical compartment of epithelial cells, or toward the immunological synapse (Figure 1). Not only is the trafficking of vesicles from the Golgi apparatus polarised but also the organelle itself exhibits intrinsic polarity. This is due to its organization into *cis, median*, and *trans* compartments. This compartmentalization dictates the polarity axis of intra-Golgi trafficking, whether it is described in terms of the vesicular transport model or the cisternal maturation model (Glick and Luini 2011a).

On a wholistic scale the Golgi apparatus and its associated elements can be subdivided into three layers: a cytoskeletal layer, the so-called Golgi matrix, and the Golgi membranes which play distinct roles in establishing cell polarity (Ravichandran, Goud, and Manneville 2020). First, the outer regions of the Golgi apparatus interact with cytoskeletal elements, mainly actin and microtubules, which shape, position, and reorient the organelle. Secondly, the Golgi membranes and associated matrix proteins, which not only participate in the selective capture of transport intermediates but also participate in signalling events during polarization of membrane trafficking. Finally, the Golgi membranes themselves serve as active signalling platforms during cell polarity events. In polarized cells, cellular materials are transported along the polarity axis. This requires polarization of membrane trafficking from the Golgi apparatus.

Studying Golgi reorientation and polarized trafficking during cell polarization has uncovered the involvement of several aforementioned polarity determinants (Bryant and Yap 2016). For instance, during directed cell migration activation of Cdc42 at the leading edge recruits and anchors motor protein dynein at the cell cortex via the Par polarity complex (Palazzo et al. 2001; Sandrine Etienne-Manneville and Hall 2003b). Dynein in turn pulls on astral microtubules to reorient the centrosome toward the leading edge (Palazzo et

al. 2001). The Golgi apparatus probably reorients via the same mechanism through its mechanical link with the centrosome (Rios 2014). Dynein has also been found at the cis-Golgi, where it associates with the actin cytoskeleton and coat proteins (J. L. Chen et al. 2005a). Polarity determinant Cdc42 has even been shown to direct intra-Golgi traffic via its interaction with coat protein I (COPI) (Park et al. 2015a).

Despite extensive research, it remains ambiguous as to whether and how external polarity cues are transduced inside the cells to polarize transport from the Golgi apparatus and conversely whether and how the Golgi apparatus could be driving cell polarization independent of external polarity cues.

Chapter 2

The Rho GTPase Cdc42

This Chapter is dedicated to the Rho GTPase Cdc42 which was first identified in the budding yeast *Saccharomyces cerevisiae* (Adams et al. 1990). The *CDC42* gene was first described as a gene likely to encode a protein that binds and hydrolyses GTP (a so-called GTPase or G protein) while bound to the inner surface of the plasma membrane. In this revolutionary study yeast mutants defective in CDC42 were unable to bud or establish cell polarity and the cells displayed delocalized plasma membrane deposition which was associated with a loss of the actin cytoskeleton organization (Adams et al. 1990). This study established Cdc42 as a key polarity determinant. Progressively, the small GTPase Cdc42 was shown to be evolutionarily conserved from yeast to mammals. Roles of Cdc42 in regulating diverse cellular functions have been demonstrated since. These include cell polarization, migration, division and also T-cell polarization, macrophage chemotaxis and phagocytosis (Sandrine Etienne-Manneville 2004; Cerione 2004; Sandrine Etienne-Manneville and Hall 2002).

It is thus not surprising that Cdc42 deficiency causes severe developmental defects in mice leading to embryonic lethality at embryonic stage E6.5 (F. Chen et al. 2000). Roles of Cdc42 during development have been demonstrated by studies using conditional knockout mice to suppress Cdc42 function. Depleting Cdc42 in neural precursor cells and neuroepithelial cells (radial glial cells) demonstrated that Cdc42 plays a pivotal role in the development of different brain regions like the telencephalon and the cerebral cortex (L. Chen et al. 2006; Peng et al. 2013). Precisely, the selective knock-out of Cdc42 in mouse telencephalon leads to a condition termed as holoprosencephaly which is associated with a loss of neural epithelium polarity (L. Chen et al. 2006) and knocking out Cdc42 in neural progenitors causes defects in formation of axon tracts (bundles of nerve fibers). Furthermore, ablating Cdc42 in neural crest stem cells, shows defects in maintenance, migration, and differentiation of these cells (Melendez, Grogg, and Zheng 2011). Emerging studies employing similar conditional knock-out methodology have revealed a number of physiologically relevant, sometimes unexpected, functions of Cdc42 in a tissue/organ-specific manner (Melendez, Grogg, and Zheng 2011). To date roles of Cdc42 have been reported in the following processes: cardiac organogenesis, pancreatic development, nervous system regulation, blood development, immune system regulation, eye development, and skin development and maintenance (Melendez, Grogg, and Zheng 2011; Woodham et al. 2017).

Considering these developmental studies, it is not surprising that *de novo* mutations of Cdc42 were identified by exome sequencing in patients exhibiting variable phenotypes. For instance, missense mutations in CDC42 gene underlie a clinically heterogeneous group of phenotypes characterized by variable growth dysregulation, facial dysmorphism, and neurodevelopmental, immunological, and haematological anomalies, including a phenotype resembling Noonan syndrome (a developmental disorder caused by dysregulated RAS signalling)(Martinelli et al. 2018; Bekhouche et al. 2020; Motokawa et al. 2018). Therefore, studying Cdc42 and its associated regulatory mechanisms are important to have a better understanding of these pathological phenotypes.

2.1 Regulation of Cdc42.

Like all monomeric GTPases, Cdc42 functions as a molecular switch, cycling between its GDP-bound inactive state and its GTP-bound active state (Figure 7). This GTPase cycle is regulated by guanosine nucleotide exchange factors (GEFs) that stimulate nucleotide exchange and GTPase-activating proteins (GAPs) that accelerate the intrinsic GTPase activity of Cdc42. Active GTP-bound Cdc42 preferentially binds to effector proteins and activate

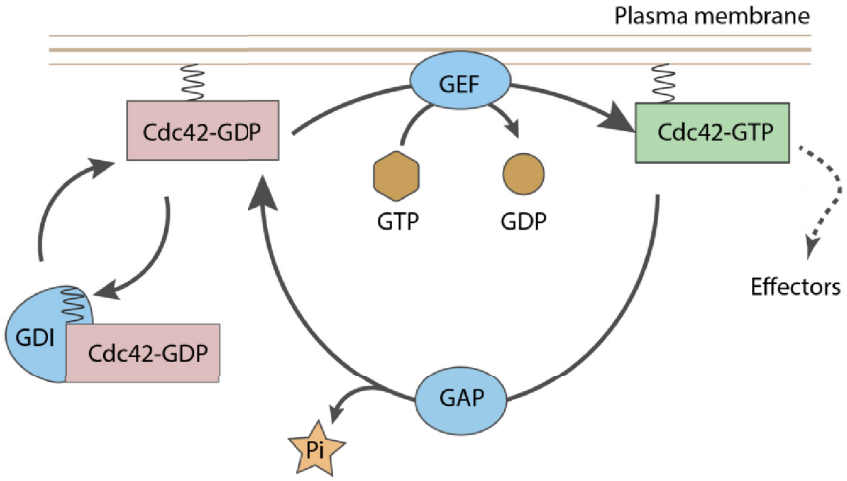

Figure.7 The Rho GTPase cycle. Cdc42 cycles between an active (GTP-bound) and an inactive (GDP-bound) state. In the active state, Cdc42 can interact with target proteins (effectors). The cycle is highly regulated by three classes of protein: in mammalian cells, guanine nucleotide exchange factors (GEFs) catalyse nucleotide exchange and mediate activation; GTPase-activating proteins (GAPs) stimulate GTP hydrolysis, leading to inactivation; and guanine nucleotide exchange inhibitors (GDIs) extract the inactive GTPase from membranes. Cdc42 is prenylated at its C terminus, and this is required for its membrane and GDI1 interaction.

downstream signalling events. An additional level of regulation is imposed on Rho GTPases through the binding to the GDI (guanosine nucleotide dissociation inhibitor) Rho GDI1 (also known as Rho GDIα), which sequesters inactive Rho proteins in the cytosol, away from their regulators and effectors (Figure 7) (Sandrine Etienne-Manneville 2004). Given the various functions associated with Cdc42, such conserved regulatory mechanisms (GEFs, GAPs and GDIs) are indispensable to for its controlled activity (Figure 6)(Arias-Romero and Chernoff 2013).

2.2 Effector proteins and cellular functions

In its GTP-bound form Cdc42 binds to and regulates several target proteins referred to as effectors, the functions of which drive downstream signalling events (Figure 8) (See Table 1 at the end of Chapter 1 for full list of mammalian Cdc42 effector proteins). Several plasma membrane-associated Cdc42 effector proteins have been identified and directly linked to the regulation of multiple cellular functions. The plasma membrane associated roles are mostly associated with initial cell polarization events, these include actin polymerization and filopodial formation, polarization of the microtubule network and organelle reorientation (Golgi-apparatus and centrosome). Other processes include clathrin independent endocytosis events.

Par polarity complex

Par6 is a direct target for Cdc42. Cdc42 induces a conformational change in Par6 upon binding, activated Par6 recruits aPKC. This is the initiation of the Par polarity complex (D. Lin et al. 2000)(see Chapter1). The PAR complex is highly conserved throughout eukaryotes (although not in yeast). In addition, several downstream targets of the PAR complex have been identified. Glycogen synthase kinase 3β (GSK3β) activity is spatially inhibited by PKCζ-induced phosphorylation and this leads to the association of the adenomatous polyposis coli protein (APC) with microtubule plus-ends (Figure.8). This is required for centrosome reorientation (Etienne-Manneville and Hall, 2003b). The Par6- aPKC complex also interacts with the tumour suppressor Lethal giant larvae (Lgl), with aPKC phosphorylating it at highly conserved residues (Sandrine Etienne-Manneville et al. 2005).

Serine/Threonine kinases

The p21-activated kinases (PAKs) are a family of Serine/Threonine protein kinases that are represented by six genes in humans (PAK 1–6), and are found in all eukaryotes sequenced to date. In addition to the conserved catalytic domain, all PAKs harbour an N-terminal regulatory domain of ~50 residues which contains a CRIB motif responsible for binding Cdc42 and Rac1-like GTPases (Bagrodia and Cerione 1999; Bokoch 2003). PAKs are

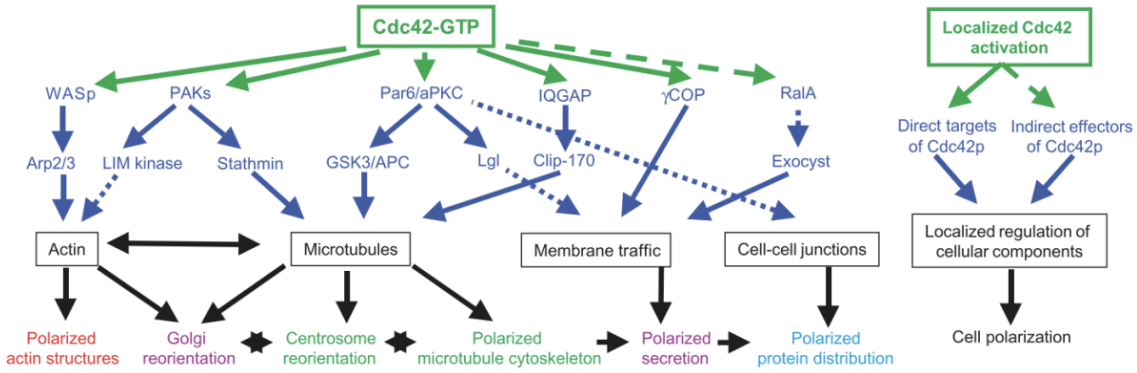

Figure 8 Cdc42 controlled signalling pathways and intracellular functions. Cell polarization requires the spatial and temporal regulation of several intracellular components. Orientation of the actin and microtubule cytoskeletons, regulation of cell contacts and organization of membrane traffic occur in concert. Multiple signalling pathways downstream of Cdc42 regulate these different cellular components (black box). These signals are transduced by different Cdc42 direct (solid line) or indirect (dotted line) effectors (blue) and involve several intermediates (blue). Cell polarization initiates from the localized activation of Cdc42, which leads to a localized regulation of cellular components and therefore to their asymmetric distribution. The different cellular components synergistically generate the general characteristics of cell polarization. Adapted from (Sandrine Etienne-Manneville 2004).

known mediators of filopodia formation. For example, PAK1 protein associates with F-actin in membrane ruffles and lamellipodia at the leading edge of polarized migrating cells. It also localizes to cell-cell contacts in epithelial cells. Additionally, PAK1 also plays an important role in actin rearrangements by regulating LIM kinase, which in turn phosphorylates and inactivates the actin-severing protein cofilin (Bishop & Hall, 2000; Bokoch, 2003).

Cdc42 also interacts with two other Serine/Threonine kinases that are involved in actin reorganization and filopodia formation, MRCKs α and β. MRCKs are Cdc42-specific effector proteins which contain a PH and a ROK-like kinase domain which can phosphorylate myosin light chain (MLC)(Etienne-Manneville, 2004). Kinase-dead MRCKα inhibits Cdc42-induced filopodia, and overexpression of MRCKα has been shown to induce extensive filopodia in mammalian cells. The *Drosophila* homologue of MRCK, Genghis Khan ('GEK') is known to be required for cytoskeletal regulation during oogenesis (Pichaud, Walther, and Nunes de Almeida 2019).

N-WASP

Another key effector protein of Cdc42 associated with the actin machinery is Wiskott–Aldrich Syndrome protein (WASp) the product of the gene mutated in Wiskott-Aldrich syndrome. WASP is expressed only in haematopoietic cells, whereas N-WASP is ubiquitously

expressed. These proteins have Cdc42- and Rac-interactive binding (CRIB) domains that bind directly and specifically to Cdc42. Activated N-WASP in turn recruits and activates the Arp2/3 complex (Figure 8). The physical interaction between the NH2 -terminal domain and the COOH-terminal effector domain of N-WASP is a regulatory interaction because it can inhibit the actin nucleation activity of the effector domain by closing the Arp2/3 binding site (Rohatgi, Ho, and Kirschner 2000). Cdc42 and Phosphatidylinositol 4,5-bisphosphate (PI(4,5)P2) reduce the affinity between the NH2 and COOH termini of WASP therefore activating WASP and enabling the recruitment of the Arp2/3 complex by N-WASP (Rohatgi, Ho, and Kirschner 2000). This pathway leads to actin polymerization and filopodia formation in migrating cells (Bishop and Hall 2000; Ridley 2006; 2015). In addition, on endomembranes, Cdc42 stimulates the formation of a branched actin network through N-WASP and WASP during endocytosis and exocytosis of vesicles at the plasma membrane, and trafficking of vesicles from the Golgi apparatus to the endoplasmic reticulum (ER). Such actin polymerization might assist the process in which a vesicle pinches off the donor membrane compartment, and/or might help drive the vesicle towards the target membrane, acting in concert with myosin motors (Ridley 2015).

IQGAP

The IQGAP family falls under the list of Cdc42 effectors. The three isoforms of the IQGAP family display a distinct expression pattern in mammalian tissues. IQGAP1 is ubiquitously expressed, while the expression of IQGAP2 is restricted to the liver and testis and IQGAP3 is found mainly in the brain and lung (Watanabe, Wang, and Kaibuchi 2015). Of the three members, IQGAP1 has been extensively studied as a Cdc42 effector protein. The GAP related domain (GRD) of the IQGAP1 inhibits the intrinsic GTPase activity of Cdc42 in vitro, stabilizing Cdc42 in its active GTP-bound form (Mataraza et al. 2003). Moreover, IQGAP1 substantially increases the pool of GTP-bound Cdc42 *in vivo*. IQGAP1 also appears to be necessary for Cdc42 to localize to the plasma membrane. Not surprisingly, overexpressed IQGAP1 modulates cell morphology by stimulating filopodia formation a phenotype associated with active Cdc42 at the plasma membrane (Watanabe, Wang, and Kaibuchi 2015). Thus, the IQGAP family is one of the critical regulators involved in mediating Rho family GTPases and their reorganization of adhesions and the cytoskeleton, including actin filaments.

2.2.1 GEFs and GAPs

Rho GEFs generally fall under two categories: the Dbl (Diffuse B-cell lymphoma) and the DOCK (Dedicator of Cytokinesis) families of GEFs. GEFs of the Dbl family are characterized by their conserved Dbl Homology (DH)/Pleckstrin Homology (PH) domains and are encoded

by the ARHGEF1 gene, thus are called ARHGEF proteins. Of the numerous Cdc42 GEFs, the Dbl proteins such as Intersectin1/2(ITSN1/2), FGD 1/4, and Tuba (ARHGEF36) are specific to Cdc42, while Abr, Asef (ARHGEF4), Vav, Dbl (ARHGEF21), and Dbs (ARHGEF14), activate both Rac and Cdc42 in vitro, and may function in a promiscuous manner (Sinha and Yang 2008). The two mammalian PAK-interacting exchange factor (PIX) proteins α-PIX and β-PIX (also known as ARHGEF6 and ARHGEF7, respectively) are a subfamily of Dbl GEFs. They were originally discovered as binding partners for the p21-activated kinases (PAK). PAK proteins which are high-affinity effectors for Cdc42 and Rac also phosphorylate PIX proteins (Sinha and Yang 2008; Ridley 2015). PIX proteins were also given alternative names: '85 kDa SH3 domain- containing proline-rich protein' (p85SPR) and 'cloned out of library-1 and -2' (cool-1 and cool-2), although the most commonly used names are α-PIX and β-PIX (W. Zhou, Li, and Premont 2016)(Figure 9).

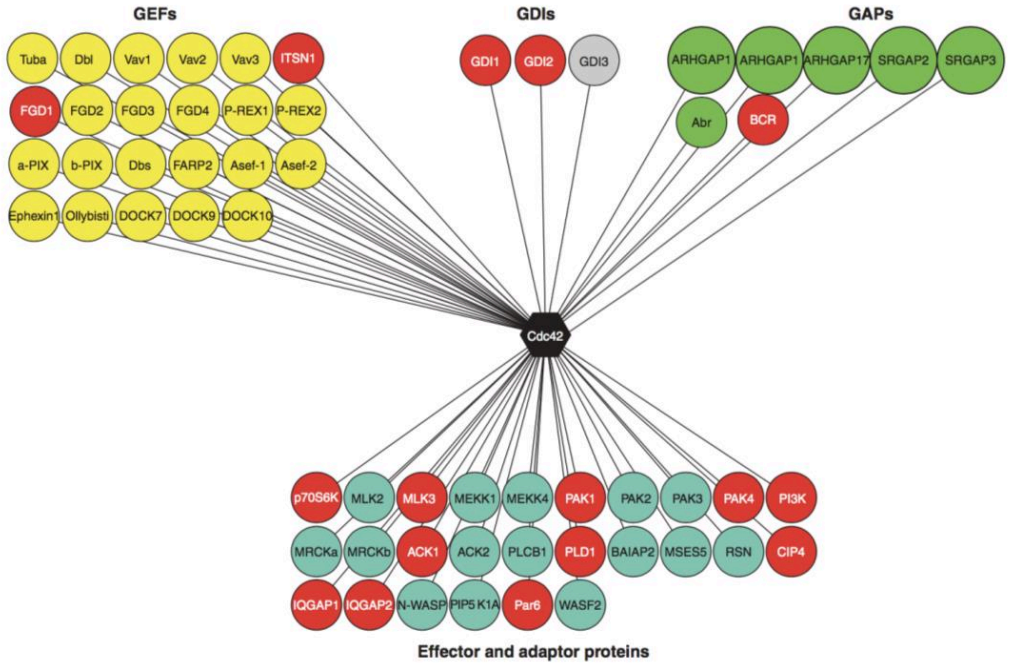

Figure 9 Proteins associated with Cdc42. Associated proteins are categorized into the three regulatory groups of proteins namely GEFs, GDIs and GAPs (top) and into effectors and adaptor proteins (bottom) associated with signalling downstream of Cdc42. Circles coloured red represent proteins interacting specifically to Cdc42 while others are promiscuous and activate other Rho GTPases too. From Romero and Chernoff. 2013.

The second group of GEFs are the DOCK proteins. The DOCK family has a distinct branch of Cdc42 activating GEFs, DOCK9 and DOCK11 (Bos, Rehmann, and Wittinghofer 2007; Sinha and Yang 2008; Sandrine Etienne-Manneville and Hall 2002). Interestingly, the DOCK GEF family contains GEFs only for Rac and Cdc42 and is conserved in plants and animals, but not in yeast, whereas the Dbl family contains GEFs for all Rho GTPases, and is conserved in yeast and mammals (Sinha and Yang 2008). With respect to Cdc42, in most of the DOCK family proteins, the DOCK homology region 2 (DHR2) domain mediates binding to GDP-bound Cdc42 (Bos, Rehmann, and Wittinghofer 2007) (Figure 9).

Although G proteins have intrinsic GTPases activity, their actual GTP hydrolysis reaction is in fact very slow, and efficient hydrolysis requires the interaction with a GAP, which accelerates the GTP hydrolysis by several orders of magnitude. Several Rho GAPs that inactivate Rho GTPases contain a Rho GAP domain. The human genome is predicted to encode between 59 and 70 proteins containing a Rho GAP domain and to date more than half of them have been characterized (Figure 9) (Pichaud, Walther, and Nunes de Almeida 2019). Similar to Rho GTPases, some GAPs show preferential tissue expression and seem to have tissue-specific functions. Moreover, several mammalian Rho GAPs have been shown to be implicated in specific Rho GTPase-mediated biological functions, including endocytosis, exocytosis, cytokinesis, cell migration, cell differentiation, cell blebbing, angiogenesis, tumour suppression and neuronal morphogenesis. This largely due to the multidomain features of Rho GAPs. ARHGAP1, also known as Cdc42GAP is the founding member of the Rho GAP family of proteins with a significant preference for Cdc42 (Tcherkezian and Lamarche-Vane 2007; Bos, Rehmann, and Wittinghofer 2007). Several other ARHGAP members have been then identified and associated with specific roles in biological processes (Figure 9). Some Rho GAPs also contain GAP domains serving as recognition modules, and could act as effectors or scaffold proteins mediating cross-talk between Rho GTPases and other signalling pathways. For example, full-length α1-chimaerin (CHN1) lacks GAP activity, but retains the ability to bind GTPases, and seems to co-operate with Rac1 and Cdc42 to promote the formation of lamellipodia and filopodia (Tcherkezian and Lamarche-Vane 2007).

2.2.2 Rho GDI Family

Rho GDIs provide a third layer of regulation to the Rho GTPase cycle by sequestering GTPases and making them unavailable to bind to effector proteins. In the Rho GDI family three members have been reported so far, which have been named GDI1 (also Rho GDI or GDIα), GDI2 (also D4- or Ly-GDI or GDIβ), and GDI3 (also GDIγ). GDI1 is ubiquitously expressed, whereas GDI2 and GDI3 show unique tissue specific expression patterns: GDI2 is expressed in hematopoietic tissues and GDI3 is expressed in brain, lung, kidney, testis and

pancreas (Sasaki and Takai 1998). Unlike the GEFs and GAPs, which catalyse a single reaction, the Rho family–specific GDIs appear to be capable of at least three distinct biochemical activities. The first activity, for which the proteins were originally named, involves the ability of the GDI to block the dissociation of GDP from Cdc42, Rac, and Rho. By blocking GDP-dissociation, GDI1 inhibits the biological activity of specific GEFs for Cdc42 and Rho. It was subsequently shown that GDI1 is also capable of inhibiting GTP hydrolysis by Rho family GTPases, blocking both GAP-catalyzed and intrinsic GTPase activity. Therefore, the GDI can intercede at two points in the GTP-binding/GTPase cycle. This implies that the GDI is able to bind to the activated, GTP-bound state of Rho proteins as well as to their inactive, GDP-bound state. In fact, GDI1 binds with essentially identical affinities to the two nucleotide-bound states of Cdc42 (Nomanbhoy and Cerione 1996). The third and important biochemical activity associated with GDIs is their ability to stimulate the release of Cdc42, Rac, and Rho from cellular membranes. The solubilization requires the GTPases to be isoprenylated in order to interact with the GDIs. In the absence of Rho GDI1, the cytosolic pool of Rho GTPases is unstable and rapidly degraded in a proteasome-dependent manner (Garcia-Mata, Boulter, and Burridge 2011). Contrary to GEFs and GAPs, there is no binding specificity (known for now) of the GDIs. For instance, GDI1 can interact with all the Rho proteins, Rac proteins and Cdc42.

Rho GDI1 has been crystallized in complex with Cdc42 (Figure 10)(Hoffman, Nassar, and Cerione 2000). The structure of Rho GDIs comprises two main domains: a C-terminal domain (amino acids 74–204), which includes the geranylgeranyl-binding pocket and is required to extract Rho GTPases from the membrane; and a ‘regulatory arm’ at the N-terminus, which inhibits exchange and hydrolysis through interactions with the switch I and switch II domains in the Rho GTPases (Keep et al. 1997). The isoprenyl-binding domain adopts an immunoglobulin-like fold, and the surface of the geranylgeranyl-binding pocket is lined with hydrophobic residues (Figure 10b). Insertion of the isoprenyl head perturbs the structure of the Rho GDI. The N-terminal region of Rho GDIs, which is flexible and disordered in solution, folds into two antiparallel helices upon formation of the complex and interacts with the switch I and switch II domains of the Rho GTPases (Figure 10). It is interesting again to note that Rho GDIs can accommodate both GTP-bound and GDP-bound forms of Rho GTPases (Nomanbhoy and Cerione 1996). Structural studies have shown that the main interaction sites between Rho GDIs and Rho GTPases are virtually unaffected by the nucleotide state (Hoffman, Nassar, and Cerione 2000).

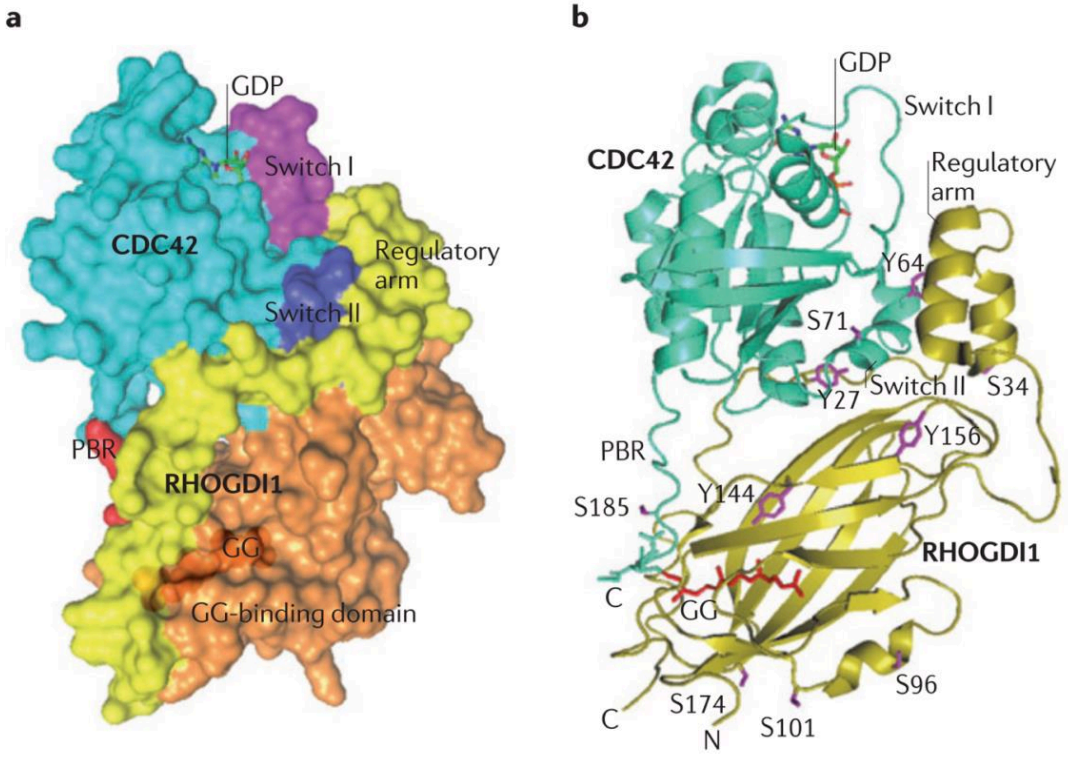

Figure 10 Rho GDI1and Cdc42 complex crystal structure. a) A space filling model showing Cdc42 in complex with Rho GDI1. The domains that play a role in the interaction are labelled on each protein respectively. b) Ribbon diagram of the crystal structure of the Cdc42-Rho GDI1 complex, where the geranylgeranyl tail is depicted in red; From Garcia-Mata ,R et al. 2011

2.2.2 Cdc42 in migrating cells

The front-rear polarization of migrating cells involves Cdc42 recruiting aPKC and activating the Par complex (Cdc42/Par6/aPKC) (Figure 6a, 8)(Etienne-Manneville and Hall 2001). Active aPKC in turn suppresses Glycogen synthase kinase 3β (GSK3β) leading to the association of the adenomatous polyposis coli protein (APC) with microtubule plus-ends and their stabilization at the leading edge of migrating cells (Etienne-Manneville 2004; Etienne-Manneville and Hall 2003a). Cdc42 together with aPKC also control Dlg1 recruitment to the cell cortex, allowing the capture of APC- positive microtubule plus-ends at the cell cortex (Etienne Manneville 2005 JCB). Plus-ends of microtubules are also stabilized by Cdc42-dependent recruitment of IQGAP and the plus-end protein CLIP-170 (Fukata et al. 2002). The stabilization of microtubules at the leading edge of migrating cells promotes the

reorientation of the MTOC towards the direction of migration involving centrosome and Golgi reorientation. Strikingly, Par6, and PKCζ, do not participate in nucleus movement but instead contribute to MTOC reorientation by maintaining the MTOC at the cell centroid. Primarily, MTOC reorientation occurs by a major rearward movement of the nucleus while the MTOC remained immobile. Nucleus movement is driven by actin retrograde flow in a myosin II dependent manner. This is mediated via Cdc42 activated MRCK that phosphorylates myosin II (Gomes, Jani, and Gundersen 2005)

With regard to actin polymerization at the leading edge, plasma membrane associated Cdc42 is the main GTPase contributing to filopodia extension, acting predominantly via mDia formins. Cdc42 also act via WASP to generate filopodia (Rohatgi, Ho, and Kirschner 2000).(see 2.2 Effectors of Cdc42) Additionally, Cdc42 can recruit and localize Rac itself at the leading edge through multiple potentially synergistic pathways which include microtubule capture at the leading edge, Rac GEF localization and directed vesicle trafficking (Ridley 2015). Rac in turn induces lamellipodium extension through the WAVE complex, which activates the Arp2/3 complex (Nobes and Hall 1999). The aforementioned roles of plasma membrane associated Cdc42 in migrating cells, can be extrapolated to other polarized cell types.

Cdc42 is also implicated in the polarized trafficking directed towards the leading edge (Figure 8). It is also implicated in intra-Golgi trafficking by interacting with coat proteins. These roles are described in detail in the following sections (See 2.3.2).

Lastly, intracellular junctions are necessary for cells migrating in a collective manner. Cdc42 effector protein IQGAP1 is implicated in regulating E-Cadherin mediated intracellular junctions in polarized migrating cells downstream of Rac and Cdc42 (Briggs and Sacks 2003; McCallum, Erickson, and Cerione 1998; Watanabe, Wang, and Kaibuchi 2015).

Summary I

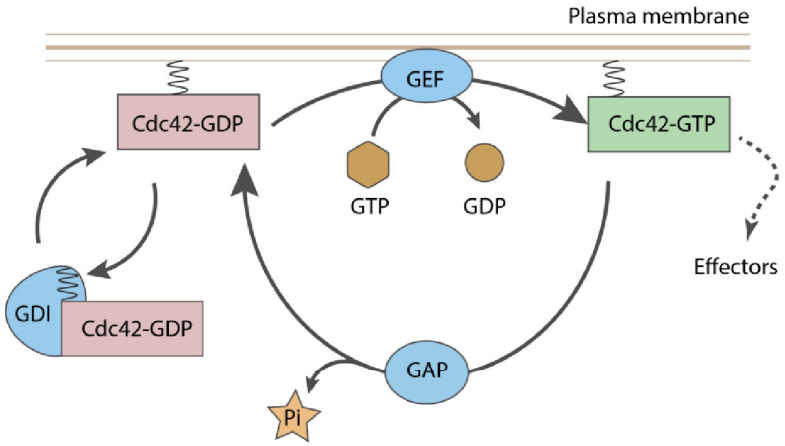

- Cdc42 is an evolutionarily conserved Rho family small G protein.
- Cdc42 cycles between an active (GTP-bound) and an inactive (GDP-bound) state. In the active state, it can interact with target proteins (effectors).
- The GTPase cycle is highly regulated by three classes of protein: in mammalian cells, GEFs catalyse nucleotide exchange and mediate activation; GAPs stimulate GTP hydrolysis, leading to inactivation; and GDIs extract the inactive GTPase from membranes.
- Cdc42 is prenylated at its C terminus, and this is required for its membrane and GDI1 interaction, regulating its subcellular localization.
- Cdc42 activates an array of effectors (~60) to regulate multiple intracellular components to establish cell polarization.
- These include cytoskeletal rearrangements (actin polymerization and polarizing microtubules), Golgi-apparatus reorientation, centrosome reorientation, polarized vesicular trafficking and localized protein distribution.

2.3 Subcellular localization of Cdc42

In their active state, GTPases are typically localized to cellular membranes. As such, compartmentalization of signalling molecules through membrane localization could provide a major mechanism modulating the outcome of intracellular signal transduction (Garcia-Mata, Boulter, and Burridge 2011; Ahearn et al. 2012; Baschieri and Farhan 2015). Given the dynamic and complex array of interactions involving Cdc42, regulatory mechanisms dictating the subcellular localization of Cdc42 are key for maintaining its controlled downstream signalling.

Distinct pools of Cdc42 have been identified in different membrane subcellular compartments. The mostly widely studied pool of Cdc42 is that associated with the plasma membrane. There is also a cytosolic pool of Cdc42 bound to Rho GDI1 (Nalbant et al. 2004; Roberts et al. 2008). Emerging roles for Cdc42 associated with other compartments like the Golgi apparatus have established the presence of additional intracellular Cdc42 pools (Farhan and Hsu 2016). Cdc42 is also delivered to the plasma membrane via polarized trafficking from the Golgi apparatus, which establishes a distinct vesicular pool (Figure 8). The Golgi-localized pool of Cdc42 is increasingly thought to be of key importance, especially for Cdc42-dependent Golgi apparatus reorientation during cell polarization (Ravichandran, Goud, and Manneville 2020). Not surprisingly, most of the earlier studies conducted to elucidate the subcellular localization of Cdc42 have considered only the ubiquitous isoform Cdc42u (see Chapter 3).

2.3.1 The plasma membrane-associated pool

The vast majority of research has been focused on studying the roles of Cdc42 at the plasma membrane. As aforementioned, we summarize here the plasma membrane associated roles of Cdc42. Several polarity-inducing stimuli activate Cdc42, such as receptor tyrosine kinases, adhesion molecules (cadherins), and G-protein coupled receptors (Cerione 2004). Active Cdc42 binds to the plasma membrane, preferably to PI(4,5)P2 enriched domains which are maintained by PTEN (Martin-Belmonte et al. 2007). Once activated, Cdc42 downstream signalling is largely driven by the Par complex, PAKs, WASp and the IQGAP protein family. (See 2.2 Effectors of Cdc42)

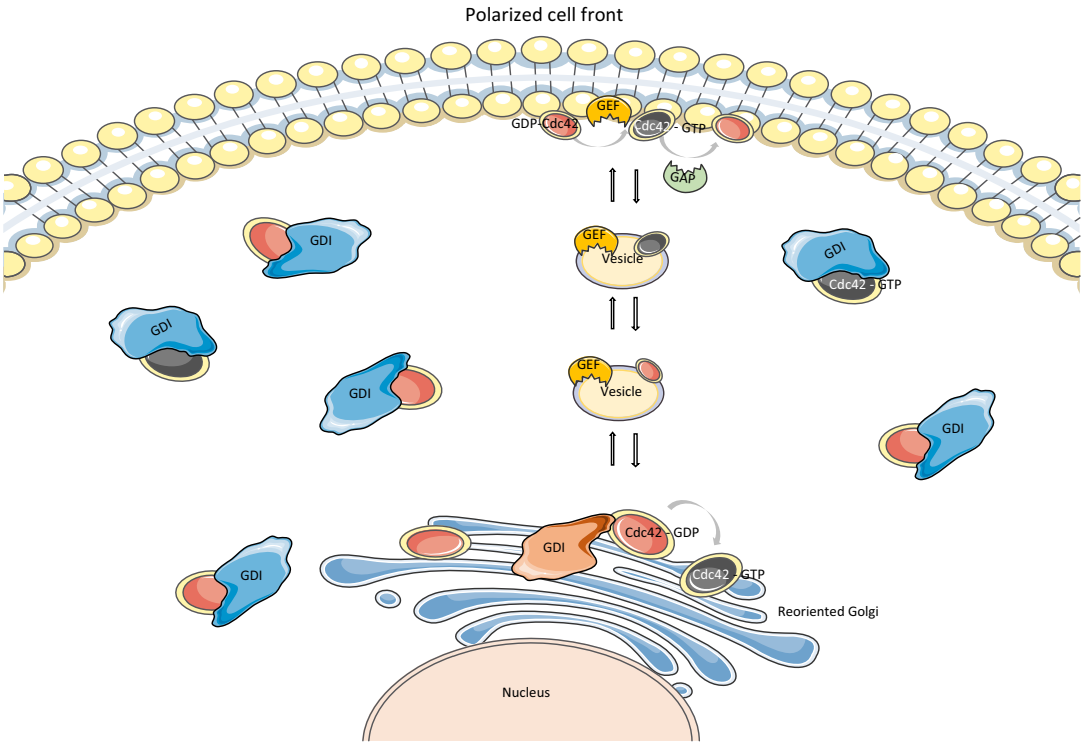

Figure 11 Schematic of the various subcellular localization of Cdc42 in a migrating cell. The distinct subcellular pools of Cdc42 include 1) the plasma membrane associated pool of Cdc42, 2) the cytosolic Rho GDI1 bound pool and 3) the vesicular pool participating in polarized trafficking towards the leading edge. The other unconventional pool of Cdc42 displayed here is the Golgi-localized pool of Cdc42 whose potential interactors are depicted in this image, such as a Golgi-localized Rho GDI, and regulation of Cdc42 activity at the Golgi-apparatus is postulated.

2.3.2 The Golgi-localized pool

More recently, interest developed in understanding the role of the Golgi-localized Cdc42 pool, when cell-based studies uncovered that this pool is activated under certain circumstances (Nalbant et al. 2004). Consistently, Cdc42 at the Golgi apparatus has been shown to interact with the Golgi matrix (Tonucci et al. 2015), golgins (Makhoul et al. 2019a) and associated cytoskeletal elements (Ravichandran, Goud, and Manneville 2020). Briefly, there exist three general models for the functions of Golgi-localized Cdc42 pool; i) the reservoir (the Golgi-localized pool acts as a reservoir to replenish the plasma membrane-associated pool), ii) localized functions (the Golgi-localized pool has a function independent

of the plasma membrane-associated pool), and iii) the polarity loop (the Golgi-localized pool synergistically coordinates with the plasma membrane-associated pool to achieve polarity events) (Figure 12) (Farhan and Hsu 2016).

To support the reservoir model (Figure 12a), studies in mammalian cells suggested that Cdc42 at the Golgi apparatus can be transported to the plasma membrane to exert its functions. A biosensor-based study, in which the reporter changed its fluorescence intensity in proportion to the level of active Cdc42, found that activation of Cdc42 at the Golgi apparatus coincides with the activation of Cdc42 at the plasma membrane (Nalbant et al. 2004). Moreover, the disruption of microtubules affects the total cellular activity of Cdc42 (Nalbant et al. 2004). Given that microtubules are involved in trafficking from the Golgi apparatus to the plasma membrane, the results suggested that Cdc42 at the Golgi could be replenishing the pool at the plasma membrane (Figure 11). Further, blocking the transport from the Golgi apparatus to the plasma membrane decreases the activity of Cdc42 at the leading edge of migrating cells (Baschieri et al. 2014).

In migrating astrocytes, an ADP-Ribosylation Factor 6 (ARF6) dependent mechanism has been demonstrated to deliver Cdc42 together with β-PIX at the leading edge (Osmani et al. 2010). ARF6 acts in the endocytic pathway by promoting endocytosis at the plasma membrane, and also recycling, which involves recycling of endosomes to the plasma membrane (Donaldson and Jackson 2011; Jackson and Bouvet 2014). Here interestingly transport of Cdc42 from the Golgi apparatus to the plasma membrane occurs indirectly, involving transit through the recycling endosome compartment (Osmani et al. 2010). Therefore, Cdc42 can be delivered to the plasma membrane both directly and indirectly via recycling endosomes. It is important to note that the presence of Rho GDIs extracting Cdc42 from endomembranes cannot compensate for the decrease of Cdc42 activity induced by microtubule depolymerisation or by knocking down ARF6 (Nalbant et al. 2004; Osmani et al. 2010).

In contrast, in the second model, Cdc42 has specific localized functions at the Golgi apparatus (Figure 12b). This model received a strong support when the role of Cdc42 in intra-Golgi transport was studied. An existing model for intra-Golgi transport is the cisternal maturation model, where the maturation of Golgi stacks mediate anterograde cargo transport and vesicles formed by the Coat Protein I (COPI) complex mediate retrograde transport of Golgi enzymes (Glick and Luini 2011b). Besides generating vesicles for retrograde Golgi transport, COPI has been found to generate tubules, which connect the Golgi stacks and promote anterograde Golgi transport (Park et al. 2015b). Cdc42 has been shown to induce membrane curvature to promote COPI tubule formation, further involving Cdc42 in bidirectional intra-Golgi transport (Park et al. 2015b). Additionally, Cdc42 has been found to control the recruitment of dynein onto COPI vesicles, which suggests a microtubule-based mechanism

that can dictate the directionality of COPI transport at the Golgi (J. L. Chen et al. 2005b). All these findings strikingly reinforce the concept of localized functions for Cdc42 residing at the Golgi apparatus.

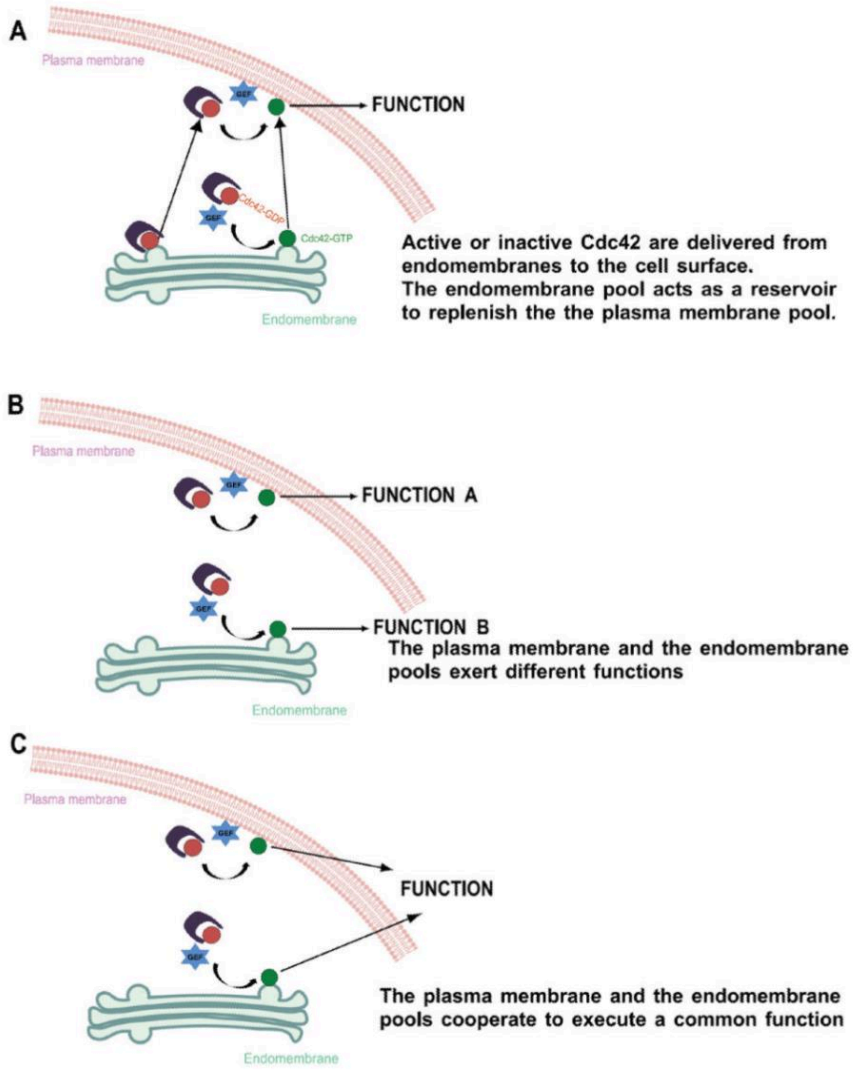

Figure 12 Schematic showing the three possible modes of action via which Golgi-localized Cdc42 can exert its functions. A) The reservoir model in which the Golgi-localized pool replenishes the plasma membrane-associated pool. B) The localized functions model in which the Golgi-localized pool exerts functions independently of other subcellular pools of Cdc42. C) The polarity loop model which depicts a coordinated function for both the plasma membrane-associated pool and the Golgi-localized pool. From Farhan and Hsu, et al. 2016

The third model, the polarity loop model, suggests that Golgi-localized Cdc42 can also act by coordinating its function with the pool at the plasma membrane for complex events of cellular polarity (Figure 12c). Several findings support this model. During directed cell migration, Cdc42 plays a microtubule-dependent role in the positioning of the Golgi apparatus and altering Golgi reorientation impairs cell migration (refer to Chapter 1)(Yadav, Puri, and Linstedt 2009). Proteins which link cytoskeletal elements to the Golgi apparatus are now being identified to interact directly or indirectly with Cdc42. For instance, AKAP350, a Golgi-localized protein involved in the nucleation of microtubules, has been shown to interact with CIP4, which acts as an effector of Cdc42 to promote the polarity of migrating cells (Tonucci et al. 2015).

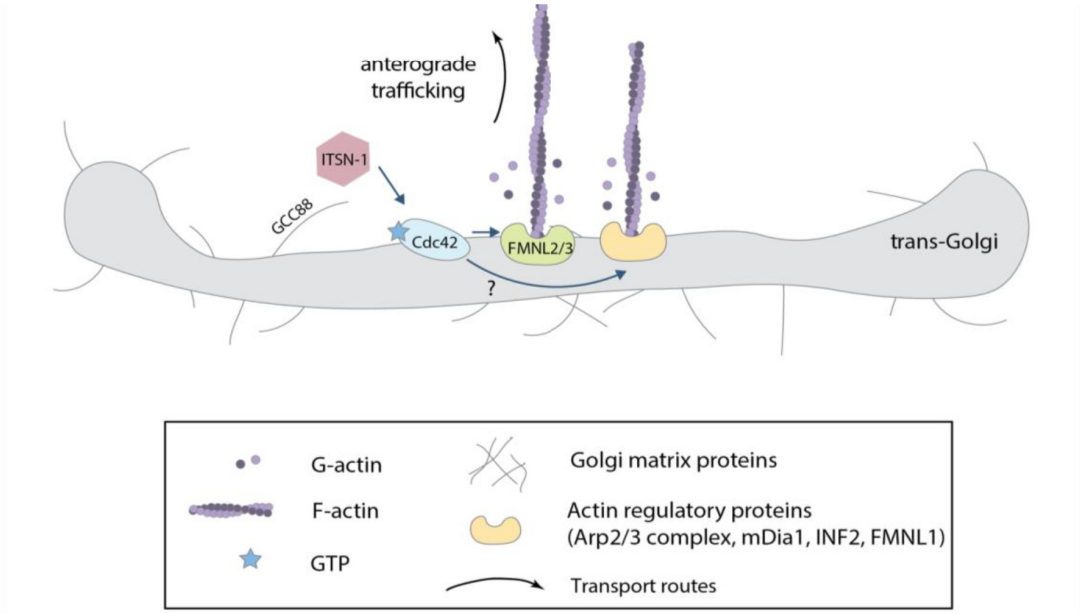

Figure 13. Cdc42-regulated actin polymerization at the trans-Golgi. The GCC88 Golgin recruits the Cdc42 GEF ITSN-1 which in turn activates Golgi-localized Cdc42. Given the residing population of actin regulatory elements at the Golgi apparatus the actin nucleation process (FMNL2/3) and actin, polymerization process is depicted at the trans-Golgi cisternae. Adapted from Ravichandran et al. 2020 COCB.

Cdc42 has been implicated in the regulation of actin at the Golgi apparatus. The actin regulatory proteins WHAMM, WAVE, Arp2/3 complex, cortactin, cofilin, profilin II, and several myosins (II, VI, 18, 1b), localize at the Golgi apparatus and at the trans-Golgi network (Egea et al. 2013). Formin family proteins FMNL2/3 also localize in the Golgi apparatus in a Cdc42 dependent manner (Kage et al. 2017a). Subsequently, Cdc42 regulators such as the

ITSN1 GEF, have been shown to be recruited by golgin GCC88 potentially activating Golgi-localized Cdc42 (Figure 13) (Makhoul et al. 2019). Lastly, a Golgi localized Rho GDI3 has also been identified but its role has not been fully uncovered yet (Brunet, Morin, and Olofsson 2002). The current approach is to study the spatial and temporal coordination of the distinct pools of Cdc42 to better understand the need for this compartmentalization. In summary, the third model largely links Golgi-localized Cdc42 to the typical "chicken-and-egg" problem of feedback loops involved in symmetry breaking during the establishment of cell polarity in mammalian cells. However, a key question remains unanswered, which is how the two isoforms of Cdc42 participate in this subcellular localization of Cdc42. Since the two isoforms have differential CaaX motifs that play a crucial role in dictating endomembrane association, the CaaX motifs govern the subcellular localization of Cdc42.

2.3.3 Can Cdc42 be recruited to other subcellular locations?

In addition to the aforementioned subcellular pools of Cdc42, other organelles where Cdc42 could be recruited to are being explored. One such organelle is the ER. It is known that Cdc42 undergoes maturation on the ER (Wang and Casey 2016). However, whether it has a specified function there is not entirely known. A recent study in yeast attempting to answer this, reports a novel Cdc42 localization with endosomal sorting complexes required for transport (ESCRT) proteins at sites of nuclear envelope and ER fission. Where Cdc42 is involved in nuclear envelope sealing and ER remodelling, by regulating ESCRT disassembly to maintain nuclear envelope integrity and ER architecture (Lu and Drubin 2020). The potential role of ER-localized mammalian Cdc42 remains to be uncovered.

Nuclear localization of overexpressed unprenylated Cdc42 has been observed in several studies. This could be due to the molecular weight of Cdc42 being lower than 40 kDa (21 kDa) making its passive diffusion through the nuclear pore complex possible. Another possibility could be due to the C-terminal PBR of Cdc42 merely resembling a cryptic nuclear localization sequence (NLS) like that of Rac1 which becomes dominant in the absence of the prenyl tail (Michaelson et al. 2008). This phenomenon remains speculative as the existence of an endogenous unprenylated pool of Cdc42 has not been previously reported. It would however not be surprising to identify an endogenous nuclear pool of Cdc42 given that actin and actin regulatory proteins have been observed in the nucleus. A potential nuclear role for Cdc42 could be unravelled eventually.

Gene name	Function	References
ACK/TNK2	Actin organization	Manser et al., 1993
Borg1/CDC42EP2	Actin organization, cell shape	Hirsch et al., 2001; Joberty et al., 1999; Joberty et al., 2001
Borg2/CDC42EP3	Actin organization, cell shape	Hirsch et al., 2001; Joberty et al., 1999; Joberty et al., 2001
Borg3/CDC42EP5	Actin organization, cell shape	Hirsch et al., 2001; Joberty et al., 1999; Joberty et al., 2001
Borg4/CDC42EP4	Actin organization	Hirsch et al., 2001; Joberty et al., 1999
Borg5/CDC42EP1	Actin organization	Hirsch et al., 2001; Joberty et al., 1999
CEP2	Pseudopodia formation	Hirsch et al., 2001
CEP5	Pseudopodia formation	Hirsch et al., 2001
CIP4/TRIP10	Actin organization	Aspenstrom, 1997
Daam1	Actin organization	Aspenstrom et al., 2006
FMNL1	Actin organization	Seth et al., 2006
IFN2	Trafficking – trancytosis.	Madrid et al., 2010
FMNL2	Actin organization	Block et al., 2012
IQGAP1	Cell morphology and motility	Kuroda et al., 1996
IQGAP2	Actin organization	Kuroda et al., 1996; LeCour et al., 2016
IQGAP3	Actin organization	Kuroda et al., 1996
IRSp53/BAIAP2	Filopodia induction	Krugmann et al., 2001
mDia2/DRF2	Actin organization	Alberts et al., 1998
mDia3	Actin organization	Yasuda et al., 2004
Mig-6/RALT	Regulates cell migration	Jiang et al., 2016
MEKK1/MAP3K1	JNK and ERK pathway activation	Fanger et al., 1997
MLK2/MAP3K10	JNK and ERK pathway activation; microtubules	Nagata et al., 1998
MLK3 /MAP3K11	JNK activation, microtubules	Nagata et al., 1998
MEKK4/MAP3K4	CSBP2 and JNK activation	Fanger et al., 1997

Table continued on next page

Gene name	Function	References
MRCKα	Actomyosin regulation	Leung et al., 1998
MRCKβ	Actomyosin regulation	Leung et al., 1998
MRCKγ	Actomyosin regulation	Leung et al., 1998
MSE55	Actin organization	Burbelo et al., 1999
N-WASP/WASL	Actin organization	Miki et al., 1998
PAK1	Actin organization, apoptosis	Manser et al., 1994
PAK2	Apoptosis, inhibition of cell growth	Gatti et al., 1999
PAK3	Dendrite development	Bagrodia et al., 1998
PAK4	Actin organization, adherens junction, adhesion, migration	Abo et al., 1998
PAK5	Neurite development, microtubule stability	Dan et al., 2002
PAK6	Actin organization, motility, adherens junction	Lee et al., 2002
PAR6A	Cell polarity	Joberty et al., 2000
PAR6B	Cell polarity	Joberty et al., 2000
PAR6G	Cell polarity	Joberty et al., 2000; Johansson et al., 2000
PIK3R1	Actin regulation, growth, motility, trafficking	Cheung et al., 2014
PLD1	Phosphatidic acid levels, cytoskeleton	Walker et al., 2000
RPS6KB1	Cell growth and proliferation	Chou and Blenis, 1996
SPEC1	Actin organization, cell shape	Pirone et al., 2000
SPEC2	Actin organization, cell shape	Pirone et al., 2000
USP6	Trafficking	Masuda-Robens et al., 2003
WASP	Actin organization	Symons et al., 1996

Tabel 1: Mammalian effectors of Cdc42. Cdc42 regulates various cellular processes via activating several downstream effectors. This list highlights the mammalian effectors of Cdc42 and the cellular functions they are associated with. With the references of their corresponding studies. Adapted from (Pichaud, Walther, and Nunes de Almeida 2019)

Chapter 3

Cdc42, two sides of a coin

3.1 Isoforms of Cdc42

The human CDC42 gene is located on chromosome 1, from which three transcripts are derived via alternative splicing, which encode two distinct Cdc42 isoforms, namely the ubiquitous Cdc42 isoform (Cdc42u) also known as the placental isoform and the so-called brain Cdc42 isoform (Cdc42b) (Marks and Kwiatkowski 1996). Cdc42 is conserved from yeast to mammals yet the alternative splicing of the Cdc42 gene product is only conserved in vertebrates (fish to mammals) (Table 2) (S. J. Lee et al. 2018).

The two isoforms share 95% identity and only have a different C-terminal exon encoding the hypervariable region. Cdc42u and Cdc42b are also referred to as E7 (Exon 7) and E6 (Exon 6) respectively. The two distinct differences between their C-terminus are 1) the amino acid at position 163 which encodes a lysine (K) for Cdc42u and an arginine (R) for Cdc42b and 2) the last 10 amino acids (Figure 14). The other key difference between the two isoforms of Cdc42 is that they are expressed in a tissue specific fashion. Cdc42u is ubiquitously expressed. In contrast, Cdc42b was initially detected in brain tissues (Marks and Kwiatkowski 1996). More recently it was also found in a range of commonly used laboratory cell lines, including HEK and MDCKII cells (Wirth et al. 2013). This splice variant may therefore also be expressed in non-brain tissue cells, underlining the need to clarify the functional differences between the two Cdc42 variants.

It is important to note that previous studies on the biological function of Cdc42 in tissues and cells have almost exclusively considered only the ubiquitous isoform of Cdc42. Therefore, less is known about the expression and functional relevance of the so-called brain isoform of Cdc42, in comparison to the numerous Cdc42 studies. In the following, we explore the differences between the two isoforms.

Species (common name)	CaaX motif Cdc42u	CCaX motif Cdc42b
Saccharomyces cerevisiae (yeast)	CAIL	-
Caenorhabditis elegans (worm)	CNIL	-
Saccoglossus kowalevskii (worm)	CVLL	-
Acanthaster planci (star fish)	CSLL	-
Danio rerio (zebra fish)	CVLL	CCIF
Xenopus tropicalis (frog)	CRLL	CCIF
Xenopus laevis (frog)	CMLL	CCIF
Nanorana parkeri (frog)	CRLL	CCIF
Callorhinchus milii (shark)	CVLL	CCIF
Python bivittatus (snake)	CVLL	CCIF
Alligator mississippiensis (alligator)	CVLL	CCIF
Gallus gallus (chicken)	CVLL	CCIF
Chelonia mydas (turtle)	CVLL	CCIF
Mus musculus (mouse)	CVLL	CCIF
Homo sapiens (human)	CVLL	CCIF

Table 2: Alternative splicing of Cdc42. Ubiquitous Cdc42 is evolutionarily conserved from yeast to mammals yet brain Cdc42 is only observed in vertebrates (fish to mammals). The CaaX and CCaX motif sequences of ubiquitous and brain Cdc42 respectively are listed here for each species. Adapted from Lee et al.2018 bioRxiv

3.2 Post-translational lipid modification

The last ten amino acids of the C-terminus in Cdc42 encodes the CaaX motif of the protein which is crucial for membrane anchorage and Rho GDI1 binding. Cdc42u terminating in amino acids CVLL encodes a classical CaaX motif (where C is a Cysteine, 'aa' corresponds to two aliphatic residues, and X is any amino acid) while Cdc42b terminates with amino acids CCIF containing a CCaX motif (Figure 14). Other examples of proteins with the

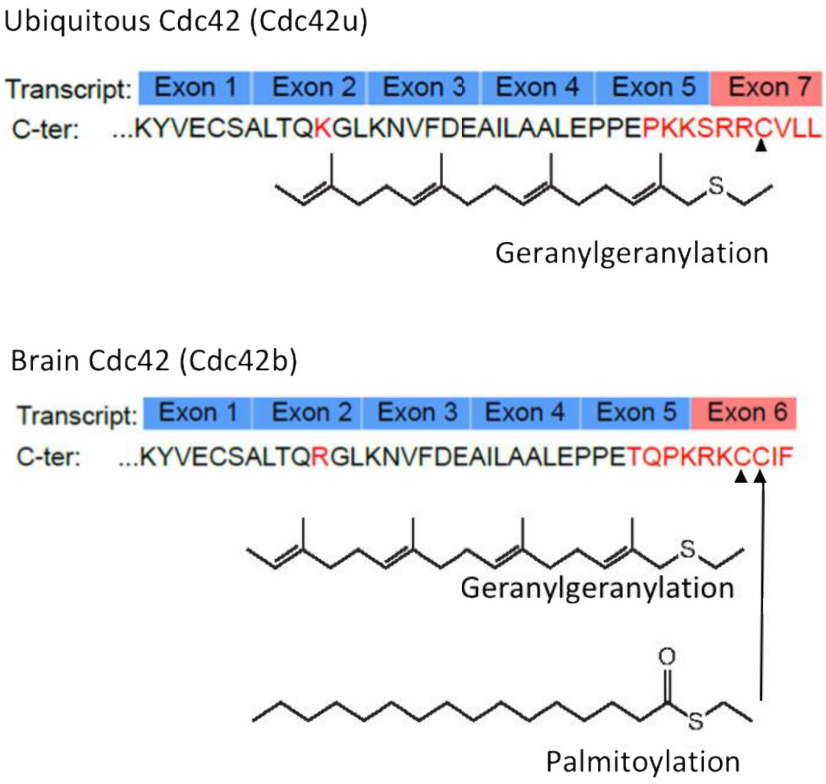

Figure 14 Differences between the two isoforms of Cdc42. The alternative splicing is depicted in the exon distribution for both isoforms. The amino acid sequence corresponding to the last unique exon is represented with unique amino acids highlighted in red. The posttranslational modifications corresponding to each isoform is indicated on the respective Cys residue and the carbon skeleton for each lipid moiety is shown.

unconventional CCaX motif include Ral, PRL and PLA2γ (A. Nishimura and Linder 2013). Both isoforms of Cdc42 undergo a canonical post-translational modification process referred to as isoprenylation on residue Cys 188 (Figure 11). Isoprenylation is the attachment of an isoprenoid moiety to a C-terminal Cys residue of target proteins. In general, the isoprenoid moieties used are farnesyl diphosphate or geranylgeranyl diphosphate, which are derived from the same biochemical pathway that produces cholesterol. For Cdc42 isoforms a 20-carbon geranylgeranyl isoprenoid moiety is added (Garcia-Mata, Boulter, and Burridge 2011).

In the case of Cdc42u, the enzyme geranylgeranyl transferase type 1 (GGTase) first adds the lipid group to the cysteine residue 188 (Figure 15a). This is an irreversible process, which occurs in the cytosol and is universal for Rho GTPases. Followed by which the endoprotease Rce1 (Ras converting enzyme 1) ensures the proteolytic cleavage of the CaaX

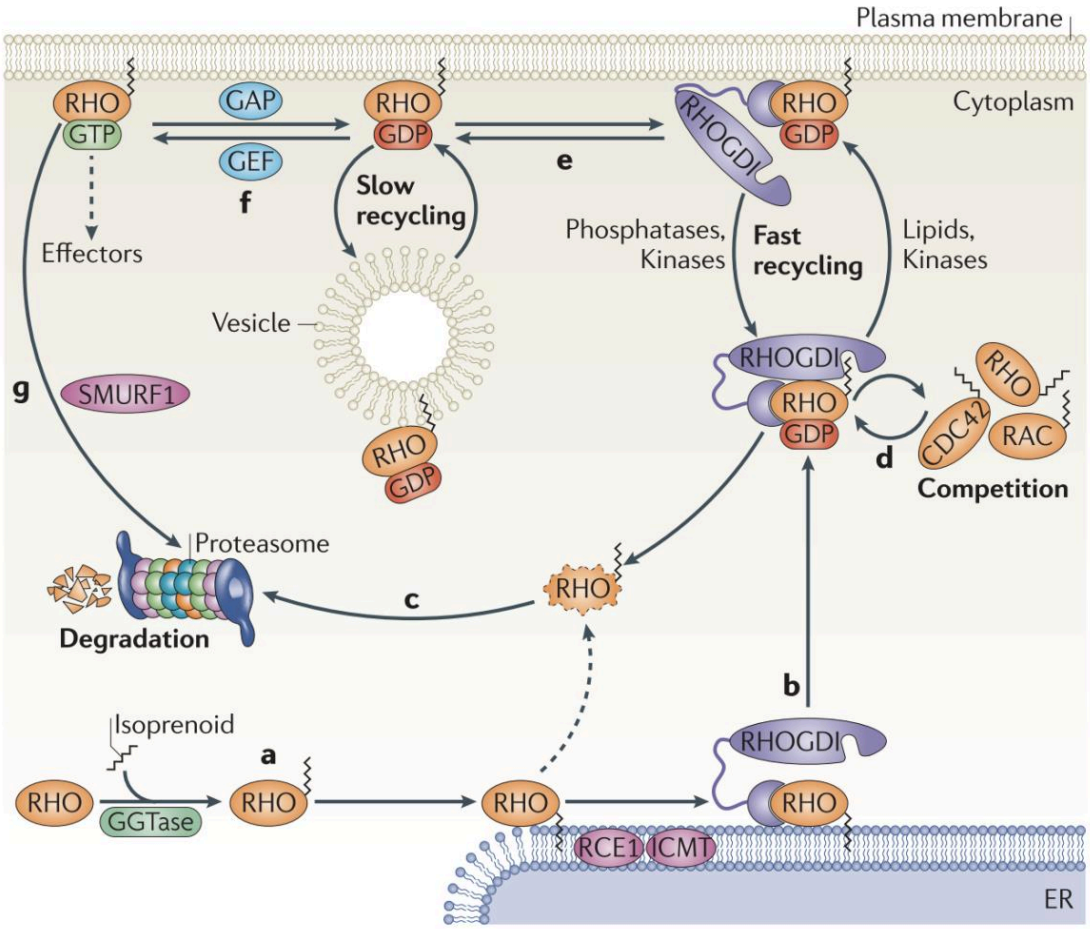

Figure 15 The Rho GDI cycle. a) Newly synthesized Rho family GTPases are geranylgeranylated by GGTase and then post-translationally modified by the protease RCE1 and ICMT at the cytoplasmic face of the ER. b) After geranyl- geranylation, Rho proteins associate with GDIs, which sequester them in the cytosol and protect them from degradation. c) Free prenylated cytosolic Rho GTPases are unstable and are rapidly degraded by the proteasome. d) Several Rho GTPases can associate with GDIs and compete for binding. e) The rate of cycling of the Rho GDI–Rho GTPase complex between the cytosol and the membrane can be regulated by post-translational modifications on both the Rho GTPase (for instance palmitoylation on Cdc42b) and the Rho GDI, which modulate the affinity of the interaction. A slower pathway for recycling Rho proteins through vesicle trafficking has also been hypothesized. f) Upon reaching the membrane, Rho GTPases can be activated by GEFs and bind to downstream effectors. Following inactivation by GTPase-activating proteins (GAPs)(this is unclear for Cdc42), Rho GTPases are extracted from the membrane by Rho GDI. g) Active Rho A can also be targeted for degradation by the ubiquitin ligase SMAD ubiquitylation regulatory factor 1 (SMURF1). From Garcia-Mata ,R et al. 2011

box (releasing the VLL residues). Lastly, the C-terminus is carboxymethylated by the enzyme Icmt (isoprenylcysteine carboxyl methyltransferase) (Figure 15b) (Gao, Liao, and Yang 2009).

In the case of Cdc42b, after prenylation at residue Cys188, C-terminal proteolysis and carboxymethylation are bypassed and S-palmitoylation (S-acylation) occurs at the adjacent Cys189 residue. S-Palmitoylation is the process by which a 16-carbon palmitate group is added to a Cys residue by a protein acyltransferase (PAT) enzyme. PATs attach the palmitate moiety through a reversible thioester linkage. Approximately 24 mammalian PAT enzymes have been identified so far. Due to their highly conserved Asp-His-His-Cys tetrapeptide motif necessary for catalysis, these enzymes are known as the DHHC protein acyltransferases (DHHC-PATs)(Rana, Lee, and Banerjee 2018). These PATs are polytopic integral membrane proteins usually found in the membranes of the ER, the Golgi apparatus, and the plasma membrane. Most importantly, S-palmitoylation is a reversible process that is controlled by depalmitoylating enzymes such as acyl protein thioesterase 1/2 (APT1/2)(Abrami et al. 2017). With regard to Cdc42 the corresponding PAT enzyme and depalmitoylase remain unknown.

It is also important to note that palmitoylation is considered as a secondary lipid modification, which either requires a primary lipid anchor (such as prenylation) or a membrane targeting motif (i.e. lipid membrane binding domains), to ensure that the target protein can be recruited to endomembranes in order to access membrane bound protein acyltransferase (PAT) enzymes (Zaballa and van der Goot 2018). Yet whether Cdc42b can be palmitoylated in the absence of its prenyl tail remains unknown.

N/H -Ras (prenylated and palmitoylated) and Rho GTPases RhoB, Rac1, Wrch-1 (prenylated and palmitoylated) have previously been reported to undergo similar dual lipid modification like Cdc42b. In addition, such reversible lipid modification with palmitate has been previously demonstrated to dynamically regulate GTPase association with membranes, and facilitate association with lipid rafts eventually triggering downstream signalling in the case of N-Ras (Navarro-Lérida et al. 2012; Linder and Deschenes 2007; Larsen et al. 2017; 2015). Yet the ability of Cdc42b CCaX motif to be both prenylated and palmitoylated in this sequence context is quite unique, similar only to that observed in few other proteins like RalA, RalB and PRL-3 proteins.

Palmitoylation can be studied *in vitro* by radiolabelling assays using radioactive palmitate or by click chemistry. Studying the palmitoylation status of the Cdc42b isoform has shown that Cdc42b undergoes alternative posttranslational processing pathways (referring to bypassing C-terminal proteolytic cleavage), generating two populations of differentially lipid modified proteins. These two mature populations of Cdc42b are 1) a dual prenyl and palmitoyl form and 2) a CaaX-processed form. These pools display different affinities for Rho GDI1 since the dual lipidation on Cdc42b perturbs insertion of its geranylgeranyl tail into the

hydrophobic pocket of Rho GDI1 (Figure 10)((Nomanbhoy and Cerione 1996; Garcia-Mata, Boulter, and Burridge 2011)). This differential Rho GDI1 binding property has been hypothesized to drive differential downstream signalling pathways and subcellular localization of Cdc42b (Nishimura and Linder 2013). The association of Cdc42 with lipid membranes is a dynamic process, such that Cdc42 has an intrinsic capability to dissociate from membranes with a time-scale of seconds. Therefore, the ability of Rho GDI to bind to the geranylgeranyl tail of Cdc42 is necessary to maintain the GTPase in the cytosol by slowing its re-association with the membrane surface eventually dictating the subcellular localization of Cdc42 between the cytosol and membranes (Figure 15b,e) (Johnson, Erickson, and Cerione 2009).

3.3 The polybasic region

In addition to the CaaX motif, other amino acids differ between the two isoforms of Cdc42. In Rho GTPases, there is a polybasic sequence in the hypervariable region preceding their geranylgeranyl tail. It is referred to as the PBR (polybasic region) and the exact positioning of these positively- charged residues in this region is conserved from yeast to humans. This region is also involved in membrane targeting and biological activity (Ahearn et al. 2012).The PBR has been reported to increase the affinity of Rho GTPases for negatively charged membranes which dictates specific biological functions. It is accepted that the carboxyl-terminal PBR of Rho GTPases might additionally contribute to their localization

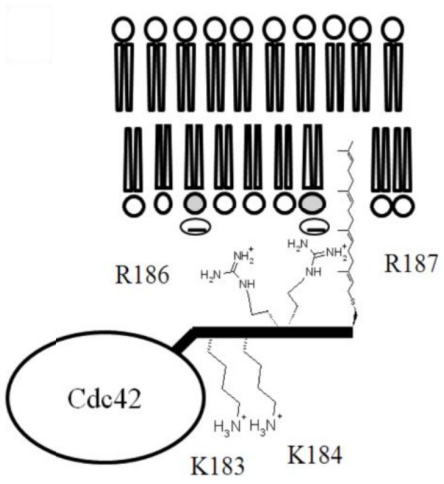

Figure 16 Schematic representation of the di-arginine motif interacting with the negatively charged membranes. Cdc42u binds with PI(4,5)P2 with its di-arginine motif made up of R186 and R187 as shown. From Johnson. J et. al 2012

and positioning at the appropriate cellular membrane sites for signal propagation. For example, Rac1 and Rac2, which differ by only 12 residues (five of which are located within the polybasic region), show significantly different subcellular localizations (Yeung et al. 2008).

With regard to the isoforms of Cdc42, the PBR is encompassed in the last 10 differential amino acids. For Cdc42u the PBR can be segregated into the di-lysine and the di-arginine motif, comprising a pair of lysine residues and arginine residues respectively. Importantly, the two sets of charged residues are separated by a serine residue (-KKSRR-). The di-lysine motif, via its interaction with the γCOP subunit of the COPI complex, plays a role in regulating intracellular trafficking as well as cell growth and transformation (J. L. Chen et al. 2005a). The di-arginine motif on the other hand is important for its association with the negatively charged lipid phosphatidylinositol PI(4,5)P2 and its ability to oncogenically transform cells (Figure 16). This property characterizes Cdc42u as an oncoprotein which enhances transformation and metastasis (Johnson, Erickson, and Cerione 2012) . In contrast, Cdc42b lacks both the di-lysine and di-arginine motifs in its PBR. The -KKSRR- sequence of Cdc42u is replaced with a -KRK- PBR sequence in Cdc42b (Figure 14) (Marks and Kwiatkowski 1996). This alternative PBR could play a role in differential subcellular localization of Cdc42b or even its downstream signalling in addition to the dual lipidation of Cdc42b. A recent study on ovarian cancer has shown that Cdc42b might behave as a tumour suppressor gene as opposed to the oncoprotein Cdc42u (He, Yuan, and Yang 2015), which may be associated to this alternative PBR and points to these amino acids are major regulators of Cdc42.

3.4 Functional relevance

To date, the functional differences between the two isoforms largely remain unknown because the great majority of studies on Cdc42 have been conducted with Cdc42u and/or its associated mutants. The expression of Cdc42b is increased in the nervous system. A switch from the exclusive production of the general isoform Cdc42u in neuronal precursors and non-neuronal cells to stable co-expression of the Cdc42b and Cdc42u isoforms at the single-neuron level is orchestrated through developmental changes. Considering that conditional inactivation of the Cdc42 gene in cortical neurons reduces the efficiency of axon formation (Garvalov et al. 2007), the role of the isoforms in neuronal differentiation has been studied. The two co-expressed isoforms have been reported to be functionally specialized during this process in neurons. The Cdc42u protein whose mRNA preferentially localizes into axons plays a role in axonogenesis (S. J. Lee et al. 2018) whereas the palmitoylation of Cdc42b accounts for its preferential localization to dendritic spines and its role in dendrite maturation (Figure 3). These findings have advanced the understanding of mechanisms

underlying axo-dendritic polarity in developing neurons and argue that co-expression of the non-redundant Cdc42 isoforms in the same cell is important during neuronal development (Yap et al. 2016).

During neurogenesis, Cdc42u specifically drives the formation of neuroprogenitor cells, whereas Cdc42b, is essential for promoting the transition of neuroprogenitor cells to neurons. The specific roles of Cdc42u and Cdc42b in neurogenesis are due to their opposing effects on mammalian target of rapamycin complex 1 also known as mechanistic target of rapamycin (mTORC1) activity. Specifically, Cdc42u stimulates mTORC1 activity and thereby induces neuroprogenitor formation, whereas Cdc42b works synergistically with activated CDC42-associated kinase (ACK) in down-regulating mammalian target of rapamycin or mechanistic target of rapamycin (mTOR) expression and promoting neuronal differentiation. It is remarkable that the two highly-similar Cdc42 splice variants regulate distinct stages of neurogenesis and neuronal differentiation (Endo, Druso, and Cerione 2020).

Considering Rac1, it has been reported that the carboxy-terminal domain of the protein was shown to participate in its interaction with its effectors such as PAK (Knaus et al. 1998; Abdrabou and Wang 2018). Therefore, studying the interactome of Cdc42 variants could be important as they encode different C-terminal domains.

Lastly; from a pathophysiologic context, in addition to their aforementioned differential roles in oncogenesis*, de novo* mutations in Cdc42u have been shown to give rise to variable developmental phenotypes. The phenotypes range from variable growth dysregulation, facial dysmorphism, and neurodevelopmental, immunological, and haematological anomalies, including a phenotype resembling Noonan syndrome, a developmental disorder caused by dysregulated RAS signalling (Martinelli et al. 2018; Bekhouche et al. 2020). In contrast, the role of Cdc42b in this context still needs to be elucidated and could aid in understanding several associated rare diseases.

Summary II

- In vertebrates, alternative splicing results in the expression of two isoforms of Cdc42, ubiquitous Cdc42 (Cdc42u) and brain Cdc42 (Cdc42b).

- The two isoforms differ in the Rho GTPase hypervariable region encoded by their carboxy terminal exon.

- Exon 6 is expressed by Cdc42b and exon 7 is expressed by Cdc42u.

- Two motifs; the CaaX motif and the PBR are modified in Cdc42 isoforms. Both motifs are responsible for membrane targeting and localization in cells.

- Cdc42u encodes a canonical CaaX motif that undergoes irreversible prenylation and its PBR is composed of a di-lysine and di-arginine motif (KKxRR).

- Cdc42b encodes a non-canonical CCaX motif that undergoes both irreversible prenylation and reversible palmitoylation and its PBR is modified.(-KRK-).

- Dually lipidated Cdc42b does not bind to GDI1

- Non-redundant functions of the isoforms have been elucidated during neurogenesis and neuronal differentiation.

Chapter 4

Membrane Models

This chapter focuses on highlighting the fundamentals of membrane biology required to understand the main characteristics of cellular membranes which could modulate Cdc42 association to membranes. Since cell membranes exhibit heterogeneous compositions and shapes, studying them *in cellulo* remains challenging. As a consequence, various in vitro membrane models have been developed which provide ideal tools to assess the interaction of membrane binding proteins such as Cdc42.

4.1 Biological membranes and the lipid bilayer

4.1.1 Biological membranes

In eukaryotic cells, membranes act as physical barriers that separate aqueous cellular components from their surroundings. Without some form of barrier distinguishing "self" from "non-self," it is difficult to define the concept of an organism and even life. The same applies for the compartmentalization of intracellular organelles by endomembranes specifically in eukaryotes. These organelles are surrounded by one or more lipid bilayers and, together, constitute the majority of membrane area present in the cell. A revolutionary step in the study of membranes was the introduction of the 'fluid mosaic model' in 1972 to depict the plasma membrane (Singer and Nicolson 1972). In this model, the lipid bilayer is represented as a fluid sheet of lipids embedded with both peripheral and transmembrane proteins. This model still forms the backbone of the standard conceptualization of membrane architecture. However, as insightful as this model has been, the emergence of new findings has weakened the generalizations the model contains. The updated view of a plasma membrane with variable thickness, variable protein distribution and mobility and higher protein density is now established (Engelman 2005; Nicolson 2014).

4.1.2 Phospholipids self-assembly

The fundamental unit of biological lipid bilayers is phospholipids. Phospholipids are amphiphilic molecules due to a hydrophilic phosphate head and a hydrophobic tail consisting of two fatty acid chains. Phospholipids have the characteristic to self-assemble

due to their amphiphilic nature, with their hydrophilic heads facing towards the aqueous solvent (either the cell external medium or the cytosol) and their hydrophobic tails buried inwards adjacent to one another. This spontaneous organization of lipids is due to the so-called hydrophobic effect, which results from a competition between hydrophilic heads and hydrophobic tails to minimize the interfacial energy: aggregation of hydrophobic tails decreases the interfacial area but simultaneously exposes hydrophilic head groups which have an intrinsic tendency to increase the interfacial area (Tanford 1978). The two most prevalent lipid assemblies in water are micelles (hexagonal phase) and bilayers (lamellar phase). Micelles are globular structures where the lipid head groups form a spherical protective shell burying the tails inward. In the cell, one example of micellar structures are lipid droplets. Bilayers on the other hand are composed of two monolayers in which the lipids are parallel to one another and the tails of each monolayer facing one another in the core of the membrane. Membranes enclosing the cell, the plasma membrane, or intracellular organelles are made of lipid bilayers. The average thickness of the plasma membrane bilayer is approximately 4 nm (Van Meer, Voelker, and Feigenson 2008).

4.1.3 Diversity of phospholipids

The hydrophilic head of the lipid defines the lipid type and can be neutral or charged. Therefore, phospholipids with certain head groups can alter the surface chemistry of a bilayer and can, for example, serve as signals as well as "anchors" for other molecules in the membranes of cells (Divecha and Irvine 1995), as is the case for Cdc42 (see below). In phospholipids, the hydrophobic tail is most often made of two aliphatic chains of varying length and degree of unsaturation. Similar to the heads, the tails of lipids can also affect membrane properties, for instance by determining the packing of the bilayer. It is important to mention that the shape factor (also called packing parameter of a lipid, defined as the ratio between the volume occupied by the head to that occupied by the tail of the lipid, differ from one lipid to the other (Kumar 1991; Vamparys et al. 2013). Another important parameter to quantify lipid shape is the lipid spontaneous curvature (Zimmerberg and Kozlov 2006; Antonny 2011; McMahon and Boucrot 2015) which corresponds to the curvature that a monolayer made solely of this lipid species would exhibit. External factors such as osmotic pressure, temperature and pH can modulate the head group projected area and chain volume (Pomorski, Nylander, and Cárdenas 2014; Pinot et al. 2018).

Phospholipids can be divided into two large classes namely glycerophospholipids and sphingolipids. Eukaryotic membranes are largely made up of polar lipids from the glycerophospholipid family, whose basic structure contains a hydrophobic diacylglycerol (DAG) backbone to which a polar phosphate group is added (Figure 17A). This fundamental structure is also the structure of the lipid species phosphatidic acid (PA). The main species of this family is phosphatidylcholine (PC), formed by the addition of a choline to the PA. PC

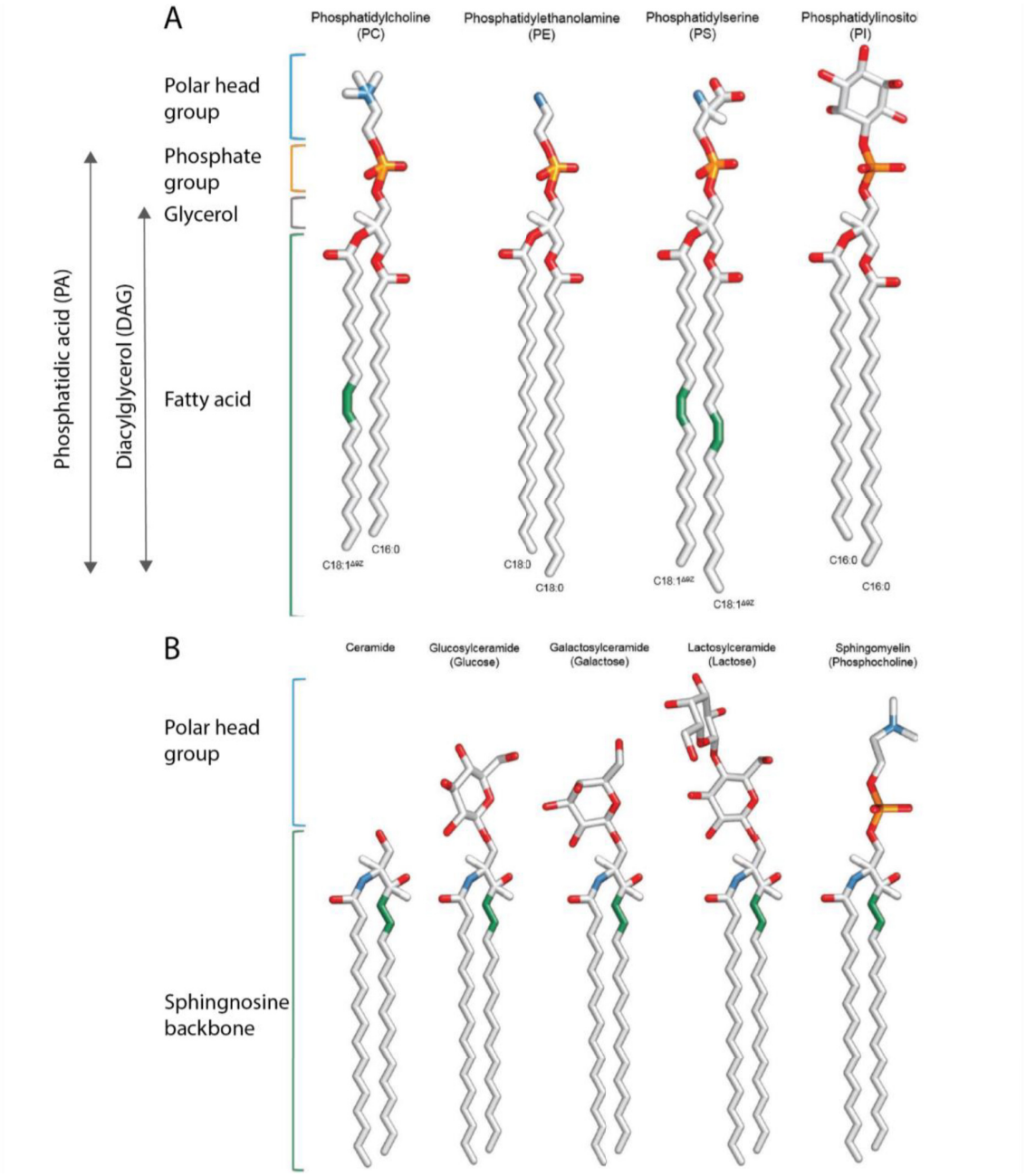

Figure 17 Classification of Phospholipids. There exist two families of phospholipids, the first being the glycerophospholipids and sphingnolipids. A) Glycerophospholipids have a diacylglycerol backbone to which a phosphate group is attached. The addition of different polar headgroup to this structure gives rise to lipids PC, PE, PS and PI shown here. B) The other class are the sphignolipids made of a 19 carbon sphingosine backbone to which various polar headgroups are attached to give rise to ceramides and sphingomyelin shown here Ortega-Anaya. J and Jiménez-Flores. 2019

lipids are zwitterionic in nature and usually have an apparent cylindrical shape. Other lipid species derived by adding differential head groups include phosphatidylethanolamine (PE), phosphatidylserine (PS) and phosphatidylinositols (PI) (Van Meer, Voelker, and Feigenson 2008).

Phosphatidylserine (PS) is a negatively charged and cylinder-shaped phospholipid mainly enriched in the inner leaflet of the plasma membrane. Phosphatidylinositols (PI) are also negatively charged due to their inositol polar head group and are minor components of the plasma membrane. PI typically represents less than 15% of the total phospholipids found in eukaryotic cells and phosphoinositides PI(4)P and PI(4,5)P2 representing the bulk of these lipids in mammals. PI lipids are known to be phosphorylated by numerous kinases and their derivatives are known to be involved in downstream signaling processes, mainly at the plasma membrane (Di Paolo and De Camilli 2006). For example, as mentioned earlier PI(4,5)P_2 is a phosphatidylinositol enriched at the plasma membrane. It interacts with the di-arginine motif of Cdc42 where it can initiate signaling activities that are essential for the oncogenic transformation of cells. PI(4,5)P2 has also been identified to behave as an activator of N-WASP, a Cdc42 effector protein, to drive actin nucleation at the plasma membrane (Rohatgi, Ho, and Kirschner 2000) (refer to Chapter 2).

The second class of phospholipids is sphingolipids (Figure 17B). They contain a backbone of sphingoid bases and a set of aliphatic amino alcohols. Sphingomyelin (SM) is the most abundant species of this family of lipids, and is composed of a phosphate-choline headgroup. Another sub-class of ceramide-based lipids is the glycosphingolipids (GSLs), consisting of a ceramide molecule attached to monosaccharides or polysaccharides. SM and GSLs are found in the outer leaflet of the plasma membrane (Van Meer, Voelker, and Feigenson 2008; D'Angelo et al. 2013).

Majority of the phospholipids are cylindrical in shape, however certain conical shaped lipids (Lipids whose lipid head group cross-sectional area is smaller than that of its acyl chains) like DAG can induce lateral lipid packing defects in the bilayer (Eichmann and Lass 2015; Campomanes, Zoni, and Vanni 2019). This is characteristic of their name as 'non-bilayer lipids' (Van Den Brink-Van Der Laan, Antoinette Killian, and De Kruijff 2004). DAG has been shown to induce packing defects similar to that induced by positive curvature (Vamparys et al. 2013). In cells, the hydrophobic spots induced by DAG's apolar head in the membrane have been shown to promote binding of membrane peripheral protein apolipophorin II (Van Den Brink-Van Der Laan, Antoinette Killian, and De Kruijff 2004). The specific membrane recruitment of RAB GTPase proteins, RAB1, RAB5 and RAB6 is primarily dependent on the hydrophobic insertion of their prenyl group into lipid packing defects induced by using a synthetic highly conical lipid, 1-2-dioleoyl-sn-glycerol DOG in GUVs (Kulakowski et al. 2018)

Apart from the phospholipids, sterols form a major class of lipids present in cell membranes. The presence of an OH group on their lipid headgroup suggests that they are slightly polar and their peculiar structure highlights that they are non-bilayer forming

molecules but can insert into membranes. Cholesterol is the major sterol present in mammalian cells (Figure 18). Since its purification from gallstones in 1789 the era of the French revolution, cholesterol has been extensively studied. It comprises of about 30% of cellular membranes and plays a key role in modulating membrane fluidity. Intracellularly, its level increases along the secretory pathway from the ER to the plasma membrane (Figure 15) (Mesmin and Maxfield 2009; Ikonen 2008).

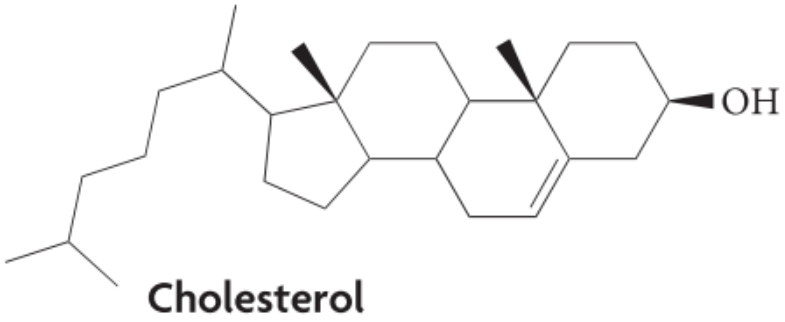

Figure 18 Cholesterol. The carbon skeleton structure of cholesterol is depicted here. The presence of aliphatic and aromatic rings distinguish it from classical phospholipids and therefore its presence affects the order of packing in membranes.

4.2 Lipid distribution in intracellular organelles

Lipids are heterogeneously distributed across endomembranes (Figure 19) (Yang, Lee, and Fairn 2018). Additionally, the bilayers of the Golgi apparatus, plasma membrane and vesicles all exhibit asymmetric lipid compositions (Wood et al. 2011; Kobayashi and Menon 2018).The ER is the main lipid and protein biosynthetic organelle (Jacquemyn, Cascalho, and Goodchild 2017). The membrane of this compartment is mostly composed of glycerophospholipids, PC and PE. The ER is responsible for producing the bulk of phospholipids and cholesterol. Ceramide, the precursor molecule for sphingolipids, is also synthesized in the ER. In spite of sterols and sphingolipid precursors being synthesized in the ER, they are rapidly transported to other organelles via vesicular trafficking. In addition to that, non-vesicular modes of transport involving membrane contact sites have also been demonstrated (Jackson, Walch, and Verbavatz 2016). These de-novo synthesized lipids are sorted in the Golgi apparatus. The cis-Golgi receives cargo from the ER and the trans-Golgi trafficking packages cargo to the plasma membrane.

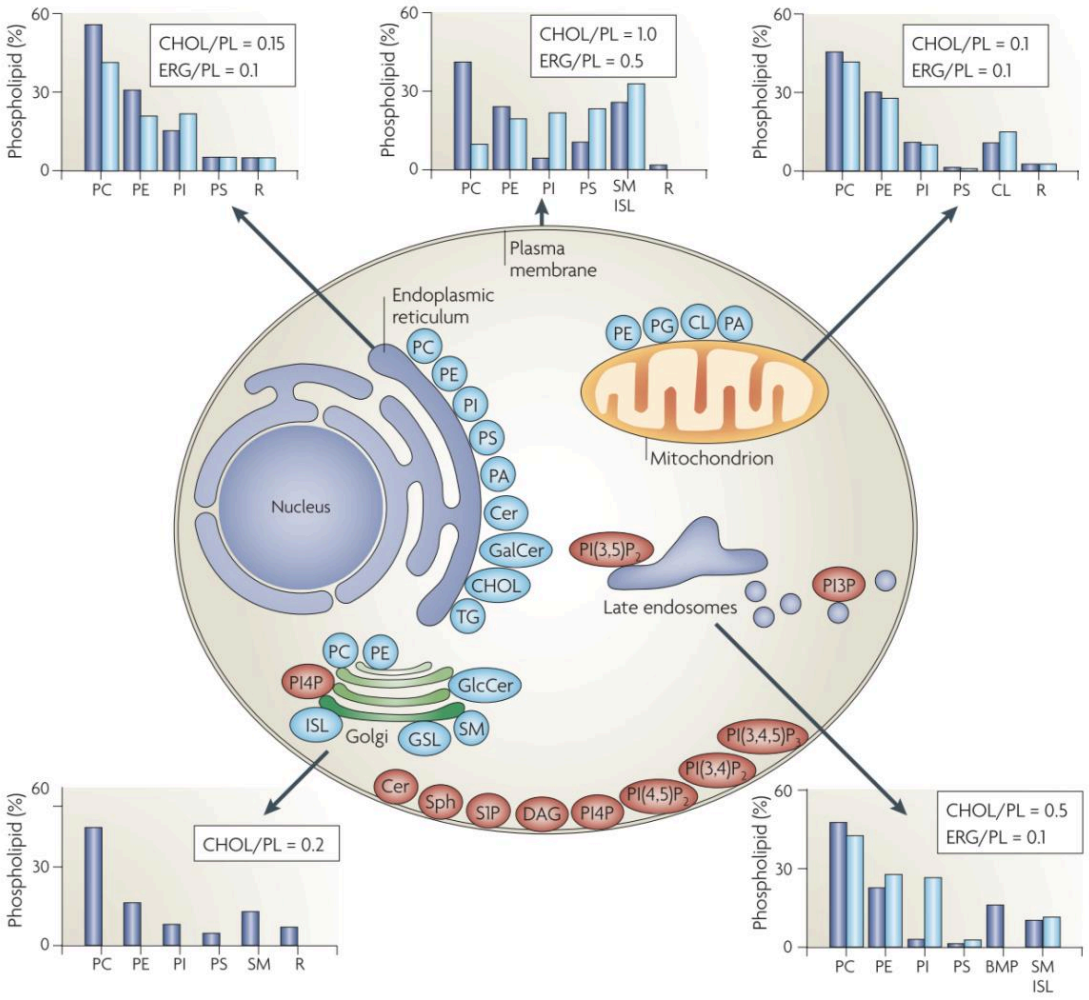

Figure 19 Lipid synthesis and distribution in endomembranes. The lipid compositions shown in graphs are expressed as a percentage of the total phospholipid (PL) in mammals (blue) and yeast (light blue). The molar ratio of CHOL (in mammals) and ergosterol (ERG in yeast) to PL is shown. The site of synthesis of the major phospholipids (blue) and lipids that are involved in signalling and organelle recognition pathways (red) is depicted. The major glycerophospholipids assembled in the ER are phosphatidylcholine (PC), phosphatidylethanolamine (PE), phosphatidylinositol (PI), phosphatidylserine (PS) and phosphatidic acid (PA). The ER also synthesizes Cer, galactosylceramide (GalCer), CHOL and ERG. Both the ER and lipid droplets participate in steryl ester and triacylglycerol (TG) synthesis. The Golgi lumen is the site of synthesis of SM, complex GSLs and yeast inositol sphingolipid (ISL) synthesis. PC is also synthesized in the Golgi, and may be coupled to protein secretion at the level of its DAG precursor. Approximately 45% of the phospholipids in the mitochondria (mostly PA and cardiolipin (CL)) are autonomously synthesized *in situ*. From Van Meer. G, et. al. 2008

With regard to lipid synthesis, the Golgi apparatus is specialized in the synthesis of complex sphingolipids, SM and GSLs (Futerman and Riezman 2005). Synthesis of PC and PE can also take place In the Golgi apparatus and the PI derivative PI(4)P is enriched at the trans-Golgi network. Notably, cholesterol levels are higher in the Golgi apparatus (in particular the trans-Golgi) than in ER membranes (Yang, Lee, and Fairn 2018).

The plasma membrane has a significantly different lipid composition from that of the ER or the Golgi apparatus (Figure 19). It is concentrated with sphingolipids and sterols which are densely packed, unlike glycerophospholipids, and can resist mechanical stress. The plasma membrane bilayer is extremely asymmetric. The outer leaflet mainly contains SM and PC while the inner leaflet is mostly composed of PE, PS along with its minor component PI(4,5)P2 (Van Meer, Voelker, and Feigenson 2008). This distribution results in a highly negatively charged inner leaflet. The plasma membrane autonomously does not synthesis structural lipids but several PI lipid derivatives, namely PI(3,4)P2, PI(4,5)P2, PI(3,4,5)P3, PI(4)P, are synthesized or degraded there (Di Paolo and De Camilli 2006). One reason could be that PI derivatives play crucial roles in recruiting cytosolic components and regulating downstream signalling.

Each of the seven PI lipids have a unique subcellular distribution with a predominant localization in subsets of membranes. Therefore, a phosphoinositide-based code represents a very effective way to define organelle identity. Phospholipids can rapidly diffuse within, but not between, membranes (unless assisted by transfer proteins). In addition, phosphoinositides can be rapidly interconverted from one species to another by strategically localized pools of kinases and phosphatases as a membrane carrier translocates from one compartment to the next (Figure 19). The existing predominant PI-based organelle identities are; PI(4,5)P2 for plasma membrane, PI(4)P for Golgi apparatus (TGN), PI(3)P for early endosome and PI(3,5)P2 for late endosome.

4.3 Lipid phase separation in membranes

Lipid bilayers made of several different lipid species can exist in different phases depending on the collective behaviour of their components. The membrane is fluid at high temperatures and in a liquid-crystal phase at lower temperatures (Subczynski et al. 2017). The two most extreme phases are the gel or solid ordered phase (So), and the liquid disordered phase (Ld). In the So phase, the lipid acyl-chains are able to undergo cis-trans isomerization. This leads to their physical extension and increased intermolecular Van der Waals interactions. Overall a highly ordered lipid packing is achieved which prevents lateral diffusion of lipids (Seu et al. 2006; Los and Murata 2004). In contrast, the Ld phase exhibits irregular packing driven by the presence of unsaturated lipids. Unsaturation present in the lipid acyl-chains leads to kinks in their structure. Additionally, this reduces the surface area accessible to other lipids and thus weakens intermolecular Van der Waals interactions.

Therefore, the Ld phase is a highly fluid state where lateral diffusion of lipids is permissible (Seu et al. 2006; Subczynski et al. 2017).

Under physiological conditions, biological membranes tend to exist in a fluid phase and can undergo phase transition under suitable external conditions. The melting temperature (Tm) of a lipid is the temperature at which it can undergo phase transition from the gel to the liquid state. A given lipid species has a unique Tm based on Its structure (Cevc 1991). For instance, lipids with longer acyl-chains occupy larger surface areas as compared to lipids with shorter chains, resulting in stronger Van der Waals interactions between aliphatic chains and an increase in their Tm. As previously mentioned, an increased level of unsaturation weakens Van der Waals interactions lowering the Tm of the lipid. Therefore, one can make the distinction between high Tm lipids that will be in a solid state at physiological conditions, and low Tm lipids that will be in a liquid state under the same conditions due to their structural differences.

In cells, the plasma membrane, which contains proteins embedded within the lipid bilayer, exhibits lipid-lipid phase separation events where localized Lo (liquid ordered) and Ld domains are observed. These micro/nanodomains have been named lipid rafts (Simons and Ikonen 1997; Munro 2003; Simons and Vaz 2004). This phenomenon is referred to as phase separation. Fundamentally, phase separation is the creation of two distinct phases from a single homogeneous mixture and can be induced by intrinsic or extrinsic factors (see below).

4.4 Model membranes for in vitro experiments

4.4.1 Techniques to form membranes in vitro

The heterogeneity and complexity of biological membranes is a bottleneck when attempting to study them in cellulo. This paved the way for the development of in vitro model membrane systems whose lipid compositions are tailored to mimic localized intracellular membrane events (Bagatolli and Sunil Kumar 2009; Sezgin and Schwille 2012). Physical parameters can also be regulated. For instance, model membranes with various geometries can be generated (Figure 20) such as, supported lipid bilayers (planar) or vesicles (spherical). In the case of spherical vesicles, the size can be customized which includes small unilamellar vesicles (SUVs) with diameters around 50 nm to giant unilamellar vesicles (GUVs) with diameters up to 10-100 µm.

Figure 20 summarizes the commonly used membrane model systems and how to generate them. Multilamellar vesicles (MLVs) can be generated via hydrating dried lipid films. Vesicles representative of biological membranes have to be unilamellar. To obtain unilamellar vesicles, SUVs (diameter between 30 and 50 nm). can be generated from MLVs by sonication. Alternatively, MLVs subjected to extrusion through polycarbonate membranes of varying

pore sizes generate large unilamellar vesicles (LUVs) (diameter between 100 nm and 1 μm) (Figure 20).

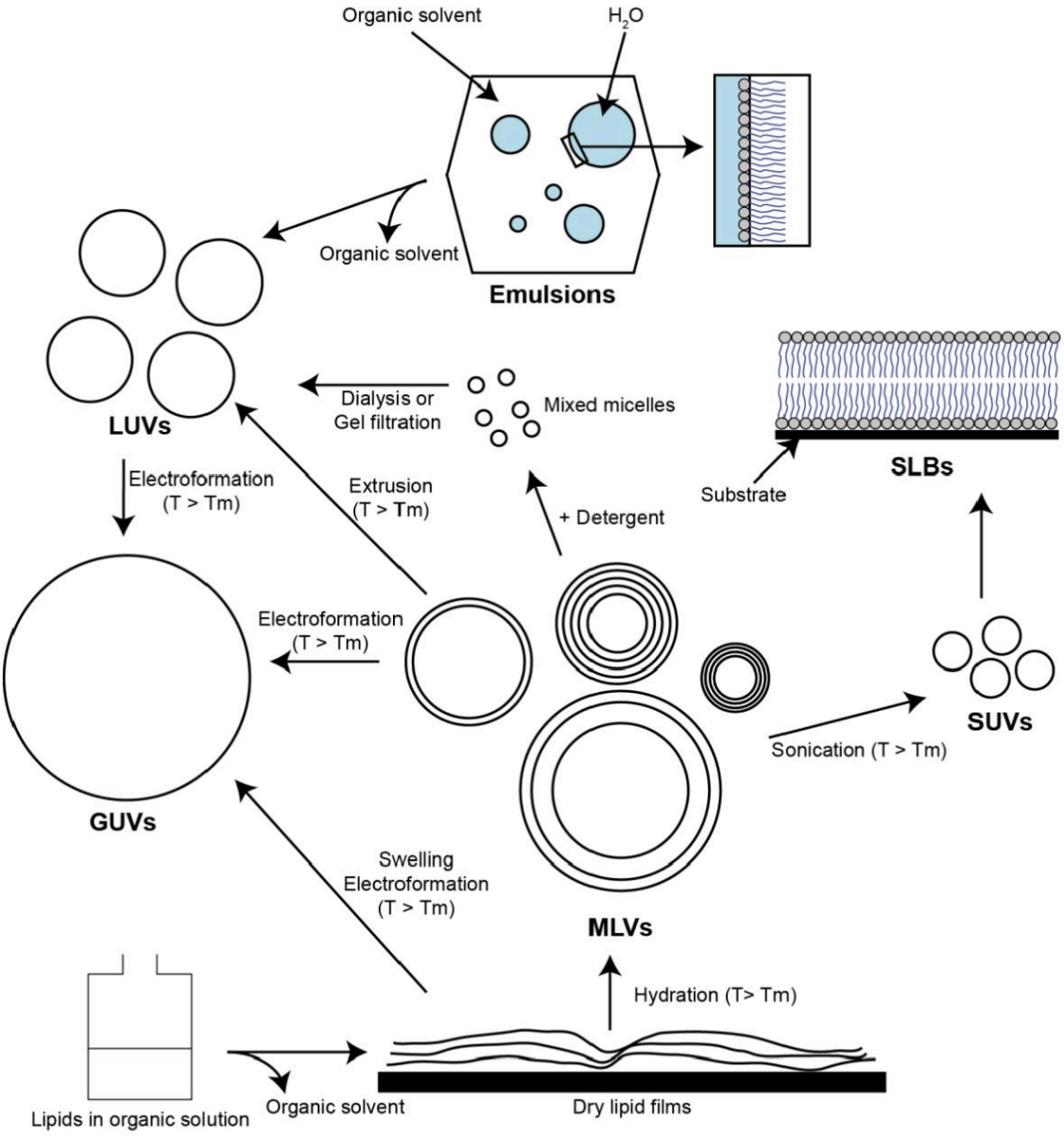

Figure 20 Membrane models and their preparation. Starting from MLVs to a broad range of unlimamellar vesicles are shown here and how to synthesize them. MLVs are generated via hydration of dry lipid films. Upon sonication MLVs generate SUVs and upon extrusion they can generate LUVs. GUVs can be synthesized via electroformation upon hydration of dry lipid films (swelling electroformation). Other methods such as synthesis via emulsions is also shown here. Adapted from (Bagatolli and Sunil Kumar, 2009).

The largest of the unilamellar vesicles are the GUVs (diameter between 1 and 100 μm). GUVs can be formed using different techniques. They can be synthesized via hydration of dried lipid films followed by electroformation under an alternating current (AC) field (Angelova et al. 2007). One particular demerit of using the classical electroformation method with ITO (Indium Tin Oxide) conducting slides as electrodes is that only growth buffers containing low levels of salts can be used. This problem can be bypassed by using an optimized electroformation method based on platinum electrodes instead (Dimova 2019). Another alternative method is gel-assisted hydration, where lipids are spread on polymer gel surfaces such as agarose or polyvinyl alcohol and GUVs are grown via hydration (Rideau, Wurm, and Landfester 2019). Unilamellar vesicles with asymmetric membranes can also be obtained using the inverted emulsion technique (Pautot et al., 2003). Here inverted emulsion droplets covered with a lipid monolayer are passed through a second monolayer within an oil-water interface. Lastly, closer to the complexity of biological membranes are the giant plasma membrane vesicles (GPMVs). They are harvested from mammalian cells with the help of vesiculants (reducing agents such as NEM and DTT) that induce cell blebbing. Subsequently, upon spontaneous pinching-off of the induced blebs, vesicles are formed which can be harvested and concentrated by centrifugation. GPMVs are mostly free of cellular compartments (Sezgin et al. 2012; Levental and Levental 2015).

GUVs have been used principally because their size and curvature allow their visualization with an optical microscope. Additionally, GUVs have found applications in several biophysical contexts in which membrane composition, tension, and geometry is controlled and manipulated using microscopy techniques (Fenz and Sengupta 2012; Bhatia et al. 2015; Morales-Penningston et al. 2010; Manneville et al. 2012). Most importantly, biochemical reconstitution assays with GUVs are widely used to understand protein sorting, interaction and dynamics (Schmid, Richmond, and Fletcher 2015).

4.4.2 Model membranes exhibiting phase separation

Studying and visualizing lipid rafts in live cells requires selective fluorescent probes and cutting-edge microscopy techniques. In spite of the development of advanced microscopy techniques in the past few decades, the study of lipid rafts in cells is still challenging (Pike 2009). Biophysicists have therefore been modifying existing membrane model systems to undergo phase separation events mimicking cell membrane associated lipid rafts, for instance with models such as supported lipid bilayers and GUVs (Dimova 2019; Liu and Fletcher 2006; Roux et al. 2005).

Phase transition occurs at a fixed melting temperature provided the system is homogenous. However, coexistence between the two phases Lo and Ld (phase separation) can be achieved in a bi-component system made up of lipids with both high and low Tm. As

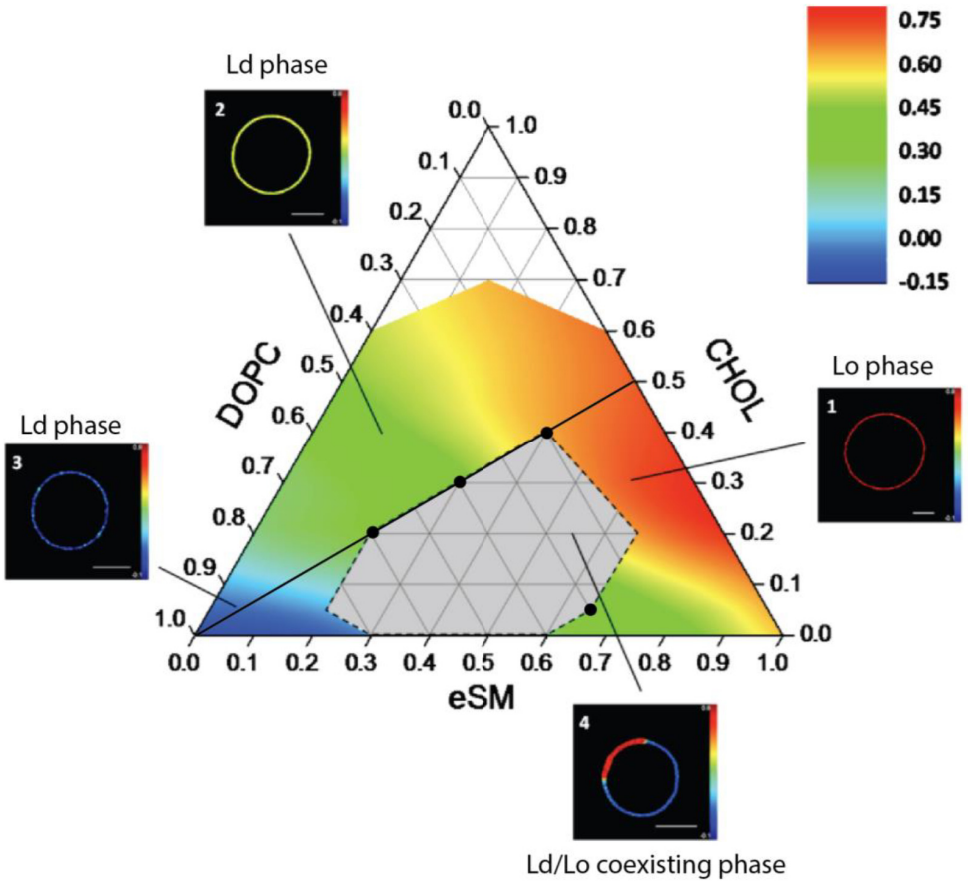

Figure 21 General polarization phase diagram for a DOPC:eSM:Chol ternary mixture at 23 °C. (A) General polarization values of lipid mixtures that do not undergo phase separation are plotted in false color, red represents the most compact lipid packing and blue for the less compact. Vesicle. General polarization images illustrate several phase states. Molar ratio compositions of the inset vesicles shown are (1), 10:60:30 (homogenous Lo phase) (2), 50:10:40 (homogenous Ld phase) (3), 90:5:5 (homogenous Ld phase) (4), 25:55:20 (phase separated Ld/Lo phase). The methodology shown here does not allow distinction between gel (So) and Lo domains. Adapted from Carravilla et al. 2015

aforementioned, cholesterol is the structural key to the formation of the Lo phase. Therefore, in GUVs synthesized with ternary lipid mixtures containing cholesterol and high/low Tm lipids, phase separation events can be observed. At a given temperature, under equilibrium conditions, thermodynamic phase separation in lipid mixtures can be predicted with phase

diagrams based on the Gibbs triangle (Figure 21) (Carravilla et al. 2015; Heberle et al. 2010). the opposite applies to DOPC lowering its Tm. The following situations can be distinguished in the phase diagram of a ternary lipid mixture: 1) pure homogeneous Ld phase when the low Tm lipid DOPC (Figure 21) is in excess; 2) pure homogeneous Lo phase when the high Tm lipid SM is in excess with moderate CHOL addition, coexistence of Lo and Ld phases occurs when the three components are in equivalent amounts (Figure 21) (Carravilla et al. 2015). At the boundary between segregated and non-segregated regions exists phase separation, which can also be triggered by external factors such as protein binding (Sorre et al. 2012).

A key finding was the discovery of a class of proteins with the ability to induce phase separation when bound to heterogenous membrane models. For example, branched actin networks formed on GUVs enriched with the PI(4,5)P2 trigger both temporal and spatial rearrangements of membrane components (Liu and Fletcher 2006). Polymerization of actin networks on the membrane induces phase separation of initially homogenous vesicles with the capacity to phase separate. This switch-like behaviour has been shown to be dependent only on the PI(4,5)P2-N-WASP link between the membrane and the actin network, while the pre-existing actin network only spatially biases the location of phase separation. This discovery showed that dynamic, membrane-bound actin networks alone can control when and where membrane domains form and may actively contribute to membrane organization during cell signalling (Liu and Fletcher 2006). It would be insightful to also identify a potential role of Cdc42, which also interacts with PI(4,5)P2, in phase separation. By using fluorescent lipids or lipophilic probes that will preferentially sort into one of the two phases, phase separation events can be observed using microscopy techniques (Figure 21) (Dimova 2019)

Part II

Objectives

Cdc42 is an evolutionarily conserved Rho GTPase controlling many cellular functions, such as cell polarity, cell migration and cell cycle, in response to various extracellular signals. Membrane association of Cdc42 is key for regulating its functions. While Cdc42 inactivated by GDI1 localizes in the cytosol, its regulators and effectors are generally membrane-associated. The regulation and functions of Cdc42 at the cell plasma membrane have been extensively studied (Sandrine Etienne-Manneville 2004; Cerione 2004). However, a significant pool of Cdc42 localizes on intracellular compartments where its specific regulation and functions remain elusive (Farhan and Hsu 2016).

Does alternative splicing influence Cdc42 localization and function?

Previous studies conducted to understand the biological function of Cdc42 in tissues and cells have mostly considered only the ubiquitous isoform of Cdc42 (Cdc42u). In vertebrates there exist two alternative splice variants of Cdc42. In addition to the ubiquitous isoform Cdc42u, a so-called brain isoform (Cdc42b) has been documented (Marks and Kwiatkowski 1996). The role of these isoforms in neurogenesis and neuronal differentiation has been studied (Yap et al. 2016; Endo, Druso, and Cerione 2020). Yet, their functional relevance with regard to cell polarity and migration remains unknown. The difference between these two isoforms lies exclusively in the carboxy-terminal domain which encompasses key amino-acid sequences responsible for Cdc42 interaction with membranes. This led us to hypothesize that alternative splicing may modulate Cdc42 localization and hence its functions.

The first aim of this study was to identify the subcellular localization of Cdc42 isoforms and determine if they had specific functions. To tackle this question, we used primary astrocytes which are an excellent model to study the role of Rho GTPases in front-to-rear cell polarization events and in cell migration (Sandrine Etienne-Manneville 2006). We also used neural precursors. Primary astrocytes and neural precursors express both isoforms of Cdc42.

This part of the study forms the article in Part IV Results Section A of this thesis. It led to the conclusion that Cdc42 isoforms have different localization and functions and pushed us to investigate whether the carboxy-terminal domain of the protein (10 last amino-acids), which is not directly involved in its GTPase activity, could influence Cdc42 interactions with other proteins (objective 2) or Cdc42 interactions with specific cellular membranes (objective 3).

Does alternative splicing affect Cdc42 interactome?

Cdc42 functions as a molecular switch, cycling between a GDP-bound inactive state and a GTP-bound active state. This GTPase cycle is regulated by GEFs that stimulate nucleotide exchange and GAPs that accelerate intrinsic GTPase activity. The human genome encodes approximately 70 Rho GEFs and 60 GAPs which exhibit overlapping functions.

In its GTP-bound form Cdc42 binds to several effector and adaptor proteins, the functions of which are regulated by Cdc42 to drive downstream signaling events. Approximately 45 mammalian Cdc42 effectors have been described (Pichaud, Walther, and Nunes de Almeida 2019). Not surprisingly, these effectors and their specific interactions with Cdc42u have been explored neglecting the second isoform Cdc42b.

A study on the regulation and functional significance of Cdc42 alternative splicing in ovarian cancer suggests a potential role of Cdc42b as a tumour suppressor gene as compared to the oncoprotein role of Cdc42u (He, Yuan, and Yang 2015). Consistently, in our lab a difference between the expression levels of Cdc42 isoforms in patient glioma samples has been reported (unpublished data). While the level of expression of Cdc42u does not differ between gliomas and the healthy brain, in contrast Cdc42b mRNA appears significantly under-expressed in gliomas.

These findings suggest that the alternative splice variants could have differential interactomes. We expected that the difference in lipid modification observed between the two isoforms would affect GDI1 binding since this interaction was reported to rely on the presence of lipid tails (Hoffman, Nassar, and Cerione 2000; A. Nishimura and Linder 2013). In addition, in the case of Rac, the carboxy-terminal domain of the protein was previously shown to participate in its interaction with its effectors such as PAK (Knaus et al. 1998; Abdrabou and Wang 2018). We sought out to determine in a non-biased manner whether alternative splicing could modify Cdc42 interactome. In the course of this study, we also collaborated with Jérôme Delon (Institut Cochin) who, together with Asma Smahi, had identified a new human mutation of Cdc42. This mutation was also particularly relevant to our study since it changed the Arginine residue (R186) of the KK-RR motif into a Cysteine which was shown to be heavily palmitoylated.

To analyze the interactomes of the two Cdc42 variants, we expressed GFP-tagged fusion proteins in HEK cells, immunoprecipitated Cdc42 using anti-GFP nanobodies and then identified the potential isoform specific interactors and regulators of Cdc42 via mass spectrometry (in collaboration with D. Loewe, F. Dingli, Institut Curie, Paris). The results we obtained are exposed in Part IV Results Section B of this thesis and in annex Article 1 (Bekhouche et al. 2020)

What is the role of the carboxy-terminal amino acids and of the CaaX box in Cdc42 interaction with the membrane?

We formulated an alternative hypothesis to explain the distinct localisation and function of Cdc42 isoforms. In parallel to studying how alternative splicing could affect the protein interactome (see Objective 2 above), we investigated whether the alternative carboxy-terminal domain may directly affect Cdc42 interaction with cellular membranes. This last C-terminal exon encompasses two characteristic features of Rho GTPases namely, the polybasic region (PBR) and the CaaX motif (Hodge and Ridley 2016). The PBR region plays a key role in membrane targeting and the CaaX box is responsible for membrane anchoring. For the two isoforms of Cdc42, both regions differ drastically.

Cdc42u has a PBR region consisting of a di-lysine and a di-arginine motif, which is absent in Cdc42b. The di-arginine motif is important for association of Cdc42u with negatively charged membranes rich in PI(4,5)P_2 in the plasma membrane (Johnson, Erickson, and Cerione 2012). Cdc42u has a classical CaaX box which is prenylated whereas Cdc42b has an alternative CCaX motif which is palmitoylated in addition to the prenylation on the Cys188 residue. This C-ter lipidation is also crucial for GDI1 binding, which in turn dictates the subcellular localization of Cdc42 (A. Nishimura and Linder 2013).

To circumvent the challenging task of studying plasma membrane interactions in cellulo we used Giant unilamellar vesicles (GUVs) as in vitro model membrane systems. GUVs are ideal as they are convenient for imaging and their lipid composition can be customized. Considering the differential membrane targeting and anchoring motifs, we dissected the role of the isoform specific membrane interactions using Cdc42 variants and mutants, carboxy-terminal constructs and GUVs of various plasma membrane- or Golgi-related composition. The results of this still on-going study are reported in Part IV Results Section C of this thesis.

Part III

Materials and Methods

3.1 In cellulo

3.1.1 Cell Biology

Cell Culture

Primary rat astrocytes were obtained from rat embryos at day E17 as previously described by Etienne-Manneville 2006. Cells were grown in 1g/L glucose DMEM supplemented with 10% FBS (Invitrogen, Carlsbad, CA), 1% penicillin-streptomycin (Gibco) and 1% Amphotericin B (Gibco) at 5% CO2 and 37°C. Medium was changed 1 day after transfection and 1 day before the experiments.

HEK 293 and HeLa cells were grown in 4.5 g/L glucose DMEM supplemented with 10% FBS (Invitrogen, Carlsbad, CA), 1% penicillin-streptomycin (Gibco) and 1% Amphotericin B (Gibco) at 5% CO2 and 37°C.

Transfection Protocol

Astrocytes were transfected with the Lonza glial cell nucleofector solution and electroporated with a Nucleofector machine (Lonza). Cells were after plated on appropriate cell culture chambers previously coated with poly-L-Ornithine (Sigma) and experiments were performed 3 days post-transfection, when optimal protein silencing or expression was observed. siRNAs used in the results section are found in the Materials and Methods section of article 1. HEK 293 cells were transiently transfected using the phosphate calcium method. 48h post-transfection cells were treated and used for protein purification, immunoprecipitation and pull-down assays. HeLa cells were seeded onto glass coverslips in 24-well plates containing complete growth medium and were transfected the following day with 0.5µg of DNA and 1µL GeneJuice-transfection reagent (Novagen) by following their user protocol. Subsequent experiments using transfected HeLa were carried out one day post-transfection.

Chemical inhibitors

All the details regarding chemical inhibitors used in the articles can be found in their respective Materials and Methods sections. 10 uM Palmostatin B, also known as APT1 inhibitor (Calbiochem), was added to HEK cells expressing GFP-tagged brain Cdc42 1h prior to protein purification. This was done to prevent depalmitoylation of brain Cdc42 by APT1 in order to increase the pool of purified palmitoylated brain Cdc42.

Immunofluorescence

HeLa cells seeded on coverslips were fixed in 4% PFA (10 minutes) and subsequently permeabilised in 0.1% Triton (10 minutes) at room temperature one day post-transfection. Seeded cells were then treated with primary anti-laminB1 antibody in PBS (1x) for 1 hour, washed 3x with PBS, and treated with secondary antibody in PBS (1x) for 1 hour. Coverslips were washed a following 3x in PBS before mounting onto microscope slides using ProLong diamond antifade mounting agent containing DAPI dye (ThermoFischer). All epifluorescence images were obtained with the Leica DM6000 inverted microscope using a 40x 1.25 NA oil-immersion objective lens. Image acquisition was performed using the Leica DFC350 FX CCD camera in conjunction with the manufacturer provided Application Suite AF software (Leica). Samples were illuminated with a white light lamp and single excitation wavelengths of 488 nm, 551 nm, and 360nm were selected using appropriate filter settings.

Live Imaging

Microinjected primary astrocytes were seeded on 35-mm glass-bottom dishes and grown to confluence for 3 days. On the day prior to wounding, the medium was changed and before imaging, HEPES buffer was added to the medium. The monolayer was wounded and cells were monitored after 4h, allowing them to polarize first. Videos were acquired on a spinning-disk confocal microscope (PerkinElmer UltraViewVox) with a heating chamber (37°C) and CO2 supply (5%).

3.1.2 Biochemistry

Electrophoresis and Western blot

Cell lysates were obtained with NuPAGE LDS Sample buffer (4X). Samples were boiled 5 minutes at 95°C before loading on precast NuPAGE Bis-Tris mini gels. Transfer was performed at 100V for 1h at 4°C on nitrocellulose membranes. Membranes were then blotted with 5% milk+TBST (0.2% Tween), after incubated with primary antibody for 1h at room temperature, washed 3 times in TBST, incubated 1h with HRP-conjugated secondary antibody. Bands were revealed with ECL chemiluminescence substrate (Pierce, ThermoScientific). Blots were imaged with Bio-Rad Gel Documentation System.

Immunoprecipitation

For GFP immunoprecipitation, HEK cells transfected with GFP tagged constructs of Cdc42 were lysed using 50mM TRIS base, Triton 2 %, 200mM NaCl as well as 1 tablet/10 ml protease inhibitor Mini-complete, EDTA-free (Roche). After removal of insoluble fragments

via centrifugation at 12,000 g for 25 min, 15ul of the lysates were stored at -20°C with the addition of 15µL of NuPAGE LDS Sample buffer (4x)(as loading control). The remaining lysates were incubated with 15 µl of GFP-Trap Agarose beads from Chromotek for 1h at 4°C on a rotary wheel. The beads were washed three times for 10mins using wash buffer (50mM TRIS base, 150mM NaCl, 1mM EDTA and 2.5 mM MgCl2 and pH adjusted to 7.5) on a rotary wheel. 20µL of NuPAGE LDS Sample buffer (4x) was added and samples prepared for western blotting.

Pull-down assays

For pull down assays with GDI1 or PAK-CRIB domain, cultured BL21 bacteria (C600003 Invitrogen) were transformed with either pGEX-GST-GDI or pGEX-GST-PAK-CRIB plasmids. The inoculated cultures were incubated overnight at 37 °C, with shaking at 250-300rpm. The following morning optical density at 600nm (OD600) was tested using a spectrophotometer. The overnight starter culture was diluted (1:50) into fresh LB media supplemented with 100 µg/mL ampicillin. The culture was incubated at 37 °C at 250–300 rpm until the OD600 was 0.8. IPTG was added to a final concentration of 1.0 mM. The culture was then incubated at 37°C at 250–300 rpm for an additional 4h, while monitoring the growth at OD600. Cells were harvested by centrifugation at 4000 × g for 20 min at 4°C. The supernatant was carefully decanted leaving ~ 15–50 ml in the centrifuge bottle. Resuspend the cells and transfer them to a 50mL centrifuge tube. Centrifuge for 20 mins at 4000x g at 4°C. The supernatant was decanted and the pellet was frozen at -20°C overnight. The following morning 5mL of Lysis buffer (25% sucrose, 150mM NaCl, 50mM Tris pH 8.8) was added to the pellet. 0.5g of lysozyme from chicken egg white (Sigma L6876-10G) was added and the lysate was incubated at RT for 30 minutes. 4uL of DNaseI recombinant (ROCHE 04536282001) was added and incubated for 30 mins, followed by centrifugation of the bacterial lysate for 30 mins at 2000rpm. The resulting supernatant contains the purified recombinant GST proteins. The supernatant was aliquoted and stored at -80 °C. Prior to the pull-down assays the protein supernatant was incubated with Glutathione Sepharose beads (GE Healthcare) for 1h at 4°C on a rotary wheel. Subsequently, the beads were washed three times with wash buffer (50mM TRIS base, 150mM NaCl, 1mM EDTA and 2.5 mM MgCl2 and pH adjusted to 7.5). Either cell lysate or purified Cdc42 were then added to the GST recombinant protein coated beads and their interaction was observed by western blotting.

Mass Spectrometry (MS) analysis

Firstly, GFP immunoprecipitation assay was carried out, for which HEK cells transfected with GFP tagged constructs of Cdc42 were lysed using 50mM TRIS base, Triton 2 %, 200mM NaCl as well as 1 tablet/10 ml protease inhibitor Mini-complete, EDTA-free (Roche). After the removal of insoluble fragments via centrifugation at 12,000 g for 25 min at 4°C, lysates were incubated with 15 µl of GFP-Trap Agarose beads from Chromotek for 1h at 4 °C on a rotary wheel. The beads were washed using a wash buffer (50mM TRIS base, 150mM NaCl, 1mM EDTA and 2.5 mM MgCl2 and pH adjusted to 7.5). Following the final wash, beads were

stored with wash buffer at 4°C prior to depositing at the Institut Curie Mass Spectrometry and Proteomics facility (LSMP).

Proteins on beads were washed twice with 100µL of 25mM NH_4HCO_3 and we performed on-beads digestion with 0.2µg of trypsin/LysC (Promega) for 1 hour in 100µL of 25mM NH_4HCO_3. Sample was then loaded onto a homemade C18 StageTips for desalting. Peptides were eluted using 40/60 MeCN/H_2O + 0.1% formic acid and vacuum concentrated to dryness.

Online chromatography was performed with an RSLCnano system (Ultimate 3000, Thermo Scientific) coupled to an Orbitrap Fusion Tribrid mass spectrometer (Thermo Scientific). Peptides were trapped on a C18 column (75µm inner diameter × 2cm; nanoViper Acclaim PepMapTM 100, Thermo Scientific) with buffer A (2/98 MeCN/H_2O in 0.1% formic acid) at a flow rate of 4.0µL/min over 4 min. Separation was performed on a 50cm x 75µm C18 column (nanoViper Acclaim PepMapTM RSLC, 2µm, 100Å, Thermo Scientific) regulated to a temperature of 55°C with a linear gradient of 5% to 25% buffer B (100% MeCN in 0.1% formic acid) at a flow rate of 300nL/min over 100 min. Full-scan MS was acquired in the Orbitrap analyzer with a resolution set to 120,000 and ions from each full scan were HCD fragmented and analyzed in the linear ion trap.

For identification the data were searched against the Homo sapiens (UP000005640) SwissProt database using Sequest HF through proteome discoverer (version 2.2). Enzyme specificity was set to trypsin and a maximum of two missed cleavage site were allowed. Oxidized methionine, N-terminal acetylation, and carbamidomethyl cysteine were set as variable modifications. Maximum allowed mass deviation was set to 10 ppm for monoisotopic precursor ions and 0.6 Da for MS/MS peaks.

The resulting files were further processed using myProMS (Poullet, Carpentier, and Barillot 2007)v3.6 (work in progress). FDR calculation used Percolator and was set to 1% at the peptide level for the whole study. The label free quantification was performed by peptide Extracted Ion Chromatograms (XICs) computed with MassChroQ version 2.2 (Valot et al. 2011). For protein quantification, XICs from proteotypic peptides shared between compared conditions (TopN matching) with no missed cleavages were used. Median and scale normalization was applied on the total signal to correct the XICs for each biological replicate. To estimate the significance of the change in protein abundance, a linear model (adjusted on peptides and biological replicates) was performed and p-values were adjusted with a Benjamini–Hochberg FDR procedure with a control threshold set to 0.05. The mass spectrometry proteomics data have been deposited to the ProteomeXchange Consortium via the PRIDE (Perez-Riverol et al. 2019) partner repository with the dataset identifier PXD017477(username: reviewer51683@ebi.ac.uk, Password: 4fNr03LX)

Radiolabelling

Radiolabelling of brain Cdc42 was performed as described in Abrami et al. 2019 for S-palmitoylated proteins. HEK cells or HeLa cells 48 hours post-transfection with different GFP-tagged Cdc42 constructs were starved for 1 hour at 37°C in IM (Glasgow minimal essential medium buffered with 10 mM HEPES pH adjusted to 7.4) and incubated for 2 hours at 37°C in IM with 200 µCi/mL of ^{3}H-palmitic acid (9,10-^{3}H(N)) (American Radiolabeled Chemicals, Inc, St Louis, Mo). The cells were washed, incubated in complete Dulbecco modified Eagle medium for 10 minutes and washed 3 times with cold PBS at 4°C, directly lysed for 30 minutes at 4°C in lysis buffer (0.5 % Nonidet P-40, 500 mM Tris pH adjusted to 7.4, 20 mM EDTA, 10 mM NaF, 2 mM benzamidine, and protease inhibitor cocktail [Roche]), and centrifuged for 3 minutes at 5000 rpm. Supernatants were subjected to preclearing with Glutathione Sepharose beads before being subjected to immunoprecipitation reaction that included overnight incubation with anti-Myc affinity gel (Thermo Scientific, Waltham, Mass). After immunoprecipitation, the washed beads were incubated for 5 minutes at 90°C in reducing sample buffer before 4% to 20% gradient SDS-PAGE and revelation with a mouse anti-GFP antibody (NovusBio NB600-313). After SDS-PAGE, the gel was incubated in a fixative solution (25% isopropanol, 65% H_2O, and 10% acetic acid), followed by a 30-minute incubation with signal enhancer Amplify NAMP100 (GE Healthcare, Chicago, Ill). The radiolabeled products were revealed using Typhoon phosphoimager after 4-6 weeks of exposure.

Protein S-acyltransferase (PAT) screen

For Protein S-acyltransferase (PAT) enzymes (zDHHC family of enzymes) identification corresponding plasmids were co-transfected with GFP-tagged Brain Cdc42 construct into Hela cells for 48 h, using *TRANS*IT–X2 according to the manufacturer's protocol (MIRUS). Followed by radiolabeling and assessing the level of palmitoylated brain Cdc42 in each given condition as described in Abrami et al. 2019 and Lakkaraju et al. 2012.

Verified siRNA for human zDHHCs were purchased from Qiagen. (see Lakkaraju et al. 2012 for siRNA knockdown)

The following siRNA were used:

zDHHC1 (5'-ACCGGCTGTGATGCTCCAATA-3')

zDHHC3 (5'TCCGTTCTCATGAATGTTTAA-3')

zDHHC7 (5'-CCCGTGGTTACTATGAATGTA-3')

zDHHC13 (5'-CAGCATAGTAGCCTTTCTATA-3')

zDHHC18 (5'-AAGCCTGATGCCAGCATGGTA-3')

zDHHC20 (5'-TACCTGTTATGAGTTGCCTATA-3')

As a control siRNA, a sequence targeting the viral glycoprotein VSV-G (5'ATTGAACAAACGAAACAAGGA-3') was used. Co-transfections of 50 nM of siRNA and GFP-tagged brain Cdc42 were carried out using *TRANS*IT-X2 (MIRUS), and the cells were radiolabelled at least 72 h after transfection (Abrami et al. 2019; Lakkaraju et al. 2012).

Protein expression and purification

Cdc42 variants and their mutants were cloned into a pCEFL-GST-GFP vector plasmid and used to purify GFP tagged proteins for the biochemical reconstitution assays (see Table 3, at the end of Part III). For protein purification, HEK cells were transiently transfected and incubated for 48h. They were washed and lysed with lysis buffer 50mM TRIS base, Triton 2 %, 200mM NaCl as well as 1 tablet/10 ml protease inhibitor Mini-complete, EDTA-free (Roche) on ice. After removal of insoluble fragments via centrifugation at 12,000 g for 25 min at 4°C, the supernatant was subjected to preclearing with Glutathione Sepharose beads for 1h at 4°C on a rotary wheel. The beads were washed three times for 10mins using wash buffer (50mM TRIS base, 150mM NaCl, 1mM EDTA and 2.5 mM MgCl2 and pH adjusted to 7.5) on a rotary wheel. Glutathione Elution was performed by adding Elution buffer (50mM TRIS base and 1M L-Glutathione reduced (Sigma-Aldrich) and pH adjusted to 8). Three rounds of elution were performed and the elute was incubated with Thrombin Sepharose beads (Thrombin CleanCleave Kit Sigma-Aldrich) overnight at room temperature. The bead slurry was centrifuged to remove Thrombin Sepharose beads and the supernatant was dialysed against PBS to remove Glutathione at 4°C. Dialysis was performed using Slide-A-Lyzer dialysis cassette (molecular weight cut off-7Kda [ThermoScientific])(Figure 22A). After dialysis to remove cut GST proteins and uncut GST-Cdc42 were removed by another round of Glutathione Sepharose beads-based pull-down assay. The final supernatant was aliquoted and snap frozen with liquid nitrogen prior to long term storage at -80°C. Before experiments, the aliquots were rapidly thawed using a water bath at 30°C and any aggregates or residual beads were removed by centrifugation.

The presence of prenylated Cdc42 was confirmed after performing GDI1 pull down assays. The pool of Cdc42 was found to be inactive as no traces of Cdc42 were bound to the PAK-CRIB in the pull-down assay (Fgure.22B). Full length Cdc42u construct co-purifies with GDI1 (Figure 22C) while C-Ter constructs do not even bind to GDI1 to begin with (Figure 22D)

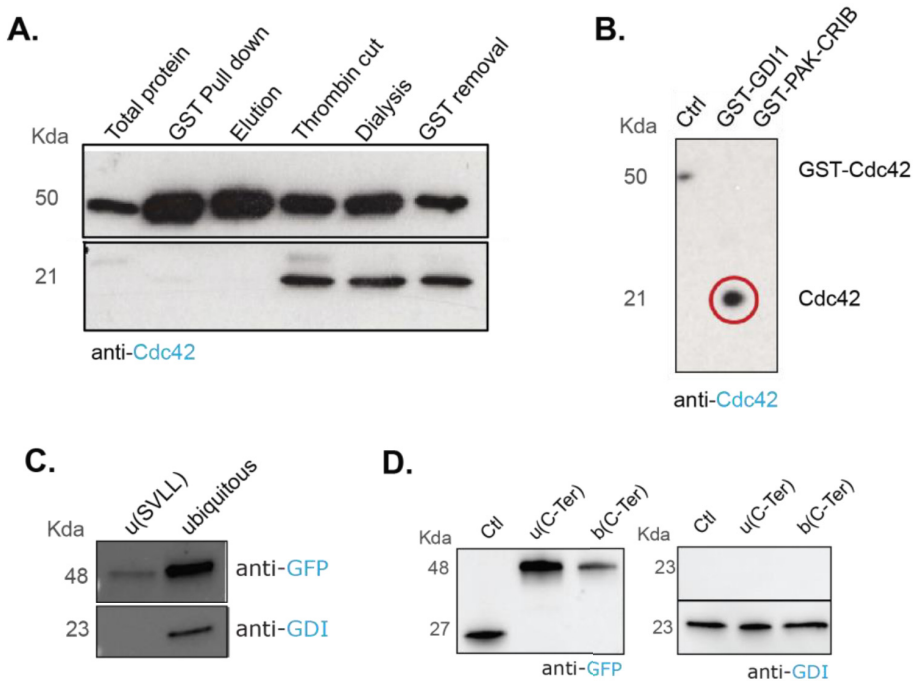

Figure. 22 Cdc42 protein purification A) Western blot showing the GST purification steps used to purify GST-tagged Cdc42 from HEK cells. HEK cells used were transiently expressing GST-tagged Cdc42 constructs. B) Pull down assay was performed with GST-GDI1 to test for prenylated Cdc42 and with GST-PAK-CRIB domain to test for the presence of active Cdc42 GTP. C) Western blot of both purified GFP-tagged unprenylated Cdc42 mutant u(SVLL) and ubiquitous Cdc42. Staining for GDI1 shows co-purification of GDI1 only with ubiquitous Cdc42. D) Western blot representing GFP immunoprecipiation assay performed with GFP-tagged Cdc42 C-Ter constructs which fail to bind to co-immunoprecipitate with GDI1 even prior to purification.

3.2. In vitro reconstitution

3.2.1 GUV Synthesis

Lipid reagents and GUV compositions

All lipids were purchased from Avanti Polar lipids unless specified. In this study, the following phase exhibiting Giant Unilamellar Vesicles (GUVs) have been used: 1) homogenous Lo or Ld GUVs; 2) heterogenous phase separated GUVs and 3) GUVs with a composition close to phase separation. Homogenous Lo and Ld vesicles were respectively composed of BrainSM:Chol and DOPC:Chol at 1:1 molar ratio . Phase separated GUVs contained BrainSM:Chol:DOPC at a molar ratio of 3:1:3 (Roux et al., 2005) and were electroformed in a 50°C dry incubator to allow lipid mixing.

The other GUVs tested were electroformed at room temperature. 'Golgi mix' (GM) was used to grow Golgi apparatus-like GUVs and was composed of 50% (mol/mol) EggPC, 19% LiverPE, 5% BrainPS, 10% LiverPI, and 16% Chol (Manneville et al. 2008). To induce lipid packing defects, EggPC was lowered to 35% to incorporate 15% 1-2-dioleoyl-sn-glycerol (DOG) (mol/mol) in the 'Golgi mix'. 'Plasma Membrane mix' (PM) was used to grow plasma membrane-like GUVs and was composed of 20% (mol/mol) EggPC, 10% LiverPE, 7.5% BrainPS, 12.5% BSM, and 50% Chol. For tests with PI(4,5)P_2 binding, 4% (mol/mol) PI(4,5)P_2 and 1% GloPIPs BODIPY TMR-PI(4,5)P2 (tebu-bio) was incorporated in the 'Plasma membrane mix' and EggPC was lowered to 15%. Other GUVs were made fluorescent by adding 0.1% (mol) of Rhodamine-PE.

Electroformation with ITO slides

GUVs were grown on conductive indium tin oxide (ITO) coated glass slides using the electroformation technique described by (Angelova et al. 2007; Manneville et al. 2012) (Figure 23A). 10µL of a 0.5 mg/mL lipid mix was dried on sequentially pre-washed (water, ethanol, water, chloroform) ITO coated slides and dried in a vacuum chamber for at least 3h. The chamber was then assembled. Sealing wax (Vitrex, Denmark) is applied around the dried lipid films of two opposing ITO glass slides. The entire chamber is immobilized using two paper clips while 4 layers of Teflon tape on each side are used as a spacer (Figure 23A). The dried lipid films were then rehydrated in a sucrose solution (osmolarity 290 mOsm) and GUVs were grown for 3h under a sinusoidal voltage (1.1V, 10Hz). Osmolarity was tested using an osmometer, to match the osmolarity of protein purification buffer. GUV growth was most of the time performed at room temperature, except in the case of phase separation where it was performed at 50°C.

Electroformation with Platinum wires

For lipid mixtures containing charged lipid ($PI(4,5)P_2$), the electroformation method using Platinum wires described by Méléard, Bagatolli, and Pott 2009 was used instead of ITO slides. The electroformation chamber is made out of a block of Teflon of 5mm thickness and 40mm length, with three regularly spaced square wells (Figure 23B). The chamber is also

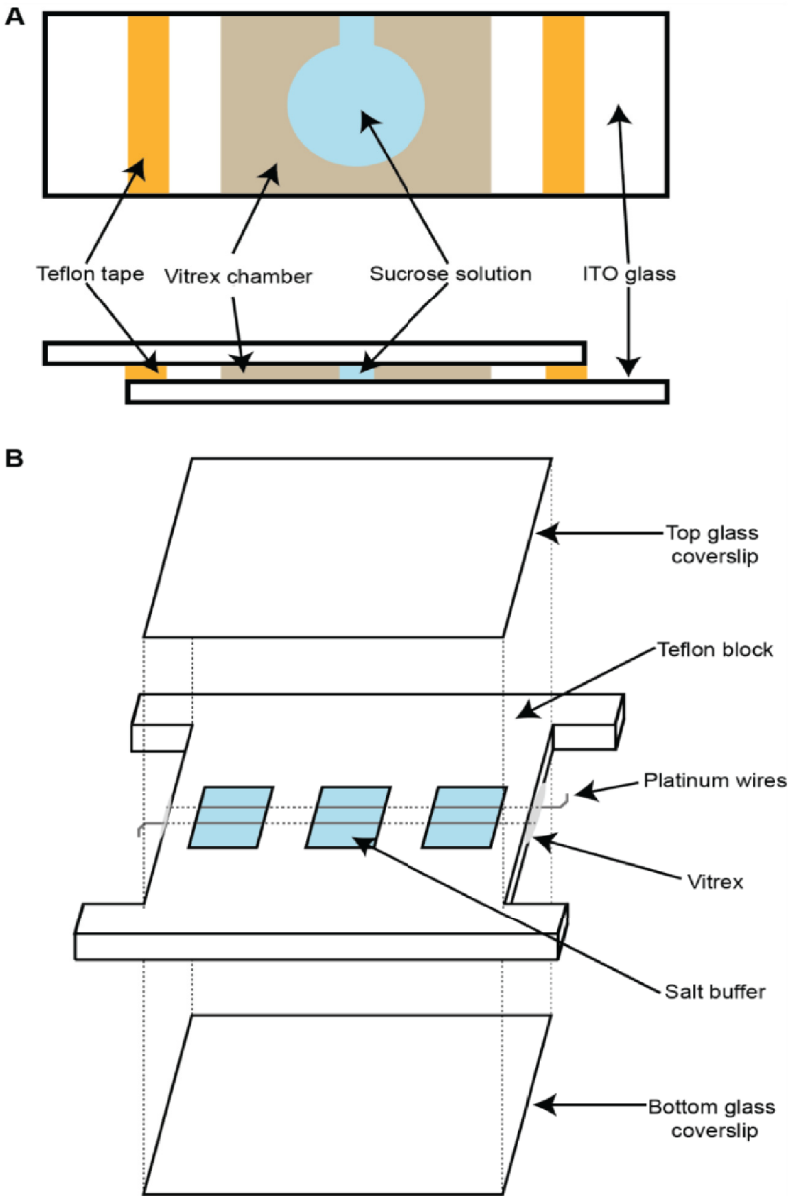

Figure.23 GUV synthesis by electroformation. (A) Conventional electroformation using ITO coated slides. (B) Electroformation with Platinum wires. From Guillaume Kulakowski thesis 'Membrane binding properties of Rab GTPases'. Biophysics UPMC.

perforated throughout its length by two narrow holes which are 3mm apart from each other. Two platinum wires of 0.5mm diameter (LS413074 Goodfellow, UK) are inserted into these holes, cross all three wells and are inserted in the hole on the opposite side of the chamber. These wires come out of the chamber by a few mm which allows us to later connect them to an electrical generator and to consequently build up an electric field inside the wells. Around 5 uL of a 3 mg/mL lipid mixture was applied drop-by-drop around the circumference of pre-washed wires and subsequent drying under high vacuum was performed.

The following steps describe the mounting of the electroformation chamber (Figure 23B). Sealing wax (Vitrex, Denmark) was applied on the side of the chamber to prevent leakage from the holes (from which the platinum wires come out). The bottom side of the chamber was closed using a glass coverslip fixed to the chamber by the anterior addition of vacuum grease (Dow Corning, USA). All the wells were filled with growth buffer and the chamber was completely sealed with a second glass coverslip. The chamber was connected to a generator through the extended platinum wires on the side and growth was performed at 4°C overnight under sinusoidal voltage (0.35 V, 500 Hz). GUVs are then collected by carefully pipetting along the surface of the wires, contact with the wire should be minimal as to avoid scraping sheets of lipids.

3.2.2 Biochemical Reconstitution assays

In the simple case of protein recruitment to differently composed GUVs, a hand-made PDMS well with a 5mm diameter hole in the middle was fixed to a pre-washed (water, ethanol, water) 22 x 40 mm glass coverslip, a circular coverslip was used to seal the top of the PDMS well to create a chamber. The chamber was incubated with 20 μL of 0.5 mg/mL β-Caesin (Sigma) for 10 minutes to prevent adhesion of the GUVs to the glass. The solution was removed and the chamber was washed using 50μL protein storage buffer. After removal of the protein storage buffer, 1 or 2 μL of GUV solution and 6-8μM proteins were added to the chamber to make up to 10 μL final volume.

3.3 Image processing and statistical analyses

Images and videos were analysed with Fiji software (Part IV, Section A-B). Statistical analysis for Figures in Article.1,(Part IV, Section A) are explained in the corresponding Figure legends and Materials and Methods section. Statistical analysis for figures in Part IV, Section B and

Figures in Part IV, Section C are explained in the corresponding Figure legends. Quantification and statistical analysis were performed using GraphPad Prism 8 software.
For *in vitro* GUV assays (Part IV, Section C), the Oval Profile plugin from ImageJ was used to measure average fluorescence intensity along the circumference of GUVs. All data are presented as the mean +/- standard error of at least three independent experiments unless specified. Statistical analysis for scatter plots was obtained with two-tailed unpaired Student's t-test with Welch's correction with p-values shown as n.s. (not significant), **** p-value <0.0001; ***p-value <0.001; **p-value <0.01; *p-value<0.05. Statistical analysis for box plots was obtained with two-tailed Student's ratio paired t-test, ****p-value <0.0001; ***p-value <0.001; **p-value <0.01; *p-value<0.05. Scale bars, 10 μm. Quantification and statistical analysis were performed using GraphPad Prism 8 software and p-values are shown as n.s. (not significant)

Table 3 List of plasmids

Plasmid	Origin
pCEFL-GST-GFP-Cdc42u	S. Guthiud
pCEFL-GST-GFP-Cdc42b	Cloned GFP Cdc42b into pCEFL vector
pCEFL-GST-GFP-Cdc42u C188S	Cloned GFP-Cdc42u into pCEFL vector and induced C188S mutation
pCEFL-GST-GFP-Cdc42b C188S	Cloned GFP-Cdc42b into pCEFL vector and induced C188S mutation
pCEFL-GST-GFP-Cdc42b C189S	Cloned GFP-Cdc42b into pCEFL vector and induced C189S mutation
pCEFL-GST-GFP-Cdc42u C-ter 10 aa	Cloned pEGFP Cdc42u C-ter 10 amino acids into pCEFL
pCEFL-GST-GFP-Cdc42b C-ter 10 aa	Cloned pEGFP Cdc42b C-ter 10 amino acids into pCEFL
pCEFL-GST-GFP-Cdc42u R186C	From J. Delon
pEGFP-Cdc42u	From S.Etienne Manneville
pEGFP-Cdc42u-G12V	From S.Etienne Manneville
pEGFP-Cdc42b	From S.Etienne Manneville
pEGFP-Cdc42b-G12V	From S.Etienne Manneville
pEGFP-Cdc42u-R186C	From J.Delon
pEGFP-Cdc42u-R186C-G12V	From J.Delon
pEGFP-Cdc42b C188S	From J.Hanisch
pEGFP-Cdc42b C189S	From J.Hanisch
pEGFP-Cdc42u C188S	From J.Hanisch
pEGFP-Cdc42u C-ter 10 aa	Cloned C-ter amino acids into pEGFP
pEGFP-Cdc42u C-ter 10 aa	Cloned C-ter amino acids into pEGFP
pEGFP-Cdc42u-ΔVLL	Deleted C-ter VLL
pEGFP-Cdc42u R187A-ΔVLL	Deleted C-ter VLL and induced R187A mutation (denoted as u(PBR))
pGEX-PAK1-CRIB	From S.Etienne Manneville
pGEX-GDI1	From S.Etienne Manneville
pEGFP-C3	Control empty vector

Part IV

Results

Section A

This part of the results section contains the version of our article in revision in the 'Journal of Cell biology' titled 'The specific localization and functions of Cdc42 isoforms'. The first aim of this study was to identify the subcellular localization of Cdc42 isoforms and determine if they had specific functions during cell migration. Primary astrocytes which are an excellent model to study the role of Rho GTPases in front-to-rear cell polarization events and in cell migration were used. We also used neural precursor cells. Most importantly, primary astrocytes and neural precursor cells express both isoforms of Cdc42.

The specific localization and functions of Cdc42 isoforms.

Jan Hänisch[1*], Kerren Murray[1*], Yamini Ravichandran[1, 2*], Vanessa Roca[1], Florent Dingli[3], Damarys Loew[3], Theresia Stradal[4], Batiste Boëda[1], Sandrine Etienne-Manneville[1]

[1]Cell Polarity, Migration and Cancer Unit, Institut Pasteur, UMR3691 CNRS, Equipe Labellisée Ligue Contre le Cancer, F-75015, Paris, France.
[2]Sorbonne Université, Collège doctoral, F-75005 Paris, France.
[3]Institut Curie, PSL Research University, Centre de Recherche, Laboratoire de Spectrométrie de Masse Protéomique, 26 rue d'Ulm, Paris 75248 Cedex 05, France
[4] Helmholtz Centre for Infection Research, Inhoffenstrasse 7, 38124 Braunschweig, Germany

Correspondance to Sandrine Etienne-Manneville. Orcid : 0000-0001-6651-3675. Cell Polarity, Migration and Cancer Unit, Institut Pasteur, 25 rue du Dr Roux, 75724 Paris cedex 15, France. sandrine.etienne-manneville@pasteur.fr

*Authors contributed equally to this work

Short Title: Cdc42 isoform specificities

Abstract

The small G-protein Cdc42 is an evolutionary conserved polarity protein and a key regulator of the cytoskeleton as well as membrane traffic. In vertebrates, alternative splicing gives rise to two Cdc42 proteins; the ubiquitously expressed isoform (Cdc42u), and the brain isoform (Cdc42b). The two isoforms only differ in their carboxy-terminal sequence, which includes the CAAX box bearing the lipid anchors of Cdc42. Here we show that these divergent sequences do not directly affect the interaction of Cdc42 and its panel of binding partners (effectors), but rather contribute to the distinct subcellular localization and function of the two proteins. In contrast to the essentially cytosolic and plasma membrane associated Cdc42u, Cdc42b localizes to intracellular membrane compartments. In astrocytes and neural precursors, which, both naturally express the two variants, we show that Cdc42u alone fulfills the polarity function required for directed persistent migration whereas Cdc42b, embodies the major isoform regulating endocytosis. Both Cdc42 isoforms act in concert by contributing their specific functions to elucidate the complex process of chemotaxis of neural precursors, demonstrating that the expression pattern of the two isoforms is decisive for the specific behavior of cells.

Introduction

Cdc42 is a small G protein of the Rho family (Etienne-Manneville and Hall, 2002). Like most Rho GTPases, it switches between a GDP-bound inactive status and a GTP-bound form that can activate a large panel of effector proteins. Through these effectors, Cdc42 participates in numerous signaling cascades regulating a wide range of cellular responses. Cdc42 is more particularly known for its fundamental role in the control of polarity during cell asymmetric division, cell differentiation, and cell migration in organisms ranging from yeast to mammals (Etienne-Manneville, 2004). Cdc42–mediated signaling controls cytoskeleton rearrangement, which affects various actin and/or microtubule-dependent cellular processes and plays a key role in endo- and exocytosis as well as vesicle transport (Chen et al., 2005; Erickson and Cerione, 2001; Ridley, 2006; Wu et al., 2000). Functional dysregulation of Cdc42 has been implicated in the pathology of several disease states and developmental disorders, including cancer (Aspenstrom, 2018; Martinelli et al., 2018). Studies using constitutively active or dominant-negative Cdc42 mutants showed that Cdc42 was an oncoprotein which promotes cellular transformation and metastasis in the context of loss of polarity (Fidyk et al., 2006; Johnson et al., 2010). On the contrary,gene knockout studies suggested that Cdc42 might function as a tumor suppressor because targeted knockout of the CDC42 gene in hepatocytes or blood stem/progenitor cells resulted in the development of hepatocellular carcinoma or myeloproliferative disease in mice (van Hengel et al., 2008). This ambiguity makes understanding the role of Cdc42 in cancer challenging.

The lacunae in the previous studies carried in cancer cells is that they have been almost exclusively focused on one isoform of Cdc42. The human Cdc42 gene which is located on chromosome 1 gives rise to three transcripts via alternative splicing, which translate into two distinct Cdc42 isoforms. The ubiquitous isoform (Cdc42u), which does not include the exon 6, but the alternative exon 7, is ubiquitously expressed (Marks and Kwiatkowski, 1996). In contrast, the so-called brain isoform (Cdc42b), generated by translation of the exons 1-6, was initially detected in brain tissue. More recently it was also found in a range of commonly used laboratory cell lines, including HEK and MDCKII cells (Wirth et al., 2013). This splice variant may thus also be expressed in non-brain tissue cells underlining the need to clarify the functional differences between the two Cdc42 variants. Using astrocytes and neural precursor cells (NPCs) (Yap et al., 2016), which both express the two Cdc42 variants, we unravel the specific functions of the two isoforms in polarity, endocytosis and cell migration.

Results and Discussion

Brain and ubiquitous Cdc42 display different intracellular localization

Alternative splicing of the Cdc42 gene gives rise to the ubiquitous or the brain isoform, which only differ in the last 10 amino acids including the CAAX box (Fig. 1A). The divergent CAAX boxes are subjected to different lipid modifications. Both isoforms are geranyl-geranylated but the brain isoform can bear an additional palmitoyl group attached to the last cysteine residue in a reversible manner (Kang et al., 2008; Nishimura and Linder, 2013). To compare the localization patterns in glial cells, constructs encoding each fluorescently-tagged Cdc42 isoform were microinjected into astrocytes and visualized in live cells. Movie 1 shows non-migrating astrocytes expressing GFP-Cdc42b together with mCherry-Cdc42u which is mainly cytosolic, whereas Cdc42b appears largely associated with intracellular compartments. We then observed the localization of Cdc42 isoforms in cells actively migrating in an in vitro wound-healing assay (Movies 2 and 3), previously shown to activate Cdc42 (Etienne- Manneville and Hall, 2001). Both isoforms accumulated at the leading edge of the plasma membrane (Fig. 1B panel 3), where Cdc42 has been shown to be recruited and activated by integrin-mediated recruitment of the GEF β-PIX (Osmani et al., 2010). Cdc42b was also clearly visible on the Golgi apparatus, co-localizing with the cis-marker GM130 (Fig.1B panel 1 and 1C) and accumulated on vesicular compartments, where it colocalized with the early endosome marker EEA1 (Fig. 1B panel 2 and 1D). In contrast, Cdc42u was rarely detectable at these sites (Movie 3, Fig.1B).

Since the two Cdc42 isoforms have different CAAX box sequences, we examined the role of lipid modifications in their specific intracellular localization. Suppression of geranyl-geranylation by a CVLL to SVLL mutation in Cdc42u CAAX motif (u(SVLL)) (Nishimura and Linder, 2013) led to its accumulation in the nucleus

(Fig. 1E). A similar CCIF to SCIF mutation in Cdc42b (b(SCIF)) to prevent all lipid modification of Cdc42b resulted in complete loss of endomembrane-binding and cytosolic distribution of the protein. In contrast, the CCIF to CSIF mutation (b(CSIF), which specifically prevents palmitoylation but not geranyl-geranylation, inhibited recruitment of Cdc42b to the plasma membrane and on endocytic vesicles but did not prevent its association with the Golgi (Fig.1E), suggesting that palmitoylation controls the recruitment of Cdc42b to the cytoplasmic vesicles.

We confirmed the role of lipid anchors in the membrane association of Cdc42 isoforms by treating cells with GGTI298, which prevents both geranyl-geranylation and palmitoylation, or with 2-bromopalmitate (2BP), a specific inhibitor of palmitoylation (Fig. S1A). We conclude that the lipid modifications of the carboxy-terminal domain of Cdc42 isoforms are crucial for their specific membrane association.

Brain and ubiquitous isoforms show similar binding partners

In order to determine whether the difference in the carboxy-terminal sequence of the two isoforms may directly affect the binding of partner proteins and effectors, we used HEK cells to perform a proteomic screen of potential interactors using GFP-trap pull-down assay followed by quantitative mass spectrometry. Following transient transfection, both GFP-tagged Cdc42 isoforms were overexpressed and displayed a similar cytoplasmic localization (Fig. 2A). Comparison of the mass spectrometry screens of both wild type (WT) isoforms did not reveal striking differences in the list of principal interactors (Fig. 2B et S2A). To assess the interaction of each isoforms with their major effectors, we then performed the quantitative mass spectrometry screen on the constitutively active V12 variants of each isoform. This assay, in which we observed the increased pull down of the classical effectors of Cdc42 like BORGs, N-WASP, IQGAPs etc, (Fig. 2C et S2B) did not show any significant difference between both isoform (Fig. 2C). These results strongly suggest that despite their divergent carboxy-terminal sequences, both Cdc42 isoforms share the same potential interactors.

Cell polarization relies on ubiquitous Cdc42

With different localization but similar potential partners, we sought for any functional differences between the two isoforms. Primary rat astrocytes were transfected with siRNAs to selectively knock down brain (si-b1, si-b2) or ubiquitous (si-u1, si-u2) Cdc42 or with a siRNA targeting a common sequence (si-both) to simultaneously inhibit expression of both isoforms. Expression of Cdc42b was assessed by immunoblotting using a Cdc42 antibody specific for the brain isoform (Fig. S1C, S1D). For lack of an antibody specific for the ubiquitous variant, we used qPCR to quantify Cdc42u expression at the mRNA level (Fig. S1E, S1F). qPCR quantification of Cdc42 upon knockdown of each isoform revealed that roughly 15% of the total Cdc42 mRNA pool in astrocytes encodes the brain isoform (Fig. S1F) (Yap et al., 2016). Cdc42 is a critical regulator of processes contributing to front-to-rear polarization and directed astrocyte migration, such as Golgi and centrosome re-positioning (Etienne- Manneville and Hall, 2001; Hehnly et al., 2010; Osmani et al., 2006; Robel et al., 2011). To determine the contribution of each Cdc42 isoform to this process, Cdc42 knockdown cells were subjected to a scratch-wound migration assay. Cell tracking revealed that knockdown of both Cdc42 isoforms did not influence the migration velocity in astrocytes, but led to a strong decrease in directionality (83% to about 55%) and persistence (85% to about 60%) of migration (Fig. 3A-3C). The specific depletion of Cdc42u led to similar results with a significant decrease in the directionality and persistence of migration, whereas Cdc42b depleted cells migrated similarly as control astrocytes (Fig. 3A-3C). Associated with the alteration of migration directionality and persistence, Golgi reorientation in cells at the wound edge was dramatically impaired following depletion of both Cdc42 isoforms,

similarly upon specific depletion of the Cdc42u (Fig. 3D). In contrast, Cdc42b knockdown had no detectable effect (Fig. 3D). To determine whether the lack of function of Cdc42b was due to its relatively low level of expression, siRNA-resistant Cdc42u (u^{RES}) or Cdc42b (b^{RES}) were expressed. u^{RES}, but not b^{RES} rescued centrosome reorientation in astrocytes depleted in both isoforms (si-both) (Fig. 3E). A non-lipid modified mutant of Cdc42u (u^{RES}(SVLL)), unable to reach the plasma membrane (Fig. 1E) did not rescue Golgi reorientation (Fig. 3E), pointing to the essential role of plasma membrane recruitment in Cdc42 polarity functions.

The Par6/aPKC polarity complex is a key mediator of Cdc42 function in astrocyte polarization. We tested whether Cdc42 isoforms differentially interacted with Par6 and aPKC by performing immunoprecipitation of constitutively active GFP-tagged Cdc42b and Cdc42u in HEK cells (Fig. S2C, S2D). We could not detect any significant difference in binding confirming the proteomic analysis of the interactome (Fig. S2A-S2D and 2B). However, depletion of Cdc42u or both Cdc42 variants, but not of Cdc42b alone, prevented PKCζ recruitment to the cell leading edge observed by immunofluorescence (Fig. 3F). Together, these observations point to the ubiquitous plasma-membrane localized Cdc42u as the main regulator of the Par6/aPKC complex, cell polarity and directed migration and strongly suggest that the subcellular localization of Cdc42 is crucial in allowing its interaction with its effectors.

Brain Cdc42 is the major Cdc42 isoform involved in endocytosis

Since Cdc42b strongly localizes to EEA1-positive endosomes (Fig. 1D), we examined the role of Cdc42 isoforms in astrocyte pinocytosis. Knockdown of both isoforms reduced by half the percentage of dextran uptake in primary astrocytes (Fig. 4A). While depletion of Cdc42u only caused a minor reduction of dextran internalization (by 10 to 20%), knockdown of Cdc42b significantly decreased the uptake rates (by approximately 40%; Fig. 4A). The predominant role of brain isoform in pinocytosis was confirmed by rescue experiments in astrocytes depleted for both isoforms. GFP-$Cdc42b^{RES}$ led to a stronger rescue than GFP-$Cdc42u^{RES}$ (Fig. 4B). The non-lipid-modified mutants of either isoform (b^{RES}(SCIF), u^{RES}(SVLL)) did not rescue dextran uptake (Fig. 4B). Furthermore, overexpression of the non-palmitoylable Cdc42b mutant (b^{RES}(CSIF)) did not restore the dextran uptake (Fig. 4F) indicating that palmitoylation, which promotes Cdc42b association with intracellular vesicles (Fig. 1E) is crucial for its function in pinocytosis. Dextran uptake experiments using specific inhibitors of lipid modification (GGTI298 or 2BP) confirmed these findings (Fig. S1B). These results show that palmitoylated Cdc42b is the major Cdc42 isoform involved in pinocytosis in migrating astrocytes.

N-WASP is a major Cdc42 effector previously shown to be involved in macropinocytosis (Kessels and Qualmann, 2002; Legg et al., 2007). We tested whether Cdc42 isoforms differentially interacted with N-WASP by performing immunoprecipitation of constitutively

active GFP-tagged Cdc42b and Cdc42u overexpressed in HEK cells (Fig. S2E). We could not detect any significant difference in the ability of N-WASP to bind the two isoforms, confirming once again the proteomic analysis of the interactome (Fig. 2B and S2G). However, when looking at the localization of N-WASP in migrating astrocytes, we found that it colocalized on large macropinosomes and accumulated at the front of the cell protrusion, together with Cdc42b (Fig. 4C). siRNA-mediated depletion of N-WASP (Fig. 4D) inhibited dextran uptake in migrating astrocytes to a similar level as Cdc42b knock-down (Fig. 4A and 4E). A double knockdown of Cdc42b and N-WASP caused similar reduction in dextran uptake (~40%) as seen for their individual depletion (Fig. 4E). Moreover, macropinocytosis was rescued by GFP-N- WASP overexpression in Cdc42b depleted cells (Fig. 4F) confirming that both proteins act within the same signaling pathway to drive pinocytosis. These data indicate that endosome-associated Cdc42b is a major regulator of N-WASP-mediated pinocytosis.

Both Cdc42 isoforms contribute their specific functions during chemotaxis of neural precursor cells

We then determined the specific functions of each Cdc42 isoform in a more physiological and complex cellular model. During development neural precursor cells (NPCs) can differentiate into mature neurons or into glial cells, such as astrocytes. When analyzing mRNA levels of Cdc42 isoforms in NPCs, we found approximately identical levels of co-expression (Fig. S3A). Like in astrocytes, Cdc42u and Cdc42b displayed distinct subcellular localization (Fig.S3B). The ubiquitous isoform was mainly visible in the cytosol and at the plasma membrane while the brain isoform localized to intracellular EEA1-positive vesicles and to the Golgi apparatus (Fig. S3B, S3C). NPCs grow in a primary 3D tissue culture system (neurospheres) and their migration can be observed when neurospheres are placed on an adhesive substrate (Durbec et al., 2008) (Fig. 5A). Using video microscopy, we first analyzed the exit of NPCs from neurospheres. Directional persistence of migration decreased when NPCs were depleted of Cdc42u (from 76% to 58-60%) or of both isoforms (to 50%), but did not require the expression of Cdc42b (Fig 5A, 5B; movies 5 and 6) or of N-WASP (Fig. S3D). We next performed dextran uptake assays in siRNA treated NPCs. Cdc42b specific depletion, like N-WASP depletion, significantly decreased dextran uptake into NPCs, whereas knockdown of Cdc42u only had a mild effect (Fig. 5C and S3E). These results confirmed in NPCs the predominant role of Cdc42u in the control of cell polarity and of Cdc42b in pinocytosis. NPCs migrate long distances from their zones of origin to their final destination where they differentiate, following gradients of chemoattractants (Leong et al., 2011). In this context, endocytosis had been shown to be required for the processing of chemotactic signals (Zhou et al., 2007). We used a Boyden chamber- based xCelligence-assay to analyze the chemotactic migration of astrocytes (Fig. 5D) and NPCs (Fig. 5E). In the absence of a gradient, astrocytes and NPCs barely migrated through the filter (Fig. S3F, S3G), whereas addition of FBS in the lower compartment induced the chemotactic migration of both astrocytes and NPCs (Fig. 5D, 5E). When astrocytes or NPCs were transfected with siRNAs targeting both

Cdc42 isoforms, chemotaxis was strongly reduced (Fig. 5D, 5E). For both cell types, a similar result was obtained following Cdc42u specific depletion. Interestingly, Cdc42b depletion led to a significant decrease in NPC chemotaxis, without altering astrocyte migratory behavior (Fig. 5D, 5E). The knockdown of N-WASP similarly resulted in decreased chemotaxis efficiency in NPCs without affecting astrocyte chemotaxis (Fig. 5F, 5G), strongly suggesting that regulation of Cdc42b- and N-WASP-mediated pinocytosis plays a key role in NPCs chemotaxis.

While Cdc42b constitutes the predominant splice variant in the regulation of macropinocytosis in astrocytes and NPCs, efficient cell polarization, directed and persistent migration as well as chemotaxis in astrocytes seem to solely require the ubiquitous isoform. The ubiquitous isoform is thus the prevalent splice variant involved in the crucial function of Cdc42 in the regulation of cell polarity. However, with the function of Cdc42b in the formation of dendritic filopodia and spines (Kang et al., 2008; Wirth et al., 2013) and its role in endocytosis and NPC chemotaxis, increasing evidence suggests that the brain variant has important specific functions that distinguish it from Cdc42u.

NPC migration is a crucial step in brain development and conditional deletion of both Cdc42 isoforms in mouse NPCs has been shown to cause malformations in the brain (Chen et al., 2006). Our results indicate that the two Cdc42 isoforms may nevertheless contribute different functions to the behavior of NPCs, underlining that the molecular regulators of NPC migration in brain development are far from being understood. A detailed characterization of regulators of NPC migration may also help to understand the molecular and genetic causes of a group of severe brain development disorders in human, together known as Neural Migration Disorders (NMDs).

In conclusion, our result show that although both Cdc42 isoforms have non- redundant functions in the cell, they surprisingly share most of their protein effectors. This strongly suggest that Cdc42 interaction with their effectors and cellular function depends on its intracellular localization which is dictated by the carboxy-terminal sequence and lipid modifications. Future work will focus on deciphering how the amino acid sequence and/or the lipid modifications lead to such radical differences in Cdc42 localization.

Materials and Methods

Antibodies and inhibitors

The following primary antibodies were used in this study: rat monoclonal anti-α-tubulin (AbDSerotec MCA77G), mouse monoclonal anti-GM130 (BD Transduction 610823), rabbit polyclonal anti-pericentrin (Covance PRB 432-C), rabbit polyclonal anti-N-WASP (Abcam AB23394), rabbit polyclonal anti-PKCζ C-20 (Santa Cruz Biotech S C-216), mouse anti-EEA1(BD biosciences 610457) and HRP coupled anti-GFP (Abcam ab6663). As secondary antibodies we used standard antibodies from Jackson ImmunoResearch: Cy5 conjugated donkey anti-mouse, Alexa Fluor 488 conjugated donkey anti-rat, TRITC conjugated donkey anti-rabbit, as well as HRP coupled donkey anti-mouse, anti-rabbit and anti-goat. For Western Blot detection of Cdc42b a custom-made isoform specific rabbit polyclonal antibody was generated by Covalab using 2 peptides for 2 immunization steps. Peptide 1 for first immunization step: C-AALEPPETQPKRK-coNH2 (Cdc42b amino acids 175-187); peptide 2 for second immunization step: C-ETQPKRK-coNH2 (Cdc42b amino acids 181-187). The antibody was subsequently purified from the anti-serum via immobilized peptide 2. DAPI in ProLong Gold Antifade Reagent (Life Tech) was used to visualize nuclei. To suppress lipid modification of Cdc42 isoforms, cells were treated overnight in 120 µM 2BP (to suppress palmitoylation; Sigma) or 20 µM GGTI298 (to suppress geranyl-geranylation and palmitoylation; Tocris)

Cell Culture

All procedures were performed in accordance with the guidelines approved by the French Ministry of Agriculture, following European standards. Preparation of neurosphere cultures was performed as described (Calaora et al., 2001). Briefly, the striata of E14 OFA rats were removed from the embryos and mechanically dissociated before cells were seeded at 1.2×10^5 cells/ml in uncoated 260 ml culture flasks (Fisher Bioblock Sc.). Culture medium consisted of DMEM/F-12 (Gibco) supplemented with 2% B27 (Gibco) and 50µg/ml gentamicin (Sigma) in the presence of 20 ng/ml EGF (R&D Systems Europe). Media were supplemented with 20 ng/ml EGF every 48h, and spheres passaged using 0.025% trypsin-EDTA (Gibco) on the fourth and sixth day in culture. Human FGF-b (RayBiotech) was also added to the medium at 10 ng/ml for the first four days of culture. For preparation of primary astrocyte cultures the telencephalon of E18 OFA rats were removed from the embryos and mechanically dissociated. Cells were plated and maintained as previously described (Etienne-Manneville, 2006) using 1g/l glucose DMEM (Gibco) supplemented with 10% FBS (Eurobio) and penicillin/streptomycin (10,000 U ml^{-1} and 10,000 µg ml^{-1}; Gibco) as culture medium. HEK and HeLa cells were cultured in 4.5g/l glucose DMEM (Gibco) supplemented with FBS and antibiotics as added for astrocytes. All cells were kept in a 37°C incubator at 5% CO2.

Proteomic screen of Cdc42 interactors and Mass Spectrometry analysis

Firstly, GFP Immunoprecipitation assay was carried out, where HEK cells transfected with GFP tagged constructs of Cdc42 were lysed using 50mM TRIS base, Triton 2 %, 200mM NaCl as well as 1 tablet/10 ml protease inhibitor Mini-complete, EDTA-free (Roche). After removal of insoluble fragments via centrifugation at 12,000 g for 25 min, lysates were incubated with 15 µl of GFP-Trap Agarose beads from Chromotek for 1h at 4 °C on a rotary wheel. The beads were washed using a wash buffer comprising of 50mM TRIS base, 150mM NaCl, 1mM EDTA and 2.5 mM MgCl2 and pH adjusted to 7.5. Following the final wash beads were stored with wash buffer in 4°C prior to depositing at the Institut Curie Mass Spectrometry and Proteomics facility (LSMP).

Where proteins on beads were washed twice with 100µL of 25mM NH_4HCO_3 and we performed on-beads digestion with 0.2µg of trypsine/LysC (Promega) for 1 hour in 100µL of 25mM NH_4HCO_3. Sample was then loaded onto a homemade C18 StageTips for desalting. Peptides were eluted using 40/60 MeCN/H_2O + 0.1% formic acid and vacuum concentrated to dryness.

Online chromatography was performed with an RSLCnano system (Ultimate 3000, Thermo Scientific) coupled to an Orbitrap Fusion Tribrid mass spectrometer (Thermo Scientific). Peptides were trapped on a C18 column (75µm inner diameter × 2cm; nanoViper Acclaim PepMapTM 100, Thermo Scientific) with buffer A (2/98 MeCN/H_2O in 0.1% formic acid) at a flow rate of 4.0µL/min over 4 min. Separation was performed on a 50cm x 75µm C18 column (nanoViper Acclaim PepMapTM RSLC, 2µm, 100Å, Thermo Scientific) regulated to a temperature of 55°C with a linear gradient of 5% to 25% buffer B (100% MeCN in 0.1% formic acid) at a flow rate of 300nL/min over 100 min. Full-scan MS was acquired in the Orbitrap analyzer with a resolution set to 120,000 and ions from each full scan were HCD fragmented and analyzed in the linear ion trap.

For identification the data were searched against the Homo sapiens (UP000005640) SwissProt database using Sequest HF through proteome discoverer (version 2.2). Enzyme specificity was set to trypsin and a maximum of two missed cleavage site were allowed. Oxidized methionine, N-terminal acetylation, and carbamidomethyl cysteine were set as variable modifications. Maximum allowed mass deviation was set to 10 ppm for monoisotopic precursor ions and 0.6 Da for MS/MS peaks.

The resulting files were further processed using myProMS (Poullet et al., 2007) v3.6 (work in progress). FDR calculation used Percolator and was set to 1% at the peptide level for the whole study. The label free quantification was performed by peptide Extracted Ion Chromatograms (XICs) computed with MassChroQ version 2.2 (Valot et al., 2011). For protein quantification, XICs from proteotypic peptides shared between compared conditions (TopN matching) with no missed cleavages were used. Median and scale normalization was applied on the total signal to correct the XICs for each biological replicate. To estimate the significance of the change in protein abundance, a linear model (adjusted on peptides and

biological replicates) was performed and p-values were adjusted with a Benjamini–Hochberg FDR procedure with a control threshold set to 0.05. The mass spectrometry proteomics data have been deposited to the ProteomeXchange Consortium via the PRIDE (Vizcaino et al., 2016) partner repository with the dataset identifier PXD017477(username: reviewer51683@ebi.ac.uk, Password: 4fNr03LX)

Cell transfection and RNAi

siRNA constructs or plasmids were introduced into rat astrocytes or NPCs by Nucleofection technology (Amaxa Biosystems) using Lonza protocols. All siRNAs were obtained from Eurofins except for a non-targeting control, which was obtained from Dharmacon. To quantify knockdowns, protein samples were analyzed using ECL immunoblotting and ImageJ. Alternatively, mRNA levels were measured using qPCR (see below). In each case, cells were analyzed 4 days after transfection with siRNAs. Transfection of HEK293 and HeLa cells with plasmids was performed with the calcium phosphate method.

si-N-WASP: 5'-CUUGUCAAGUAGCUCUUAA(dTdT)-3'
si-both: 5'-UGAUGGUGCUGUUGGUAAA(dTdT)-3'
si-Pl1: 5'-CAAUAAUGACAGACGACCU(dTdT)-3'
si-Pl2: 5'-GCAAUAUUGGCUGCCUUGGUU(dTdT)-3'
si-Br1: 5'-CCAUUUAACAAUCGACUUA(dTdT)-3'
si-Br2: 5'-ACUCAACCCAAAAGGAAGUUU(dTdT)-3'

Real time qPCR

For isolation of total RNA striatal neurospheres or cultured astrocytes were prepared from E14 or E18 rat embryos respectively. RNA was isolated by using the RNeasy Mini Kit (QIAGEN) followed by the digestion of contaminating genomic DNA (Turbo DNA Free). RNA concentration and purity were determined by spectrophotometry. cDNA synthesis was performed according to kit instructions (VILO cDNA synthesis; Invitrogen). Quantitative real-time PCR was performed using Applied Biosystems custom TaqMan Gene Expression Assays designed using the Taqman Assay Search Tool (Life Technologies) for the ubiquitous Cdc42 isoform. Assay Rn00821429_g1 was used to quantify panCdc42 mRNA levels (both isoforms). As endogenous control we used PGK1 (assay Rn00821429_g1) and Ppia (assay Rn00690933_m1) (all from Life Technologies) for astrocytes and Casc3 (Rn00595941_m1) and Eif2b1 (Rn00596951_m1) for neural precursor cells. Real-time PCR amplification was performed on a Sequence Detection System (7500; Applied Biosystems) using TaqMan Universal MMix II (Life Technologies) according to the manufacturer's instructions. Thermal cycling conditions were as follows: 50°C for 2 min, 95°C for 10 min followed by 40 cycles of 95°C for 15 s, and 60°C for 1 min. Data were collected and analyzed with the SDS software v2.0.6 (Applied Biosystems). The comparative CT Method ($\Delta\Delta C_T$) was used as described in the AB7500 SDS guidelines.

Live spinning disk confocal microscopy

To study protein localization in live cells, plasmids encoding the GFP- or mCherry tagged protein were microinjected into wound border astrocytes plated on glass bottom dishes (MatTek) and scratched 1h before microinjection. Live imaging was done 4-8h laterusing a spinning disk confocal microscope (Perkin Elmer Ultra View ERS) equipped with a heating chamber (37°C) and CO2 supply (5%).

Centrosome/Golgi reorientation and PKCzeta localization assays

Scratch-induced cell polarization of astrocytes was studied as detailed previously (Etienne-Manneville, 2006). Briefly, a monolayer of astrocytes plated on poly-L-ornithine (Sigma) coated coverslips was scratched and fixed 8h later followed by immunostaining of centrosome, Golgi and microtubules. Wound border cells were counted as polarized when the centrosome and Golgi were situated within the 90° or 120°C section of a virtual circle drawn around the nucleus that faces the wound (see Fig. 4B). Images were acquired on a Leica DM6000 epifluorescence microscope equipped with 40×, NA 1.25 and a 63×, NA 1.4 objective lenses and were recorded with a CCD camera (CoolSNAP HQ, Roper Scientific) using Leica LAS AF software. PKCzeta accumulation at the cell front was studied in knockdown cells situated on poly-L-ornithine coated cover slips and fixed 4h after wounding.

Cell Spreading Assays

Sixteen-well E-plates (Ozyme) were pre-coated with 25µg/ml Fibronectin (Sigma) for NPCs or used uncoated for astrocytes. Single cell suspensions of $1x10^5$ NPC or $5x10^4$ astrocytes in 100µl of normal culture medium were added per well. Each condition (control or siRNA Transfected) was run in triplicate wells. Cell adhesion and spreading was measured as changes in impedance measured on the xCelligence RTCA DP Analyzer (ACEA Biosciences) according to the manufacturer's instructions.

Cell Migration Assays

Astrocyte wound healing and neurosphere migration assays: For live imaging of astrocyte wound healing experiments, Transfected astrocytes were seeded into poly-L-ornithin (Sigma) coated 12-well standard plastic dishes using normal cell culture medium. Cell monolayers were scratched immediately before image acquisition followed by addition of 20mMHepes (Sigma) as well as antioxidant (Sigma) to the medium and addition of liquid paraffin on top of the medium. Video time-lapse data were acquired on a Zeiss Axiovert 200M microscope equipped with a 37°C humidified heating chamber as well as CO2 supply (5%) by taking pictures every 15min over 16h and analyzed by manual tracking of cells using ImageJ, as described previously (Camand et al., 2012). For tracking of NPCs, neurospheres obtained from suspension cultures of transfected cells were plated into fibronectin coated

12-well plastic dishes immediately before life imaging followed by addition of Hepes, antioxidant and paraffin as for astrocytes. Images were taken every 5 min for NPCs.

Chemotaxis assays

The bottom wells of sixteen-well C.I.M plates (Ozyme) were filled with 160µl of normal culture medium for astrocytes or NPCs containing 10% FBS in both cases. The upper wells were filled with 50µl of normal culture medium without FBS (but containing B27 in case of NPCs). After 1h of equilibration in the incubator, single cell suspensions of $1x10^5$ NPC or $5x10^4$ astrocytes in 100µl medium (without FBS) were added to the upper wells plated in the upper wells. Each condition (control or siRNA Transfected) was run in triplicate wells on the xCelligence RTCA DP Analyzer according to user guidelines. Cell migration was measured as changes in impedance with the slopes of cell migration being compared over 10h.

Endocytosis assays

Neurospheres were incubated for 1.5h at 37°C in 1mg/ml Texas Red labeled dextran (10 kDa Invitrogen), extensively washed and plated on poly-L-ornithine and fibronectin coated glass coverslips for 4h, before being fixed in 4% paraformaldehyde. Transfected astrocytes were plated on poly-L-ornithine coated coverslips and scratched 4d later followed by addition of 1mg/ml fluorescent dextran. Cells were fixed in PFA after 1.5 h and analyzed on the Leica DM6000 epifluorescence microscope described above. The relative amount of dextran uptake was determined using ImageJ to quantify the number of fluorescence maxima per cell after background subtraction.

Pull down assays

HEK cells were either transfected with plasmids encoding a GFP-tagged interaction partner or used non-transfected to test interactions with an endogenous protein. Cells were lysed using pull down buffer containing 500mM NaCl, 15mM KCl, 8mM TRIS base, 12mM HEPES free base, 3mM MgCl2, 10% (v/v) glycerol, 1% (v/v) Triton X-100 as well as 1 tablet/10ml protease inhibitor Mini-complete, EDTA-free (Roche). After removal of insoluble compounds via centrifugation, lysates were incubated with glutathione sepharose beads (GE Healthcare) coated with the other interaction partner for 30min at 4°C on a rotary wheel. Subsequently, beads were washed three times for 10min with the same buffer containing however doubled amounts of NaCl on the rotary wheel, followed by detection of associated proteins using Western Blotting.

Acknowledgements

This work was supported by the Centre National de la Recherche Scientifique and the Institut Pasteur. B.Boeda is a full-time INSERM researcher at the CNRS. J.Hänisch was funded by a Marie Curie post-doctoral grant. Y.Ravichandran was funded by the Polarnet ITN (Innovative Training Network) part of the European Commission and the Fondation pour la Recherche

Médicale. We would like to thank members of the SEM lab for support and discussion. We gratefully acknowledge the Imagopole of Institut Pasteur (Paris, France).

The authors declare no conflict of interest.

Figure 1

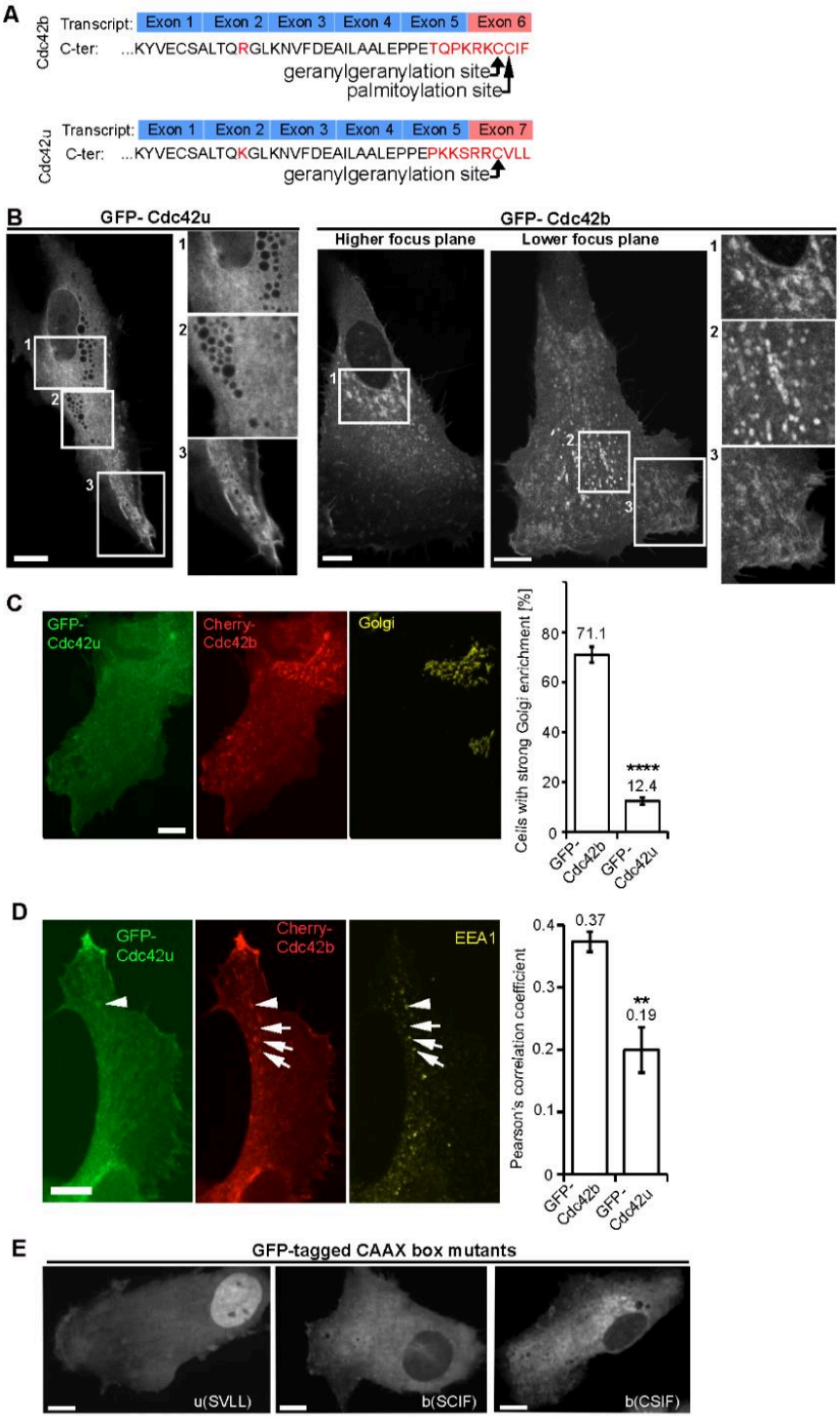
A
Cdc42b
Transcript: Exon 1 Exon 2 Exon 3 Exon 4 Exon 5 Exon 6
C-ter: ...KYVECSALTQRGLKNVFDEAILAALEPPETQPKRKCCIF
geranylgeranylation site
palmitoylation site
Cdc42u
Transcript: Exon 1 Exon 2 Exon 3 Exon 4 Exon 5 Exon 7
C-ter: ...KYVECSALTQKGLKNVFDEAILAALEPPEPKKSRRCVLL
geranylgeranylation site
B
GFP- Cdc42u
GFP- Cdc42b
Higher focus plane
Lower focus plane
C
GFP-Cdc42u
Cherry-Cdc42b
Golgi
Cells with strong Golgi enrichment [%]
71.1
****
12.4
GFP-Cdc42b
GFP-Cdc42u
D
GFP-Cdc42u
Cherry-Cdc42b
EEA1
Pearson's correlation coefficient
0.37
**
0.19
GFP-Cdc42b
GFP-Cdc42u
E
GFP-tagged CAAX box mutants
u(SVLL)
b(SCIF)
b(CSIF)

Figure 1: Localization and GDI binding of brain Cdc42 (Cdc42b) and ubiquitous Cdc42 (Cdc42u). (A) Transcribed exons and translated carboxy-terminal protein sequences of brain and ubiquitous Cdc42. (B) Confocal section images of live astrocytes expressing GFP-tagged Cdc42u or Cdc42b 5h after wounding. Right panels show higher magnification of the corresponding boxed area and highlight the different localization of the two isoforms (see corresponding movies 2 and 3). (C) Confocal stack images of GFP- Cdc42u and mCherry-Cdc42b expressing astrocytes 5h after wounding stained with anti-GM130 (cis-Golgi marker). The histogram displays the percentage of cells showing a strong colocalisation of each Cdc42 construct with GM130. (D) Confocal stack images of GFP-Cdc42u and mCherry-Cdc42b expressing astrocytes 5h after wounding stained with anti-EEA1 (early endosomes marker). The histogram displays the percentage of cells showing a strong colocalisation of each Cdc42 construct with EEA1. (E) Confocal section images showing localization patterns of GFP-tagged non-palmitoylable Cdc42b (brCSIF) or non-lipid-modified brain (br(SCIF)) or ubiquitous Cdc42 (pl(SVLL)) in live astrocytes 5h after wounding. All data are presented as means ±SEM from 3 independent experiments. All p-values were calculated using two-sided unpaired Student's t-test. ****p-value <0.0001; ***p-value <0.001; **p-value <0.01; *p-value<0.05. Scale bars: 10 μm.

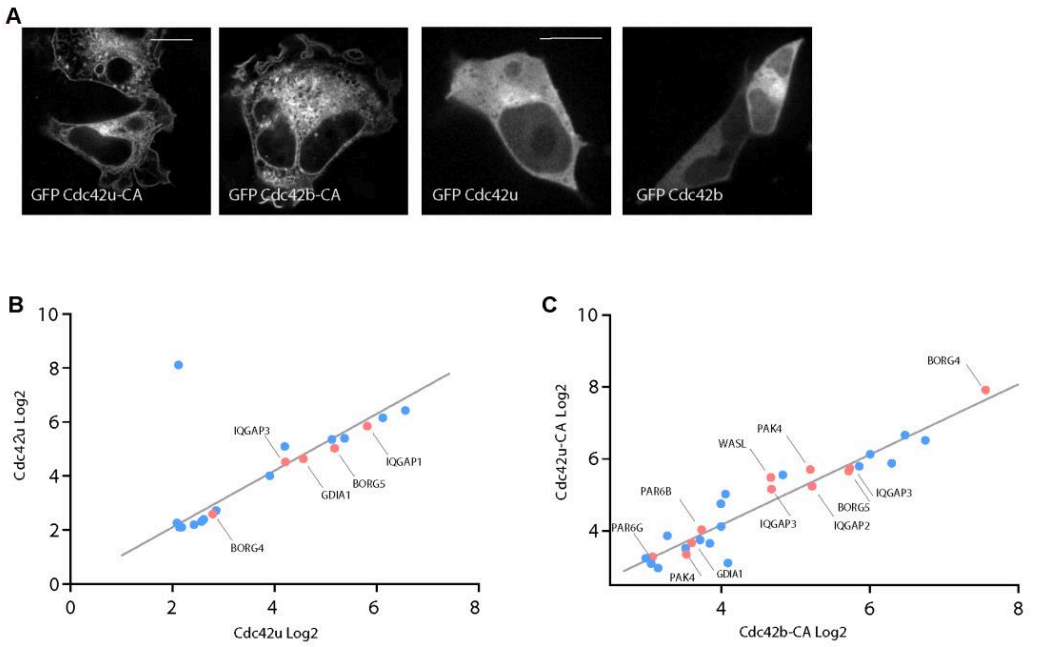

Figure 2: Cdc42u and Cdc42b share the same panel of binding partners
(A) Spinning disk images of HEK cells expressing the indicated GFP Cdc42 constructs 24h after transfection. (B-C) Graphs show common proteins or binding partners obtained by using quantitative label-free mass spectrometry analysis of proteins associated with Cdc42b-WT (wild type) and Cdc42u-WT (B) which have a peptide ratio ≥ 4 compared to GFP or Cdc42b-CA (constitutively active) and Cdc42u-CA (C) which have a peptide ratio ≥ 7 compared to GFP, p-value ≤ 0.05. Peptides used to calculate significance are ≥ 6 and number of replicates = 4. The lists of proteins corresponding to the respective WT and CA correlation plots are included in the supplementary material. (Figure S2A, S2B). Data extraction and statistical analysis was performed using myProMS software(see methods).

Figure 3

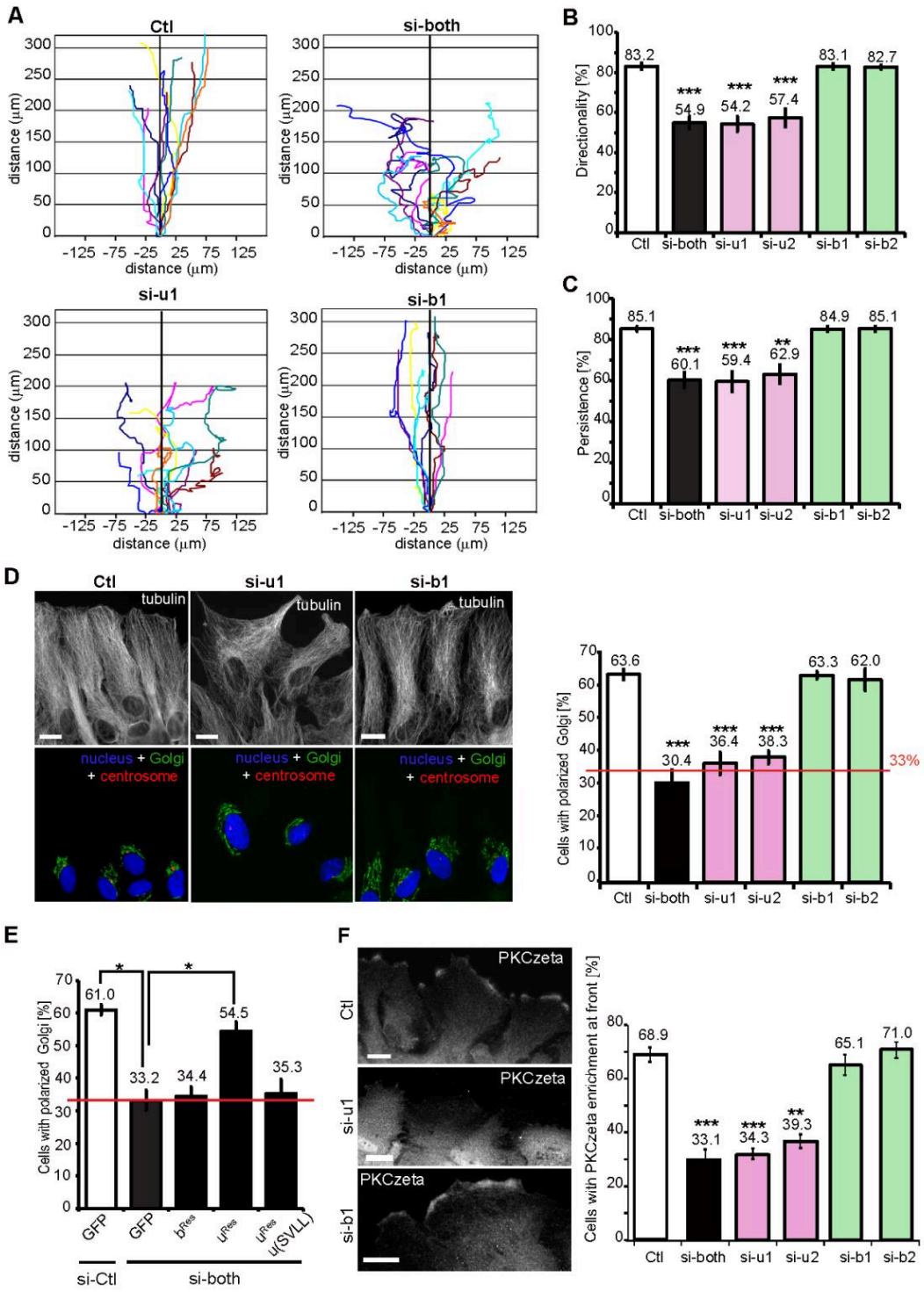
A
Ctl
si-both
si-u1
si-b1
distance (μm)
distance (μm)
B
Directionality [%]
83.2
54.9
54.2
57.4
83.1
82.7
Ctl
si-both
si-u1
si-u2
si-b1
si-b2
C
Persistence [%]
85.1
60.1
59.4
62.9
84.9
85.1
D
Ctl
si-u1
si-b1
tubulin
nucleus + Golgi + centrosome
Cells with polarized Golgi [%]
63.6
30.4
36.4
38.3
63.3
62.0
33%
E
Cells with polarized Golgi [%]
61.0
33.2
34.4
54.5
35.3
GFP
GFP
bRes
uRes
uRes u(SVLL)
si-Ctl
si-both
F
PKCzeta
Ctl
si-u1
si-b1
Cells with PKCzeta enrichment at front [%]
68.9
33.1
34.3
39.3
65.1
71.0

Figure 3: Cdc42u, but not Cdc42b control cell polarization and directed and persistent migration of astrocytes. (A) Representative trajectories of astrocytes transfected with siRNAs against the ubiquitous (si-pla1), the brain (si-br1) or both (si- both) Cdc42 isoforms and migrating in a wound healing assays for 16h. (B-C) Directionality (B) and persistence (C) of astrocytes transfected with the indicated siRNA and migrating in wound healing assays. Graphs show data presented as means ±SEM of 5 independent experiments. (D) Immunofluorescence images of astrocytes transfected with the indicated siRNA and fixed 8h after wounding. Images show microtubules (anti- tubulin, white), *cis*-Golgi (anti-GM130, green), centrosome (anti-pericentrine, red) and the nucleus (DAPI, blue). Quantification of Golgi orientation in astrocytes transfected with the indicated siRNA, 8h after wounding, in shown on the right panel. (E) Quantification of Golgi reorientation in a rescue experiment using astrocytes transfected with control siRNA or with a siRNA targeting both Cdc42 isoforms together with the indicated control (GFP) or GFP-tagged Cdc42 constructs. (F) Fluorescence images showing PKCzeta localization in wound-edge astrocytes transfected with the indicated siRNA. The graph on the right shows the percentage of cells showing PKCzeta accumulation at the cell front. Graphs show data presented as means ±SEM of 4 (for E) or 3 (for F) independent experiments. Red lines indicate the values expected for random positioning of the Golgi apparatus. Ctl: Control cells transfected with non-targeting siRNA. All p- values were calculated using two-sided unpaired Student's t-test. ****p-value<0.0001; ***p-value <0.001; **p-value <0.01; *p-value<0.05. Scale bars: 10 μm.

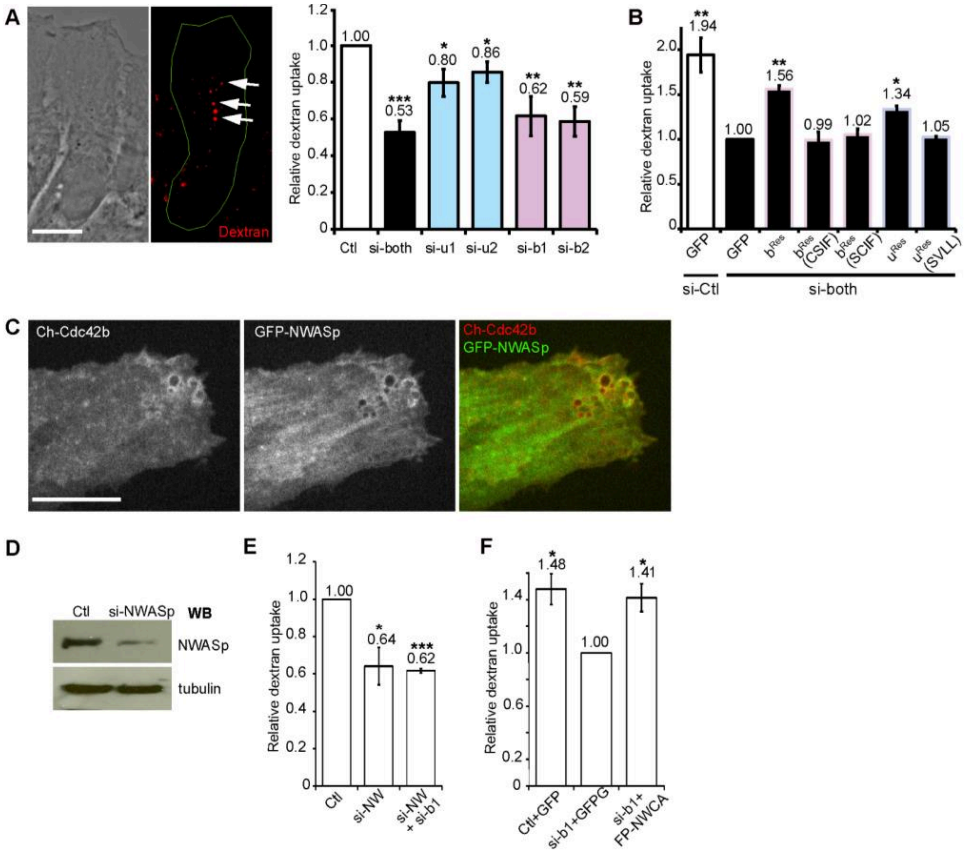

Figure 4: Cdc42b, N-WASP, but not Cdc42u control pinocytosis (A) Phase and fluorescence images showing dextran uptake in control migrating astrocytes. On the right, the graph shows the relative dextran uptake in astrocytes pretreated with the indicated Cdc42 siRNAs. (B) Quantification of relative dextran uptake in a rescue experiment using control or Cdc42-depleted astrocytes expressing the indicated Cdc42 construct. (C) Confocal section images from migrating astrocytes showing co-localization of mCherry- Cdc42b and GFP-N-WASP at the wound edge of migrating astrocytes 6h after wounding. (D) Western Blot showing N-WASP expression in control (Ctl) and N-WASP siRNA transfected astrocytes. Tubulin was used as loading control. (E) Quantification of the relative dextran uptake in astrocytes treated with indicated siRNAs against Cdc42b and/or N-WASP (si-NW) compared to control cells. (F) Quantification of relative dextran uptake in a rescue experiment using control or br-Cdc42-depleted astrocytes expressing the GFP or GFP-N-WCA (constitutively active N-WASP) constructs. All graphs show data presented as means ±SEM of n=3 experiments with at least 150 cells analyzed per condition and were normalized to the values obtained for si-both treated and GFP expressing cells. All p-values were calculated using two-sided unpaired Student's t-test.***p-value <0.001; **p-value <0.01; *p-value<0.05. Scale bars: 10 µm.

Figure 5

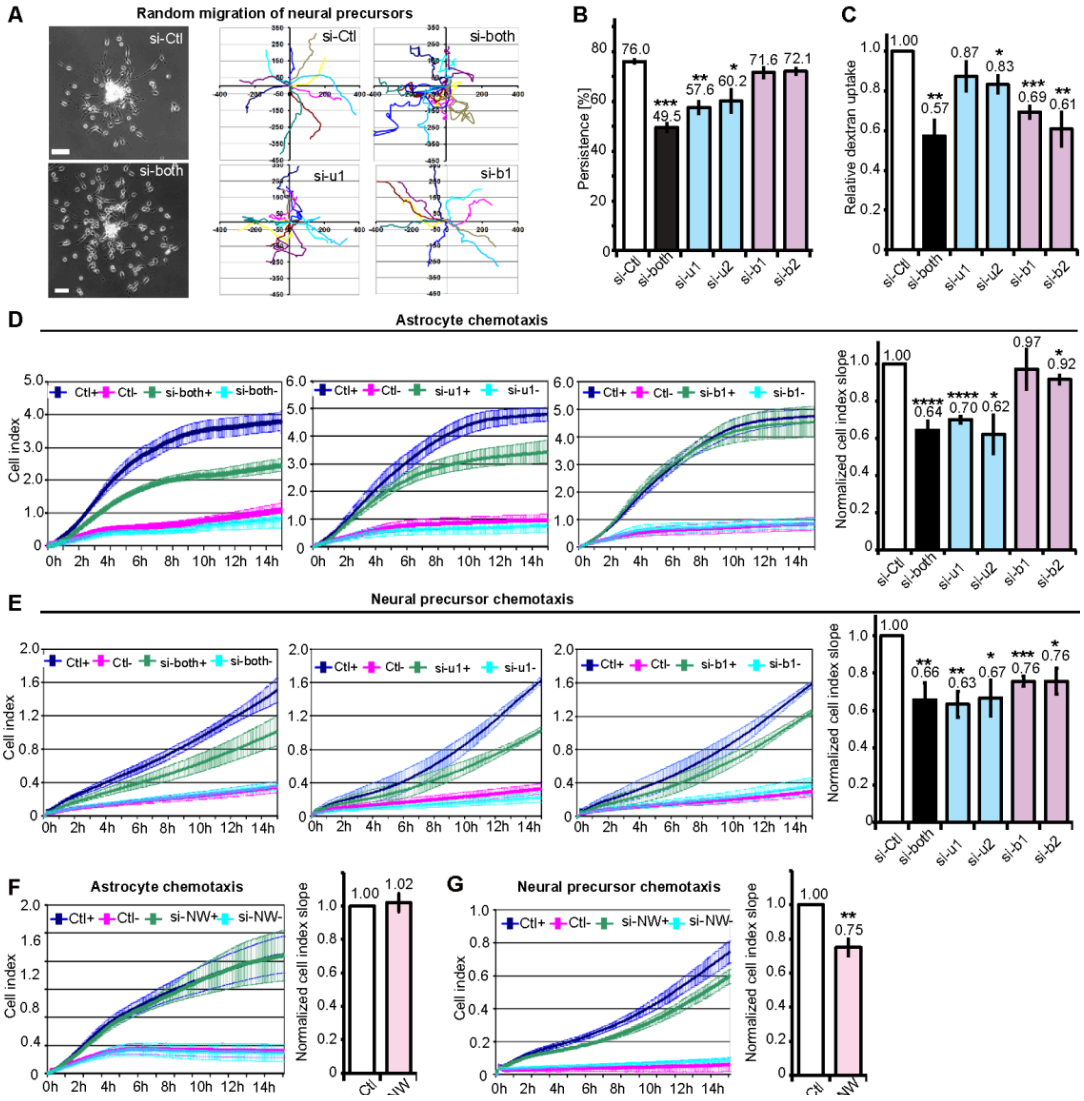
A
Random migration of neural precursors
si-Ctl
si-both
si-u1
si-b1
B
Persistence [%]
76.0
49.5
57.6
60.2
71.6
72.1
C
Relative dextran uptake
1.00
0.57
0.87
0.83
0.69
0.61
D
Astrocyte chemotaxis
Ctl+ Ctl- si-both+ si-both-
Ctl+ Ctl- si-u1+ si-u1-
Ctl+ Ctl- si-b1+ si-b1-
Cell index
0h 2h 4h 6h 8h 10h 12h 14h
Normalized cell index slope
1.00
0.64
0.70
0.62
0.97
0.92
E
Neural precursor chemotaxis
1.00
0.66
0.63
0.67
0.76
0.76
F
Astrocyte chemotaxis
Ctl+ Ctl- si-NW+ si-NW-
1.00
1.02
G
Neural precursor chemotaxis
1.00
0.75
si-Ctl
si-both
si-u1
si-u2
si-b1
si-b2

Figure 5: Cdc42 isoforms cooperate to promote neural precursor cell (NPC) chemotaxis. (A-B) Random migration of NPCs transfected with the indicated siRNA out of neurospheres. (A) Phase contrast images show transfected NPCs migrating out of neurospheres 5h after plating. Representative cell trajectories over 4h of migration are shown in the right panels. (B) Persistence of NPC migration calculated for the time period between 100min and 300min after plating. (C) Relative dextran uptake into NPCs transfected with the indicated siRNAs. Data, normalized to the control, represent means ± SEM from 3 independent experiments with at least 150 cells analyzed per condition. (D- G) Astrocyte and NPC migration in Boyden chamber-based xCelligence system assays. +: bottom well contains FBS; -: no FBS in bottom well (negative control to measure non-chemotactic migration). Curves show the impedance measurement over time in the bottom well. The graphs show the curve slopes, which indicate the rate of migration in chemotactic conditions in which FBS was contained in the bottom wells. Slopes represent means ± SEM of at least 3 independent experiments and were normalized to the control. (D-E) Chemotactic migration of astrocytes (D) or NPCs (E) upon knockdown of Cdc42 isoforms. (F-G) Effects of N-WASP (si-NW) knockdown on chemotactic migration of astrocytes (F) or NPCs (G). All p-values were calculated using two-sided unpaired Student's t-test. ****p-value<0.0001; ***p-value <0.001; **p-value <0.01; *p-value<0.05. Scale bars: 100 μm.

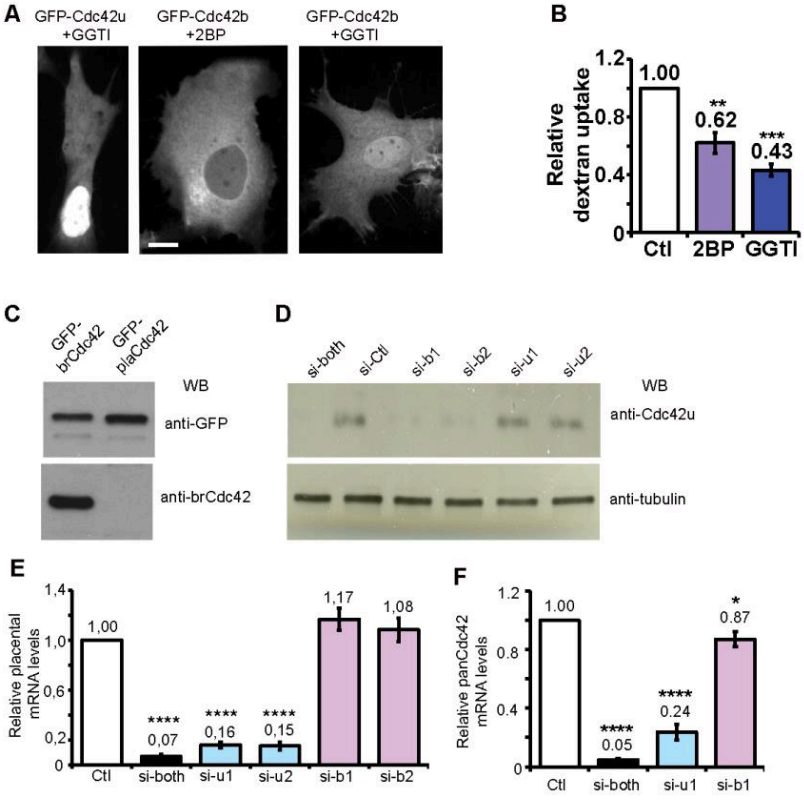

Figure S1: Inhibitors of lipid modifications confirm the role of Cdc42 geranyl-geranylation and palmitoylation in the localization and endocytic function of Cdc42b. (A) Localization of GFP-Cdc42b or GFP-Cdc42u in astrocytes pretreated overnight with inhibitors suppressing palmitoylation (2BP, 120µM) or geranylgeranylation (GGTI, 20µM). Astrocytes where treated with GGTI298, which prevents both geranyl-geranylation and palmitoylation, or with 2-bromopalmitate (2BP), a specific inhibitor of palmitoylation. (B) Histogram showing the relative dextran uptake observed in treated cells compared to control cells (Ctl). (C) Western Blot analysis of HEK cells expressing GFP-tagged Cdc42b or Cdc42u using anti-GFP antibody and a polyclonal rabbit anti-Cdc42b antibody designed to specifically detect the brain Cdc42 isoform. (D) Western Blot analysis of astrocyte lysates using anti- Cdc42b to specifically detect Cdc42 brain isoform and anti-tubulin as loading control. Astrocytes were transfected with siRNA designed against both Cdc42 isoforms (si-both), the brain isoform (si-br1, si-br2), or the ubiquitous Cdc42 variant (sipla1, sipla2). (E) QPCR data using a TaqMan assay specifically detecting the ubiquitous Cdc42 in astrocytes transfected with the indicated siRNA. (F) Full Cdc42 mRNA levels were measured using a TaqMan assay that recognizes both Cdc42 isoforms (panCdc42) in astrocytes transfected with the indicated siRNA. All data are presented as means ±SEM from 3 independent experiments. All p-values were calculated using two-sided unpaired Student's t-test. ****p-value <0.0001; ***p-value <0.001; **p-value <0.01; *p-value<0.05. Scale bars: 10 µm.

Figure S2

A

Gene	Cdc42b/GFP				Cdc42u/GFP				Description
	Ratio	Log2	p-value	Peptides used	Ratio	Log2	p-value	Peptides used	
FIGNL2	94	6.6	0.004038	8	86	6.4	7.45E-06	8	Putative fidgetin-like protein 2
FAM89A	70	6.1	0.000188	16	71	6.2	0.000223	16	Protein FAM89A
IQGAP1	56	5.8	2.5E-193	422	58	5.8	1.2E-216	414	Ras GTPase-activating-like protein IQGAP1
CDC42SE2	41	5.4	5.27E-08	16	42	5.4	1.39E-09	16	CDC42 small effector protein 2
CDC42EP1	36	5.2	1.78E-44	85	33	5.0	4.33E-53	89	Cdc42 effector protein 1
IQGAP2	35	5.1	9.99E-59	172	41	5.4	4.21E-61	166	Ras GTPase-activating-like protein IQGAP2
GDIA1	24	4.6	5.69E-06	24	25	4.6	1.18E-05	25	Rho GDP-dissociation inhibitor 1
IQGAP3	19	4.2	1.98E-45	162	23	4.5	3.84E-53	169	Ras GTPase-activating-like protein IQGAP3
CHD1	18	4.2	0.033993	7	34	5.1	0.049715	7	Chromodomain-helicase-DNA-binding protein 1
MYL6	15	3.9	1.03E-11	39	16	4.0	1.12E-13	40	Myosin light polypeptide 6
CDC42SE1	7	2.9	0.011289	13	7	2.7	0.000521	15	CDC42 small effector protein 1
CDC42EP4	7	2.8	2.96E-05	21	6	2.6	1.21E-05	22	Cdc42 effector protein 4
TNPO1	6	2.6	1.02E-23	96	5	2.4	3.36E-23	108	Transportin-1
DLEC1	6	2.6	0.021645	8	5	2.3	0.017569	8	Deleted in lung and esophageal cancer protein 1
XPO4	5	2.4	2.04E-17	48	5	2.2	2.24E-17	59	Exportin-4
CDC42EP2	5	2.2	2.72E-06	37	4	2.1	3.24E-06	41	Cdc42 effector protein 2
CSE1L	4	2.1	4.36E-47	190	4	2.1	1.18E-42	197	Exportin-2
CDC42	4	2.1	0.029057	39	278	8.1	8.72E-12	39	Cell division control protein 42 homolog
IPO5	4	2.1	6.57E-55	268	5	2.3	5.38E-67	294	Importin-5

B

Gene	Cdc42b-CA/GFP				Cdc42u-CA/GFP				Description
	Ratio	Log2	p-value	Peptides used	Ratio	Log2	p-value	Peptides used	
BORG4	189	7.6	1.036E-11	22	242	7.9	1.85E-12	22	Cdc42 effector protein 4
FAM89A	89	6.5	9.599E-05	16	101	6.7	5.02E-05	16	Protein FAM89A
FIGNL2	107	6.7	0.0005983	8	92	6.5	9.81E-05	8	Putative fidgetin-like protein 2
BORG1	64	6.0	3.056E-20	41	70	6.1	5.99E-16	35	Cdc42 effector protein 2
ACSF2	78	6.3	0.0125883	7	59	5.9	0.002924	7	Acyl-CoA synthetase family member 2, mitochondrial
CDC42SE2	58	5.9	3.708E-08	16	56	5.8	5.29E-10	16	CDC42 small effector protein 2
IQGAP1	53	5.7	1.6E-188	430	54	5.7	3.1E-205	409	Ras GTPase-activating-like protein IQGAP1
PAK4	37	5.2	9.071E-38	64	52	5.7	1.38E-42	59	Serine/threonine-protein kinase PAK 4
BORG5	52	5.7	1.124E-51	89	51	5.7	9.19E-51	85	Cdc42 effector protein 1
WIPF1	28	4.8	1.587E-06	22	47	5.6	3.55E-07	20	WAS/WASL-interacting protein family member 1
WASL	25	4.7	1.189E-21	58	45	5.5	1.49E-25	54	Neural Wiskott-Aldrich syndrome protein
IQGAP2	37	5.2	1.391E-59	180	38	5.2	1.81E-68	169	Ras GTPase-activating-like protein IQGAP2
IQGAP3	26	4.7	8.247E-53	178	36	5.2	4.94E-59	170	Ras GTPase-activating-like protein IQGAP3
TNPO2	17	4.1	0.0102385	8	33	5.0	0.000814	8	Transportin-2
CDC42BPB	16	4.0	1.749E-19	101	27	4.8	7.28E-25	99	Serine/threonine-protein kinase MRCK beta
MYL6	16	4.0	7.743E-13	41	17	4.1	1.08E-13	42	Myosin light polypeptide 6
PARD6B	13	3.7	1.926E-17	56	16	4.0	5.87E-19	53	Partitioning defective 6 homolog beta
WIPF2	10	3.3	7.123E-06	26	15	3.9	1.22E-06	26	WAS/WASL-interacting protein family member 2
CDC42BPA	13	3.7	7.513E-60	212	13	3.8	1.01E-52	208	Serine/threonine-protein kinase MRCK alpha
GDIA1	12	3.6	0.0004117	24	13	3.7	0.000166	23	Rho GDP-dissociation inhibitor 1
ISOC1	14	3.8	0.03559	8	13	3.7	0.029438	8	Isochorismatase domain-containing protein 1
TTC9C	11	3.5	0.0426658	6	11	3.5	0.047361	6	Tetratricopeptide repeat protein 9C
PAK2	12	3.5	4.932E-13	49	10	3.4	9.03E-13	48	Serine/threonine-protein kinase PAK 2
PARD6G	8	3.1	2.165E-05	16	10	3.3	2.82E-05	15	Partitioning defective 6 homolog gamma
DNMBP	8	3.0	8.002E-22	119	9	3.2	2.74E-22	117	Dynamin-binding protein
CDC42SE1	17	4.1	0.0007614	15	9	3.1	0.01929	14	CDC42 small effector protein 1
BIN3	8	3.1	5.681E-06	22	9	3.1	2.23E-06	23	Bridging integrator 3
DLEC1	9	3.1	0.0030675	8	8	3.0	0.001019	8	Deleted in lung and esophageal cancer protein 1

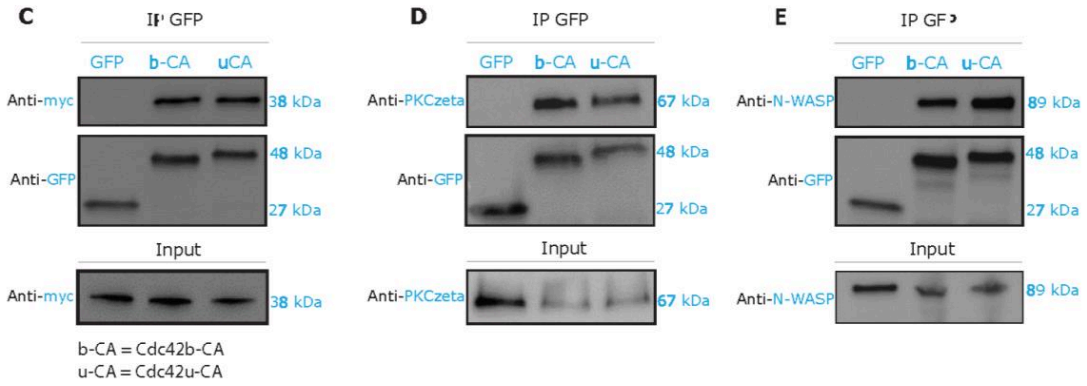

b-CA = Cdc42b-CA
u-CA = Cdc42u-CA

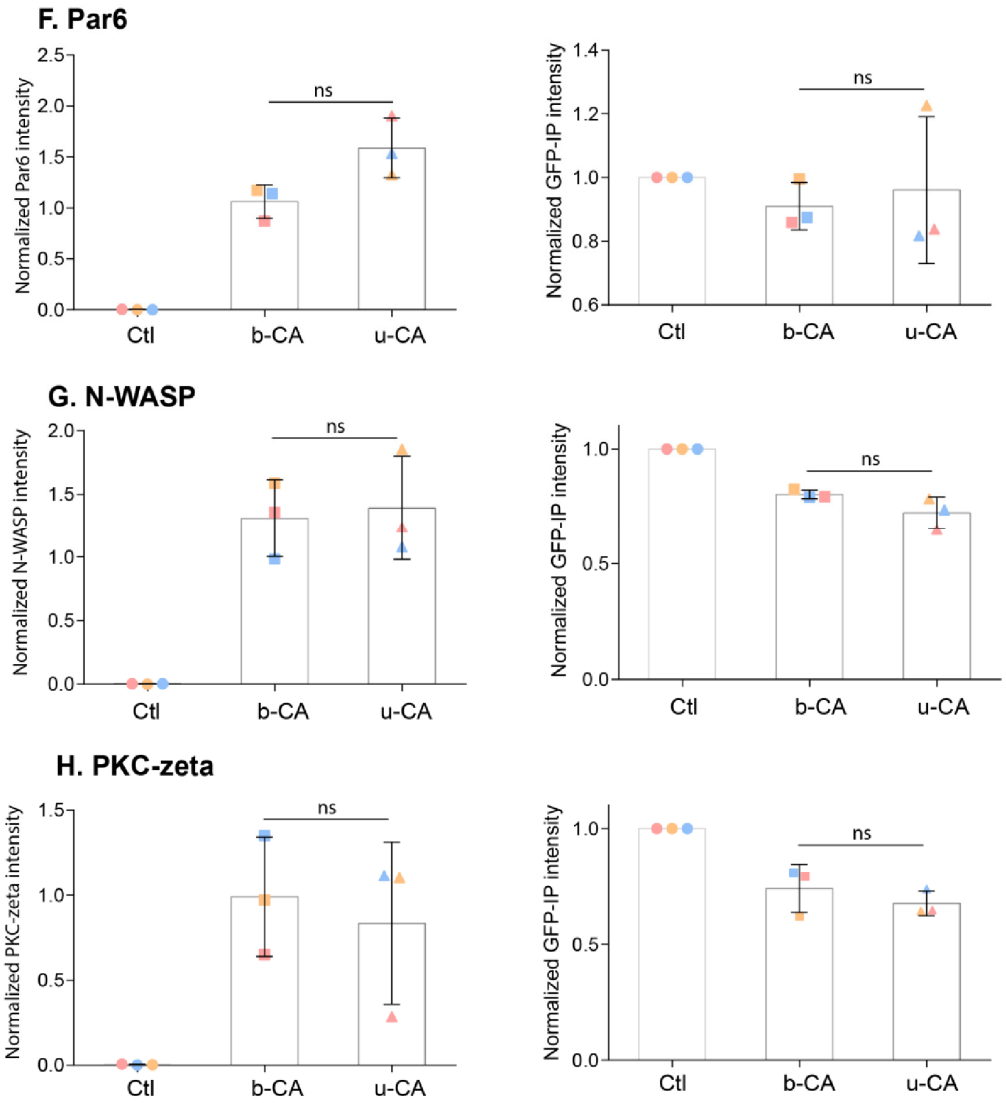

Figure S2: (A-B) Table displaying top binding partners of Cdc42 obtained by quantitative label-free mass spectrometry analysis: corresponding to either Cdc42b and Cdc42u (A), with a cut-off peptide ratio of ≥ 4 compared to GFP and (B) Cdc42b-CA (constitutively active) and Cdc42u-CA with a cut-off peptide ratio of ≥ 7 compared to GFP, p-value ≤ 0.05. Peptides used to calculate significance are ≥ 6 and number of replicates is four. **(C-G)** GFP immunoprecipitation of transiently expressed constitutively active Cdc42 variants in HEK cells to identify co-immunoprecipitation (Co-IP) of Cdc42 effector proteins Par6, PKCzeta and N-WASP. **(C-E)** Western blots of the GFP immunoprecipitation assays using GFP-Cdc42b-CA (b-CA), GFP-Cdc42u-CA (u-CA) and control GFP. **C)** myc-tagged Par6 was co-transfected with the GFP tagged proteins. Staining for anti-myc revealed levels of co-

immunoprecipitated myc-Par6 with Cdc42 variants. **D)** Staining for anti-PKCzeta revealed levels of co-immunoprecipitated endogenous PKCzeta with Cdc42 variants. **E)** Staining for anti-N-WASP revealed levels of co-immunoprecipitated endogenous N-WASP with Cdc42 variants. Control GFP did not co-immunoprecipitate with any of the three Cdc42 effector proteins. F-H) Quantitative analysis of the co-immunoprecipitation showed that there both b-CA and u-CA bound Par6, PKCzeta and N-WASP similarly. No significant differences in the immunoprecipitated levels of u-CA and b-CA were detected. Statistical analysis was performed using Wilcoxon matched pair t-test on values from three independent experiments.

Figure S3

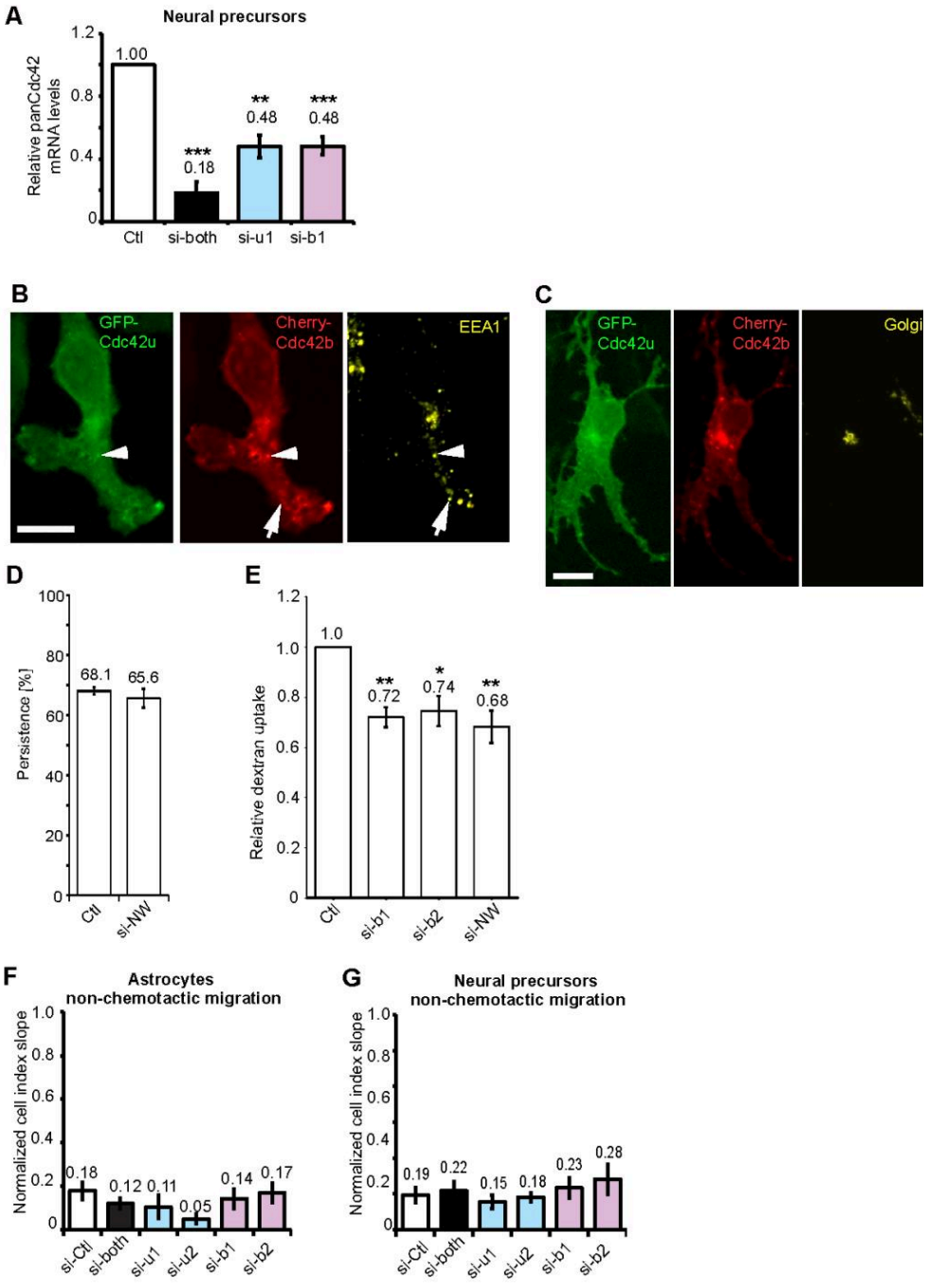
A
Neural precursors
Relative panCdc42 mRNA levels
1.00
0.18
0.48
0.48
Ctl
si-both
si-u1
si-b1
B
GFP-Cdc42u
Cherry-Cdc42b
EEA1
C
GFP-Cdc42u
Cherry-Cdc42b
Golgi
D
Persistence [%]
68.1
65.6
Ctl
si-NW
E
Relative dextran uptake
1.0
0.72
0.74
0.68
Ctl
si-b1
si-b2
si-NW
F
Astrocytes
non-chemotactic migration
Normalized cell index slope
0.18
0.12
0.11
0.05
0.14
0.17
si-Ctl
si-both
si-u1
si-u2
si-b1
si-b2
G
Neural precursors
non-chemotactic migration
Normalized cell index slope
0.19
0.22
0.15
0.18
0.23
0.28
si-Ctl
si-both
si-u1
si-u2
si-b1
si-b2

Figure S3: (A) Full Cdc42 mRNA levels were measured using a TaqMan assay that recognizes both Cdc42 isoforms (panCdc42) in neural precursors transfected with the indicated siRNA. (B, C) Fluorescence images of NPCs expressing GFP-Cdc42u and mCherry-Cdc42b, fixed and stained with anti EEA1 (early endosome marker) (B) and anti-GM130 (Golgi) (C). (D) Random migration of NPCs transfected with the indicated siRNA out of neurospheres. The histogram shows the direction persistence calculated for the time period between 100min and 300min after plating. (E) Quantification of relative dextran uptake in NPCs transfected with the indicated siRNA. (F-G) Astrocyte (F) and NPC (G) migration in Boyden chamber-based xCelligence system assays. Graphs show the curve slopes which indicate the rate of migration in non-chemotactic conditions (no FBS in lower well). Histograms show data presented as means ±SEM of 3 independent experiments. All p-values were calculated using two-sided unpaired Student's t-test. ****p-value<0.0001, ***p-value <0.001; **p- value <0.01; *p-value<0.05. Scale bars: 10 μm.

Movie S1: Cdc42u and Cdc42b display distinct intracellular localization. Movie showing mCherry-Cdc42u and GFP-Cdc42b expressing astrocytes. Fluorescent images were taken using spinning disk microscopy every 10 sec (total length: 12:20 min). Bar: 10 μm.

Movie S2: GFP-Cdc42u is mainly cytosolic. Movie showing a GFP-Cdc42u expressing migrating astrocyte, 5h after wounding. Fluorescent images were taken using spinning disk microscopy every 10 sec (total length: 13:20 min). Bar: 10 μm.

Movie S3: GFP-Cdc42b localizes to Golgi, vesicles and the plasma membrane. Movie showing a GFP-Cdc42b expressing migrating astrocyte 5h after wounding. Fluorescent images were taken using spinning disk microscopy every 10 sec (total length: 20 min). Bar 10 μm.

References

Aspenstrom, P. 2018. Activated Rho GTPases in Cancer-The Beginning of a New Paradigm. *International journal of molecular sciences*. 19.

Calaora, V., B. Rogister, K. Bismuth, K. Murray, H. Brandt, P. Leprince, M. Marchionni, and M. Dubois-Dalcq. 2001. Neuregulin signaling regulates neural precursor growth and the generation of oligodendrocytes in vitro. *J Neurosci*. 21:4740-4751. Camand, E., F. Peglion, N. Osmani, M. Sanson, and S. Etienne-Manneville. 2012. N- cadherin expression level modulates integrin-mediated polarity and strongly impacts on the speed and directionality of glial cell migration. *J Cell Sci*. 125:844- 857.

Chen, J.L., R.V. Fucini, L. Lacomis, H. Erdjument-Bromage, P. Tempst, and M. Stamnes. 2005. Coatomer-bound Cdc42 regulates dynein recruitment to COPI vesicles. *J Cell Biol*. 169:383-389.

Chen, L., G. Liao, L. Yang, K. Campbell, M. Nakafuku, C.Y. Kuan, and Y. Zheng. 2006. Cdc42 deficiency causes Sonic hedgehog-independent holoprosencephaly. *Proc Natl Acad Sci U S A*. 103:16520-16525.

Durbec, P., I. Franceschini, F. Lazarini, and M. Dubois-Dalcq. 2008. In vitro migration assays of neural stem cells. *Methods Mol Biol*. 438:213-225.

Erickson, J.W., and R.A. Cerione. 2001. Multiple roles for Cdc42 in cell regulation. *Curr Opin Cell Biol*. 13:153-157.

Etienne-Manneville, S. 2004. Cdc42--the centre of polarity. *J Cell Sci*. 117:1291-1300.

Etienne-Manneville, S. 2006. In vitro assay of primary astrocyte migration as a tool to study Rho GTPase function in cell polarization. *Methods Enzymol*. 406:565-578.

Etienne-Manneville, S., and A. Hall. 2001. Integrin-mediated activation of Cdc42 controls cell polarity in migrating astrocytes through PKCzeta. *Cell*. 106:489-498.

Etienne-Manneville, S., and A. Hall. 2002. Rho GTPases in cell biology. *Nature*. 420:629- 635.

Fidyk, N., J.B. Wang, and R.A. Cerione. 2006. Influencing cellular transformation by modulating the rates of GTP hydrolysis by Cdc42. *Biochemistry*. 45:7750-7762.

Hehnly, H., W. Xu, J.L. Chen, and M. Stamnes. 2010. Cdc42 regulates microtubule- dependent Golgi positioning. *Traffic*. 11:1067-1078.

Johnson, E., D.D. Seachrist, C.M. DeLeon-Rodriguez, K.L. Lozada, J. Miedler, F.W. Abdul-Karim, and R.A. Keri. 2010. HER2/ErbB2-induced breast cancer cell migration and invasion require p120 catenin activation of Rac1 and Cdc42. *J Biol Chem*. 285:29491-29501.

Kang, R., J. Wan, P. Arstikaitis, H. Takahashi, K. Huang, A.O. Bailey, J.X. Thompson, A.F. Roth, R.C. Drisdel, R. Mastro, W.N. Green, J.R. Yates, 3rd, N.G. Davis, and A. El-Husseini. 2008. Neural palmitoyl-proteomics reveals dynamic synaptic palmitoylation. *Nature*. 456:904-909.

Kessels, M.M., and B. Qualmann. 2002. Syndapins integrate N-WASP in receptor- mediated endocytosis. *EMBO J*. 21:6083-6094.

Legg, J.A., G. Bompard, J. Dawson, H.L. Morris, N. Andrew, L. Cooper, S.A. Johnston,

G. Tramountanis, and L.M. Machesky. 2007. N-WASP involvement in dorsal ruffle formation in mouse embryonic fibroblasts. *Mol Biol Cell*. 18:678-687.
Leong, S.Y., C.H. Faux, A. Turbic, K.J. Dixon, and A.M. Turnley. 2011. The Rho kinase pathway regulates mouse adult neural precursor cell migration. *Stem Cells*. 29:332- 343.
Marks, P.W., and D.J. Kwiatkowski. 1996. Genomic organization and chromosomal location of murine Cdc42. *Genomics*. 38:13-18.
Martinelli, S., O.H.F. Krumbach, F. Pantaleoni, S. Coppola, E. Amin, L. Pannone, K. Nouri,
L. Farina, R. Dvorsky, F. Lepri, M. Buchholzer, R. Konopatzki, L. Walsh, K. Payne,
M.E. Pierpont, S.S. Vergano, K.G. Langley, D. Larsen, K.D. Farwell, S. Tang, C. Mroske, I. Gallotta, E. Di Schiavi, M. Della Monica, L. Lugli, C. Rossi, M. Seri, G. Cocchi, L. Henderson, B. Baskin, M. Alders, R. Mendoza-Londono, L. Dupuis,
D.A. Nickerson, J.X. Chong, G. University of Washington Center for Mendelian,
N. Meeks, K. Brown, T. Causey, M.T. Cho, S. Demuth, M.C. Digilio, B.D. Gelb, M.J. Bamshad, M. Zenker, M.R. Ahmadian, R.C. Hennekam, M. Tartaglia, and
G.M. Mirzaa. 2018. Functional Dysregulation of CDC42 Causes Diverse Developmental Phenotypes. *American journal of human genetics*. 102:309-320.
Nishimura, A., and M.E. Linder. 2013. Identification of a novel prenyl and palmitoyl modification at the CaaX motif of Cdc42 that regulates RhoGDI binding. *Mol Cell Biol*. 33:1417-1429.
Osmani, N., F. Peglion, P. Chavrier, and S. Etienne-Manneville. 2010. Cdc42 localization and cell polarity depend on membrane traffic. *J Cell Biol*. 191:1261-1269.
Osmani, N., N. Vitale, J.P. Borg, and S. Etienne-Manneville. 2006. Scrib controls Cdc42 localization and activity to promote cell polarization during astrocyte migration. *Curr Biol*. 16:2395-2405.
Poullet, P., S. Carpentier, and E. Barillot. 2007. myProMS, a web server for management and validation of mass spectrometry-based proteomic data. *Proteomics*. 7:2553- 2556.
Ridley, A.J. 2006. Rho GTPases and actin dynamics in membrane protrusions and vesicle trafficking. *Trends Cell Biol*. 16:522-529.
Robel, S., S. Bardehle, A. Lepier, C. Brakebusch, and M. Gotz. 2011. Genetic deletion of cdc42 reveals a crucial role for astrocyte recruitment to the injury site in vitro and in vivo. *J Neurosci*. 31:12471-12482.
Valot, B., O. Langella, E. Nano, and M. Zivy. 2011. MassChroQ: a versatile tool for mass spectrometry quantification. *Proteomics*. 11:3572-3577.
van Hengel, J., P. D'Hooge, B. Hooghe, X. Wu, L. Libbrecht, R. De Vos, F. Quondamatteo,
M. Klempt, C. Brakebusch, and F. van Roy. 2008. Continuous cell injury promotes hepatic tumorigenesis in cdc42-deficient mouse liver. *Gastroenterology*. 134:781- 792.
Vizcaino, J.A., A. Csordas, N. del-Toro, J.A. Dianes, J. Griss, I. Lavidas, G. Mayer, Y. Perez-Riverol, F. Reisinger, T. Ternent, Q.W. Xu, R. Wang, and H. Hermjakob. 2016. 2016 update of the PRIDE database and its related tools. *Nucleic Acids Res*. 44:D447-456.

Wirth, A., C. Chen-Wacker, Y.W. Wu, N. Gorinski, M.A. Filippov, G. Pandey, and E. Ponimaskin. 2013. Dual lipidation of the brain-specific Cdc42 isoform regulates its functional properties. *Biochem J*. 456:311-322.
Wu, W.J., J.W. Erickson, R. Lin, and R.A. Cerione. 2000. The gamma-subunit of the coatomer complex binds Cdc42 to mediate transformation. *Nature*. 405:800-804.
Yap, K., Y. Xiao, B.A. Friedman, H.S. Je, and E.V. Makeyev. 2016. Polarizing the Neuron through Sustained Co-expression of Alternatively Spliced Isoforms. *Cell reports*. 15:1316-1328.
Zhou, P., M. Porcionatto, M. Pilapil, Y. Chen, Y. Choi, K.F. Tolias, J.B. Bikoff, E.J. Hong, M.E. Greenberg, and R.A. Segal. 2007. Polarized signaling endosomes coordinate BDNF-induced chemotaxis of cerebellar precursors. *Neuron*. 55:53-68.

Additional results

We report differential subcellular localization of Cdc42 isoforms our article. Cdc42b is Golgi-localized in immobile astrocytes (Article.1, Figure 1C) and we also observe that palmitoylation of Cdc42b promotes its association with vesicles (Article.1, Figure 1E). Whether palmitoylation of Cdc42b occurs in the Golgi apparatus, which is responsible for its association with vesicles has not been explored in the article. No enzyme responsible for palmitoylating Cdc42b has been reported so far. Therefore, we sought to identify the enzyme responsible for palmitoylation of Cdc42b and its subcellular localization

Golgi localized zDHHC3 and zDHHC7 PAT enzymes are potential candidates for palmitoylating brain Cdc42

We therefore investigated whether palmitoylation of Cdc42b could take place in the Golgi apparatus and could regulate vesicular trafficking of Golgi-localized Cdc42b. Palmitoylation of Cdc42b occurs through S-acylation (A. Nishimura and Linder 2013). Protein acyltransferases (PATs) are known to orchestrate S-acylation in mammalian cells. Due to the highly conserved Asp-His-His-Cys tetrapeptide motif necessary for catalysis, these enzymes are known as the DHHC protein acyltransferases (DHHC-PATs)(Rana, Lee, and Banerjee 2018). These PATs are polytopic integral membrane proteins usually found in the membranes of the ER, the Golgi apparatus, and the plasma membrane. Approximately 24 mammalian PATs enzymes have been identified so far. For our PAT screen, we chose a group of 9 PAT enzymes which include, zDHHC1 (ER-localized), zDHHC3 (Golgi-localized), zDHHC6 (ER-localized), zDHHC7 (Golgi-localized), zDHHC13 (ER-localized), zDHHC15 (ER-localized), zDHHC17 (Golgi-localized), zDHHC18 (Golgi-localized) and zDHHC20 (Golgi-PM-localized)(Cho and Park 2016). To screen the PAT proteins, we co-transfected individual PAT enzymes with GFP-tagged Cdc42b in HeLa cells. Followed by radiolabeling of palmitoylated Cdc42b prior to performing a GFP immunoprecipitation assay (see materials). Autoradiography revealed the levels of palmitoylated Cdc42b in each condition. zDHHC3 co-transfection resulted in the highest level of palmitoylated Cdc42b followed by zDHHC7 (Figure 24A). Control Cdc42b alone also exhibited a palmitoylation signal but lower as compared to zDHHC3 and ZDHHC7 co-transfection (Figure 24A).

We further tested whether knockdown of zDHHC3 and zDHHC7 PAT enzymes resulted in lower levels of palmitoylated Cdc42b along with other PAT enzymes. We observed that knockdown of zDHHC3 and zDHHC7 resulted in the absence of palmitoylated Cdc42b (Figure 24B). We also observed a distinct reduction in palmitoylated Cdc42b upon zDHHC1 (Figure 24B). With these findings, we can suggest that Golgi-localized zDHHC3 and zDHHC7 PATs are potential candidates for Cdc42b palmitoylation, which should be investigated further.

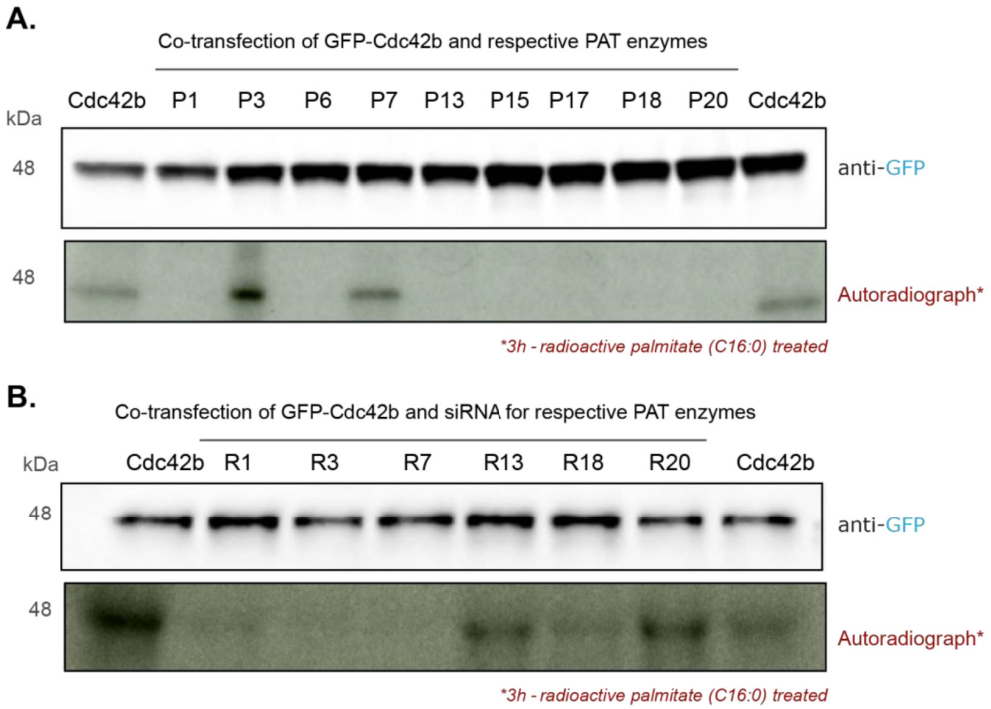

Figure 24 Golgi localized zDHHC3 and zDHHC7 PAT enzymes are potential candidates for palmitoylating brain Cdc42.

A) Western blot of GFP immunoprecipitation assay performed with control Cdc42b and co-transfection of Cdc42b with individual PAT enzymes in HeLa cells. PAT enzymes are labelled as P1 for zDHHC1, P3 for zDHHC3 and so on. The autoradiograph corresponding to the IP shows the signal from radiolabeled palmitoylation on Cdc42b under each condition. The strongest signal is observed for zDHHC3 followed by zDHHC7. Bands are also observed for control Cdc42b lanes. No signal was observed for other PAT enzymes. **B)** Western blot of GFP immunoprecipitation assay performed with control Cdc42b and co-transfection of Cdc42b along with knockdown of individual PAT enzymes in HeLa cells. Conditions where knockdown of PAT enzymes was performed are labelled as R1 for zDHHC1, R3 for zDHHC3 and so on. The autoradiograph corresponding to the IP shows the signal from radiolabeled palmitoylation on Cdc42b under each condition. The strongest signal is observed for control Cdc42b, bands are also observed for control other PAT enzymes. Only a faint signal was observed with zDHHC1 and no signal was observed for PAT enzymes zDHHC3 and zDHHC7.

Section B

This part of the results section contains findings from a collaborative study done with Jérôme Delon (Institut Cochin). This study reports the identification of a patient with a R186C mutation in the C-terminal region of Cdc42u and molecular mechanisms behind its pathogenicity (see Annex for corresponding article). Cdc42u is largely plasma membrane associated, yet the R186C mutation resulted in the accumulation of Cdc42u in the Golgi apparatus. The R186C mutant was also shown to be highly palmitoylated making Cdc42u more Cdc42b like. Therefore, we wanted to delineate whether this subcellular mislocalization of R186C mutant was associated to its de novo dual lipidation. Eventually also address whether it's mislocalization was responsible for the autoinflammatory phenotype displayed by the patient. If so, this would strengthen our conclusion (Article.1 Section. A) that subcellular localization is key for Cdc42 functionality.

R186C mutant localizes in the Golgi apparatus

Jérôme Delon and co-workers identified an R186C mutation in the C-terminal region of ubiquitous Cdc42u in a young adult patient presenting an autoinflammatory phenotype. The patient had developed a severe form of generalized pustular psoriasis following bone marrow transplant in his childhood. The R186C mutation was also identified to undergo a gain of function, palmitoylation on the carboxy terminal domain of ubiquitous Cdc42 (Figure 25A, see Annex). This palmitoylation was shown to be responsible for ubiquitous Cdc42 being trapped in the Golgi apparatus (Figure 25B), indicating a defect in subcellular localization of Cdc42u. The palmitoylation of ubiquitous Cdc42u now makes it dually lipidated and traps it in the Golgi apparatus, displaying brain Cdc42b like subcellular localization. Therefore, we collaborated in this study to identify the molecular mechanisms behind the R186C entrapment in the Golgi apparatus and eventually cause of its pathogenicity.

To identify the differences between the interactome of R186C and ubiquitous Cdc42 we performed mass spectrometry. Qualitative analysis showed that both wildtype and constitutively active R186C were capable of binding known Cdc42 effectors (see Annex Article, for PRIDE database access). Further quantitative comparisons were performed with each condition using their fold change versus GFP, a value indicative of how many times true peptides are pulled down with our target sample versus control GFP. The resulting fold change values were used to generate correlation plots of common proteins between both conditions. For wildtype R186C versus ubiquitous Cdc42 the list of common proteins is slightly uncorrelated and the fold change of GDI1 for R186C is lower than that of ubiquitous Cdc42 (Figure 25C). With regard to constitutively active proteins, several effector proteins were correlated such as WASp, CEP4 (Cdc42 effector protein [Cdc42EP2]), WIPF2 (WASp interacting protein family 2). The number of proteins of more in the case of constitutive active conditions as compared to wildtype condition (Figure 25D). The proteomic analysis mainly showed that R186C has the tendency to bind classical interactors of Cdc42 in both wildtype and constitutively active conditions.

GDI1 binds to the geranylgeranyl moiety on the C-ter of Cdc42. Co-immunoprecipitation of GDI1 with R186C was assessed compared to ubiquitous Cdc42 (Figure 25E). R186C displayed strikingly impaired GDI1 binding as opposed to ubiquitous Cdc42. Unprenylated u(SVLL) was used a negative control for its inability to bind to GDI1. This suggests that the highly palmitoylated R186C displays impaired GDI1 like palmitoylated brain Cdc42.

N-WASP is a known effector of Cdc42. We performed co-immunoprecipitation assays to evaluate the ability of constitutively active R186C to bind to effectors as opposed to constitutively active ubiquitous Cdc42. R186C is capable of binding N-WASP similar to

ubiquitous Cdc42 (Figure 25F). This suggests that R186C mutant is capable of binding an array of classical effectors yet the molecular mechanism behind its pathogenicity is its inability to be extracted from the Golgi apparatus by GDI1. These results indicate that the subcellular localization of the R186C mutant is crucial despite having the ability to bind known interactors.

Figure.25

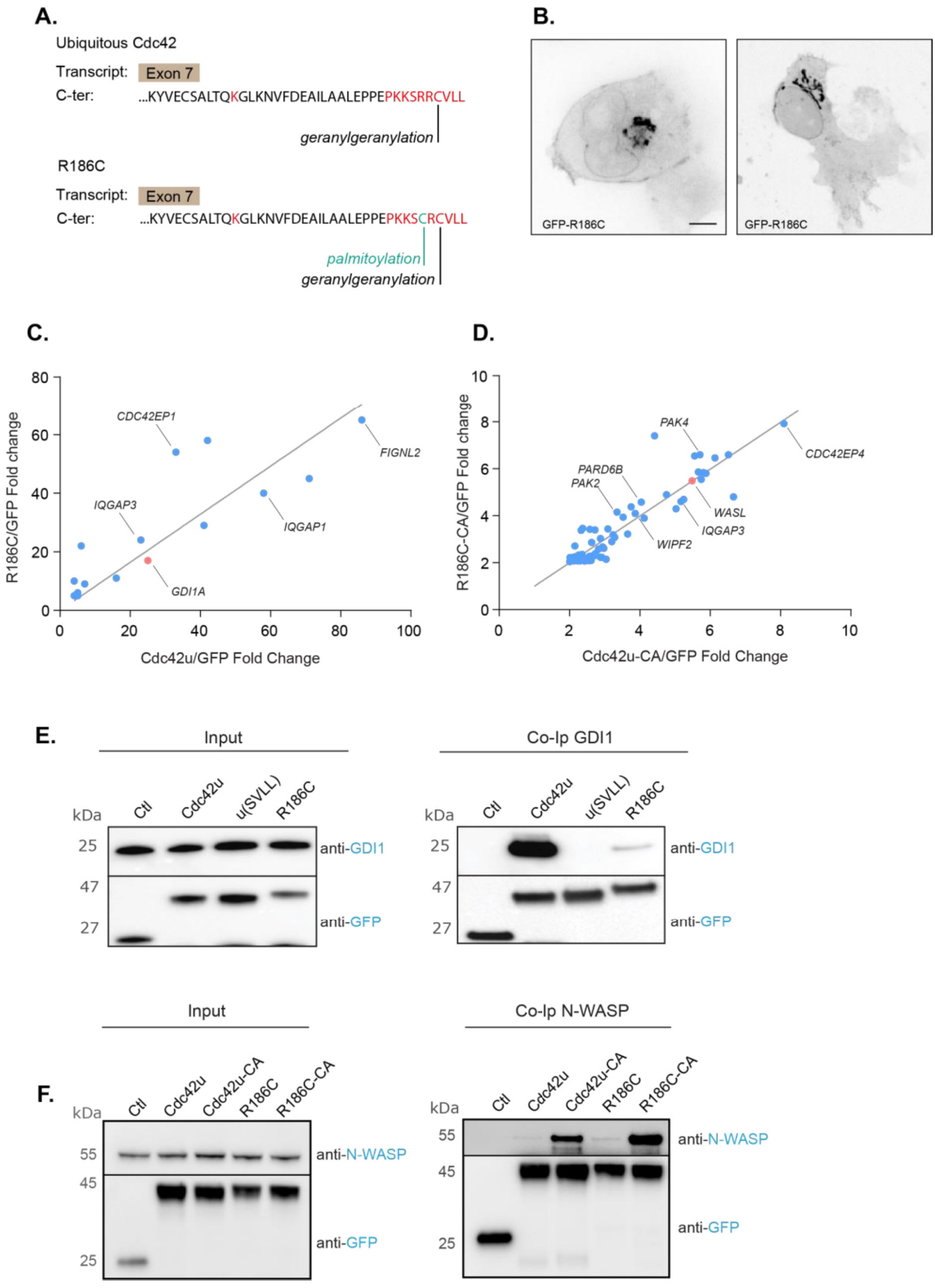
A.
Ubiquitous Cdc42
Transcript: Exon 7
C-ter: ...KYVECSALTQKGLKNVFDEAILAALEPPEPKKSRRCVLL
geranylgeranylation
R186C
Transcript: Exon 7
C-ter: ...KYVECSALTQKGLKNVFDEAILAALEPPEPKKSCRCVLL
palmitoylation
geranylgeranylation
B.
GFP-R186C
GFP-R186C
C.
R186C/GFP Fold change
Cdc42u/GFP Fold Change
CDC42EP1
FIGNL2
IQGAP3
IQGAP1
GDI1A
D.
R186C-CA/GFP Fold change
Cdc42u-CA/GFP Fold Change
PAK4
CDC42EP4
PARD6B
PAK2
WASL
IQGAP3
WIPF2
E.
Input
Co-Ip GDI1
kDa
Ctl
Cdc42u
u(SVLL)
R186C
anti-GDI1
anti-GFP
F.
Input
Co-Ip N-WASP
kDa
Ctl
Cdc42u
Cdc42u-CA
R186C
R186C-CA
anti-N-WASP
anti-GFP

Figure 25 (A-B) R186C patient mutant localizes in the Golgi apparatus

A) Schematic showing the mutation R186C on ubiquitous Cdc42 background which also results in a gain of function being palmitoylation. **B)** Spinning disk live images (inverted LUT) of both HEK cells (left) and astrocytes (right) transiently expressing R186C, which exhibits a distinct localization in the Golgi apparatus. Scale bar 10μm. **(C-F) R186C binding to GDI1 is impaired**. **C)** Mass spectrometry based proteomic analysis. Correlation plots were made to compare between wildtype R186C and Cdc42u. The correlation plot represents common proteins between R186C and Cdc42u having a significant fold change ≥ 4 compared to GFP and peptides used to calculate significance are ≥ 6. Quantitative analysis was performed by calculating foldchange for each peptide. Foldchange is the number of peptides bound to Cdc42 versus control GFP. GDI1A (gene name for GDI1) was highlighted and shown to have a lower foldchange for R186C compared to Cdc42u. Data from four independent samples. **D)** The correlation plot represents common proteins between constitutively active R186C-CA and Cdc42u-CA having a significant fold change ≥ 4 compared to GFP and peptides used to calculate significance are ≥ 6. Log2 values of fold change were plotted. The CA correlation plot has more interactors compared to wildtype and several known effectors of Cdc42 are annotated (annotations correspond to gene names of respective proteins). Data from four independent samples. **E)** Western blot of GFP immunoprecipitation assay performed with Cdc42u, u(SVLL), R186C and control GFP. Staining for co-immunoprecipitation (Co-Ip) of GDI1 shows that R186C exhibits significantly impaired GDI1 binding while Cdc42u strongly binds to GDI1. **F)** Western blot of GFP immunoprecipitation assay performed with Cdc42u, R186C, their respective constitutively active forms (G12V mutant) and control GFP. R186C-CA is capable of co-immunoprecipitating with N-WASP, a known effector of Cdc42 similar to Cdc42u-CA.

Section C

This section contains results from an ongoing *in vitro* study using giant unilamellar vesicles to address the membrane anchorage and targeting ability of Cdc42 variants purified from mammalian cells. To explain the distinct localization and function of Cdc42 isoforms in cells, we investigated whether the alternative carboxy-terminal domain may directly affect Cdc42 interaction with membranes. This last C-terminal exon encompasses two characteristic features of Rho GTPases namely, the polybasic region (PBR) and the CaaX motif (Hodge and Ridley 2016). In cells, the PBR region plays a key role in membrane targeting and the CaaX box is responsible for membrane insertion. For the two isoforms of Cdc42, both regions differ drastically. Cdc42u has a classical CaaX box, which is prenylated whereas Cdc42b has an alternative CCaX motif, which is palmitoylated in addition to the prenylation on the Cys188 residue. To circumvent the challenging task of studying plasma membrane interactions *in cellulo* we used Giant unilamellar vesicles (GUVs) as in vitro model membrane systems. GUVs are ideal as they are convenient for imaging and their lipid composition can be customized. Considering the differential membrane targeting and anchoring motifs, we dissected the role of the isoform specific membrane interactions using Cdc42 variants and mutants, carboxy-terminal only constructs and GUVs of various plasma membrane- or Golgi-related composition.

Prenylated Cdc42 proteins intrinsically prefer Golgi-apparatus like vesicles.

In cells, brain Cdc42 (Cdc42b) localizes in the Golgi apparatus and ubiquitous Cdc42 (Cdc42u) is largely plasma membrane associated. Posttranslational lipid modifications on CaaX motifs of proteins are essential for membrane interaction. To test whether the differences in subcellular localization of Cdc42 variants is due to their differential post translational lipid modifications, we performed *in vitro* binding assays using giant unilamellar vesicles (GUVs). Cdc42 variants and their specific lipid mutants were first generated by inducing a point mutation on the carboxy terminal amino acids Cys 188 of Cdc42u and either Cys 188 or Cys 189 residues of Cdc42b. (Figure 26A). GFP-tagged constructs of Cdc42 variants and their corresponding lipid mutants were expressed and purified from mammalian cells. Notably, prenylated Cdc42 were soluble due to their co-purification in complex with GDI1. All purified proteins were incubated with GUVs of different lipid composition, either Golgi apparatus-like (GM) GUVs or plasma membrane-like (PM) GUVs. Unprenylated u(SVLL) and b(SCIF) failed to be recruited on either GUVs (Figure 26B). Prenylated Cdc42 variants and non-palmitoylable brain Cdc42 b(CSIF) bound to both GM and PM GUVs (Figure 26B). This confirms that prenylated Cdc42 proteins are capable of membrane anchorage, which is in agreement with previous membrane model studies (Park et al. 2015a; Johnson, Erickson, and Cerione 2012). These results also indicate that palmitoylation of Cdc42b is not essential for membrane anchorage.

Surprisingly, average intensity quantifications of prenylated Cdc42 proteins indicated that both Cdc42 variants and non-palmitoylable brain Cdc42 b(CSIF), all significantly prefer GM GUVs as opposed to PM GUVs (Figure 26C-E). To quantify the preference of each Cdc42 protein towards GM GUVs versus PM GUVs, GM/PM binding ratios were calculated for each protein. All three proteins had no significant differences in their GM/PM ratios (approximately 2-fold) (Figure 26F). There are three major differences between GM GUVs and PM GUVs: 1) their Chol:Phospholipid (PL) ratio (1:1 [mol/mol] for PM GUVs and 1:5 for GM GUVs); 2) GM GUVs are twice negatively charged as compared to PM GUVs; and 3)Sphingomyelin (SM) is not incorporated in GM GUVs. This indicates that prenylated Cdc42 proteins have intrinsic preference for negatively charged membranes with lower concentrations of Cholesterol. The inner leaflet of the plasma membrane also has a 1:1 Chol:PL ratio similar to our PM GUVs (Van Meer, Voelker, and Feigenson 2008). Thus, it is surprising that Cdc42u which is largely plasma membrane associated in cells prefers GM GUVs as opposed to PM GUVs. Therefore, these results with model membranes indicate that Cdc42 intrinsically prefers GM GUVs that have a lower Chol:PL ratio.

Figure.26

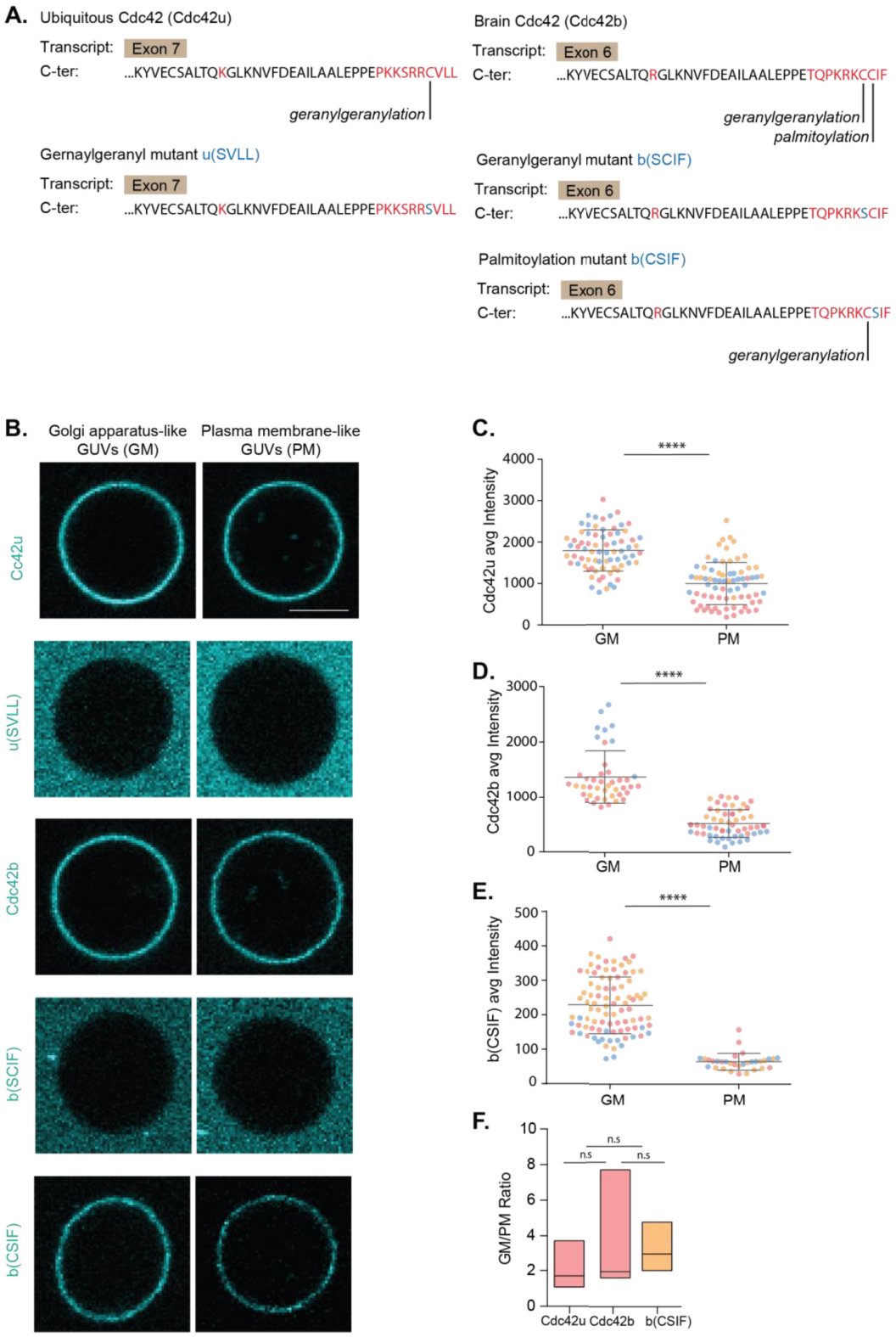
A.
Ubiquitous Cdc42 (Cdc42u)
Transcript: Exon 7
C-ter: ...KYVECSALTQKGLKNVFDEAILAALEPPEPKKSRRCVLL
geranylgeranylation
Gernaylgeranyl mutant u(SVLL)
Transcript: Exon 7
C-ter: ...KYVECSALTQKGLKNVFDEAILAALEPPEPKKSRRSVLL
Brain Cdc42 (Cdc42b)
Transcript: Exon 6
C-ter: ...KYVECSALTQRGLKNVFDEAILAALEPPETQPKRKCCIF
geranylgeranylation
palmitoylation
Geranylgeranyl mutant b(SCIF)
Transcript: Exon 6
C-ter: ...KYVECSALTQRGLKNVFDEAILAALEPPETQPKRKSCIF
Palmitoylation mutant b(CSIF)
Transcript: Exon 6
C-ter: ...KYVECSALTQRGLKNVFDEAILAALEPPETQPKRKCSIF
geranylgeranylation
B.
Golgi apparatus-like GUVs (GM)
Plasma membrane-like GUVs (PM)
Cc42u
u(SVLL)
Cdc42b
b(SCIF)
b(CSIF)
C.
Cdc42u avg Intensity
****
GM
PM
D.
Cdc42b avg Intensity
****
GM
PM
E.
b(CSIF) avg Intensity
****
GM
PM
F.
GM/PM Ratio
n.s
n.s
n.s
Cdc42u
Cdc42b
b(CSIF)

Figure 26 Cdc42 intrinsically prefers Golgi-apparatus like GUVs

A) Schematic showing the various point mutations induced to generate Cdc42 variant specific posttranslational lipid modification mutants (referred to as lipid mutants). **B)** Confocal images showing Cdc42 variants and their respective lipid mutants were bound to Golgi apparatus-like GUVs (GM) and plasma membrane-like GUVs (PM). The unprenylated Cdc42 mutants u(SVLL) and u(SCIF) fail to bind to both GM and PM GUVs. Prenylated Cdc42 proteins, Cdc42u, Cdc42b and non-palmitoylable b(CSIF) are able to bind to both GM and PM GUVs. (Scale bar = 10 μm) **C-E)** The scatter plots representing the grey scale intensity values (mean ± SEM) calculated along the circumference of the GUVs represented in B), show that Cdc42u, Cdc42b and b(CSIF) all significantly preferentially bind to GM GUVs as opposed to PM GUVs. Statistical analysis was performed using two tailed unpaired t-test with Welch's correction, ****= $p<0.0001$. The different colour codes used for the dots represent sets of data from three individual experiments. (number of GUVs used (n), C) n=74, 73, D) n=43, 54 and F) n=90, 32 for GM and PM conditions respectively). **F)** Box plot showing mean intensity ratio of GM versus PM binding was calculated for Cdc42 proteins using the mean of three individual experiments. (mean ± SEM, bounds=95% confidence interval). The average GM/PM ratios of Cdc42u, Cdc42b and b(CSIF) depicted in the graph show that all three proteins prefer GM GUVs versus PM GUVs in similar folds, (n.s. means non-significant). Statistical analysis was performed using two tailed ratio paired t-test.

Prenylated Cdc42 variants segregate specifically to Ld domains.

The plasma membrane, which is enriched in saturated lipids and cholesterol, has been shown to exist in both liquid-disordered (Ld) and liquid-ordered (Lo) phases (so-called raft phase), while intracellular membranes composed of unsaturated lipids and low cholesterol levels rather behave as Ld phases (Simons and Vaz 2004). Therefore, the existence of lipid Lo domains in the plasma membrane is widely accepted as opposed to their putative existence in Golgi-apparatus membranes (Levental, Levental, and Heberle 2020). Thus, we studied whether Cdc42 variants are recruited to specific domains. We used both phase separated GUVs (3:1:3, DOPC:Chol:SM) and pure liquid disordered (Ld) or liquid ordered (Lo) GUVs. Both Cdc42 variants segregated specifically to Ld domains on GUVs displaying phase separation (Figure 27A) and recruitment was only observed on Ld vesicles but not on Lo vesicles (Figure 27B). This is similar to other monoprenylated proteins such as Rab1, Rab5 and Rab6 (Kulakowski et al. 2018) with the hypothesis that unsaturation in the geranylgeranyl moiety lead to preferential insertion of the geranylgeranyl moiety into Ld membranes. However, this raises the question why the saturated palmitoyl moiety of brain Cdc42 species does not influence recruitment of brain Cdc42 to Lo domain like other palmitoylated GTPases such as N-RAS (Levental et al. 2010)

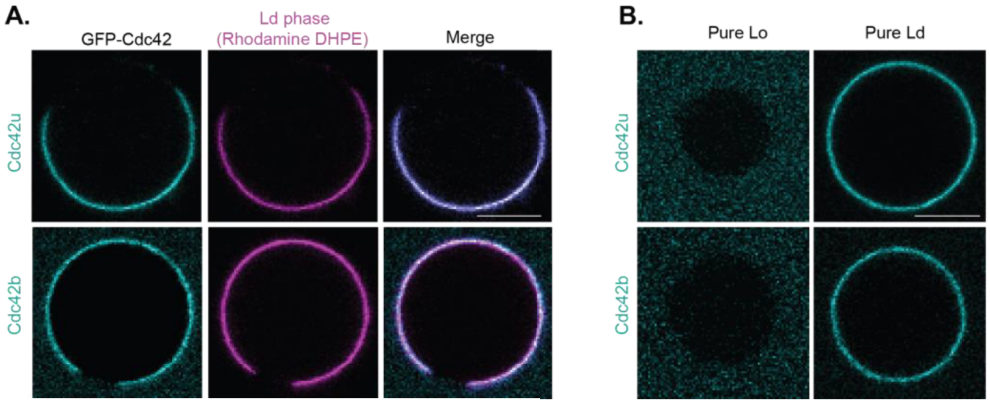

Figure 27 Prenylated Cdc42 binds to liquid disordered (Ld) membrane domains

A) Confocal images of phase separated GUVs composed of DOPC:Chol:SM (3:1:3 mol/mol ratio) showing that both GFP-tagged Cdc42u and Cdc42b preferentially bind to Ld domains. The Ld phase was visualized by the addition of fluorescent Rhodamine-DHPE, a Ld phase marker. Scale bar, 10 µm. **B)** Confocal images showing GFP-tagged Cdc42 variants bind only to pure Ld vesicles composed of DOPC:Chol (1:1 mol/mol ratio) and fail to bind to pure Lo vesicles composed of Chol:SM (1:1 mol/mol ratio). Scale bar, 10µm.

Cdc42 variants prefer lipid packing defects

The Ld phase is characterized by the assembly of unsaturated lipids which are known to promote lipid packing defects (Vamparys et al. 2013). To explain the preferential binding of prenylated Cdc42 variants to Ld membranes, we hypothesized that Cdc42 membrane recruitment depends on the presence of lipid packing defects in endomembranes. To test this hypothesis, we performed recruitment experiments with GM GUVs containing 15% 1-2-dioleoyl-sn-glycerol (DOG) (EggPC was lowered to 35%) denoted 'GM+DOG' in the following. DOG is a highly conical-shaped lipid that has been shown to induce the formation of packing defects similar to those found on positively curved membranes (Vamparys et al. 2013). Both Cdc42 variants show significantly increased membrane recruitment in the presence of DOG (Figure 28A,B), i.e. in presence of higher amounts of lipid packing defects. To quantify the preference of each Cdc42 protein towards GM GUVs versus GM+DOG GUVs, GM+DOG/GM binding ratios were calculated for each protein. We report here that lipid packing defects are instrumental in specific membrane recruitment of prenylated Cdc42 variants by ameliorating the hydrophobic insertion of their prenyl group into lipid packing defects. The same is observed with monoprenylated Rabs (Rab1, Rab5 and Rab6) (Kulakowski et al. 2018). However, Cdc42u showed a significantly higher preference for DOG lipids (1.3 fold) when compared to Cdc42b (Figure 28B),

We hypothesized that the difference in affinity between Cdc42 variants for membranes with lipid packing defects could be due to the palmitoylated pool of brain Cdc42. For this purpose, we used Palmostatin B (chemical inhibitor of depalmitoylase enzyme APT1) to prevent depalmitoylation of brain Cdc42 (Cdc42b+Palm B) during purification (Figure 28E). We then tested the membrane recruitment of Cdc42b+Palm B on DOG incorporated GUVs (Figure 28B). Interestingly, preliminary results suggest that increased palmitoylated Cdc42b slightly increases its affinity to DOG incorporated GUVs as compared to Cdc42b (Figure 28F,H). However, this is still not equivalent to the preference for lipid packing defects shown by Cdc42u. Therefore, the differences in the preference towards membranes with lipid packing defects between Cdc42u and Cdc42b may be due to the differences in the amino acid sequence of brain Cdc42 and/or to their differential binding to GDI1 (A. Nishimura and Linder 2013).

Figure 28

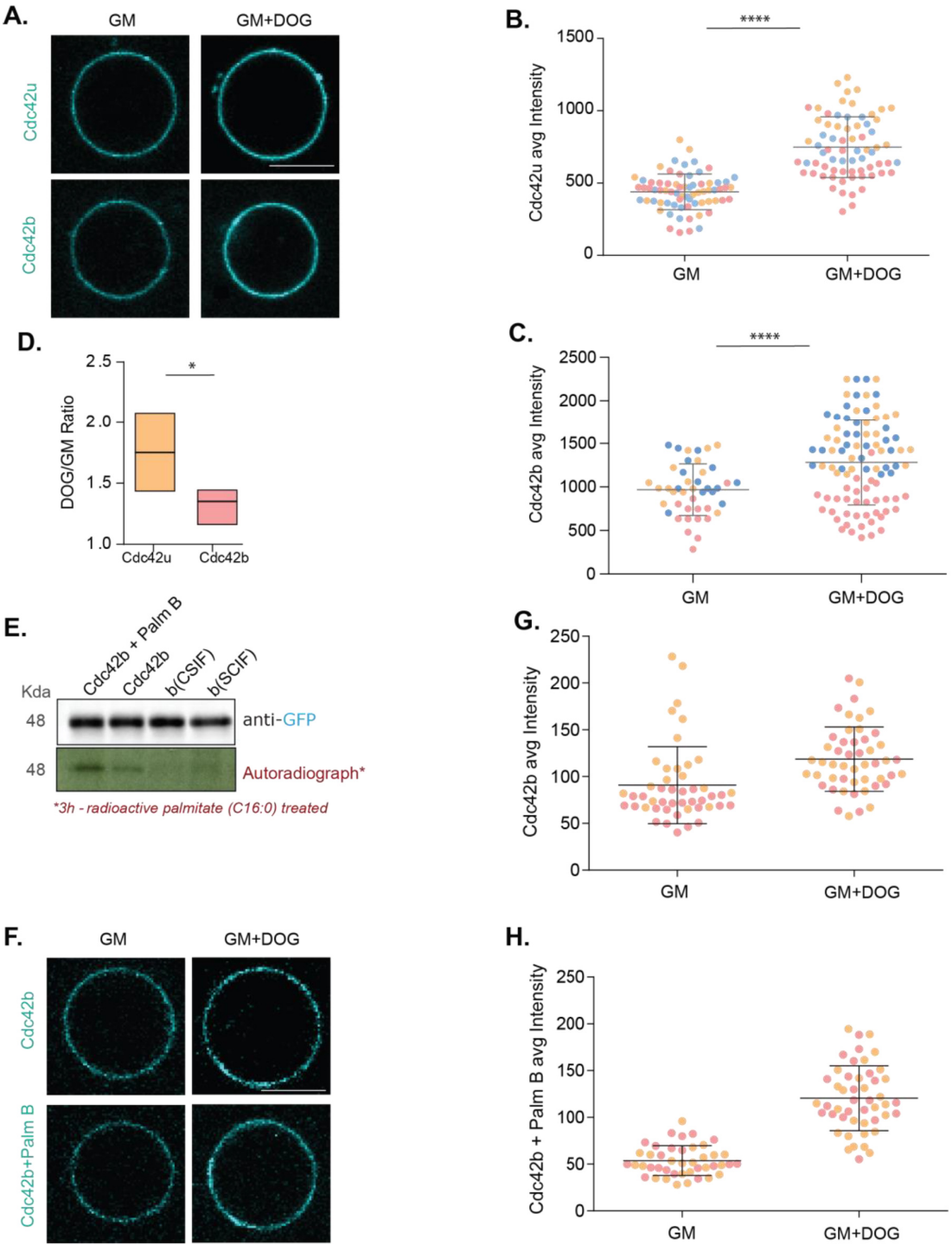
A.
GM
GM+DOG
Cdc42u
Cdc42b
B.
****
Cdc42u avg Intensity
1500
1000
500
0
GM
GM+DOG
C.
****
Cdc42b avg Intensity
2500
2000
1500
1000
500
0
GM
GM+DOG
D.
*
DOG/GM Ratio
2.5
2.0
1.5
1.0
Cdc42u
Cdc42b
E.
Cdc42b + Palm B
Cdc42b
b(CSIF)
b(SCIF)
Kda
48
anti-GFP
48
Autoradiograph*
*3h - radioactive palmitate (C16:0) treated
G.
Cdc42b avg Intensity
250
200
150
100
50
0
GM
GM+DOG
F.
GM
GM+DOG
Cdc42b
Cdc42b+Palm B
H.
Cdc42b + Palm B avg Intensity
250
200
150
100
50
0
GM
GM+DOG

Figure 28 (A-D) Cdc42 variants prefer lipid packing defects

A) Lipid packing defects were induced by adding 15% DOG to the Golgi apparatus-like composition (GM+DOG). Confocal images showing both Cdc42u and Cdc42b prefer GM+DOG GUVs compared to control GM GUVs. Scale bar, 10 μm. **B-C)** The scatter plots representing mean grey scale intensity values (mean ± SEM) of the GUVs represented in A), show that both Cdc42 variants significantly prefer GM+DOG GUVs compared to control GM GUVs. (****=t-test, $p<0.0001$). The different colour codes used for the dots represent sets of data from three individual experiments. (number of GUVs used (n) in graphs; B) n=70, 70 and D) n=43,93 for GM and GM+DOG conditions respectively) **D)** Box plot showing mean intensity ratio of GM+DOG versus GM binding for both Cdc42 variants. (mean ± SEM, bounds=95% confidence interval). Cdc42u significantly prefers GM+DOG GUVs compared to Cdc42b. (*=t-test, $p=0.045$). **(E-H) Use of Palmostatin B to increase palmitoylated pool of brain Cdc42 E)** Western blot showing GFP immunoprecipitation (IP) of brain Cdc42 and its lipid mutants b(SCIF) and non-palmitoylable b(CSIF) from HEK cells. Palmostatin-B (Palm-B) was added to one condition of HEK cells expressing brain Cdc42 (see Materials and Methods). The autoradiograph corresponding to the IP shows the signal from radiolabeled palmitoylation on the Cdc42 proteins. The Palm-B treated sample shows the highest radio signal, followed by control brain Cdc42. No signal was observed with b(CSIF) and a faint signal is noticed with the b(SCIF) lane. **F)** Confocal images showing Cdc42b and Cdc42b purified after Palmostatin B treatment (Cdc42b+Palm B) were bound to GM GUVs and GM+DOG GUVs. Scale bar, 10 μm. **G-H)** The scatter plots representing mean grey intensity values (mean ± SEM) from preliminary experiments (N=2) show that Cdc42b+Palm B tends to prefer GM+DOG GUVs more than control brain Cdc42. (number of GUVs used (n) in graphs; G) n=46,48 and H) n=42,47 for GM and GM+DOG conditions respectively).

Cdc42u prefers PI(4,5)P2 rich vesicles while Cdc42b does not.

The last 10 carboxy terminal amino acids, which are different for Cdc42 variants, encompasses their polybasic region (PBR). The PBR has been shown to be essential for membrane targeting of GTPases (Ahearn et al. 2012; Michaelson et al. 2001). The PBR of Cdc42u is composed of a di-lysine and di-arginine motif (Figure 29A). The positively charged di-arginine motif and its distinct placement has been shown to be essential for its interaction with the negatively charged phosphatidylinositol PI(4,5)P_2 upon membrane anchorage via the geranylgeranyl moiety (Johnson, Erickson, and Cerione 2012). PI(4,5)P_2 is known to be enriched at the plasma membrane. In contract, brain Cdc42 lacks this motif (Figure 29A). We hypothesized that the di-arginine motif could be responsible for the plasma membrane recruitment and enrichment of Cdc42u. Because Cdc42b lacks the di-arginine motif, it could fail to interact with PI(4,5)P_2 and would associate to a lesser extent to the plasma membrane. To test this hypothesis, we used PM GUVs composed of 5% PI(4,5)P_2 (EggPC was reduced to 15%), denoted 'PM+PIP2' in the following, and compared the membrane recruitment of Cdc42u and Cdc42b. We observed that Cdc42u and Cdc42b were both recruited on PM+PIP2 GUVs (Figure 29B,C). Yet Cdc42u displayed significantly increased membrane recruitment to PM+PIP2 GUVs, while Cdc42b did not distinguish between PM+PIP2 GUVs and control PM GUVs (Figure 29D,E). Cdc42u showed almost four-fold increased affinity for PM+PIP2 GUVs (Figure 29F). This indicates that the di-arginine motif is crucial for plasma membrane targeting and may dictate the subcellular localization of Cdc42 variants in cells. Consistently, plasma membrane targeting of K-RAS, the only RAS protein which is not palmitoylated, is largely dependent on its polybasic region(Ahearn et al. 2012). Additionally, unlike palmitoylated RAS proteins (H/N-RAS) which are primarily Golgi-localized, K-RAS is stably associated to the plasma membrane.

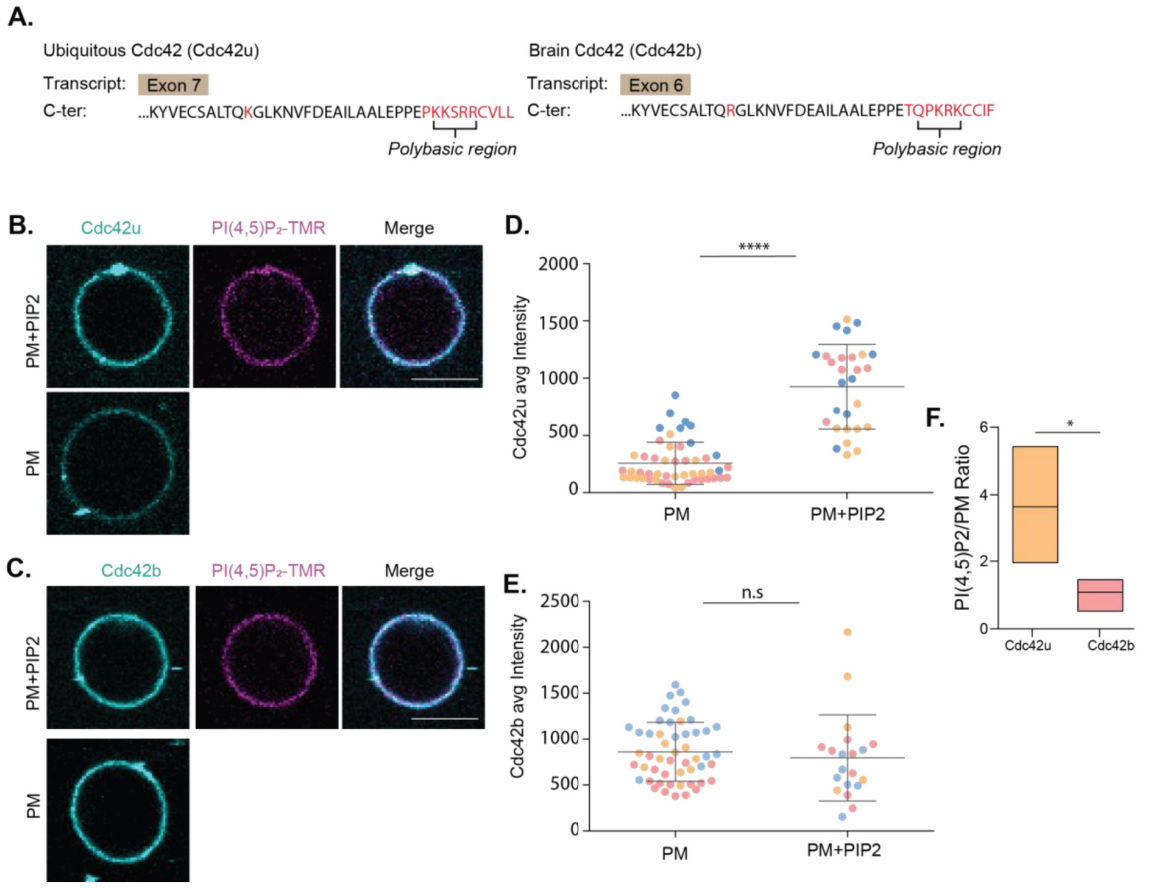

Figure 29 Ubiquitous Cdc42 interacts with PI(4,5)P_2 while brain Cdc42 does not.

A) Schematic showing the differences in the PBR of Cdc42 variants. **B-C)** To test the influence of the PBR region on Cdc42 variants binding to membranes, we added 5% PI(4,5)P_2 to the plasma membrane-like composition (PM+PIP2). Confocal images showing Cdc42u and Cdc42b binding to PM+PIP2 GUVs (cyan) was visualized along with control PM GUVS. PI(4,5)P_2 incorporation in the GUVs was visualized by the addition of fluorescent TMR-PI(4,5)P_2 (magenta). Scale bar, 10 µm. **D-E)** The scatter plots representing mean grey scale intensity values (mean ± SEM) of the GUVs represented in B), show that Cdc42u significantly binds more to PM+PIP2 GUVs than to control PM GUVs (****=t-test, p<0.0001), while Cdc42b does not demonstrate this differential binding (n.s). (number of GUVs used (n) in graphs; D) n=50, 28 and E) n=51,20 for conditions PM and PM+PIP2 respectively) **F)** Box plot showing mean intensity ratio of PM+PIP2 versus PM binding (mean ± SEM, bounds=95% confidence interval). The plot shows that Cdc42u binds to PM+PIP2 GUVs two-fold more than control PM GUVs (*=t-test, p=0.0185) while brain shows no significant difference (n.s.).

C-ter amino acids of Cdc42 variants interact contrarily with Golgi apparatus like vesicles

We next investigated whether the last 10 differential carboxy terminal amino acids of Cdc42 variants (Figure 30A) play a role in specific membrane recruitment of Cdc42 variants. For that purpose, we studied the recruitment of GFP tagged to the Cdc42 C-ter amino acids (referred to as u(C-ter) for Cdc42u and b(C-ter) for Cdc42b). Notably, Cdc42 C-ter alone does not have the ability to interact with GDI1 therefore, it does not co-purify as a complex with GDI1. In astrocytes, we observe an enriched Golgi apparatus like localization for b(C-ter) (Figure 30B) while u(C-ter) is mostly cytosolic. Therefore, we tested the membrane recruitment of u(C-ter) and b(C-ter) using GM and PM like GUVs (Figure 30C). Interestingly, we observe that u(C-ter) alone does not distinguish between GM and PM like GUVs (Figure 30D), while b(C-ter) significantly demonstrates increased membrane recruitment on GM GUVs compared to PM GUVs (Figure 30E). b(C-ter) prefers GM GUVs three-fold more than PM GUVs (Figure 30E). These findings indicate that b(C-ter) alone prefers GM membranes with lower Chol:PL ratio while u(C-ter) loses its ability to selectively bind to GM membranes. The key difference between earlier experiments performed with full length Cdc42u membrane recruitment is the presence of GDI1. Therefore, the absence of GDI1 seems to be responsible for u(C-ter) to lose its ability to specifically bind to GM membranes. This suggests that GDI1 association and dissociation with Cdc42 could influence the membrane anchorage of Cdc42 proteins and possibly their membrane association dynamics too. In addition to accommodating the geranylgeranyl moiety on the C-ter of Cdc42, GDI1 also interacts with other upstream domains on Cdc42. For Cdc42u, it is also reported that Lys 184 and Arg 186 interact with GDI1 (Nomanbhoy and Cerione 1996), however the interaction between the PBR of Cdc42b and GDI1 is not known.

We then studied the ability of the potentially differentially lipid modified Cdc42 C-ter variants to sense lipid packing defects. For this purpose, we used GM supplemented with 15% DOG GUVs mentioned above (GM+DOG GUVs) as Golgi membranes demonstrate more packing defects as opposed to plasma membrane . Preliminary experiments show that both C-ter proteins were capable of binding to DOG incorporated GUVs (Figure 30G). However, unlike full length Cdc42 proteins, b(C-ter) tends to strongly dislike (0.2 fold) DOG incorporated GUVs (Figure 30H,J), while u(C-ter) approximately has a slight preference towards DOG membranes (1.5 fold) (Figure 30I). Prenylated proteins prefer membranes with lipid packing defects This unexpected behaviour of Cdc42 variant C-ter could again be due to their inability to bind to GDI1. This suggests that GDI1 has an essential role in the membrane recruitment and sensing of Cdc42 variants.

Figure 30

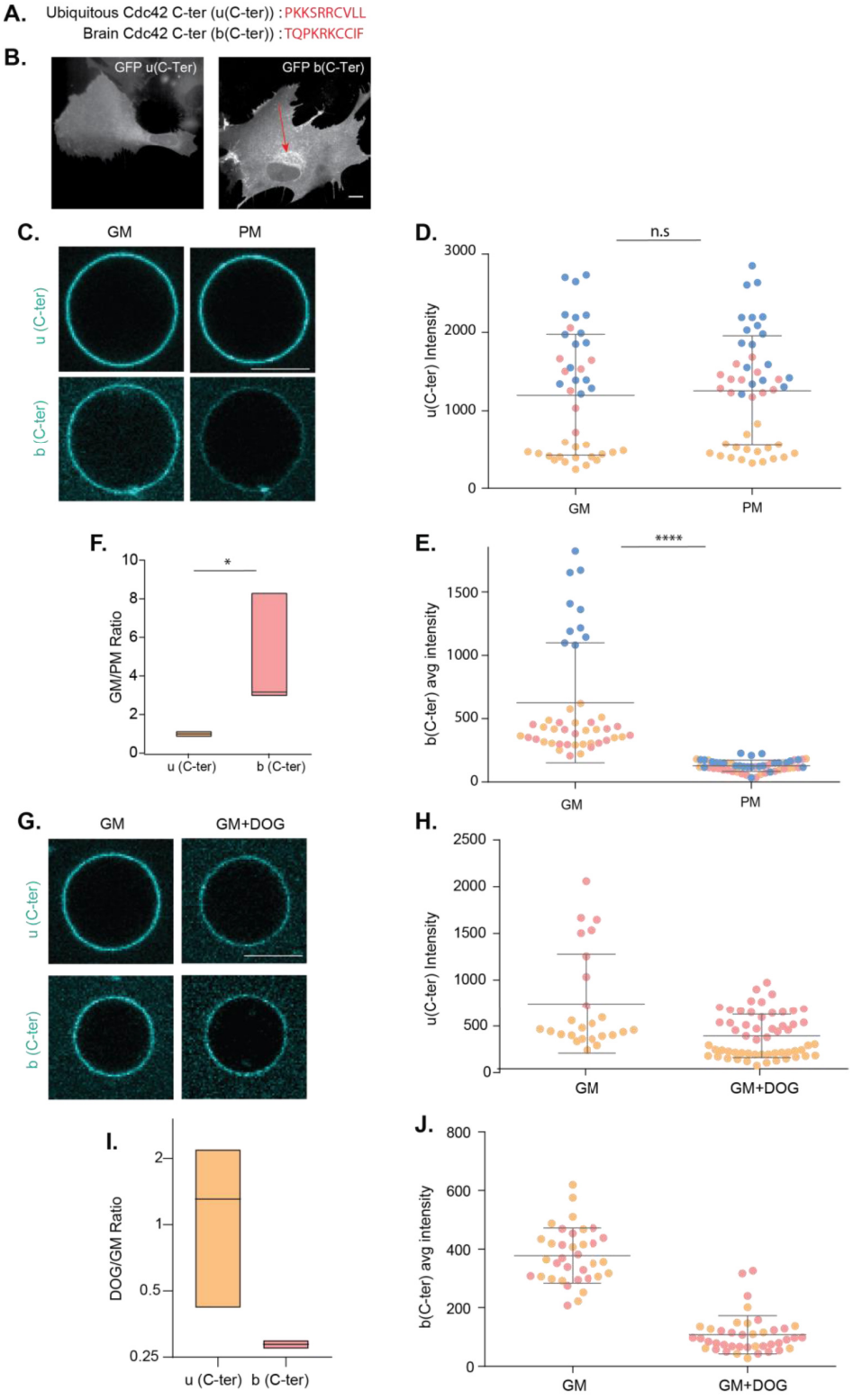
A.
Ubiquitous Cdc42 C-ter (u(C-ter)) : PKKSRRCVLL
Brain Cdc42 C-ter (b(C-ter)) : TQPKRKCCIF
B.
GFP u(C-Ter)
GFP b(C-Ter)
C.
GM
PM
u (C-ter)
b (C-ter)
D.
n.s
u(C-ter) Intensity
3000
2000
1000
0
GM
PM
F.
*
GM/PM Ratio
10
8
6
4
2
0
u (C-ter)
b (C-ter)
E.
****
b(C-ter) avg intensity
1500
1000
500
0
GM
PM
G.
GM
GM+DOG
u (C-ter)
b (C-ter)
H.
u(C-ter) Intensity
2500
2000
1500
1000
500
0
GM
GM+DOG
I.
DOG/GM Ratio
2
1
0.5
0.25
u (C-ter)
b (C-ter)
J.
b(C-ter) avg intensity
800
600
400
200
0
GM
GM+DOG

Figure 30(A-F) C-ter amino acids of Cdc42 variants interact differently with GM GUVs

A) Schematic showing Cdc42 variant specific last 10 amino acids, which were fused to GFP to express proteins, referred to as u(C-ter) and b(C-ter). **B)** Spinning disk live images of Cdc42 C-ter proteins expressed in astrocytes, where u(C-Ter) is cytosolic and b(C-ter) shows perinuclear endomembrane localization indicated by the red arrow. Scale bar, 10 µm. **C)** Confocal images showing C-ter proteins were bound to GM and PM GUVs. Scale bar, 10 µm. **D-E)** The scatter plots representing mean grey scale intensity values (mean ± SEM) of the GUVs represented in C) show that u(C-ter) does not distinguish between GM and PM GUVs while b(C-ter) significantly binds to GM GUVs(****=t=test, $p<0.0001$). (number of GUVs used (n) in graphs; D) n=41, 47 and E) n=46, 55 for GM and PM conditions respectively) **F)** Box plot showing mean intensity ratio of GM versus PM binding (mean ± SEM, bounds=95% confidence interval). The plot shows that b(C-ter) binds to GM GUVs three-fold more than PM GUVs (*=t-test, $p=0.0334$) which is significantly more than b(C-ter) whose ratio is close to 1. **(G-J) C-ter amino acids of Cdc42 variants and lipid packing defects G)** Lipid packing defects were induced by adding 15%DOG to the GM GUV composition. C-ter proteins were bound to control GM GUVs and GM+DOG GUVs. Scale bar, 10 µm. **H-J)** Average intensity quantifications from preliminary (N=2) experiments show that u(C-ter) and b(C-ter) proteins tend to bind better to GM GUVs and do not prefer GUVs with lipid packing defects. (number of GUVs used (n) in graphs H) n=24,56 and I) n=34,40 for conditions GM and GM+DOG respectively). **I)** Box plot showing mean intensity ratio of DOG versus GM binding (mean ± SEM, bounds=95% confidence interval) for Cdc42 C-ter proteins. The u(C-ter) ratio tends to show a slight preference(1.5 fold) towards DOG GUVs as compared to GM. b(C-ter) however does not prefer DOG GUVs (0.2 fold).

R186C Cdc42u patient mutant

To confirm whether all Cdc42 proteins intrinsically prefer Golgi-like membranes we tested the membrane recruitment of the R186C Cdc42u patient mutant. This mutant is highly palmitoylated on R186C residue and is prenylated on Cys 188. We tested its membrane recruitment using GM and PM GUVs. R186C was capable of binding both GM and PM GUVs (Figure 31A). Not surprisingly, we observed significantly increased membrane recruitment of R186C on GM GUVs as compared to PM GUVs (Figure 31B). While comparing its GM/PM ratio, the R186C mutant had a significantly higher ratio than control Cdc42u (Figure 31C). This indicates that prenylated Cdc42 proteins intrinsically prefer GM membranes.

We demonstrated earlier that Cdc42u interacts with PI(4,5)P_2 enriched PM (PM+PIP2) GUVs. Since the R186C mutant undergoes a mutation on residue R186, which is part of the di-arginine motif in the PBR of Cdc42u, we wanted to test whether the mutation impaired membrane interaction with PI(4,5)P_2 enriched GUVs(Figure 31D). Preliminary experiments suggest that R186C does not interact preferentially with PM+PIP2 GUVs unlike control Cdc42u (Figure 31E). This in agreement with the role of the Cdc42u di-arginine motif in enhancing PI(4,5)P_2 enriched plasma membrane interaction.

Figure 31

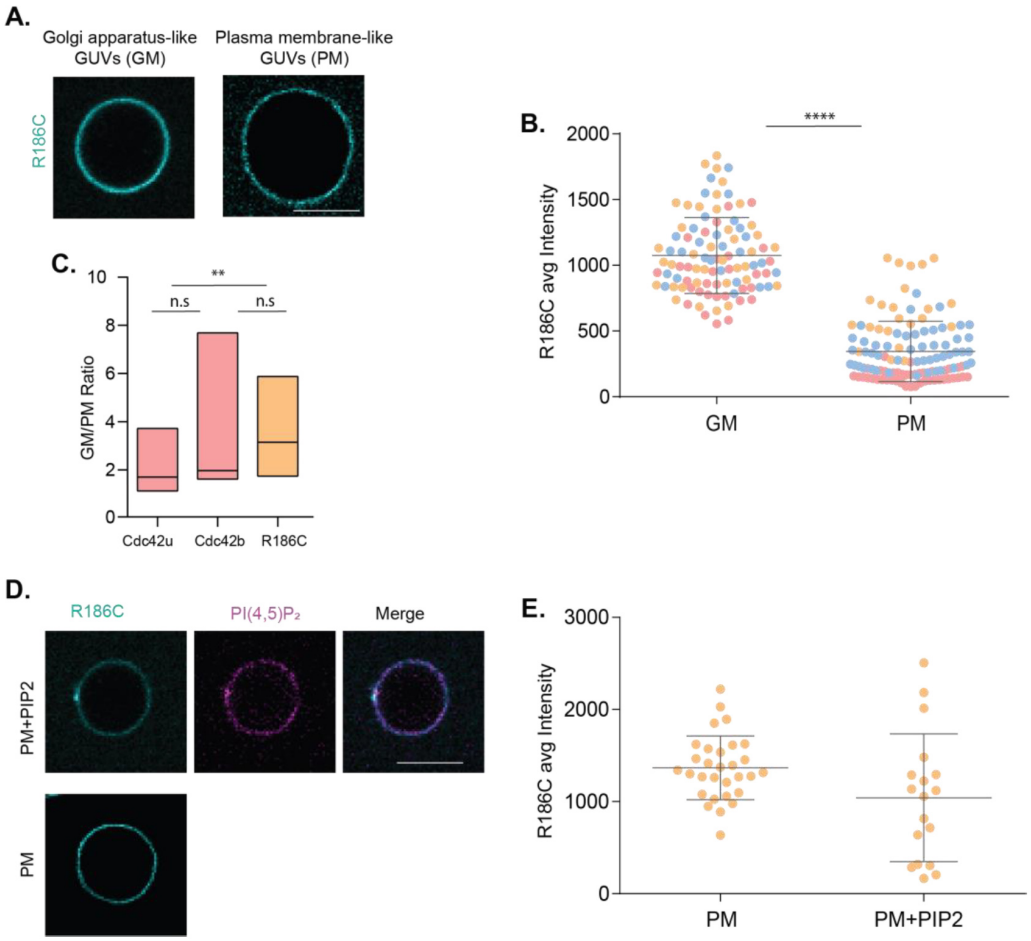
A.
Golgi apparatus-like GUVs (GM)
Plasma membrane-like GUVs (PM)
R186C
B.
****
R186C avg Intensity
2000
1500
1000
500
0
GM
PM
C.
**
n.s
n.s
GM/PM Ratio
10
8
6
4
2
0
Cdc42u
Cdc42b
R186C
D.
R186C
PI(4,5)P2
Merge
PM+PIP2
PM
E.
R186C avg Intensity
3000
2000
1000
0
PM
PM+PIP2

Figure 31 R186C Cdc42u patient mutant

A) Confocal images showing purified R186C mutant protein was bound to GM and PM GUVs. Scale bar, 10 μm. **B)** The scatter plots representing mean grey scale intensity values (mean ± SEM) of the GUVs represented in A), show that R186C significantly binds preferentially to GM GUVs (****=t-test, $p<0.0001$). (Number of GUVs used (n); n=99,117 for GM and PM conditions respectively) **C)** Box plot showing mean intensity ratio of GM versus PM binding (mean ± SEM, bounds=95% confidence interval). Ratios of R186C were compared with that of Cdc42u and Cdc42b. R186C approximately binds GM GUVs three-fold more than PM GUVs. The GM/PM ratio of R186C is significantly higher than that of Cdc42u (**=t-test, p=0.0088). **D)** Confocal images showing R186C mutant protein (cyan) was bound to PM+PIP2 GUVs. $PI(4,5)P_2$ incorporation in the GUVs was visualized by the addition of fluorescent TMR-$PI(4,5)P_2$ (magenta). Scale bar, 10 μm. **E)** The scatter plots representing mean grey scale intensity values (mean ± SEM) of the GUVs represented in D), of a preliminary experiment (N=1) suggests that R186C does not preferentially interact with $PI(4,5)P_2$. (Number of GUVs used (n); n=30,18 for PM and PM+PIP2 conditions respectively).

Section D

During the course of my PhD, we have initiated a project entitled 'Cdc42 in the nucleus' carried out by three different master students under my co-supervision (Gregoire Mathonnet [Jan-June 2018], Astrid Boström [Sept 2018-Sept 2019] and Dylan Ramage [Sept 2019-June2020]). This project focuses on understanding what could drive the distinct nuclear accumulation of unprenylated Cdc42 lipid mutants observed during this study (see Article 1). Our main objective being to identify a potential role of Cdc42 in the nucleus. This section only contains selective results from this nuclear study that supports the role of the polybasic region being a major regulator of subcellular localization of Cdc42 variants.

C-terminal amino acids of Cdc42 variants encode a cryptic NLS.

This project was initiated after the proteomic analysis data we obtained for Cdc42 variants showed that karyopherins (protein family involved in nucleocytoplasmic transport) (Mosammaparast and Pemberton 2004) were significantly pulled down with Cdc42 variants (Article.1, Figure S2A,B). A few examples include Transportin-1/2, Exportin-4 and Importin-5. Previously, we had also observed that chemically inhibiting prenylation made Cdc42 variants accumulate in the nucleus in astrocytes (Article.1, Figure 1E, S1A). Similar nuclear accumulation was seen when expressing unprenylated Cdc42 mutant u(SVLL) in astrocytes (Figure 32A). This distinct nuclear accumulation has also been observed for other unprenylated mutants of Rho GTPases such as Rac and RhoA (Michaelson et al. 2008; Abdrabou and Wang 2018). However, we observed a striking difference between the subcellular localization of unprenylated mutants of Cdc42 variants (u(SVLL) versus b(SCIF)) (Figure 32A). u(SVLL) is distinctly more nuclear than b(SCIF). Interestingly, the double lipid mutant b(SSIF) is however capable of accumulating into the nucleus, but still does not manage to accumulate as much as u(SVLL) (Figure 32A). This made us investigate whether Cdc42 could be transported into the nucleus in a selective manner.

For a protein to be actively imported into the nucleus via karyopherins it needs to have a nuclear localization sequence (NLS)(B. J. Lee et al. 2006). Therefore, we ran an *in silico* NLS prediction for Cdc42 variants using cNLS Mapper. Proteins having a classical NLS (cNLS) can fall under two groups, either monopartite (sequence consisting of a single stretch of basic amino acids) or bipartite (consisting of two stretches of basic amino acids separated by a linker region) (B. J. Lee et al. 2006). Interestingly, both Cdc42 variants were predicted to encode a bipartite NLS encoded by 28 and 29 C-ter amino acids for Cdc42u and Cdc42b respectively (Figure 32A). Both variants were predicted to have a monopartite NLS. However, wildtype Cdc42 variants, which encode these NLS, do not demonstrate nuclear accumulation. This is because the Cdc42 NLS is only dominant in the absence of its C-ter prenylation. This type of NLS is referred to as a cryptic NLS, which is also observed in the case of Rac1(Michaelson et al. 2008). Despite having similar cryptic NLS regions, lipid mutants of Cdc42 variants localize differently to the nucleus (u(SVLL) and b(SSIF)). This could be due to the differences in the polybasic residues of their cryptic NLS.

Figure 32

A.

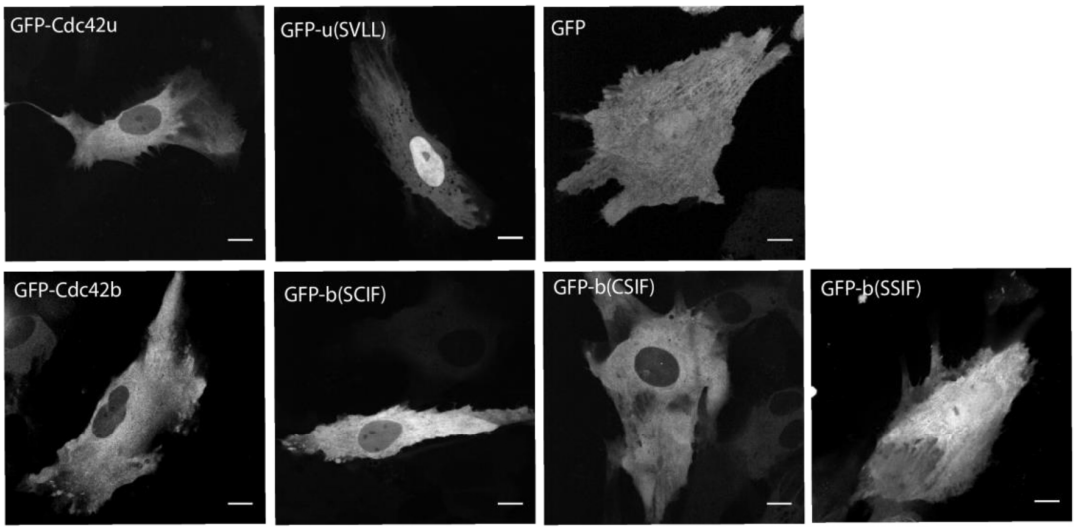

B.

Predicted NLSs in query sequence

```
QTIKCVVVGDGAVGKTCLLISYTTNKFPSEYVPTVFDNYAVTVMIGGEPY 50
TLGLFDTAGQEDYDRLRPLSYPQTDVFLVCFSVVSPSSFENVKEKWVPEI 100
THHCPKTPFLLVGTQIDLRDDPSTIEKLAKNKQKPITPETAEKLARDLKA 150
VKYVECSALTQKGLKNVFDEAILAALEPPEPKKSRRCVLL            190
```

Predicted monopartite NLS

Pos.	Sequence	Score

Predicted bipartite NLS

Pos.	Sequence	Score
161	QKGLKNVFDEAILAALEPPEPKKSRRC	5.1
161	QKGLKNVFDEAILAALEPPEPKKSRRCV	5.2
162	KGLKNVFDEAILAALEPPEPKKSRRC	5.9

C.

Predicted NLSs in query sequence

```
QTIKCVVVGDGAVGKTCLLISYTTNKFPSEYVPTVFDNYAVTVMIGGEPY 50
TLGLFDTAGQEDYDRLRPLSYPQTDVFLVCFSVVSPSSFENVKEKWVPEI 100
THHCPKTPFLLVGTQIDLRDDPSTIEKLAKNKQKPITPETAEKLARDLKA 150
VKYVECSALTQRGLKNVFDEAILAALEPPETQPKRKCCIF            190
```

Predicted monopartite NLS

Pos.	Sequence	Score

Predicted bipartite NLS

Pos.	Sequence	Score
161	QRGLKNVFDEAILAALEPPETQPKRKCCI	5.5
162	RGLKNVFDEAILAALEPPETQPKRKCCI	8.6

Figure 32 Nuclear accumulation of unprenylated Cdc42 mutants

A) Spinning disk live images of astrocytes transiently expressing GFP-tagged Cdc42 proteins. Cdc42u, Cdc42b and non-palmitoylable b(CSIF) do not accumulate in the nucleus. Unprenylated b(SCIF) tends to accumulate slightly more in the nucleus compared to wildtype brain Cdc42. Unprenylated u(SVLL) mutant shows a distinct nuclear enrichment. Brain double mutant b(SSIF) tends to enter the nucleus similar to that observed with control GFP. **B-C)** NLS prediction was performed for **B)** Cdc42u and **C)** Cdc42b using cNLS Mapper, available at http://nls-mapper.iab.keio.ac.jp/. Both proteins have their predicted NLS situated in their carboxy terminal comprising of 28 and 29 amino acids highlighted in red for Cdc42u and Cdc42b respectively. They both lack a monopartite NLS and their respective scores for a bipartite NLS are represented.

The PBR is essential for nuclear accumulation of ubiquitous Cdc42

The PBR has been shown to play a key role in defining the strength of the cryptic NLS of the GTPase Rac1(Abdrabou and Wang 2018; Michaelson et al. 2008). We hypothesized that disrupting the Cdc42u PBR might impair the nuclear enrichment of Cdc42u. For this purpose, we first generated a u(ΔVLL) mutant that lacks the last three amino acids of the CaaX box to recreate a mutant representative of CaaX box processing. Followed by which another mutation targeting the PBR was introduced in the ΔVLL background. The resulting double mutant, ΔVLL R187A Cdc42, herein referred to as the u(PBR) mutant, harboured a novel amino acid substitution of a basic arginine to a neutral alanine at position 187 and was designed in an attempt to weaken the NLS potential conferred by Cdc42 PBR. Position 187 is immediately upstream of the CaaX box cysteine residue and is therefore the basic residue of Cdc42 PBR closest to the NLS-blocking lipid tail under physiological conditions. This one amino acid substitution is predicted to kill an existing NLS present in Cdc42 C-terminus according to the *in silico* NLS prediction software NLS mapper (Figure 33B). GFP tagged u(PBR) was transfected into HeLa cells along with Cdc42u and ΔVLL, the cells were fixed and stained as before imaging.

Epifluorescence images of transfected HeLa cells show the PBR mutant enriched primarily within the nucleus, to a similar degree as seen for ΔVLL. However, there appeared to be a distinctly stronger GFP signal coming from the cytoplasm of PBR mutant transfected HeLa cells compared with those transfected with ΔVLL (Figure 33A). Transfection quantification of u(PBR) confirms that its nuclear localization is significantly greater than both Cdc42u as well as the GFP control. However, statistical analysis also revealed a significant difference in the nuclear localization of ΔVLL Cdc42 and u(PBR) mutated Cdc42, showing the PBR double mutant as significantly less nuclear (Figure 33C). This result confirms that Cdc42u PBR is at least partly responsible for its nuclear targeting since mutation of PBR residues reduces the observable nuclear pool of Cdc42. Yet again we report here the role of the PBR as being crucial for subcellular localization.

Figure 33

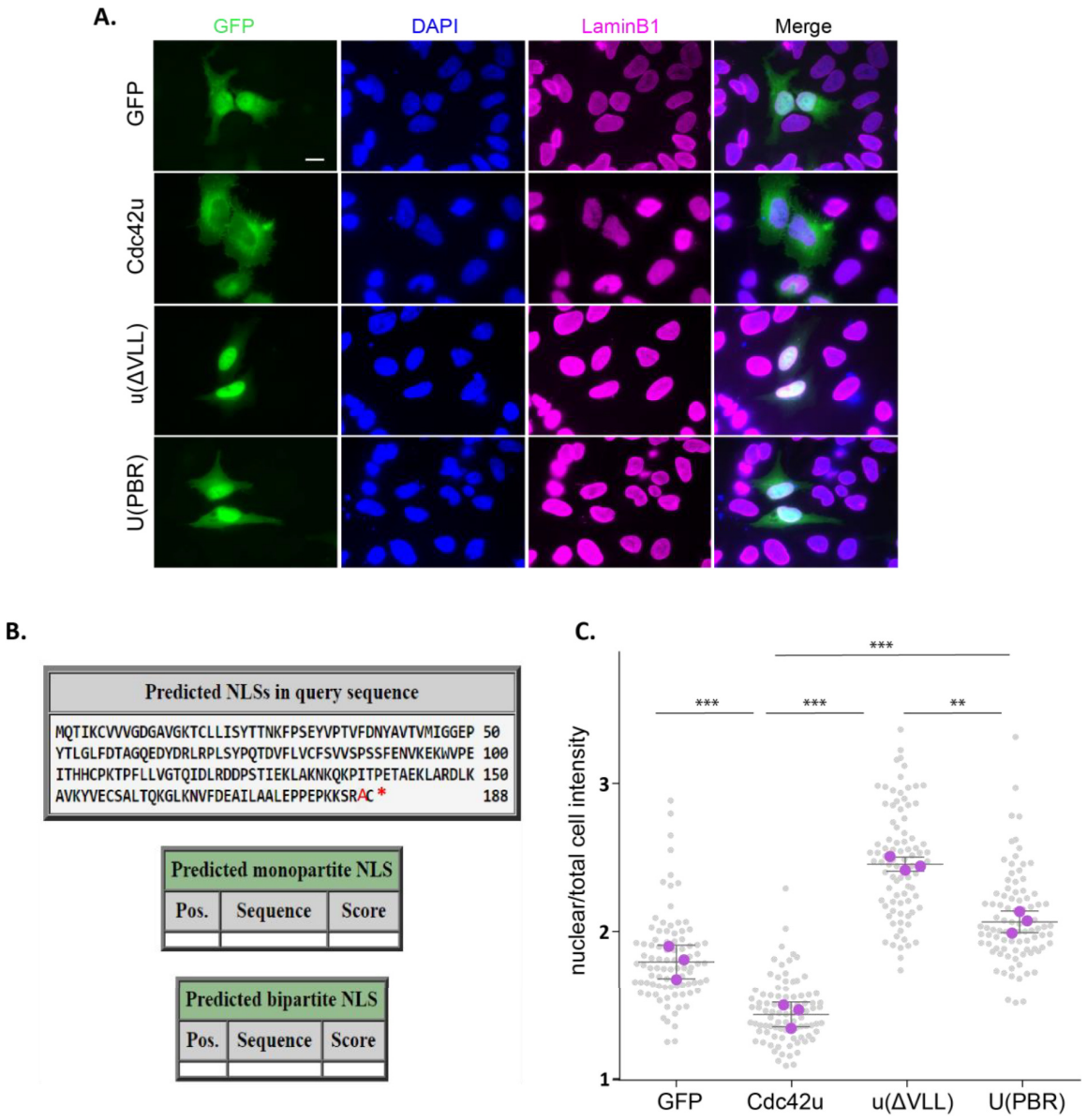
A.
GFP
DAPI
LaminB1
Merge
GFP
Cdc42u
u(ΔVLL)
U(PBR)
B.
Predicted NLSs in query sequence
MQTIKCVVVGDGAVGKTCLLISYTTNKFPSEYVPTVFDNYAVTVMIGGEP 50
YTLGLFDTAGQEDYDRLRPLSYPQTDVFLVCFSVVSPSSFENVKEKWVPE 100
ITHHCPKTPFLLVGTQIDLRDDPSTIEKLAKNKQKPITPETAEKLARDLK 150
AVKYVECSALTQKGLKNVFDEAILAALEPPEPKKSRAC* 188
Predicted monopartite NLS
Pos.
Sequence
Score
Predicted bipartite NLS
Pos.
Sequence
Score
C.
***
***
***
**
nuclear/total cell intensity
3
2
1
GFP
Cdc42u
u(ΔVLL)
U(PBR)

Figure 33 PBR is essential for nuclear accumulation of ubiquitous Cdc42

A)Epifluorescence images of fixed HeLa cells stained with anti laminB1 antibodies (magenta) and DAPI (blue). transiently expressing GFP-tagged Cdc42u, truncated u(ΔVLL) and truncated u(PBR) mutant. **B)** R187A mutation affecting Cdc42 PBR is predicted to eliminate a C-terminal NLS according to cNLS Mapper, available at http://nls-mapper.iab.keio.ac.jp/. **C)** Nuclear/total cell intensity ratio was quantified for each cell (grey dot) by measuring the mean nuclear grey value and dividing this with the total cell mean grey value, 30 cells were used in each replica. this value with the total cell mean grey value, with 30 cells being used in each replica. Statistical analysis using the mean ratio of each replica (purple dot) was performed by an unpaired two tailed t-test (mean ± SEM n=3). Scale bar=10μm (Δ VLL : truncated non lipidated GFP Cdc42u, Δ VLL CA : truncated non lipidated and constitutively active GFP Cdc42u).

Part V

Discussion

This interdisciplinary study addresses three key aspects- subcellular localization, function and regulation of Cdc42 variants observed in vertebrates. On a cellular scale, their roles associated with front-to-rear cell polarization and directed migration have been elucidated, in parallel to other studies demonstrating the functions of Cdc42 variants during neurogenesis and neuronal differentiation (Yap et al. 2016; Endo, Druso, and Cerione 2020).

Localization and functions of Cdc42 variants

Subcellular localization of Cdc42 is key for both its function and regulation (Osmani et al. 2010; Mitin et al. 2012; Makowski, Tran, and Field 2017). Here we report differential subcellular localization of Cdc42 variants upon microinjection in primary rat astrocytes. The ubiquitous isoform Cdc42u is predominantly cytosolic and plasma membrane-associated, whereas the brain isoform Cdc42b is enriched in the Golgi apparatus in immobile astrocytes within a confluent monolayer and, during migration, in vesicles participating in polarized trafficking towards the leading edge. This is suggestive of the existence of two distinct subcellular pools of Cdc42, 1) the plasma membrane-associated Cdc42u and 2) Golgi-localized Cdc42b. These subcellular pools of Cdc42 have been previously described. Yet, most studies have focused on the plasma membrane-associated Cdc42 pool (Farhan and Hsu 2016; Phuyal and Farhan 2019). Here we emphasize that this distinct subcellular localization could be isoform specific in cells expressing both variants. However, we have also noticed that Cdc42u localises, albeit not at high concentration, at the Golgi apparatus too. This may explain some functions for Cdc42u described at the Golgi apparatus obtained by other groups after overexpression of GFP tagged Cdc42u (Baschieri et al. 2014; Kage et al. 2017b). Another possibility is that these studies in fact used Cdc42b and not Cdc42u, as in Etienne-Manneville and Hall 2001; and Osmani et al. 2006.

Furthermore, studying the role of Cdc42 isoforms during cell polarization unravels-striking differences. Emphasis has been made on Cdc42u as the major isoform involved in cell polarity (Article.1, Figure 3). Cdc42u knockdown phenocopies the polarity defects observed with the knockdown of both isoforms which leads to the loss of persistence and directionality of migrating cells, along with cells failing to reorient their Golgi apparatus. We also report that Cdc42u is responsible for recruiting aPKC to the leading edge and therefore is primarily involved in the Par6/aPKC polarity complex. Whereas, Cdc42b does not seem to

play a role in initial cell polarization events, which could be explained by its weaker, and possibly delayed interaction with the leading-edge plasma membrane.

It is important however to note that the expression of Cdc42 isoforms in astrocytes is skewed by a ratio of 17:3 (Cdc42u:Cdc42b)(Yap et al. 2016). Therefore, it was important to address whether the dispensable role of Cdc42b in cell polarization could be due to its low expression level. This surely is not the case since even overexpression of Cdc42b in cells lacking both isoforms does not rescue the defects observed with Golgi reorientation, while overexpression of Cdc42u does (Article.1, Figure 3E).

Neural precursor cells (NPCs) were also used as they display an equivalent level of expression of the two Cdc42 variants (1:1 ratio)(Article.1, Figure S3A). Primarily NPCs are a more physiological and complex cellular model, and during development, they can differentiate into mature neurons or into glial cells, such as astrocytes (Zahr, Kaplan, and Miller 2019). Most importantly, they exhibit co-expression of the isoforms and have been used to elucidate their role in neuronal differentiation (Yap et al. 2016). Like in astrocytes, Cdc42u and Cdc42b display distinct subcellular localization in NPCs. The ubiquitous isoform was mainly visible in the cytosol and at the plasma membrane while the brain isoform localized to intracellular EEA1-positive vesicles and to the Golgi apparatus. Yet again, directional persistence of migration decreased when NPCs were depleted of Cdc42u or of both isoforms, but did not require the expression of Cdc42b (Article.1, Figure 5A, B).These findings reinforce the role of Cdc42u as the isoform exclusively associated with cell polarity establishment both in astrocytes and NPCs.

To further assess the role of plasma membrane-associated Cdc42u as a polarity regulator, two key questions need to be addressed: 1) what is the role of Cdc42 variants in the formation of filopodia at the leading edge of migrating astrocytes? and 2) what is the role of Cdc42u in reorienting the Golgi apparatus at the leading edge, which has previously been shown to be a microtubule dependent process regulated by the Cdc42/Par6/aPKC complex (Palazzo et al. 2001; Sandrine Etienne-Manneville and Hall 2001).

We studied the functional relevance of Cdc42b in macropinocytosis in astrocytes and in endocytosis in NPCs, after observing that palmitoylation of Cdc42b promotes its association with vesicles in astrocytes (Article.1, Figure 1E). Our findings highlight that palmitoylated Cdc42b embodies the major isoform regulating macropinocytosis in migrating astrocytes. In NPCs, chemotaxis is an endocytosis-dependent pathway (P. Zhou et al. 2007) and yet again Cdc42b regulates this process. Cdc42b governs macropinocytosis in astrocytes and endocytosis in NPCs in an N-WASP dependent manner (Article.1, Figure 4, 5).N-WASP has previously been shown to be involved in endocytosis (Kessels and Qualmann 2002; Legg et al. 2007). When observing the localization of N-WASP in migrating astrocytes, we found that it colocalized with Cdc42b on large macropinosomes and accumulated at the front of the cell protrusion (Article.1, Figure 4C). Notably, Cdc42b-driven N-WASP mediated endocytosis is

one of the clathrin-independent endocytic routes regulated by Cdc42. Among the many other clathrin-independent endocytosis (CIE) processes, Cdc42 is a major regulator of the CLIC/GEEC pathway (S. Mayor, Parton, and Donaldson 2014). Therefore, dissecting the isoform specific role in the CLIC/GEEC pathway will be crucial to confirm the exclusive role of Cdc42b in Cdc42 dependent CIE processes both in astrocytes and NPCs.

The functional relevance of Cdc42b localized on vesicles associated with polarized trafficking either toward or from the leading edge still remains unanswered. More precisely, what regulates the loading of palmitoylated Cdc42b on vesicles from the Golgi apparatus, and what is the nucleotide-bound state (activity) of Cdc42b as it exits from the Golgi apparatus via vesicles directed to the leading edge and possibly back to the Golgi apparatus remains unclear. Considering previous work conducted in migrating astrocytes, we know that Cdc42 accumulation and activation at the wound edge results from wound-induced integrin signalling (Sandrine Etienne-Manneville and Hall 2001) and Arf6-dependent vesicular delivery of Cdc42 along with its GEF β-PIX. Yet only after β-PIX interacts with Scrib (Osmani et al. 2006) and Src kinase phosphorylates β-PIX (Feng et al. 2006) at the leading edge does β-PIX activate Cdc42 (as opposed to activating Rac in absence of Src phosphorylation). This in turn results in the generation of a Cdc42-mediated polarity signalling via the Cdc42/Par6/aPKC complex (Sandrine Etienne-Manneville and Hall 2003b). Therefore, Cdc42b could possibly only be activated upon reaching the leading edge and remain inactive on vesicles. However, this still does not explain what regulates palmitoylated Cdc42b loading onto vesicles in the first place.

In summary, while the brain isoform Cdc42b constitutes the predominant splice variant in the regulation of macropinocytosis in astrocytes and NPCs, efficient cell polarization, directed and persistent migration as well as chemotaxis in astrocytes seem to require only the ubiquitous isoform Cdc42u. Cdc42u is thus the prevalent splice variant involved in the crucial function of Cdc42 in the regulation of cell polarity. However, with the function of Cdc42b in the formation of dendritic filopodia and spines (Kang et al. 2008; Wirth et al. 2013) and its role in endocytosis and NPC chemotaxis, increasing evidence suggests that the brain variant has important specific functions that distinguish it from Cdc42u (Yap et al. 2016; Endo, Druso, and Cerione 2020). NPC migration is a crucial step in brain development and conditional deletion of both Cdc42 isoforms in mouse NPCs has been shown to cause malformations in the brain (L. Chen et al. 2006). Our results indicate that the two Cdc42 isoforms may nevertheless contribute different functions to the behaviour of NPCs, underlining that the molecular regulators of NPC migration in brain development are far from being understood. A detailed characterization of regulators of NPC migration may also help to understand the molecular and genetic causes of a group of severe brain development disorders in human, known together as Neural Migration Disorders (Copp and Harding 1999; Schwarz, Stichel, and Luhmann 2000).

Does alternative splicing affect Cdc42 interactome?

The Cdc42 variants have distinct functions associated with cell polarization and cell migration. This raises the question as to whether they have differential interactomes. They share 95% sequence identity, yet their differences are observed in the C-ter hypervariable region of Rho GTPases. The effector binding domain is upstream of Cdc42, identical for both Cdc42 variants. Yet, considering Rac for which the C-terminal polybasic region (PBR) was previously shown to participate in its interaction with effectors such as PAK (Knaus et al. 1998; Abdrabou and Wang 2018), we have studied the differential interactome of Cdc42 variants. Using astrocytes to perform proteomic analysis is technically challenging, because microinjecting astrocytes limits the yield of Cdc42 expressing cells which is insufficient for mass spectrometry. Proteomic analysis was thus performed using HEK cells in which the overexpression Cdc42 variants display similar subcellular localization. Upon analysing the interactomes of both wildtype and constitutively active Cdc42 variants, we observed that they qualitatively pull-down identical interactors involved in polarity pathways and Rho GTPase downstream signalling. Quantitatively, the fold change for each of these interactors is approximately linearly correlated, suggesting that they both tend to pull down similar levels of interactors. It is however important to note that the levels of sample Cdc42 variants were skewed to begin with, since Cdc42u is more expressed compared to Cdc42b. Yet both variants pulled-down interactors with similar ratios (Article.1, Figure 2,S2).This can be explained by Cdc42 sample saturation. Interestingly, despite sample saturation, we still observe that both variants are capable of pulling down similar interactors, the same is validated via immunoprecipitation assays. Therefore, the subcellular localization of Cdc42 variants happens to be a predominant determinant of Cdc42 functions. To further confirm this, we would have to use proximity-ligation approaches or BioID screens prior to proteomic analysis (Roux et al. 2018) to obtain a more precise understanding of the differential interactomes of Cdc42 variants in situ. However, a BioID screen would probably raise the same technical problems and prevent precise localization of the proteins due to overexpression in HEK cells.

In conclusion, our results show that although both Cdc42 isoforms have non-redundant functions in the cell, they surprisingly share most of their protein effectors. This strongly suggests that Cdc42 interaction, with their effectors and cellular function depends on its intracellular localization, which is dictated by the carboxy-terminal sequence and lipid modifications.

During the course of this study a collaboration was set up with Jerome Delon (Institut Cochin) to perform proteomic analysis for a Cdc42u patient mutant containing a heterozygous mutation resulting in a substitution of the arginine residue at position 186 to

a cysteine residue (R186C). The cysteine substitution results in a gain of function being an additional palmitoylation. Therefore, the patient now expresses a pool of Cdc42u which is dually lipidated similar to Cdc42b. Interestingly, this highly palmitoylated R186C Cdc42u mutant is distinctly Golgi-localized (see Annex Article.1, Figure 1D,E). Phenotypically this patient suffers from a condition posing a combination phenotype of a pustular psoriasis disease and a myelodysplastic syndrome. We expressed the R186C mutant both in astrocytes and HEK cells and observed strikingly enriched Golgi-localization (Figure 25B). We further performed mass spectrometry analysis for the R186C mutant to decipher whether it has a differential interactome when compared to Cdc42u. Both wildtype and constitutively active R186C pull down classical interactors of Cdc42. However, with wildtype R186C, some proteins are upregulated or downregulated as compared to Cdc42u. One such candidate protein is GDI1. Performing co-immunoprecipitation assays with R186C confirmed that its GDI1 binding is significantly impaired. This is due to the dual lipidation of R186C perturbing the geranylgeranyl moiety from accessing the hydrophobic pocket of GDI1. However, the proteomic analysis still indicates that Cdc42u and R186C have the tendency to bind similar interactors despite having strikingly different localization in both astrocytes and HEK cells. These results further show that the functional alteration of R186C is mainly due to its perturbed subcellular localization and failure to be extracted from Golgi membranes (see Annex article II)

Interaction of Cdc42 variants with cellular membranes

Irreversible prenylation of the classical CaaX motif is crucial for membrane binding (Mitin et al. 2012). In the case of Cdc42 variants the prenylation (addition of a geranylgeranyl moiety) on both the classical CaaX motif of Cdc42u and the CCaX motif of Cdc42b has been shown to be essential for their membrane anchorage both *in vivo* and *in vitro* (Nalbant et al. 2004; Johnson, Erickson, and Cerione 2009; Akiyuki Nishimura and Linder 2019). Prenylation is also required for binding to GDI1 (Nomanbhoy and Cerione 1996). Unprenylated Cdc42 mutants tend to display perturbed subcellular localization, especially showing distinct nuclear accumulation (u(SVLL), b(SSIF)) (Article.1, Figure 1E)(Figure 32A). Chemically inhibiting prenylation also results in nuclear accumulation of Cdc42u and Cdc42b (Article.1, Figure S1A). Similar nuclear accumulation of unprenylated mutants has been observed with other Rho GTPases such as RhoA and Rac (Michaelson et al. 2008; Guilluy, Dubash, and García-Mata 2011). Thus, prenylation is considered a key regulatory factor of protein subcellular localization.

In addition to prenylation, Cdc42b undergoes palmitoylation (S-acylation) which is a reversible lipid modification. The dual-lipidation on Cdc42b affects its binding to GDI1 (A. Nishimura and Linder 2013) which could alter its subcellular localization as is the case with the highly palmitoylated patient R186C mutant which fails to bind to GDI1 (Figure 25E). It is also important to note that palmitoylation is considered as a secondary lipid modification

which either requires a primary lipid anchor (such as prenylation) or a membrane targeting motif to ensure that the target protein can be recruited to endomembranes in order to access membrane bound palmityoltransferase (PAT) enzymes (Zaballa and van der Goot 2018). Yet whether Cdc42b can be palmitoylated in the absence of its prenyl tail remains unknown. Our findings with regard to b(SCIF) not accumulating in the nucleus and b(SSIF) shuttling to the nucleus, raises the possibility that b(SCIF) could be palmitoylated in the absence of prenylation (C188S) which would prevent its entry into the nucleus (Figure 32A).

To study the regulatory mechanisms behind the subcellular localization of Cdc42b, we first had to consider the presence of two species of Cdc42b,1) palmitoylated Cdc42 and 2) non-palmitoylated Cdc42 (A. Nishimura and Linder 2013). Unlike prenylation, palmitoylation is reversible and the ratios of these two palmitoylation-dependent Cdc42b species at a given time point is not exactly known. Microinjected non-palmitoylable mutant (b(CSIF)) shows an accumulation in the Golgi apparatus similar to that of Cdc42b observed upon chemically inhibiting palmitoylation using 2BP in migrating astrocytes (Article.1, Figure S1A), confirming that palmitoylation of Cdc42b is necessary for its association with vesicles. Thus, palmitoylation is essential for the trafficking of Cdc42b which is similar to the palmitoylation dependent trafficking of specific Ras GTPases (H/N-Ras) (Ahearn et al. 2012).

The mechanism behind the distinct Golgi-localization of Cdc42b still remains to be answered. However, we hypothesized that the accumulation of Cdc42b at the Golgi apparatus is also possibly due to its dual lipidation similar to the Golgi-localization of dually lipidated RAS GTPases. RAS palmitoylation takes place on the cytosolic face of the Golgi apparatus, where the DHHC9–GPC16 PAT resides. Dually lapidated (farnesylated and palmitoylated) RAS proteins have more than 100-fold higher membrane affinity than only farnesylated RAS and therefore palmitoylation of RAS at the Golgi serves as an affinity trap for the protein (Ahearn et al. 2012). To test whether the same applies to Cdc42, we sought out to identify the PAT required for palmitoylating Cdc42b. We report Golgi-localized DHHC3 and DHHC7 as potential candidates (Figure 24). Therefore, similar to N-Ras and H-Ras, Cdc42b is probably dually lipidated at the Golgi apparatus setting up its own affinity trap with Golgi membranes, eventually promoting its own subcellular trafficking through vesicular transport. Alternatively, Cdc42b could still exit the Golgi-apparatus via Rho GDI1 extraction. However, the addition of a palmitoyl group adjacent to the prenyl tail sterically inhibits Cdc42b from binding to Rho GDI1 (A. Nishimura and Linder 2013; Hodge and Ridley 2016). This could explain the Golgi localization of Cdc42b. Considering the existing models (Figure 12) to describe the interactions between Golgi-localized and plasma membrane pools of Cdc42 (Farhan and Hsu 2016), 'the Golgi affinity trap' hypothesis would be in line/agreement with the reservoir model, where Golgi-localized Cdc42b is trafficked to the leading edge once Cdc42u polarizes the cell.

In support of 'the Golgi affinity trap' hypothesis, are the findings from the study conducted with the patient mutation R186C in Cdc42u. This *de novo* mutation results in a gain of function with an additional palmitoylation on C186. The R186C Cdc42u mutant now exhibits the same subcellular localization as Cdc42b. This highly palmitoylated mutant is found to be accumulated in the Golgi apparatus as compared to the mostly plasma membrane-associated Cdc42u. Not surprisingly, due to its palmitoylation, the binding of the R186C Cdc42u mutant to Rho GDI1 is also strongly impaired(Figure 25E). However, this mutant does not participate in vesicular trafficking. This results in its inability to be extracted from the Golgi apparatus (Bekhouche et al. 2020). These findings again reinforce the role of dually lipidated proteins setting up affinity traps in organelles where they are primarily palmitoylated and emphasize the crucial role played by subcellular localization on the function and regulation of Cdc42 variants.

Additionally, we tested the role of only the last 10 differential carboxy amino acids in subcellular localization in astrocytes. We observe that Cdc42b C-ter is localized in perinuclear endomembranes as opposed to Cdc42u C-ter. Indicating that in the absence of other protein interactions which require upstream domains of Cdc42 (for example GDI1 binding requires Switch I and Switch II domains), the Cdc42 variants C-ter alone are also capable of differentially localizing (Figure 30B).

Interaction of Cdc42 variants with model membranes

All the aforementioned findings point toward subcellular localization of Cdc42 isoforms being instrumental in their function and regulation. Therefore, studying membrane targeting and anchorage of Cdc42 variants is essential to decipher how the C-ter amino acid sequence and/or the lipid modifications lead to such radical differences in Cdc42 localisation. *In vitro* model membrane systems (giant unilamellar vesicles, GUVs) were used to tackle the technical challenge of dissecting membrane association *in cellulo*. We report that both Cdc42 variants preferentially bind to Golgi apparatus-like GUVs (lower in cholesterol (Chol) and sphingomyelin (SM)) over plasma membrane-like GUVs (Figure 26). The same is observed for the non-palmitoylable Cdc42b mutant and the R186C Cdc42u mutant.

Surprisingly these findings with GUVs suggest that Cdc42 intrinsically prefers Golgi apparatus-like GUVs compared to plasma membrane-like GUVs. Since *in cellulo* findings show that Cdc42u is more plasma membrane-associated, this is likely due to the absence of $PI(4,5)P_2$ and/or the presence of SM and high Chol in the plasma membrane-like GUVs. Not surprisingly, when studying the binding of Cdc42 variants to liquid disordered (Ld)/liquid ordered (Lo) phase separated GUVs, Cdc42 preferentially binds to the Ld phase as opposed to the Chol and SM-rich Lo phase (Figure 27). The same preference for the Ld phase has been demonstrated for other prenylated GTPases like RABs (Kulakowski et al. 2018) or for myristolyated proteins like Arfs (Manneville et al. 2008). These findings indicate that

preferential binding to Golgi-apparatus-like GUVs and to Ld vesicles is mainly due to the C-ter prenylation since both Cdc42 variants, the non-palmitoylable b(CSIF) mutant and the R186C mutant all exhibit this preference in GUVs (Figure 26, 31).

It is important to note that, in our *in vitro* assay, Cdc42 proteins are purified along with Rho GDI1. For this purpose, only the C-ter (last 10 amino acids) of Cdc42 variants were used for GUV reconstitution assays. The C-ter on its own is incapable of binding to GDI1, since upstream Cdc42 domains (Switch I and Switch II) are absent (Hoffman, Nassar, and Cerione 2000; Garcia-Mata, Boulter, and Burridge 2011). This characteristic of the C-ter constructs allowed us to observe the membrane interaction of only the differential PBR and CaaX/CCaX motifs (Figure 30A). Surprisingly, we observe that the C-ter of Cdc42u does not preferentially bind to either plasma membrane-like GUVs or Golgi apparatus-like GUVs, while the C-ter of Cdc42b still prefers Golgi apparatus-like GUVs (Figure 30D-F) which also corresponds to what we observe in astrocytes (Figure 30B). These results suggest that differential membrane binding depends on GDI association and dissociation. In order to confirm this, FRAP experiments will have to be performed to assess the association and dissociation dynamics of Cdc42 variants and test whether it depends on GDI1 (Pincet et al. 2016; Kulakowski et al. 2018). Alternatively, it will also be insightful to mutate Cdc42 variants to abolish their binding to GDI1, by taking advantage of the existing Cdc42 R66A mutation that fails to bind to GDI1 (Q. Lin et al. 2003). Adapting this strategy might however pose the technical difficultly of protein aggregation due to insolubility, since GDI1 is necessary to mask the lipid tail and ensure the solubility of lipid modified Cdc42. Note however that the C-ter constructs are soluble but fail to bind to GDI1. The solubility of the C-ter constructs is probably the result of residual detergent in the protein storage buffer. Detergents have been previously used to solubilize lipid modified Cdc42 (Park et al. 2015a; McCallum, Erickson, and Cerione 1998).

Further, we demonstrate that the di-arginine motif present on Cdc42u is necessary for its preferential binding to PI(4,5)P_2 incorporated plasma membrane-like GUVs (Figure 29D). This was previously reported in a small liposome study (Johnson, Erickson, and Cerione 2012). Interestingly, we show that Cdc42b fails to distinguish between PI(4,5)P_2 containing GUVs and control GUVs (Figure 29E). This is due to the absence of the PI(4,5)P_2 interacting di-arginine motif in the PBR of Cdc42. These findings can be extrapolated to explain the plasma-membrane associated Cdc42u subcellular localization in astrocytes and NPCs. Also, preliminary results (N=1) obtained with the purified R186C mutant on PI(4,5)P_2 incorporated GUVs demonstrates no preferential binding, in agreement with the observation that the di-arginine motif of R186C is disrupted by its additional palmitoylation (Figure 31E).

The membrane binding of dually lipdiated N-RAS was shown to be dependent on the amount of lipid packing defects induced by curvature (Larsen et al. 2015; 2017). We studied whether this is the case for palmitoylated Cdc42b. Lipid packing defects were induced in Golgi

apparatus-like GUVs by adding diacylglycerols (DAG). Surprisingly, both Cdc42 variants preferred GUVs with packing defects. We chemically attempted to increase the ratio of palmitoylated Cdc42b, which showed a slight increase in its preference for GUVs with lipid packing defects. However, the potential role of palmitoylated Cdc42b sensing lipid packing defects and membrane curvature still remains to be elucidated, for instance by pulling membrane nanotubes to induce membrane curvature (Prévost et al. 2017; Kulakowski et al. 2018).

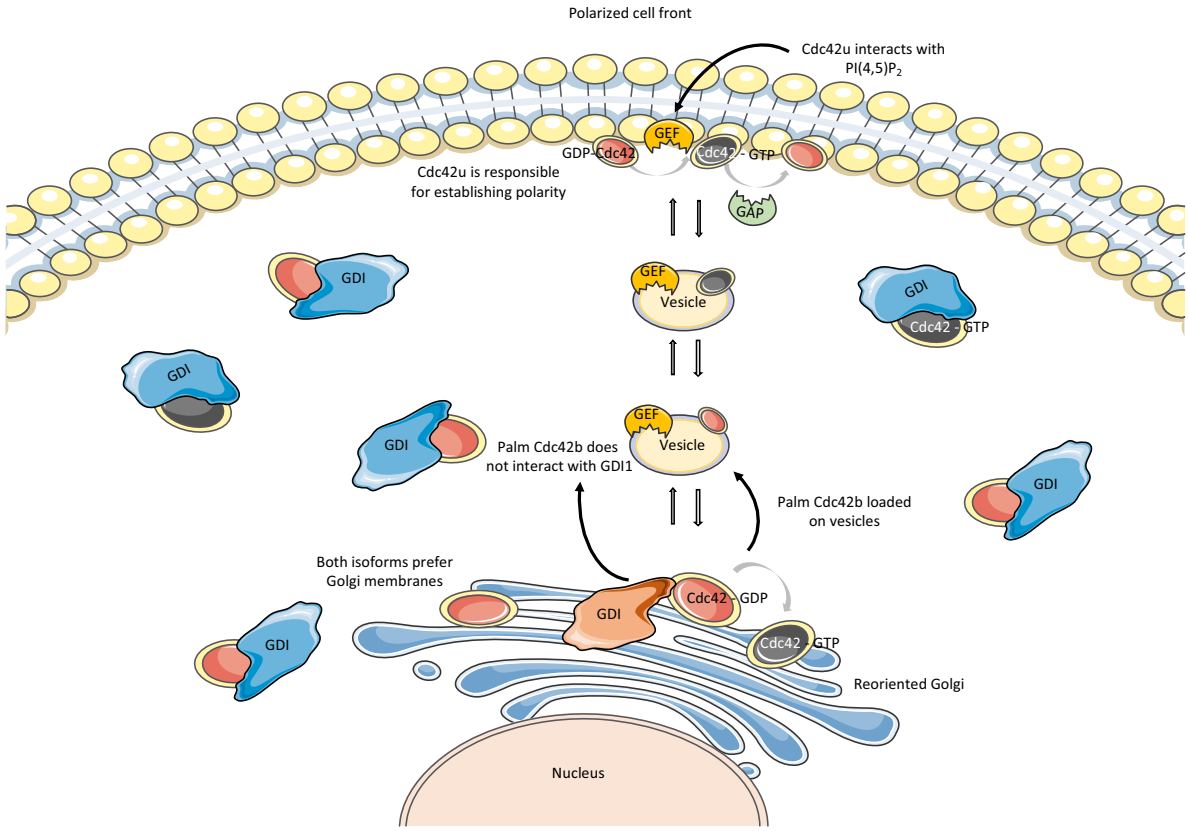

Figure 34 Localization, function and regulation of Cdc42 isoforms.
Summary of our key findings on the subcellular localization of Cdc42 isoforms. Both isoforms prefer Golgi-like membranes. We know that palmitoylated Cdc42 fails to interact with GDI1, thus we observe that palmitoylation promotes Cdc42b association with vesicles. At the plasma membrane, Cdc42u plays the role of the major isoform involved in establishing cell polarity. It also specifically interacts with PI(4,5)P2 enriched membranes.

Part IV

Conclusion and Perspective

In conclusion, our study emphasizes the crucial role of subcellular localization in the function of Cdc42 variants and of the R186C patient mutant. We show that, although they have similar interactors, Cdc42 variants have different cellular functions. Cdc42u is the major variant associated with initial polarization events, while Cdc42b regulates micropinocytosis. Because both Cdc42 variants intrinsically prefer Golgi apparatus-like membranes *in vitro*, we formulated the hypothesis along which both Cdc42 variants are initially localized to the Golgi apparatus, but Cdc42u is extracted more efficiently by GDI1 compared to palmitoylated Cdc42b. In addition to impaired GDI1 extraction, Cdc42b may be retained in the Golgi apparatus by an affinity trap mechanism similar to that reported for other dually lipidated GTPases like H/N-RAS. Vesicular transport would then be the only mode of exit from the Golgi apparatus for Cdc42b, potentially inducing a temporal lag in the delivery of Cdc42b to the leading edge when compared to cytosolic GDI1-bound Cdc42u. Impaired GDI1 extraction is also observed for the Golgi-localized and dually lipidated R186C mutant. This mutant also fails to localize with vesicles in cells and thus remains trapped at the Golgi apparatus being causative for its pathological phenotype (Bekhouche et al. 2020).

How Cdc42 variants initially localize to the Golgi apparatus is the main question that arises at the end of this study. Since Cdc42 prenylation occurs at the cytosol, as for other GTPases which are prenylated by GGTase1, and protein maturation (CaaX box processing) occurs on the ER membrane (Wang and Casey 2016), how prenylated Cdc42 variants enter the Golgi apparatus after protein maturation is not clear. This could be the starting point of a new study tracking initial Cdc42 interactors regulating the subcellular localization of Cdc42. In the case of H/N-RAS, before palmitoylation, newly synthesized Ras can reversibly bind ER and Golgi membranes and traffic between them via a soluble cytosolic intermediate (binding to VPS35 that maintains farnesylated N-RAS in the cytosol [M. Zhou et al. 2016]) (Goodwin et al. 2005). Such mode of ER to Golgi localization still needs to be elucidated for Cdc42. Several questions remain to be answered. For instance, could prenylated Cdc42 be extracted from the ER by GDI1 and delivered to the Golgi apparatus? Considering the role of coatmer-bound Cdc42u in intra-Golgi trafficking (J. L. Chen et al. 2005a), could there be a bias towards anterograde (*cis* to *trans* Golgi) versus retrograde COPI trafficking (from *cis* Golgi to the ER) (Farhan and Hsu 2016; Park et al. 2015a)? Then, how does mature Cdc42 move from the ER to the *cis*-Golgi?

Another unknown phenomenon is how Cdc42b is depalmitoylated ? Could depalmitoylation dictate the recycling of Cdc42b back to the Golgi apparatus as is the case with H/N-RAS? Depalmitoylation at the plasma membrane gives rise to a transiently depalmitoylated pool of H/N-RAS that is returned to the Golgi complex and/or to the ER by non-vesicular transport, where it can again interact with PAT enzymes and re-enter the secretory pathway(Goodwin et al. 2005). Similarly, for Cdc42b, depalmitoylation could result in its association to GDI and redistribution into the cytosol or re-entry into the Golgi apparatus. Additionally, Cdc42b could also be recycled via endosomes. Likewise, upon reaching the plasma membrane, palmitoylated H/N-RAS can undergo endocytosis (Goodwin et al. 2005). While Cdc42b shows similarities with H/N-RAS, certain regulatory parameters need to be taken into consideration. In the case of Cdc42, GDIs can extract Cdc42 and the presence of the Golgi localized Rho GDI3 has been demonstrated (Brunet, Morin, and Olofsson 2002). IQGAP1 has also been shown to extract Cdc42 from Golgi membranes (McCallum, Erickson, and Cerione 1998). This introduces the additional complexity of membrane extraction proteins for Cdc42 which are not interactors of H/N-RAS. The role of these players could help better understanding the regulation of Cdc42 subcellular localization.

These findings will be instrumental in better understanding the fundamental role of Cdc42 variants both physiologically and in a pathophysiological context. Studying *de novo* mutations in Cdc42u have been shown to give rise to variable developmental phenotypes such as variable growth dysregulation, facial dysmorphism, and neurodevelopmental in humans. A group of Cdc42u mutations have also been reported in the exons1-5 common to both Cdc42 variants(such as Y64C, Y23C, S83P and so on). Yet no studies have been reported on whether these mutations or the pathogenicity observed in the patients are also associated with the functioning of brain Cdc42. In our study we confirm the non-redundant functions of Cdc42 variants in parallel to other studies (Endo, Druso, and Cerione 2020; Yap et al. 2016). Therefore, it would be insightful to study the functional role of brain Cdc42 in these patients. Eventually enabling us to better diagnose patients with rare diseases.

References

Abdrabou, Abdalla, and Zhixiang Wang. 2018. "Post-Translational Modification and Subcellular Distribution of Rac1: An Update." *Cells* 7 (12): 263. https://doi.org/10.3390/cells7120263.

Abrami, Laurence, Tiziano Dallavilla, Patrick A. Sandoz, Mustafa Demir, Béatrice Kunz, Georgios Savoglidis, Vassily Hatzimanikatis, and F. Gisou van Der Goot. 2017. "Identification and Dynamics of the Human ZDHHC16-ZDHHC6 Palmitoylation Cascade." *ELife* 6: 1–24. https://doi.org/10.7554/eLife.27826.

Abrami, Laurence, Robin A. Denhardt-Eriksson, Vassily Hatzimanikatis, and F. Gisou van der Goot. 2019. "Dynamic Radiolabeling of S-Palmitoylated Proteins." In *Methods in Molecular Biology*, 2009:111–27. Humana Press Inc. https://doi.org/10.1007/978-1-4939-9532-5_9.

Adams, Alison E.M., Douglas I. Johnson, Richard M. Longnecker, Barbara F. Sloat, and John R. Pringle. 1990. "CDC42 and CDC43, Two Additional Genes Involved in Budding and the Establishment of Cell Polarity in the Yeast Saccharomyces Cerevisiae." *Journal of Cell Biology* 111 (1): 131–42. https://doi.org/10.1083/jcb.111.1.131.

Aguilar-Aragon, Mario, Alex Tournier, and Barry Thompson. 2019. "A Fence Function for Adherens Junctions in Epithelial Cell Polarity." *BioRxiv*, April, 605808. https://doi.org/10.1101/605808.

Ahearn, Ian M., Kevin Haigis, Dafna Bar-Sagi, and Mark R. Philips. 2012. "Regulating the Regulator: Post-Translational Modification of RAS." *Nature Reviews Molecular Cell Biology*. Nature Publishing Group. https://doi.org/10.1038/nrm3255.

Angelova, M. I., S. Soléau, Ph. Méléard, F. Faucon, and P. Bothorel. 2007. "Preparation of Giant Vesicles by External AC Electric Fields. Kinetics and Applications." In *Trends in Colloid and Interface Science VI*, edited by C Helm, M Lösche, and H Möhwald, 127–31. Darmstadt: Steinkopff. https://doi.org/10.1007/bfb0116295.

Arias-Romero, Luis E., and Jonathan Chernoff. 2013. "Targeting Cdc42 in Cancer." *Expert Opinion on Therapeutic Targets*. https://doi.org/10.1517/14728222.2013.828037.

Bagrodia, Shubha, and Richard A. Cerione. 1999. "PAK to the Future." *Trends in Cell Biology*. Elsevier Ltd. https://doi.org/10.1016/S0962-8924(99)01618-9.

Baschieri, Francesco, Stefano Confalonieri, Giovanni Bertalot, Pier Paolo Di Fiore, Wolfgang Dietmaier, Marcel Leist, Piero Crespo, Ian G. MacAra, and Hesso Farhan. 2014. "Spatial Control of Cdc42 Signalling by a GM130-RasGRF Complex Regulates Polarity and

Tumorigenesis." *Nature Communications* 5. https://doi.org/10.1038/ncomms5839.

Baschieri, Francesco, and Hesso Farhan. 2015. "Endomembrane Control of Cell Polarity: Relevance to Cancer." *Small GTPases* 6 (2): 104–7. https://doi.org/10.1080/21541248.2015.1018402.

Bekhouche, Bahia, Aurore Tourville, Yamini Ravichandran, Rachida Tacine, Laurence Abrami, Michael Dussiot, Andrea Khau-Dancasius, et al. 2020. "A Toxic Palmitoylation of Cdc42 Enhances NF-KB Signaling and Drives a Severe Autoinflammatory Syndrome." *Journal of Allergy and Clinical Immunology*, April. https://doi.org/10.1016/j.jaci.2020.03.020.

Bentley, Marvin, and Gary Banker. 2016. "The Cellular Mechanisms That Maintain Neuronal Polarity." *Nature Reviews Neuroscience*. https://doi.org/10.1038/nrn.2016.100.

Bishop, Anne L., and Alan Hall. 2000. "Rho GTPases and Their Effector Proteins." *Biochemical Journal* 348 (2): 241–55. https://doi.org/10.1042/bj3480241.

Bokoch, Gary M. 2003. "Biology of the P21-Activated Kinases." *Annual Review of Biochemistry*. https://doi.org/10.1146/annurev.biochem.72.121801.161742.

Boncompain, Gaelle, and Aubrey V. Weigel. 2018. "Transport and Sorting in the Golgi Complex: Multiple Mechanisms Sort Diverse Cargo." *Current Opinion in Cell Biology* 50 (February): 94–101. https://doi.org/10.1016/j.ceb.2018.03.002.

Bos, Johannes L., Holger Rehmann, and Alfred Wittinghofer. 2007. "GEFs and GAPs: Critical Elements in the Control of Small G Proteins." *Cell*. https://doi.org/10.1016/j.cell.2007.05.018.

Briggs, Michael W., and David B. Sacks. 2003. "IQGAP1 as Signal Integrator: Ca2+, Calmodulin, Cdc42 and the Cytoskeleton." *FEBS Letters* 542 (1–3): 7–11. https://doi.org/10.1016/S0014-5793(03)00333-8.

Brunet, Nicolas, Annie Morin, and Birgitta Olofsson. 2002. "RhoGDI-3 Regulates RhoG and Targets This Protein to the Golgi Complex through Its Unique N-Terminal Domain." *Traffic* 3 (5): 342–58. https://doi.org/10.1034/j.1600-0854.2002.30504.x.

Bryant, David M., and Alpha S. Yap. 2016. "Editorial Overview: Membrane Traffic and Cell Polarity." *Traffic* 17 (12): 1231–32. https://doi.org/10.1111/tra.12433.

Butler, Mitchell T., and John B. Wallingford. 2017. "Planar Cell Polarity in Development and Disease." *Nature Reviews Molecular Cell Biology*. https://doi.org/10.1038/nrm.2017.11.

Capuana, Lavinia, Astrid Boström, and Sandrine Etienne-Manneville. 2020. "Multicellular Scale Front-to-Rear Polarity in Collective Migration." *Current Opinion in Cell Biology*. Elsevier Ltd. https://doi.org/10.1016/j.ceb.2019.10.001.

Cerione, Richard A. 2004. "Cdc42: New Roads to Travel." *Trends in Cell Biology* 14 (3): 127–32. https://doi.org/10.1016/j.tcb.2004.01.008.

Chen, F., L. Ma, M. C. Parrini, X. Mao, M. Lopez, C. Wu, P. W. Marks, et al. 2000. "Cdc42 Is Required for PIP2-Induced Actin Polymerization End Early Development but Not for

Cell Viability." *Current Biology*. Vol. 10. https://doi.org/10.1016/S0960-9822(00)00571-6.

Chen, Ji Long, Raymond V. Fucini, Lynne Lacomis, Hediye Erdjument-Bromage, Paul Tempst, and Mark Stamnes. 2005a. "Coatomer-Bound Cdc42 Regulates Dynein Recruitment to COPI Vesicles." *Journal of Cell Biology* 169 (3): 383–89. https://doi.org/10.1083/jcb.200501157.

Chen, Lei, Guanghong Liao, Linda Yang, Kenneth Campbell, Masato Nakafuku, Chia Yi Kuan, and Yi Zheng. 2006. "Cdc42 Deficiency Causes Sonic Hedgehog-Independent Holoprosencephaly." *Proceedings of the National Academy of Sciences of the United States of America* 103 (44): 16520–25. https://doi.org/10.1073/pnas.0603533103.

Cho, Eunsil, and Mikyoung Park. 2016. "Palmitoylation in Alzheimer's Disease and Other Neurodegenerative Diseases." *Pharmacological Research*. Academic Press. https://doi.org/10.1016/j.phrs.2016.06.008.

Chou, Fu Sheng, Rong Li, and Pei Shan Wang. 2018. "Molecular Components and Polarity of Radial Glial Cells during Cerebral Cortex Development." *Cellular and Molecular Life Sciences* 75 (6): 1027–41. https://doi.org/10.1007/s00018-017-2680-0.

Copp, Andrew J., and Brian N. Harding. 1999. "Neuronal Migration Disorders in Humans and in Mouse Models - An Overview." *Epilepsy Research* 36 (2–3): 133–41. https://doi.org/10.1016/S0920-1211(99)00047-9.

Cotteret, Sophie, and Jonathan Chernoff. 2002. "The Evolutionary History of Effectors Downstream of Cdc42 and Rac." *Genome Biology*. BioMed Central. https://doi.org/10.1186/gb-2002-3-2-reviews0002.

Davey, Crystal F., and Cecilia B. Moens. 2017. "Planar Cell Polarity in Moving Cells: Think Globally, Act Locally." *Development (Cambridge)*. https://doi.org/10.1242/dev.122804.

Devreotes, Peter N., Sayak Bhattacharya, Marc Edwards, Pablo A. Iglesias, Thomas Lampert, and Yuchuan Miao. 2017. "Excitable Signal Transduction Networks in Directed Cell Migration." *Annual Review of Cell and Developmental Biology* 33 (1): 103–25. https://doi.org/10.1146/annurev-cellbio-100616-060739.

Donaldson, Julie G., and Catherine L. Jackson. 2011. "ARF Family G Proteins and Their Regulators: Roles in Membrane Transport, Development and Disease." *Nature Reviews Molecular Cell Biology*. https://doi.org/10.1038/nrm3117.

Drubin, David G., and W. James Nelson. 1996. "Origins of Cell Polarity." *Cell*. https://doi.org/10.1016/S0092-8674(00)81278-7.

Egea, Gustavo, Carla Serra-Peinado, Laia Salcedo-Sicilia, and Enric Gutiérrez-Martínez. 2013. "Actin Acting at the Golgi." *Histochemistry and Cell Biology* 140 (3): 347–60. https://doi.org/10.1007/s00418-013-1115-8.

Endo, Makoto, Joseph E. Druso, and Richard A. Cerione. 2020. "The Two Splice Variant Forms of Cdc42 Exert Distinct and Essential Functions in Neurogenesis." *Journal of Biological Chemistry* 295 (14): 4498–4512. https://doi.org/10.1074/jbc.RA119.011837.

Etienne-Manneville, S. 2008. “Polarity Proteins in Migration and Invasion.” *Oncogene*. https://doi.org/10.1038/onc.2008.347.

Etienne-Manneville, Sandrine. 2004. “Cdc42 - The Centre of Polarity.” *Journal of Cell Science* 117 (8): 1291–1300. https://doi.org/10.1242/jcs.01115.

Etienne-Manneville, S. 2006. “In Vitro Assay of Primary Astrocyte Migration as a Tool to Study Rho GTPase Function in Cell Polarization.” *Methods in Enzymology* 406: 565–78. https://doi.org/10.1016/S0076-6879(06)06044-7.

Etienne-Manneville, S. 2013. “Microtubules in Cell Migration.” *Annual Review of Cell and Developmental Biology* 29: 471–99. https://doi.org/10.1146/annurev-cellbio-101011-155711.

Etienne-Manneville, Sandrine, and Alan Hall. 2001. “Integrin-Mediated Activation of Cdc42 Controls Cell Polarity in Migrating Astrocytes through PKCζ.” *Cell* 106 (4): 489–98. https://doi.org/10.1016/S0092-8674(01)00471-8.

Etienne-Manneville, S. 2002. “Rho GTPases in Cell Biology.” *Nature* 420 (6916): 629–35. https://doi.org/10.1038/nature01148.

Etienne-Manneville, S. 2003a. “Cdc42 Regulates GSK-3β and Adenomatous Polyposis Coli to Control Cell Polarity.” *Nature* 421 (6924): 753–56. https://doi.org/10.1038/nature01423.

Etienne-Manneville, S 2003b. “Cell Polarity: Par6, APKC and Cytoskeletal Crosstalk.” *Current Opinion in Cell Biology* 15 (1): 67–72. https://doi.org/10.1016/S0955-0674(02)00005-4.

Etienne-Manneville, Sandrine, Jean Baptiste Manneville, Sarah Nicholls, Michael A. Ferenczi, and Alan Hall. 2005. “Cdc42 and Par6-PKCη Regulate the Spatially Localized Association of Dlg1 and APC to Control Cell Polarization.” *Journal of Cell Biology* 170 (6): 895–901. https://doi.org/10.1083/jcb.200412172.

Faber-Elman, A., A. Solomon, J. A. Abraham, M. Marikovsky, and M. Schwartz. 1996. “Involvement of Wound-Associated Factors in Rat Brain Astrocyte Migratory Response to Axonal Injury: In Vitro Simulation.” *Journal of Clinical Investigation* 97 (1): 162–71. https://doi.org/10.1172/JCI118385.

Farhan, Hesso, and Victor W. Hsu. 2016. “Cdc42 and Cellular Polarity: Emerging Roles at the Golgi.” *Trends in Cell Biology* 26 (4): 241–48. https://doi.org/10.1016/j.tcb.2015.11.003.

Feng, Qiyu, Dan Baird, Xu Peng, Jianbin Wang, Thi Ly, Jun Lin Guan, and Richard A. Cerione. 2006. “Cool-1 Functions as an Essential Regulatory Node for EGF Receptor- and Src-Mediated Cell Growth.” *Nature Cell Biology* 8 (9): 945–56. https://doi.org/10.1038/ncb1453.

Fukata, Masaki, Takashi Watanabe, Jun Noritake, Masato Nakagawa, Masaki Yamaga, Shinya Kuroda, Yoshiharu Matsuura, Akihiro Iwamatsu, Franck Perez, and Kozo Kaibuchi. 2002. “Rac1 and Cdc42 Capture Microtubules through IQGAP1 and CLIP-170.” *Cell* 109

(7): 873–85. https://doi.org/10.1016/S0092-8674(02)00800-0.

Gao, Juehua, Jie Liao, and Guang Yu Yang. 2009. "CAAX-Box Protein, Prenylation Process and Carcinogenesis." *American Journal of Translational Research* 1 (3): 312–25. http://www.ncbi.nlm.nih.gov/pubmed/19956441%0Ahttp://www.pubmedcentral.nih.gov/articlerender.fcgi?artid=PMC2776320.

Garcia-Mata, Rafael, Etienne Boulter, and Keith Burridge. 2011. "The 'Invisible Hand': Regulation of RHO GTPases by RHOGDIs." *Nature Reviews Molecular Cell Biology*. https://doi.org/10.1038/nrm3153.

Garvalov, Boyan K., Kevin C. Flynn, Dorothee Neukirchen, Liane Meyn, Nicole Teusch, Xunwei Wu, Cord Brakebusch, James R. Bamburg, and Frank Bradke. 2007. "Cdc42 Regulates Cofilin during the Establishment of Neuronal Polarity." *Journal of Neuroscience* 27 (48): 13117–29. https://doi.org/10.1523/JNEUROSCI.3322-07.2007.

Glick, Benjamin S., and Alberto Luini. 2011a. "Models for Golgi Traffic: A Critical Assessment." *Cold Spring Harbor Perspectives in Biology* 3 (11). https://doi.org/10.1101/cshperspect.a005215.

Gnanaguru, Gopalan, Galina Bachay, Saptarshi Biswas, Germán Pinzón-Duarte, Dale D. Hunter, and William J. Brunken. 2013. "Laminins Containing the Β2 and Γ3 Chains Regulate Astrocyte Migration and Angiogenesis in the Retina." *Development (Cambridge)* 140 (9): 2050–61. https://doi.org/10.1242/dev.087817.

Goldstein, Bob, and Ian G. Macara. 2007. "The PAR Proteins: Fundamental Players in Animal Cell Polarization." *Developmental Cell*. https://doi.org/10.1016/j.devcel.2007.10.007.

Gomes, Edgar R., Shantanu Jani, and Gregg G. Gundersen. 2005. "Nuclear Movement Regulated by Cdc42, MRCK, Myosin, and Actin Flow Establishes MTOC Polarization in Migrating Cells." *Cell* 121 (3): 451–63. https://doi.org/10.1016/j.cell.2005.02.022.

Goodwin, J. Shawn, Kimberly R. Drake, Carl Rogers, Latasha Wright, Jennifer Lippincott-Schwartz, Mark R. Philips, and Anne K. Kenworthy. 2005. "Depalmitoylated Ras Traffics to and from the Golgi Complex via a Nonvesicular Pathway." *Journal of Cell Biology* 170 (2): 261–72. https://doi.org/10.1083/jcb.200502063.

Griffith, Jason W., and Andrew D. Luster. 2013. "Targeting Cells in Motion: Migrating toward Improved Therapies." *European Journal of Immunology* 43 (6): 1430–35. https://doi.org/10.1002/eji.201243183.

Guilluy, Christophe, Adi D. Dubash, and Rafael García-Mata. 2011. "Analysis of RhoA and Rho GEF Activity in Whole Cells and the Cell Nucleus." *Nature Protocols* 6 (12): 2050–60. https://doi.org/10.1038/nprot.2011.411.

Guo, Yusong, Daniel W. Sirkis, and Randy Schekman. 2014. "Protein Sorting at the Trans-Golgi Network." *Annual Review of Cell and Developmental Biology* 30 (1): 169–206. https://doi.org/10.1146/annurev-cellbio-100913-013012.

He, Xiaolong, Chengfu Yuan, and Jilai Yang. 2015. "Regulation and Functional Significance of CDC42 Alternative Splicing in Ovarian Cancer." *Oncotarget* 6 (30): 29651–63.

https://doi.org/10.18632/oncotarget.4865.

Hodge, Richard G., and Anne J. Ridley. 2016. “Regulating Rho GTPases and Their Regulators.” *Nature Reviews Molecular Cell Biology*. Nature Publishing Group. https://doi.org/10.1038/nrm.2016.67.

Hoffman, Gregory R., Nicolas Nassar, and Richard A. Cerione. 2000. “Structure of the Rho Family GTP-Binding Protein Cdc42 in Complex with the Multifunctional Regulator RhoGDI.” *Cell* 100 (3): 345–56. https://doi.org/10.1016/S0092-8674(00)80670-4.

Izumi, Yasushi, Tomonori Hirose, Yoko Tamai, Syu Ichi Hirai, Yoji Nagashima, Toyoshi Fujimoto, Yo Tabuse, Kenneth J. Kemphues, and Shigeo Ohno. 1998. “An Atypical PKC Directly Associates and Colocalizes at the Epithelial Tight Junction with ASIP, a Mammalian Homologue of Caenorhabditis Elegans Polarity Protein PAR-3.” *Journal of Cell Biology* 143 (1): 95–106. https://doi.org/10.1083/jcb.143.1.95.

Jackson, Catherine L., and Samuel Bouvet. 2014. “Arfs at a Glance.” *Journal of Cell Science* 127 (19): 4103–9. https://doi.org/10.1242/jcs.144899.

Johnson, Jared L., Jon W. Erickson, and Richard A. Cerione. 2009. “New Insights into How the Rho Guanine Nucleotide Dissociation Inhibitor Regulates the Interaction of Cdc42 with Membranes.” *Journal of Biological Chemistry* 284 (35): 23860–71. https://doi.org/10.1074/jbc.M109.031815.

Johnson, Jared L., Jon W. Erickson, and Richard A. Cerione. 2012. “C-Terminal Di-Arginine Motif of Cdc42 Protein Is Essential for Binding to Phosphatidylinositol 4,5-Bisphosphate-Containing Membranes and Inducing Cellular Transformation.” *Journal of Biological Chemistry* 287 (8): 5764–74. https://doi.org/10.1074/jbc.M111.336487.

Johnston, Daniel St. 2018. “Establishing and Transducing Cell Polarity: Common Themes and Variations.” *Current Opinion in Cell Biology* 51 (April): 33–41. https://doi.org/10.1016/j.ceb.2017.10.007.

Kage, Frieda, Anika Steffen, Adolf Ellinger, Carmen Ranftler, Christian Gehre, Cord Brakebusch, Margit Pavelka, Theresia Stradal, and Klemens Rottner. 2017a. “FMNL2 and -3 Regulate Golgi Architecture and Anterograde Transport Downstream of Cdc42.” *Scientific Reports* 7 (1). https://doi.org/10.1038/s41598-017-09952-1.

Kang, Rujun, Junmei Wan, Pamela Arstikaitis, Hideto Takahashi, Kun Huang, Aaron O. Bailey, James X. Thompson, et al. 2008. “Neural Palmitoyl-Proteomics Reveals Dynamic Synaptic Palmitoylation.” *Nature*. Nature Publishing Group. https://doi.org/10.1038/nature07605.

Keep, Nicholas H., Maria Barnes, Igor Barsukov, Ramin Badii, Lu Yun Lian, Anthony W. Segal, Peter C.E. Moody, and Gordon C.K. Roberts. 1997. “A Modulator of Rho Family G Proteins, RhoGDI, Binds These G Proteins via an Immunoglobulin-like Domain and a Flexible N-Terminal Arm.” *Structure* 5 (5): 623–33. https://doi.org/10.1016/S0969-2126(97)00218-9.

Kessels, Michael M., and Britta Qualmann. 2002. “Syndapins Integrate N-WASP in Receptor-

Mediated Endocytosis." *EMBO Journal* 21 (22): 6083–94. https://doi.org/10.1093/emboj/cdf604.

Kimelberg, Harold K., and Maiken Nedergaard. 2010. "Functions of Astrocytes and Their Potential As Therapeutic Targets." *Neurotherapeutics*. Vol. 7. Neurotherapeutics. https://doi.org/10.1016/j.nurt.2010.07.006.

Knaus, Ulla G., Yan Wang, Abina M. Reilly, Dawn Warnock, and Janis H. Jackson. 1998. "Structural Requirements for PAK Activation by Rac GTPases." *Journal of Biological Chemistry* 273 (34): 21512–18. https://doi.org/10.1074/jbc.273.34.21512.

Kulakowski, Guillaume, Hugo Bousquet, Jean Baptiste Manneville, Patricia Bassereau, Bruno Goud, and Lena K. Oesterlin. 2018. "Lipid Packing Defects and Membrane Charge Control RAB GTPase Recruitment." *Traffic* 19 (7): 536–45. https://doi.org/10.1111/tra.12568.

Ladoux, Benoit, René Marc Mège, and Xavier Trepat. 2016. "Front-Rear Polarization by Mechanical Cues: From Single Cells to Tissues." *Trends in Cell Biology*. https://doi.org/10.1016/j.tcb.2016.02.002.

Lakkaraju, Asvin K.K., Laurence Abrami, Thomas Lemmin, Sanja Blaskovic, Béatrice Kunz, Akio Kihara, Matteo Dal Peraro, and Françoise Gisou Van Der Goot. 2012. "Palmitoylated Calnexin Is a Key Component of the Ribosome-Translocon Complex." *EMBO Journal* 31 (7): 1823–35. https://doi.org/10.1038/emboj.2012.15.

Lang, Charles F., and Edwin Munro. 2017. "The PAR Proteins: From Molecular Circuits to Dynamic Self-Stabilizing Cell Polarity." *Development (Cambridge)*. https://doi.org/10.1242/dev.139063.

Larsen, Jannik B., Celeste Kennard, Søren L. Pedersen, Knud J. Jensen, Mark J. Uline, Nikos S. Hatzakis, and Dimitrios Stamou. 2017. "Membrane Curvature and Lipid Composition Synergize To Regulate N-Ras Anchor Recruitment." *Biophysical Journal* 113 (6): 1269–79. https://doi.org/10.1016/j.bpj.2017.06.051.

Larsen, Jannik B, Martin Borch Jensen, Vikram K. Bhatia, Søren L. Pedersen, Thomas Bjørnholm, Lars Iversen, Mark Uline, et al. 2015. "Membrane Curvature Enables N-Ras Lipid Anchor Sorting to Liquid-Ordered Membrane Phases." *Nature Chemical Biology* 11 (3): 192–94. https://doi.org/10.1038/nchembio.1733.

Lawson, Campbell D., and Keith Burridge. 2014. "The On-off Relationship of Rho and Rac during Integrin-Mediated Adhesion and Cell Migration." *Small GTPases*. https://doi.org/10.4161/sgtp.27958.

Lee, Brittany J., Ahmet E. Cansizoglu, Katherine E. Süel, Thomas H. Louis, Zichao Zhang, and Yuh Min Chook. 2006. "Rules for Nuclear Localization Sequence Recognition by Karyopherinβ2." *Cell* 126 (3): 543–58. https://doi.org/10.1016/j.cell.2006.05.049.

Lee, Seung Joon, Amar Kar, Riki Kawaguchi, Priyanka Patel, Pabitra Sahoo, Byron Aguilar, Kelsey Lantz, et al. 2018. "Selective Axonal Translation of Prenylated Cdc42 MRNA Isoform Supports Axon Growth." *BioRxiv*, 366369. https://doi.org/10.1101/366369.

Legg, John A., Guillaume Bompard, John Dawson, Hannah L. Morris, Natalie Andrew, Lisa

Cooper, Simon A. Johnston, Giorgos Tramountanis, and Laura M. Machesky. 2007. "N-WASP Involvement in Dorsal Ruffle Formation in Mouse Embryonic Fibroblasts." *Molecular Biology of the Cell* 18 (2): 678–87. https://doi.org/10.1091/mbc.E06-06-0569.

Levental, Ilya, Kandice R. Levental, and Frederick A. Heberle. 2020. "Lipid Rafts: Controversies Resolved, Mysteries Remain." *Trends in Cell Biology*. Elsevier Ltd. https://doi.org/10.1016/j.tcb.2020.01.009.

Levental, Ilya, Daniel Lingwood, Michal Grzybek, Ünal Coskun, and Kai Simons. 2010. "Palmitoylation Regulates Raft Affinity for the Majority of Integral Raft Proteins." *Proceedings of the National Academy of Sciences of the United States of America* 107 (51): 22050–54. https://doi.org/10.1073/pnas.1016184107.

Lin, Dan, Amelia S. Edwards, James P. Fawcett, Geraldine Mbamalu, John D. Scott, and Tony Pawson. 2000. "A Mammalian PAR-3-PAR-6 Complex Implicated in Cdc42/Rac1 and APKC Signalling and Cell Polarity." *Nature Cell Biology* 2 (8): 540–47. https://doi.org/10.1038/35019582.

Lin, Qiong, Reina N. Fuji, Wannian Yang, and Richard A. Cerione. 2003. "RhoGDI Is Required for Cdc42-Mediated Cellular Transformation." *Current Biology* 13 (17): 1469–79. https://doi.org/10.1016/S0960-9822(03)00613-4.

Linder, Maurine E., and Robert J. Deschenes. 2007. "Palmitoylation: Policing Protein Stability and Traffic." *Nature Reviews Molecular Cell Biology* 8 (1): 74–84. https://doi.org/10.1038/nrm2084.

Lu, Michelle Seiko, and David G. Drubin. 2020. "Cdc42 GTPase Regulates ESCRTs in Nuclear Envelope Sealing and ER Remodeling." *The Journal of Cell Biology* 219 (8). https://doi.org/10.1083/jcb.201910119.

Makhoul, Christian, Prajakta Gosavi, Regina Duffield, Bronwen Delbridge, Nicholas A. Williamson, and Paul A. Gleeson. 2019a. "Intersectin-1 Interacts with the Golgin GCC88 to Couple the Actin Network and Golgi Architecture." *Molecular Biology of the Cell* 30 (3): 370–86. https://doi.org/10.1091/mbc.E18-05-0313.

Makowski, Stefanie L., Thuy TT Tran, and Seth J. Field. 2017. "Emerging Themes of Regulation at the Golgi." *Current Opinion in Cell Biology*. https://doi.org/10.1016/j.ceb.2017.01.004.

Manneville, Jean Baptiste, Jean François Casella, Ernesto Ambroggio, Pierre Gounon, Julien Bertherat, Patricia Bassereau, Jean Cartaud, Bruno Antonny, and Bruno Goud. 2008. "COPI Coat Assembly Occurs on Liquid-Disordered Domains and the Associated Membrane Deformations Are Limited by Membrane Tension." *Proceedings of the National Academy of Sciences of the United States of America* 105 (44): 16946–51. https://doi.org/10.1073/pnas.0807102105.

Manneville, Jean Baptiste, Cécile Leduc, Benoit Sorre, and Guillaume Drin. 2012. "Studying In Vitro Membrane Curvature Recognition by Proteins and Its Role in Vesicular Trafficking." *Methods in Cell Biology* 108: 47–71. https://doi.org/10.1016/B978-0-12-

386487-1.00003-1.

Marei, Hadir, and Angeliki Malliri. 2017. “GEFs: Dual Regulation of Rac1 Signaling.” *Small GTPases*. Taylor and Francis Inc. https://doi.org/10.1080/21541248.2016.1202635.

Marks, Peter W., and David J. Kwiatkowski. 1996. “Genomic Organization and Chromosomal Location of Murine CDC42.” *Genomics* 38 (1): 13–18. https://doi.org/10.1006/geno.1996.0586.

Martin-Belmonte, Fernando, Ama Gassama, Anirban Datta, Wei Yu, Ursula Rescher, Volker Gerke, and Keith Mostov. 2007. “PTEN-Mediated Apical Segregation of Phosphoinositides Controls Epithelial Morphogenesis through Cdc42.” *Cell*. Vol. 128. https://doi.org/10.1016/j.cell.2006.11.051.

Martinelli, Simone, Oliver H.F. Krumbach, Francesca Pantaleoni, Simona Coppola, Ehsan Amin, Luca Pannone, Kazem Nouri, et al. 2018. “Functional Dysregulation of CDC42 Causes Diverse Developmental Phenotypes.” *American Journal of Human Genetics* 102 (2): 309–20. https://doi.org/10.1016/j.ajhg.2017.12.015.

Mataraza, Jennifer M., Michael W. Briggs, Zhigang Li, Ronald Frank, and David B. Sacks. 2003. “Identification and Characterization of the Cdc42-Binding Site of IQGAP1.” *Biochemical and Biophysical Research Communications* 305 (2): 315–21. https://doi.org/10.1016/S0006-291X(03)00759-9.

Mattila, Pieta K., and Pekka Lappalainen. 2008. “Filopodia: Molecular Architecture and Cellular Functions.” *Nature Reviews Molecular Cell Biology*. Nature Publishing Group. https://doi.org/10.1038/nrm2406.

Mayor, Roberto, and Sandrine Etienne-Manneville. 2016. “The Front and Rear of Collective Cell Migration.” *Nature Reviews Molecular Cell Biology*. https://doi.org/10.1038/nrm.2015.14.

Mayor, Roberto, and Eric Theveneau. 2012. “The Neural Crest.” *Development (Cambridge)* 140 (11): 2247–51. https://doi.org/10.1242/dev.091751.

Mayor, Satyajit, Robert G. Parton, and Julie G. Donaldson. 2014. “Clathrin-Independent Pathways of Endocytosis.” *Cold Spring Harbor Perspectives in Biology* 6 (6). https://doi.org/10.1101/cshperspect.a016758.

McCallum, Sandra J., Jon W. Erickson, and Richard A. Cerione. 1998. “Characterization of the Association of the Actin-Binding Protein, IQGAP, and Activated Cdc42 with Golgi Membranes.” *Journal of Biological Chemistry* 273 (35): 22537–44. https://doi.org/10.1074/jbc.273.35.22537.

Meer, Gerrit Van, Dennis R. Voelker, and Gerald W. Feigenson. 2008. “Membrane Lipids: Where They Are and How They Behave.” *Nature Reviews Molecular Cell Biology*. Nature Publishing Group. https://doi.org/10.1038/nrm2330.

Méléard, Philippe, Luis A. Bagatolli, and Tanja Pott. 2009. “Giant Unilamellar Vesicle Electroformation. From Lipid Mixtures to Native Membranes Under Physiological Conditions.” *Methods in Enzymology*. Academic Press. https://doi.org/10.1016/S0076-

6879(09)65009-6.

Melendez, Jaime, Matthew Grogg, and Yi Zheng. 2011. “Signaling Role of Cdc42 in Regulating Mammalian Physiology.” *Journal of Biological Chemistry*. American Society for Biochemistry and Molecular Biology. https://doi.org/10.1074/jbc.R110.200329.

Michaelson, David, Wasif Abidi, Daniele Guardavaccaro, Mo Zhou, Ian Ahearn, Michele Pagano, and Mark R. Philips. 2008. “Rac1 Accumulates in the Nucleus during the G2 Phase of the Cell Cycle and Promotes Cell Division.” *Journal of Cell Biology* 181 (3): 485–96. https://doi.org/10.1083/jcb.200801047.

Michaelson, David, Joseph Silletti, Gretchen Murphy, Peter D’Eustachio, Mark Rush, and Mark R. Philips. 2001. “Differential Localization of Rho GTPases in Live Cells: Regulation by Hypervariable Regions and RhoGDI Binding.” *Journal of Cell Biology* 152 (1): 111–26. https://doi.org/10.1083/jcb.152.1.111.

Mitin, Natalia, Patrick J. Roberts, Emily J. Chenette, and Channing J. Der. 2012. “Posttranslational Lipid Modification of Rho Family Small GTPases.” *Methods in Molecular Biology* 827: 87–95. https://doi.org/10.1007/978-1-61779-442-1_6.

Mosammaparast, Nima, and Lucy F. Pemberton. 2004. “Karyopherins: From Nuclear-Transport Mediators to Nuclear-Function Regulators.” *Trends in Cell Biology*. Trends Cell Biol. https://doi.org/10.1016/j.tcb.2004.09.004.

Motokawa, Midori, Satoshi Watanabe, Akiko Nakatomi, Tatsuro Kondoh, Tadashi Matsumoto, Kanako Morifuji, Hirotake Sawada, et al. 2018. “A Hot-Spot Mutation in CDC42 (p.Tyr64Cys) and Novel Phenotypes in the Third Patient with Takenouchi-Kosaki Syndrome.” *Journal of Human Genetics* 63 (3): 387–90. https://doi.org/10.1038/s10038-017-0396-5.

Müller, Matthias P., and Roger S. Goody. 2018. “Molecular Control of Rab Activity by GEFs, GAPs and GDI.” *Small GTPases*. https://doi.org/10.1080/21541248.2016.1276999.

Nalbant, Perihan, Louis Hodgson, Vadim Kraynov, Alexei Toutchkine, and Klaus M. Hahn. 2004. “Activation of Endogenous Cdc42 Visualized in Living Cells.” *Science* 305 (5690): 1615–19. https://doi.org/10.1126/science.1100367.

Navarro-Lérida, Inmaculada, Sara Sánchez-Perales, María Calvo, Carles Rentero, Yi Zheng, Carlos Enrich, and Miguel A. Del Pozo. 2012. “A Palmitoylation Switch Mechanism Regulates Rac1 Function and Membrane Organization.” *EMBO Journal* 31 (3): 534–51. https://doi.org/10.1038/emboj.2011.446.

Nishimura, A., and M. E. Linder. 2013. “Identification of a Novel Prenyl and Palmitoyl Modification at the CaaX Motif of Cdc42 That Regulates RhoGDI Binding.” *Molecular and Cellular Biology* 33 (7): 1417–29. https://doi.org/10.1128/mcb.01398-12.

Nishimura, Akiyuki, and Maurine E. Linder. 2019. “Monitoring RhoGDI Extraction of Lipid-Modified Rho GTPases from Membranes Using Click Chemistry.” In *Methods in Molecular Biology*, 2009:297–306. Humana Press Inc. https://doi.org/10.1007/978-1-4939-9532-5_22.

Nobes, Catherine D., and Alan Hall. 1995. “Rho, Rac, and Cdc42 GTPases Regulate the Assembly of Multimolecular Focal Complexes Associated with Actin Stress Fibers, Lamellipodia, and Filopodia.” *Cell* 81 (1): 53–62. https://doi.org/10.1016/0092-8674(95)90370-4.

Nobes, Catherine D., and Alan Hall. 1999. “Rho GTPases Control Polarity, Protrusion, and Adhesion during Cell Movement.” *Journal of Cell Biology*. Vol. 144. https://doi.org/10.1083/jcb.144.6.1235.

Nomanbhoy, Tyzoon K., and Richard A. Cerione. 1996. “Characterization of the Interaction between RhoGDI and Cdc42Hs Using Fluorescence Spectroscopy.” *Journal of Biological Chemistry* 271 (17): 10004–9. https://doi.org/10.1074/jbc.271.17.10004.

Ori-McKenney, Kassandra M., Lily Yeh Jan, and Yuh Nung Jan. 2012. “Golgi Outposts Shape Dendrite Morphology by Functioning as Sites of Acentrosomal Microtubule Nucleation in Neurons.” *Neuron* 76 (5): 921–30. https://doi.org/10.1016/j.neuron.2012.10.008.

Osmani, Naël, Florent Peglion, Philippe Chavrier, and Sandrine Etienne-Manneville. 2010. “Cdc42 Localization and Cell Polarity Depend on Membrane Traffic.” *Journal of Cell Biology* 191 (7): 1261–69. https://doi.org/10.1083/jcb.201003091.

Osmani, Naël, Nicolas Vitale, Jean Paul Borg, and Sandrine Etienne-Manneville. 2006. “Scrib Controls Cdc42 Localization and Activity to Promote Cell Polarization during Astrocyte Migration.” *Current Biology* 16 (24): 2395–2405. https://doi.org/10.1016/j.cub.2006.10.026.

Palazzo, Alexander F., Hazel L. Joseph, Ying Jiun Chen, Denis L. Dujardin, Arthur S. Alberts, K. Kevin Pfister, Richard B. Vallee, and Gregg G. Gundersen. 2001. “Cdc42, Dynein, and Dynactin Regulate MTOC Reorientation Independent of Rho-Regulated Microtubule Stabilization.” *Current Biology* 11 (19): 1536–41. https://doi.org/10.1016/S0960-9822(01)00475-4.

Park, Seung Yeol, Jia Shu Yang, Angela B. Schmider, Roy J. Soberman, and Victor W. Hsu. 2015a. “Coordinated Regulation of Bidirectional COPI Transport at the Golgi by CDC42.” *Nature* 521 (7553): 529–32. https://doi.org/10.1038/nature14457.

Peng, Xu, Qiong Lin, Yang Liu, Yixin Jin, Joseph E. Druso, Marc A. Antonyak, Jun Lin Guan, and Richard A. Cerione. 2013. “Inactivation of Cdc42 in Embryonic Brain Results in Hydrocephalus with Ependymal Cell Defects in Mice.” *Protein and Cell* 4 (3): 231–42. https://doi.org/10.1007/s13238-012-2098-2.

Perez-Riverol, Yasset, Attila Csordas, Jingwen Bai, Manuel Bernal-Llinares, Suresh Hewapathirana, Deepti J. Kundu, Avinash Inuganti, et al. 2019. “The PRIDE Database and Related Tools and Resources in 2019: Improving Support for Quantification Data.” *Nucleic Acids Research* 47 (D1): D442–50. https://doi.org/10.1093/nar/gky1106.

Phuyal, Santosh, and Hesso Farhan. 2019. “Multifaceted Rho GTPase Signaling at the Endomembranes.” *Frontiers in Cell and Developmental Biology* 7 (July): 127. https://doi.org/10.3389/fcell.2019.00127.

Pichaud, Franck, Rhian F. Walther, and Francisca Nunes de Almeida. 2019. “Regulation of Cdc42 and Its Effectors in Epithelial Morphogenesis.” *Journal of Cell Science* 132 (10). https://doi.org/10.1242/jcs.217869.

Pincet, Frédéric, Vladimir Adrien, Rong Yang, Jérôme Delacotte, James E. Rothman, Wladimir Urbach, and David Tareste. 2016. “FRAP to Characterize Molecular Diffusion and Interaction in Various Membrane Environments.” *PLoS ONE* 11 (7). https://doi.org/10.1371/journal.pone.0158457.

Poullet, Patrick, Sabrina Carpentier, and Emmanuel Barillot. 2007. “MyProMS, a Web Server for Management and Validation of Mass Spectrometry-Based Proteomic Data.” *Proteomics* 7 (15): 2553–56. https://doi.org/10.1002/pmic.200600784.

Prévost, Coline, Feng Ching Tsai, Patricia Bassereau, and Mijo Simunovic. 2017. “Pulling Membrane Nanotubes from Giant Unilamellar Vesicles.” *Journal of Visualized Experiments* 2017 (130): e56086. https://doi.org/10.3791/56086.

Price, Leo S., Jie Leng, Martin Alexander Schwartz, and Gary M. Bokoch. 1998. “Activation of Rac and Cdc42 by Integrins Mediates Cell Spreading.” *Molecular Biology of the Cell* 9 (7): 1863–71. https://doi.org/10.1091/mbc.9.7.1863.

Rana, Mitra S., Chul Jin Lee, and Anirban Banerjee. 2018. “The Molecular Mechanism of DHHC Protein Acyltransferases.” *Biochemical Society Transactions*. Portland Press Ltd. https://doi.org/10.1042/BST20180429.

Ravichandran, Yamini, Bruno Goud, and Jean Baptiste Manneville. 2020. “The Golgi Apparatus and Cell Polarity: Roles of the Cytoskeleton, the Golgi Matrix, and Golgi Membranes.” *Current Opinion in Cell Biology* 62: 104–13. https://doi.org/10.1016/j.ceb.2019.10.003.

Ridley, Anne J. 2006. “Rho GTPases and Actin Dynamics in Membrane Protrusions and Vesicle Trafficking.” *Trends in Cell Biology* 16 (10): 522–29. https://doi.org/10.1016/j.tcb.2006.08.006.

Ridley, Anne J.. 2015. “Rho GTPase Signalling in Cell Migration.” *Current Opinion in Cell Biology*. https://doi.org/10.1016/j.ceb.2015.08.005.

Ridley, Anne J., Hugh F. Paterson, Caroline L. Johnston, Dagmar Diekmann, and Alan Hall. 1992. “The Small GTP-Binding Protein Rac Regulates Growth Factor-Induced Membrane Ruffling.” *Cell* 70 (3): 401–10. https://doi.org/10.1016/0092-8674(92)90164-8.

Rios, Rosa M. 2014. “The Centrosome - Golgi Apparatus Nexus.” *Philosophical Transactions of the Royal Society B: Biological Sciences*. https://doi.org/10.1098/rstb.2013.0462.

Roberts, Patrick J., Natalia Mitin, Patricia J. Keller, Emily J. Chenette, James P. Madigan, Rachel O. Currin, Adrienne D. Cox, Oswald Wilson, Paul Kirschmeier, and Channing J. Der. 2008. “Rho Family GTPase Modification and Dependence on CAAX Motif-Signaled Posttranslational Modification.” *Journal of Biological Chemistry* 283 (37): 25150–63. https://doi.org/10.1074/jbc.M800882200.

Rohatgi, Rajat, Hsin Yi Henry Ho, and Marc W. Kirschner. 2000. “Mechanism of N-WASP Activation by CDC42 and Phosphatidylinositol 4,5-Bisphosphate.” *Journal of Cell Biology* 150 (6): 1299–1309. https://doi.org/10.1083/jcb.150.6.1299.

Roux, Kyle J., Dae In Kim, Brian Burke, and Danielle G. May. 2018. “BioID: A Screen for Protein-Protein Interactions.” *Current Protocols in Protein Science* 91 (1): 19.23.1-19.23.15. https://doi.org/10.1002/cpps.51.

Sasaki, Takuya, and Yoshimi Takai. 1998. “The Rho Small G Protein Family-Rho GDI System as a Temporal and Spatial Determinant for Cytoskeletal Control.” *Biochemical and Biophysical Research Communications*. Vol. 245. https://doi.org/10.1006/bbrc.1998.8253.

Schwarz, Petra, Christine C. Stichel, and Heiko J. Luhmann. 2000. “Characterization of Neuronal Migration Disorders in Neocortical Structures: Loss or Preservation of Inhibitory Interneurons?” *Epilepsia* 41 (7): 781–87. https://doi.org/10.1111/j.1528-1157.2000.tb00243.x.

Simons, Kai, and Winchil L.C. Vaz. 2004. “Model Systems, Lipid Rafts, and Cell Membranes.” *Annual Review of Biophysics and Biomolecular Structure*. Annual Reviews. https://doi.org/10.1146/annurev.biophys.32.110601.141803.

Sinha, Soniya, and Wannian Yang. 2008. “Cellular Signaling for Activation of Rho GTPase Cdc42.” *Cellular Signalling* 20 (11): 1927–34. https://doi.org/10.1016/j.cellsig.2008.05.002.

Sofroniew, Michael V. 2015. “Astrogliosis.” *Cold Spring Harbor Perspectives in Biology* 7 (2): a020420. https://doi.org/10.1101/cshperspect.a020420.

Spano, Daniela, Chantal Heck, Pasqualino De Antonellis, Gerhard Christofori, and Massimo Zollo. 2012. “Molecular Networks That Regulate Cancer Metastasis.” *Seminars in Cancer Biology* 22 (3): 234–49. https://doi.org/10.1016/j.semcancer.2012.03.006.

St Johnston, Daniel, and Julie Ahringer. 2010. “Cell Polarity in Eggs and Epithelia: Parallels and Diversity.” *Cell*. https://doi.org/10.1016/j.cell.2010.05.011.

Tabuse, Yo, Yasushi Izumi, Fabio Piano, Kenneth J. Kemphues, Johji Miwa, and Shigeo Ohno. 1998. “Atypical Protein Kinase C Cooperates with PAR-3 to Establish Embryonic Polarity in Caenorhabditis Elegans.” *Development* 125 (18): 3607–14. https://pubmed.ncbi.nlm.nih.gov/9716526/.

Tcherkezian, Joseph, and Nathalie Lamarche-Vane. 2007. “Current Knowledge of the Large RhoGAP Family of Proteins.” *Biology of the Cell* 99 (2): 67–86. https://doi.org/10.1042/bc20060086.

Thompson, Barry J. 2013. “Cell Polarity: Models and Mechanisms from Yeast, Worms and Flies.” *Development (Cambridge)* 140 (1): 13–21. https://doi.org/10.1242/dev.083634.

Tonucci, Facundo M., Florencia Hidalgo, Anabela Ferretti, Evangelina Almada, Cristián Favre, James R. Goldenring, Irina Kaverina, Arlinet Kierbel, and M. Cecilia Larocca. 2015. “Centrosomal AKAP350 and CIP4 Act in Concert to Define the Polarized Localization of

the Centrosome and Golgi in Migratory Cells." *Journal of Cell Science* 128 (17): 3277–89. https://doi.org/10.1242/jcs.170878.

Valot, Benoît, Olivier Langella, Edlira Nano, and Michel Zivy. 2011. "MassChroQ: A Versatile Tool for Mass Spectrometry Quantification." *Proteomics* 11 (17): 3572–77. https://doi.org/10.1002/pmic.201100120.

Vamparys, Lydie, Romain Gautier, Stefano Vanni, W. F.Drew Bennett, D. Peter Tieleman, Bruno Antonny, Catherine Etchebest, and Patrick F.J. Fuchs. 2013. "Conical Lipids in Flat Bilayers Induce Packing Defects Similar to That Induced by Positive Curvature." *Biophysical Journal* 104 (3): 585–93. https://doi.org/10.1016/j.bpj.2012.11.3836.

Wang, Mei, and Patrick J. Casey. 2016. "Protein Prenylation: Unique Fats Make Their Mark on Biology." *Nature Reviews Molecular Cell Biology*. Nature Publishing Group. https://doi.org/10.1038/nrm.2015.11.

Watanabe, Takashi, Shujie Wang, and Kozo Kaibuchi. 2015. "IQGAPS as Key Regulators of Actin-Cytoskeleton Dynamics." *Cell Structure and Function* 40 (2): 69–77. https://doi.org/10.1247/csf.15003.

Watson, Leah J., Guendalina Rossi, and Patrick Brennwald. 2014. "Quantitative Analysis of Membrane Trafficking in Regulation of Cdc42 Polarity." *Traffic* 15 (12): 1330–43. https://doi.org/10.1111/tra.12211.

Wennerberg, Krister, Kent L. Rossman, and Channing J. Der. 2005. "The Ras Superfamily at a Glance." *Journal of Cell Science* 118 (5): 843–46. https://doi.org/10.1242/jcs.01660.

Wirth, Alexander, Chen Wacker Chen, Yao Wen Wu, Nataliya Gorinski, Mikhail A. Filippov, Ghanshyam Pandey, and Evgeni Ponimaskin. 2013. "Dual Lipidation of the Brain-Specific Cdc42 Isoform Regulates Its Functional Properties." *Biochemical Journal* 456 (3): 311–22. https://doi.org/10.1042/BJ20130788.

Woodham, Emma F., Nikki R. Paul, Benjamin Tyrrell, Heather J. Spence, Karthic Swaminathan, Michelle R. Scribner, Evangelos Giampazolias, et al. 2017. "Coordination by Cdc42 of Actin, Contractility, and Adhesion for Melanoblast Movement in Mouse Skin." *Current Biology* 27 (5): 624–37. https://doi.org/10.1016/j.cub.2017.01.033.

Yadav, Smita, Sapna Puri, and Adam D. Linstedt. 2009. "A Primary Role for Golgi Positioning in Directed Secretion, Cell Polarity, and Wound Healing." Edited by Jennifer Lippincott-Schwartz. *Molecular Biology of the Cell* 20 (6): 1728–36. https://doi.org/10.1091/mbc.E08-10-1077.

Yap, Karen, Yixin Xiao, Brad A. Friedman, H. Shawn Je, and Eugene V. Makeyev. 2016. "Polarizing the Neuron through Sustained Co-Expression of Alternatively Spliced Isoforms." *Cell Reports* 15 (6): 1316–28. https://doi.org/10.1016/j.celrep.2016.04.012.

Yeung, Tony, Gary E. Gilbert, Jialan Shi, John Silvius, Andras Kapus, and Sergio Grinstein. 2008. "Membrane Phosphatidylserine Regulates Surface Charge and Protein Localization." *Science* 319 (5860): 210–13. https://doi.org/10.1126/science.1152066.

Zaballa, María Eugenia, and F. Gisou van der Goot. 2018. "The Molecular Era of Protein S-

Acylation: Spotlight on Structure, Mechanisms, and Dynamics." *Critical Reviews in Biochemistry and Molecular Biology*. Taylor & Francis. https://doi.org/10.1080/10409238.2018.1488804.

Zahr, Siraj K., David R. Kaplan, and Freda D. Miller. 2019. "Translating Neural Stem Cells to Neurons in the Mammalian Brain." *Cell Death and Differentiation*. Nature Publishing Group. https://doi.org/10.1038/s41418-019-0411-9.

Zhou, Mo, Heidi Wiener, Wenjuan Su, Yong Zhou, Caroline Liot, Ian Ahearn, John F. Hancock, and Mark R. Philips. 2016. "VPS35 Binds Farnesylated N-Ras in the Cytosol to Regulate N-Ras Trafficking." *Journal of Cell Biology* 214 (4): 445–58. https://doi.org/10.1083/jcb.201604061.

Zhou, Pengcheng, Marimelia Porcionatto, Mariecel Pilapil, Yicheng Chen, Yoojin Choi, Kimberley F. Tolias, Jay B. Bikoff, Elizabeth J. Hong, Michael E. Greenberg, and Rosalind A. Segal. 2007. "Polarized Signaling Endosomes Coordinate BDNF-Induced Chemotaxis of Cerebellar Precursors." *Neuron* 55 (1): 53–68. https://doi.org/10.1016/j.neuron.2007.05.030.

Zhou, Wu, Xiaobo Li, and Richard T. Premont. 2016. "Expanding Functions of GIT Arf GTPase-Activating Proteins, PIX Rho Guanine Nucleotide Exchange Factors and GIT-PIX Complexes." *Journal of Cell Science* 129 (10): 1963–74. https://doi.org/10.1242/jcs.179465.

Annexes

The first article corresponds to the study that was an outcome of our collaboration with Jerome Delon. Selected results have been described in Part IV, Section B. This study reports the identification of an R186C Cdc42 patient mutant with an autoinflammatory phenotype and molecular mechanism associated with its pathogenicity. The article is titled, '*A toxic palmitoylation of Cdc42 enhances NF-kB signaling and drives a severe autoinflammatory syndrome*'.

The second is a review article titled, '*The Golgi apparatus and cell polarity: Roles of the cytoskeleton, the Golgi matrix, and Golgi membranes.*

Article 1 - A toxic palmitoylation of Cdc42 enhances NF-kB signaling and drives a severe autoinflammatory syndrome

Letter to the Editor

A toxic palmitoylation of Cdc42 enhances NF-κB signaling and drives a severe autoinflammatory syndrome

To the Editor:

Autoinflammatory diseases result from the dysregulation of innate immune responses. Here, we show that (1) a mutation in the C-terminal region of the Cdc42 Rho guanosine triphosphatase (GTPase) leads to palmitoylation and is involved in a severe, complex immunohematoautoinflammatory phenotype and (2) a direct link between the Cdc42-mutated form and enhanced NF-κB signaling pathway is responsible for the patient's inflammatory phenotype.

The clinical and laboratory data of our patient (referred to as patient A.S.) are detailed in the Methods section in this article's Online Repository at www.jacionline.org. The main clinical characteristics were severe neonatal dermatitis and flare-ups of a nonspecific urticarial, scaling rash. This rash worsened, with the formation of well-confined psoriasiform plaques and development of chronic psoriasiform erythroderma that was resistant to various lines of treatment (Fig 1, *A* and see Fig E1, *A-D* in this article's Online Repository at www.jacionline.org). The patient also displayed acute episodes of hepatomegaly with cytolysis; mild facial dysmorphia; a permanent nonspecific inflammatory syndrome with occasional monocytosis; and in adulthood, mild hypereosinophilia and hyper-IgE that were putatively related to a skin barrier defect. There was no evidence of an autoimmune disease during childhood. No major infections or allergies were observed, but a chronic staphylococcal colonization that probably acts as a triggering factor for worsening skin inflammation was seen.

Using whole exome sequencing, we identified a *de novo* c.556C>T (p.R186C) heterozygous mutation in cell division cycle 42 *(CDC42)* (Fig 1, *B* and see Fig E1, *E* and *F*). The mutation affects only the ubiquitously expressed Cdc42 form and not the brain form (see Fig E1, *G* and *H*). Cdc42 alternates between an inactive, cytosolic guanosine diphosphate–bound form and an active, membranous guanosine triphosphate–bound form; this cycle allows Cdc42 to interact with effectors and thus activate various biologic functions.[1,2] The cytosol/membrane cycle is regulated by guanosine diphosphate dissociation inhibitors (GDIs), which extract Cdc42 from endomembranes and plasma membranes and sequester it in the cytosol. Binding to membranes requires that Rho GTPases be lipidated by a geranyl-geranyl anchor attached to a cysteine residue in its C-terminal hypervariable region, C188 in Cdc42 (Fig 1, *C*).

Whereas wild-type (WT) Cdc42 is distributed in the cytosol, nuclear envelope and in the Golgi apparatus to a small extent, we found that Cdc42 R186C is abnormally anchored in the Golgi apparatus (Fig 1, *D* and see Fig E2, *A* in this article's Online Repository at www.jacionline.org). We studied whether the mutant Cdc42 influenced the WT protein's localization. Quantification of the Pearson coefficient for the signals from WT Cdc42 versus for those from Cdc42 R186C showed that the 2 proteins localize independently of each other (see Fig E2, *B*). Furthermore, the Golgi localization of Cdc42 R186C is stable over time (see Fig E2, *C*). Using constitutively active and dominant-negative mutant forms of Cdc42, we showed that the localization defect is independent of Cdc42 activation state (see Fig E2, *D*). Lastly, the localization of Cdc42 R186C was specifically related to the cysteine at position 186, because substitution with a serine or leucine did not have much impact on localization of Cdc42 (see Fig E2, *E-G*).

Curiously, the R186C mutation introduces a cysteine in a position that is palmitoylated in the related small GTPase H-Ras (see Fig E3, *A* in this article's Online Repository at www.jacionline.org). In Cdc42 immunoprecipitation experiments, we demonstrated that Cdc42 R186C is palmitoylated (Fig 1, *E*). Interestingly, Cdc42 R186C no longer located to the Golgi when palmitoylation was pharmacologically blocked (Fig 1, *F* and see Fig E3, *B-C*). Thus, the cysteine 186 caused Cdc42 palmitoylation and leads to retention of the protein in the Golgi apparatus.

We then hypothesized that this localization defect might modify the molecular partners with which Cdc42 could interact; we confirmed this hypothesis in mass spectrometry analyses. Interaction with GDI1 was significantly reduced by the R186C mutation (Fig 1, *G*). The crystal structure of the Cdc42/GDI1 complex shows that GDI1 interacts extensively with the lipidated hypervariable region and buries the geranyl-geranyl lipid inside a hydrophobic pocket.[3] Importantly, the R186 residue is also buried inside the GDI1 (see Fig E4, *A* in this article's Online Repository at www.jacionline.org). We therefore reasoned that the substitution of R186 by a palmitoylated cysteine would impair GDI1 binding. Biochemical experiments showed that Cdc42 R186C fails to interact with GDI1 (Fig 1, *H*). As a control for the lack of GDI1 interaction, we used another mutant described in other autoinflammatory patients, C188Y, which has been predicted to lack lipidation.[4]

We next investigated the functional consequences of the aberrant localization of Cdc42 R186C. Given that Cdc42 controls actin filament polymerization, we wondered whether actin polymerization would be affected. The cells of patient A.S. contained around 30% less F-actin than normal (Fig 2, *A*). Expression of Cdc42 R186C in starved CEM cells recapitulated the actin polymerization defect (Fig 2, *B*). In view of the patient's systemic inflammatory phenotype, we found that his fibroblasts overproduced proinflammatory cytokines (Fig 2, *C* and see Fig E5 in this article's Online Repository at www.jacionline.org) in an NF-κB-dependent manner (Fig 2, *D*). Accordingly, the patient's cells displayed increases in p65 NF-κB phosphorylation and nuclear translocation (Fig 2, *E* and *F*). Moreover, Cdc42 R186C expression in control fibroblasts was sufficient to increase IL-8 and IL-1β production to levels similar to those measured in the patient's cells (Fig 2, *G*). Remarkably, expression of Cdc42 R186C or C188Y induced NF-κB hyperactivation, whereas no activation was observed with these variants carrying a dominant negative mutation (Fig 2, *H*), indicating that these mutants must be activated by guanosine triphosphate to induce NF-κB signaling. Lastly, inhibition of palmitoylation reversed the NF-κB hyperactivation induced by Cdc42 R186C, indicating that the Golgi retention of Cdc42 is responsible for NF-κB overstimulation (Fig 2, *I*). Our results thus support a direct link between the Cdc42 R186C mutation and the cellular inflammatory phenotype and show that this is mediated by NF-κB.

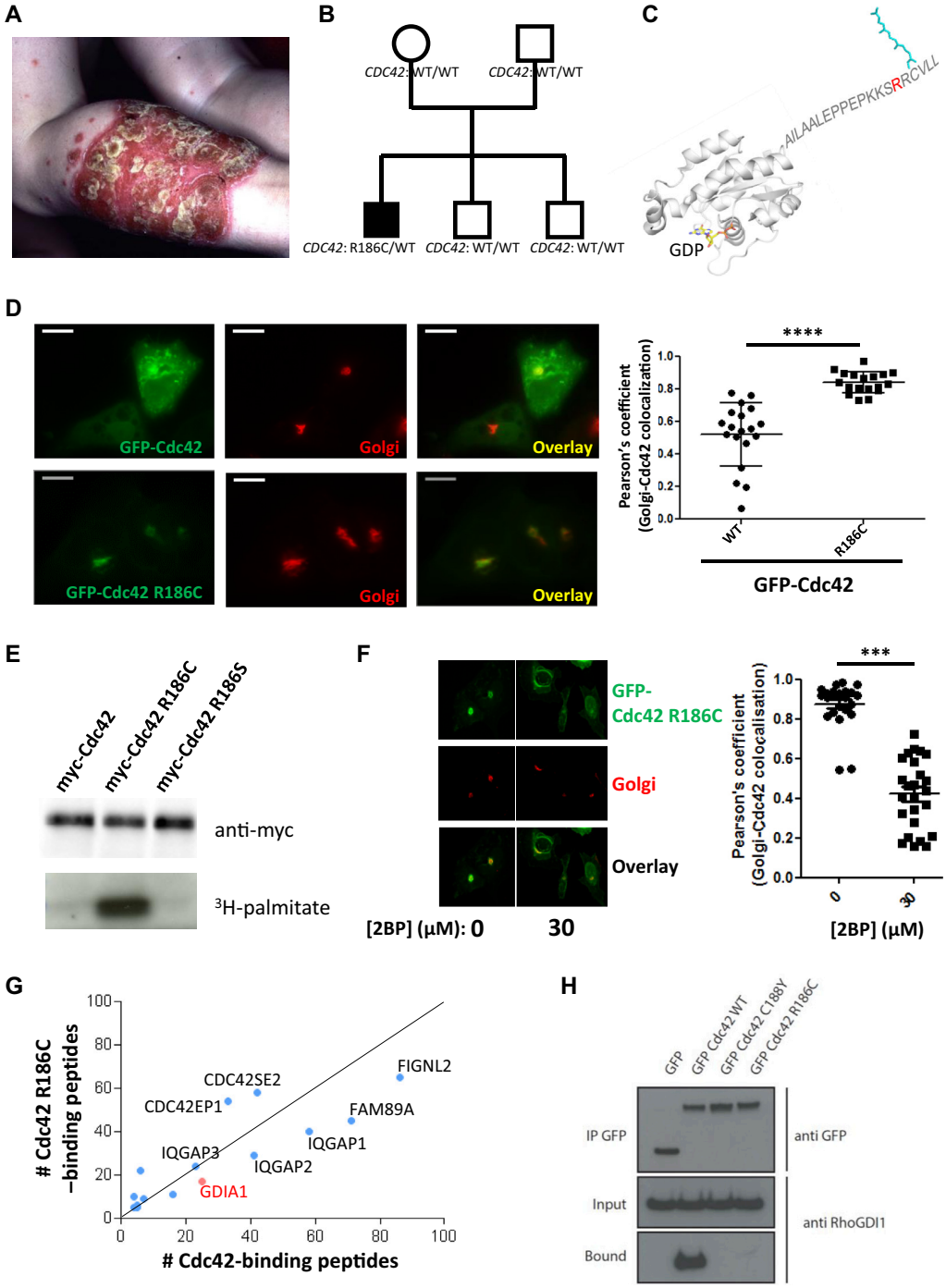

FIG 1. A, Pustular psoriasiform lesions and severe psoriasiform erythrodema. **B,** Pedigree. **C,** Structure of Cdc42, highlighting the mutated R186 (*red*). **D,** Staining of the Golgi apparatus in human bone marrow endothelial (HBMEC) cells transfected with the WT or R186C Cdc42. Scale bars = 20 μm. **E,** Western blot showing the amount of palmitate borne by the WT or mutant Cdc42. **F,** HBMECs expressing green fluorescent protein (GFP)-Cdc42 R186C treated with 2-bromo-palmitate (2BP [*left*]) and quantification of the staining (*right*). **G,** Mass spectrometry analysis. The *x* axis and *y* axis represent the numbers of peptides from the indicated Cdc42 partners that bind to WT and R186C Cdc42, respectively. Dots that fall on the line correspond to partners that bind equally well to WT and R186C Cdc42. **H,** The GDI1-Cdc42 interaction as monitored by coimmunoprecipitation and Western blot experiments. *GDP,* Guanosine diphosphate; *IP,* immunoprecipitation.

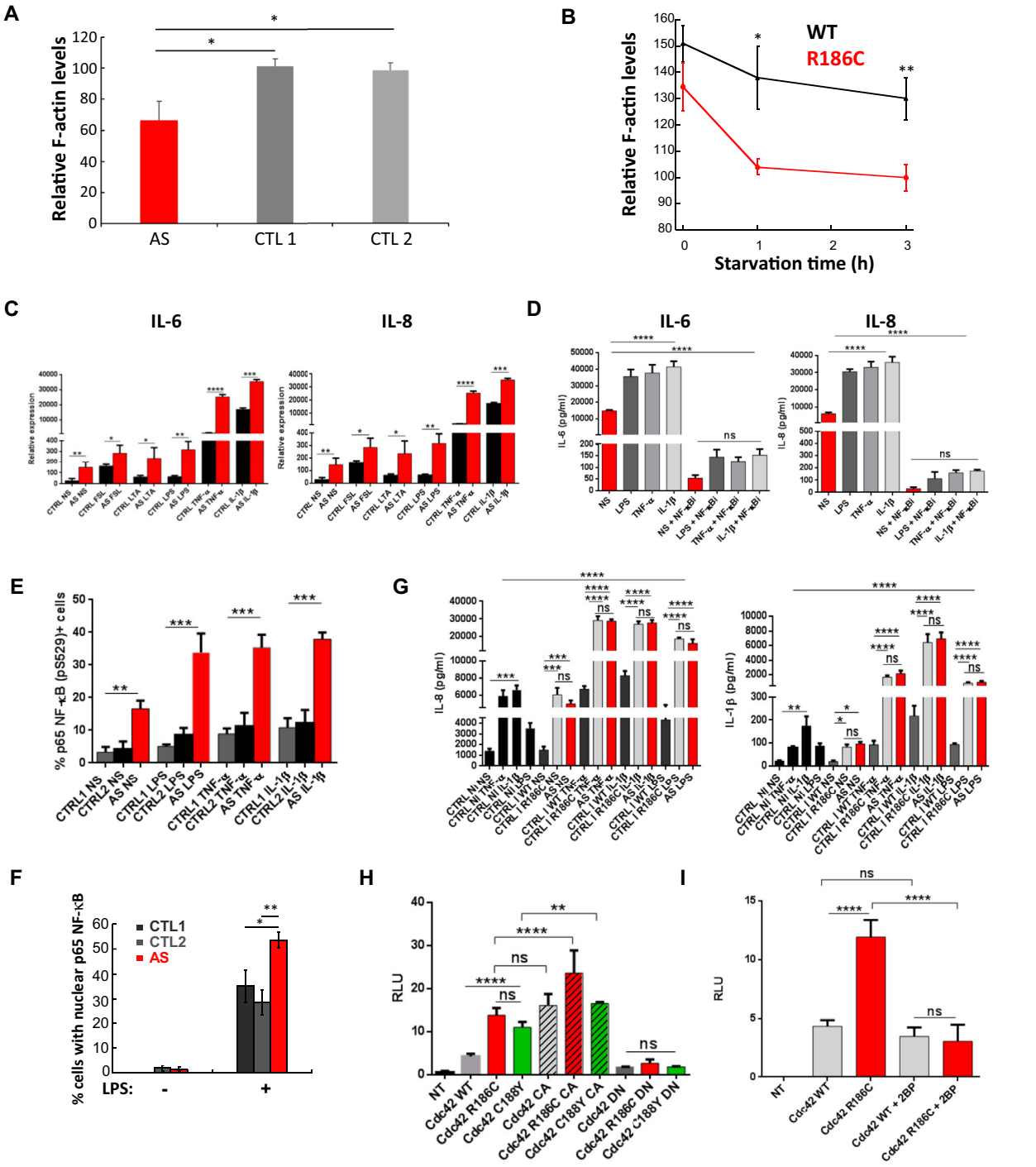

FIG 2. A, F-actin levels in patient and control fibroblasts. **B,** F-actin levels measured in starved CEM cells transfected with WT or R186C Cdc42. **C,** Relative mRNA expression of IL-6 and IL-8 in control and patient fibroblasts. **D,** ELISA quantification of IL-6 and IL-8 expression in the absence or presence of an NF-κB inhibitor in patient fibroblasts. Analysis of p65 NF-κB phosphorylation (**E**) and nuclear translocation (**F**). **G,** IL-8 and IL-1β production in control or patient fibroblasts not infected or infected with a lentivirus encoding WT or R186C Cdc42. **H,** NF-κB luciferase activity following transfection of the indicated constructs. **I,** NF-κB luciferase activity following expression of WT or R186C Cdc42 in the absence or presence of 2BP. *AS,* Autoinflammatory syndrome; *CTL*, control; *ns*, not significant; *NS*, no stimulation; *NT*, no transfection.

Our in-depth molecular characterization of the Cdc42 R186C mutant is in line with recent reports on other patients who had autoinflammatory syndromes and carried C-terminal variants of Cdc42.[4,5] In our study, the doubly lipidated R186C Cdc42 mutant was retained in the Golgi (see Fig E4, *B*). This impaired its plasma membrane anchoring and resulted in actin polymerization defects and hyperactivation of NF-κB signaling.

In conclusion, our study identifies a strong link between impaired cytosol/membrane cycling of Cdc42 resulting from abnormal double lipidation, partial defects in actin polymerization, and hyperactivation of NF-κB signaling, which can explain the pathophysiology of the disease. More broadly, our findings are consistent with reports in the literature that link inflammation with actin turnover[6] and membrane targeting of Rho GTPases.[7-9] Thus, further investigation of the various consequences of *CDC42* mutations are required because these mutations arise in a broad spectrum of clinical phenotypes. Ultimately, it offers the possibility of designing specific therapeutic targeting of this pathway that is newly involved in autoinflammatory diseases.

We thank patient A.S. and his family for participating in this research.

Bahia Bekhouche, MSc[a]*
Aurore Tourville, MSc[b]*
Yamini Ravichandran, MTech[c,d]
Rachida Tacine, BSc[b]
Laurence Abrami, PhD[e]
Michael Dussiot, MSc[a]
Andrea Khau-Dancasius, MD[a]
Olivia Boccara, MD[f]
Meriem Khirat, MD[b]
Marianne Mangeney, PhD[b]
Florent Dingli, MSc[g]
Damarys Loew, PhD[g]
Batiste Boëda, PhD[c]
Pénélope Jordan, MD[h]
Thierry Jo Molina, MD, PhD[a,i]
Nathalia Bellon, MD[f]
Sylvie Fraitag, MD[j]
Smail Hadj-Rabia, MD, PhD[f]
Stéphane Blanche, MD, PhD[k]
Anne Puel, PhD[l]
Sandrine Etienne-Manneville, PhD[c]
F. Gisou van der Goot, PhD[e]
Jacqueline Cherfils, PhD[m]
Olivier Hermine, MD, PhD[a,n]
Jean-Laurent Casanova, MD, PhD[l,o,p]
Christine Bodemer, MD, PhD[f]‡
Asma Smahi, PhD[a]‡
Jérôme Delon, PhD[b]‡

From [a]the Institut Imagine, INSERM U1163, CNRS ERL 8254, Université Paris Descartes, Sorbonne Paris-Cité, Laboratoire d'Excellence GR-Ex, Paris, France; [b]the Université de Paris, Institut Cochin, INSERM, U1016, CNRS, UMR8104, Paris, France; [c]the Cell Polarity, Migration and Cancer Unit, Institut Pasteur, UMR3691 CNRS, Equipe Labellisée Ligue Contre le Cancer, Paris, France; [d]Sorbonne Université, Collège doctoral, F-75005 Paris, France; [e]the Global Health Institute, School of Life Sciences, EPFL, Lausanne, Switzerland; [f]the Department of Dermatology, Reference Center for Genodermatoses (MAGEC), Necker- Enfants Malades Hospital (AP-HP), Paris Descartes-Sorbonne Paris Cité University, Imagine Institute, Paris, France; [g]the Institut Curie, PSL Research University, Centre de Recherche, Laboratoire de Spectrométrie de Masse Protéomique, Paris, France; [h]the Fédération de Génétique, Service de Génétique Moléculaire, Hôpital Necker-Enfants Malades, Paris, France; [i]the Department of Pathology, Necker Enfants Malades, Université de Paris, France; [j]the Department of Pathology, reference centre MAGEC, Necker-Enfants Malades Hospital, APHP; [k]Unité d'Immunologie Hématologie Rhumatologie Pédiatrique, Necker-Enfants Malades Hospital (AP-HP5), Paris Descartes-Sorbonne Paris Cité University, France; [l]the Laboratory of Human Genetics of Infectious Diseases, Necker Branch, INSERM U1163, Descartes University, Imagine Institute, Paris, France; [m]the Laboratoire de Biologie et Pharmacologie Appliquée, CNRS and Ecole Normale Supérieure Paris-Saclay, Cachan, France; [n]the Department of Hematology, Hôpital Necker AP-HP, Paris, France; [o]the St. Giles Laboratory of Human Genetics of Infectious Diseases, Rockefeller Branch, Rockefeller University, New York, NY, Howard Hughes Medical Institute, New York, NY; and [p]the Department of Pediatric Immunology and Hematology, Necker-Enfants Malades Hospital (AP-HP), Paris Descartes-Sorbonne Paris Cité University, Paris, France. E-mail: christine.bodemer@aphp.fr, asma.smahi@inserm.fr, jerome.delon@inserm.fr.

*These authors contributed equally to this work as first authors.

‡These authors contributed equally to this work.

Supported by INSERM, CNRS, Université de Paris, Association pour la Recherche contre le Cancer (to J.D.), Ligue Contre le Cancer (to S.E.M.), Société Française de Dermatologie (to A.S., C.B., and J.D.), Agence Nationale de la Recherche (RIDES to A.S., J.D., and J.C.), the European Union Horizon 2020 Marie Skłodowska-Curie research and innovation program (MSCA-ITN-2015-675407 to S.E.M.), Institut Pasteur, the Région Ile de France and the Fondation pour la Recherche Médicale (J.C. and D.L.).

Disclosure of potential conflict of interest: The authors declare that they have no relevant conflicts of interest.

REFERENCES

1. Rougerie P, Delon J. Rho GTPases: masters of T lymphocyte migration and activation. Immunol Lett 2012;142:1-13.
2. Cherfils J, Zeghouf M. Regulation of small GTPases by GEFs, GAPs, and GDIs. Physiol Rev 2013;93:269-309.
3. Hoffman GR, Nassar N, Cerione RA. Structure of the Rho family GTP-binding protein Cdc42 in complex with the multifunctional regulator RhoGDI. Cell 2000;100:345-56.
4. Gernez Y, de Jesus AA, Alsaleem H, Macaubas C, Roy A, Lovell D, et al. Severe autoinflammation in 4 patients with C-terminal variants in cell division control protein 42 homolog (CDC42) successfully treated with IL-1β inhibition. J Allergy Clin Immunol 2019;144:1122-5.
5. Lam MT, Coppola S, Krumbach OHF, Prencipe G, Insalaco A, Cifaldi C, et al. A novel disorder involving dyshematopoiesis, inflammation, and HLH due to aberrant CDC42 function. J Exp Med 2019;216:2778-99.
6. Pfajfer L, Mair NK, Jimenez-Heredia R, Genel F, Gulez N, Ardeniz O, et al. Mutations affecting the actin regulator WD repeat-containing protein 1 lead to aberrant lymphoid immunity. J Allergy Clin Immunol 2018;142:1589-604.e11.
7. Akula MK, Shi M, Jiang Z, Foster CE, Miao D, Li AS, et al. Control of the innate immune response by the mevalonate pathway. Nat Immunol 2016;17:922-9.
8. Park YH, Wood G, Kastner DL, Chae JJ. Pyrin inflammasome activation and RhoA signaling in the autoinflammatory diseases FMF and HIDS. Nat Immunol 2016;17:914-21.
9. Akula MK, Ibrahim MX, Ivarsson EG, Khan OM, Kumar IT, Erlandsson M, et al. Protein prenylation restrains innate immunity by inhibiting Rac1 effector interactions. Nat Commun 2019;3975.

https://doi.org/10.1016/j.jaci.2020.03.020

METHODS

Patient A.S.

Patient A.S. was born at term to healthy, nonconsanguineous, white parents. His biological father was confirmed by a paternity test. From his first few days of life onward, patient A.S. displayed episodes of fever, hepatosplenomegaly, pancytopenia, and a diffuse maculopapular rash with frequent relapses and a progressive worsening of his general condition. When he was 2 months of age, an acute episode of pancytopenia prompted a clinical investigation. This investigation revealed extramedullary hematopoiesis (in a needle liver biopsy specimen), nonspecific lymphoid hyperplasia (in a lymph node biopsy specimen), and a relatively acellular bone marrow. The skin biopsy specimen showed a moderately intense, nonspecific inflammatory infiltrate. Although systemic treatment with high-dose steroids led to some improvement, the patient became corticoid dependent. At the age of 11 months, A.S. displayed relapses of more strongly inflammatory, scaly, erythematous skin lesions and fluctuating hepatosplenomegaly with cytolysis. These conditions had a severe impact on growth (–4 SDs). At the age of 16 months, the patient's health worsened, with a moderate bone marrow fibrosis, persistent skin flare-ups, and episodes of fever and cytolysis with a nonspecific inflammatory syndrome. There were no signs of infection or autoimmune disease. Splenectomy performed when the patient was 23 months old showed extramedullary hematopoiesis and no evidence of neoplastic disease. Allogeneic bone marrow transplantation was performed when the patient was 24 months old; immune reconstitution was good, with 100% donor chimerism. However, scaly cutaneous lesions with a psoriasiform aspect appeared just 6 days after the transplant, despite the absence of any signs of graft-versus-host disease. We did not observe vacuolization or necrosis of basal layer keratinocytes or lymphocytic exocytosis (ie, satellite cell necrosis) on multiple sections. The skin lesions worsened gradually; 8 months after the transplantation, the patient's whole body was affected by erythroderma. On a skin biopsy specimen, sterile pustular psoriasis-type lesions were noted (Fig 1, *A*). The fever and pancytopenia disappeared totally, whereas hepatomegaly and liver cytolysis persisted. The patient is now a 23-year-old adult with permanent, severe, psoriasiform erythroderma; flares of more pronounced, painful skin inflammation (Fig 1, *A* and Fig E1, *A-D*); chronic *Staphylococcus aureus* skin infections; and recurrent episodes of liver cytolysis. Viral infections and the staphylococcal skin infections worsen the organ inflammation. Clinically, we have observed aortic insufficiency, mild facial dysmorphy, acquired hypophosphatemic rickets, growth retardation, a nonspecific inflammatory syndrome, monocytosis of varying intensity (>1000/mm^3), hypereosinophilia (>600/mm^3), and hyper-IgE (>700 IU/mL). The patient's clinical characteristics (flares of inflammation in different organs, episodes of fever, and a nonspecific inflammatory syndrome) are suggestive of an autoinflammatory disease. After transient improvements, the patient has failed to respond to treatments with various immunosuppressants and/or biologics (including anti–IL-1 receptor and anti–TNF-α, which have been tested in severe and pustular psoriasis) (Fig E1).

Constructs

The pEGFP-C3 vector was from Clontech (Mountain View, Calif). The pEGFP-C3-Cdc42 plasmid was provided by L.I. Salazar-Fontana.[E1] Constitutively active L61Q and dominant negative T17N mutants that mimic the guanosine triphosphate– and guanosine diphosphate–bound forms of Cdc42 respectively, were previously described.[E2] The pRK5-myc-Cdc42 plasmids were all obtained from Addgene. The Cdc42 mutants (R186C, R186S, R186L or C188Y) were generated by site-directed mutagenesis (Quickchange kit, Agilent Technologies, Les Ulis, France).

WT and R186C Cdc42 were also subcloned in the pLenti-III-CMV vector from Applied Biological Materials Inc (Richmond, British Columbia, Canada).

Cells

The lymphoblastoid T-cell line CEM was grown in RPMI 1640 medium plus Glutamax medium (Gibco, Illkirch, France) supplemented with 10% heat-inactivated FCS, antibiotics (50 U/mL of penicillin and 50 μg/mL of streptomycin [Gibco]), 10 mM sodium pyruvate (Gibco), and 10 mM HEPES (Gibco).

Primary human peripheral blood T cells (PBTs) were purified from the blood of healthy donors (provided by Etablissement Français du Sang) by using a Ficoll gradient separation before negative selection with a cocktail of antibodies (EasySep Human T cell isolation kit [Stem Cell Technologies, Grenoble, France]) according to the manufacturer's recommendation. PBTs were grown in complete RPMI 1640 medium supplemented by 10% human AB serum.

Primary human fibroblasts from the patient and healthy donors were obtained from skin biopsy specimens.

Human bone marrow endothelial cell (HBMEC), HEK 293T, RPE1 cell lines and primary human fibroblasts were cultivated in complete Dulbecco modified Eagle medium (Gibco).

Transfections and transductions

CEM cells (2×10^6) were centrifuged for 5 minutes at 1200 rpm and washed once in PBS (Gibco). The cells were then transfected by nucleofection with 5 μg of DNA in 100 μL of Cell Line Nucleofector Solution V (Lonza, Levallois-Perret, France) by using the C-016 program (Amaxa Biosystems). After transfection, 500 μL of complete RPMI medium was added to the cells, which were then deposited in 6-well plates containing 2 mL of medium. The plate was incubated overnight.

The transfection of the HBMEC cells was carried out according to the same protocol but with 3 μg of DNA for 0.5×10^6 cells in 100 μL of Cell Line Nucleofector Solution V (Lonza) with the program U-015. For the cotransfection experiments, 0.5×10^6 HBMEC cells were transfected with 2.5 μg of each of the plasmids of interest encoding for GFP-Cdc42 R186C together with either Myc-Cdc42 WT or an empty vector. The PBTs were transfected with 5 μg of DNA for 5×10^6 cells in 100 μL of Human T-Cell Nucleofector Solution (Lonza) with the program U-014 (Amaxa Biosystems). The HEK cells were transfected with plasmids encoding green fluorescent protein (GFP)-tagged Cdc42 variants by using calcium phosphate transfection or a Lipofectamine LTX Kit (Life Technologies, Carlsbad, Calif). The RPE1 cells were transfected by using Fugene (Promega, Madison, Wis). Lentiviral production and fibroblasts infection were performed as described.[E3]

Biochemistry

To detect palmitoylation, the RPE1 cells that had been transfected 48 hours earlier with different Myc-tagged constructs were starved for 1 hour at 37°C in IM (Glasgow minimal essential medium buffered with 10 mM HEPES [pH 7.4]) and incubated for 2 hours at 37°C in IM with 200 μCi/mL of ^{3}H-palmitic acid (9,10-^{3}H(N)) (American Radiolabeled Chemicals, Inc, St Louis, Mo). The cells were washed, incubated in complete Dulbecco modified Eagle medium for 10 minutes, washed 3 times with cold PBS at 4°C, directly lysed for 30 minutes at 4°C in lysis buffer (0.5 % Nonidet P-40, 500 mM Tris [pH 7.4], 20 mM EDTA, 10 mM NaF, 2 mM benzamidine, and protease inhibitor cocktail [Roche, Basel, Switzerland]), and centrifuged for 3 minutes at 5000 rpm. Supernatants were subjected to preclearing with G Sepharose beads before being subjected to immunoprecipitation reaction that included overnight incubation with anti-Myc affinity gel (Thermo Scientific, Waltham, Mass). After immunoprecipitation, the washed beads were incubated for 5 minutes at 90°C in reducing sample buffer before 4% to 20% gradient SDS-PAGE and revelation with a mouse anti-Myc 9E10 antibody (Covance, Princeton, NJ). After SDS-PAGE, the gel was incubated in a fixative solution (25% isopropanol, 65% H_2O, and 10% acetic acid), followed by a 30-minute incubation with signal enhancer Amplify NAMP100 (GE Healthcare, Chicago, Ill). The radiolabeled products were revealed by using Typhoon phosphoimager.

For GDI1 coimmunoprecipitation assay, the HEK cells were lysed by using 50 mM TRIS base, Triton 2%, and 200 mM NaCl, as well as 1 tablet/10 mL of the protease inhibitor Mini-complete, EDTA-free (Roche). After removal of insoluble fragments via centrifugation at 12,000 *g* for 25 min, the lysates were incubated with 15 μL of GFP-Trap Agarose beads from Chromotek (Planegg, Germany) for 1 hour at 4°C on a rotary wheel. The beads were then washed 3 times for 10 minutes with wash buffer (250 mM NaCl and 0.1 % Triton in

PBS) followed by detection of GDI1 interaction with GFP-tagged Cdc42 variants by using Western blot. The primary antibodies used were anti–GFP–horseradish peroxidase (Novus Biologicals, Centennial, Colo) and anti–Rho GDIα (Santa Cruz Biotechnology, Santa Cruz, Calif).

All biochemistry experiments are representative of at least 3 independent experiments.

Proteomics and mass spectrometry analysis

GFP immunoprecipitation assays were carried out as described earlier with 1 exception; namely, a special wash buffer was used to wash the Chromotek beads after the binding assays. The mass spectrometry wash buffer was prepared by using 50 mM TRIS base, 150 mM NaCl, 1 mM EDTA, and 2.5 mM $MgCl_2$ (pH adjusted to 7.5). Following the final wash, the beads were stored with wash buffer at 4°C before deposition at the Institut Curie Mass Spectrometry and Proteomics facility (LSMP).

The proteins on the beads were washed twice with 100 μL of 25 mM NH_4HCO_3, after which we performed on-bead digestion with 0.2 μg of Trypsin/LysC (Promega) for 1 hour in 100 μL of 25 mM NH_4HCO_3. The samples were then loaded onto homemade C18 StageTips for desalting. Peptides were eluted by using 40:60 MeCN/H_2O plus 0.1% formic acid and vacuum-concentrated to dryness.

Online chromatography was performed with an RSLCnano system (Ultimate 3000, Thermo Scientific) coupled to an Orbitrap Fusion Tribrid mass spectrometer (Thermo Scientific). Peptides were trapped on a C18 column (75-μm inner diameter × 2 cm; nanoViper Acclaim PepMapTM 100, Thermo Scientific) with buffer A (2/98 MeCN/H_2O in 0.1% formic acid) at a flow rate of 4 μL/min over 4 minutes. Separation was performed on a 50 cm × 75-μm C18 column (nanoViper Acclaim PepMapTM RSLC, 2 μm, 100 Å, Thermo Scientific) regulated to a temperature of 55°C with a linear gradient of 5% to 25% buffer B (100% MeCN in 0.1% formic acid) at a flow rate of 300 nL/min over 100 minutes. Full-scan MS was performed by using the Orbitrap analyzer with a resolution set to 120,000, and ions from each full scan were high-density collisional dissociation–fragmented and analyzed in the linear ion trap.

For identification, the data were searched against the *Homo sapiens* (UP000005640) SwissProt database by using Sequest HF through proteome discoverer (version 2.2). Enzyme specificity was set to trypsin, and a maximum of 2 missed cleavage sites were allowed. Oxidized methionine, N-terminal acetylation, and carbamidomethyl cysteine were set as variable modifications. The maximum allowed mass deviation was set to 10 ppm for monoisotopic precursor ions and 0.6 Da for MS/MS peaks.

The resulting files were further processed by using myProMS E4 v3.6 (work in progress). The false discovery rate calculation was performed by using Percolator and was set to 1 % at the peptide level for the whole study. The label-free quantification was performed by peptide extracted ion chromatograms (XICs) computed with MassChroQ version 2.2.[E5] For protein quantification, XICs from proteotypic peptides shared between compared conditions (TopN matching) with no missed cleavages were used. Median and scale normalization was applied on the total signal to correct the XICs for each biologic replicate. To estimate the significance of the change in protein abundance, a linear model (adjusted on peptides and biologic replicates) was performed and *P* values were adjusted with a Benjamini-Hochberg false discovery rate procedure with a control threshold set to 0.05.

The mass spectrometry proteomics data have been deposited with the ProteomeXchange Consortium via the PRIDE[E6] partner repository, with the data set identifier PXD016251 (username, reviewer94457@ebi.ac.uk; password, MrXYoj4j).

For each indicated partner (*blue dots*), the number of identified peptides that bind to mutant Cdc42 R186C is shown as a function of the number of peptides binding to WT Cdc42. Partners that fall on the black line bind WT and mutant Cdc42 equally well.

Treatments of cells

CEM and HBMEC cells were incubated overnight in complete culture medium containing 30 μM 2-bromo-palmitate (Sigma, St Louis, Mo).

Cells were stimulated with FSL-1 (a TLR2/6 agonist [1 μg/mL]), LTA (a TLR2 agonist [10 μg/mL]), LPS (a TLR4 agonist [1 μg/mL]), TNF-α (20 ng/mL), and IL-1β (20 ng/mL) for 24 hours.

RNA extraction and cDNA synthesis

Total RNA was extracted from patient and healthy control fibroblasts stimulated or left unstimulated with a Qiagen (Hilden, Germany) RNA mini kit according to the manufacturer's instructions. cDNA was synthesized thanks to ready-to-use iScript cDNA supermix (BioRad, Hercules, Calif).

Real-time quantitative PCR

Real-time quantitative PCR was performed with Syber Green PCR master mix (Life Technologies) according to the manufacturer's instructions. The results were read with the CFX384 Real Time System machine. Relative expression of mRNA was determined by the $2^{-\Delta\Delta C(t)}$ method by using *GAPDH* and *ACTIN* as housekeeping genes.

ELISA

Supernatants were collected, and ELISA (InvivoGen, San Diego, Calif) for different cytokines was performed according to the manufacturer's instructions. Absorbance results were read with the Infinite f200 pro TECAN machine.

NF-κB luciferase activity

HEK 293T cells were transfected with NF-κB–dependent firefly luciferase vector (Ig-κLUC), *Renilla* luciferase vector as an internal control, and different constructions of Cdc42 following the manufacturer's indications. The cells were lysed in passive lysis buffer, and luciferase activity was read in the Infinite f200 pro TECAN machine.

Immunofluorescence

After cells were washed with PBS, they were fixed with 4% paraformaldehyde (Electron Microscopy Sciences, Hatfield, Pa) for 10 minutes. They were then washed once in PBS containing 1 % BSA (Sigma) and twice in a permeabilization buffer (PBS containing 0.1% saponin [Fluka Biochemika, Illkirch, France] and 0.2% BSA). The cells were incubated for 45 minutes with the following primary antibodies: anti-GM130 (Santa Cruz Biotechnology), anti-p65 NF-κB (Santa Cruz Biotechnology), or an anti-myc tag Alexa Fluor 488 antibody (Cell Signaling Technology, Danvers, Mass; 9B11). After they were washed in the permeabilization buffer, the cells were incubated for 30 minutes with secondary anti-goat or anti-mouse antibodies conjugated to Alexa Fluor 568 (Invitrogen, Carlsbad, Calif). After an additional wash, the cells were incubated with Hoechst (Sigma) for 5 minutes to stain nuclei in blue.

For the cotransfection experiments, the cells were stained according to the same protocol except for the myc staining that was performed by using an unconjugated anti-myc tag antibody (Santa Cruz Biotechnology, 9E10) followed by an AMCA anti-mouse antibody (Jackson ImmunoResearch, Ely, United Kingdom).

The images were acquired by using a Nikon TE300 fluorescence microscope, a Cascade Photometrics camera, and Metamorph version 7.8.9.0 software. Three oil immersion objectives were used: 40×, 60×, and 100×. Z-stack images were generated, and then (after deconvolution and projection) the Pearson coefficient (PC) was measured on Fiji (ImageJ software, version 1.51u) by using a macro containing the Coloc2 plugin. This coefficient measures the degree of overlap between 2 stainings and was used to quantify the degree of colocalization between Cdc42 and the Golgi apparatus. A PC value of 0 means that there is no colocalization between the 2 stainings. By contrast, a PC value of 1 means that there is a perfect colocalization between Cdc42 and the Golgi.

All immunocytochemistry experiments and quantifications shown are representative of at least 3 independent experiments.

The degree of p65 NF-κB nuclear translocation was quantified on Fiji from randomly acquired images by measuring the mean fluorescence intensity of the staining in the nucleus divided by the mean fluorescence intensity in the cytosol with use of the same size regions. A ratio higher than 1 was considered to be the hallmark of a cell presenting p65 NF-κB nuclear translocation.

Flow cytometry

The transfected CEM cells were used directly or serum-starved during the indicated times in RPMI medium alone. The cells were then fixed and permeabilized as previously explained. Actin filaments were stained with 0.5 U/mL of phalloidin Alexa Fluor 647 (Invitrogen). The amount of filamentous actin (F-actin) present in the CEM cells was measured by flow cytometry (FACSCalibur, BD Biosciences, Le Pont de Claix, France) and analyzed with Flowjo version 7 software.

Alexa Fluor 488 Mouse Anti NF-κB p65 (pS529) from BD Biosciences was used on fibroblasts.

Statistical analyses

Statistical analyses were carried out by using GraphPad Prism 5 software (GraphPad Software Inc, La Jolla, Calif). The results represent the means plus or minus SEs of at least 3 independent experiments. The levels of significance were calculated by ANOVA or the Student *t* test: $*P < .05$; $**P < .01$; $***P < .001$, $****P < .0001$.

REFERENCES

E1. Salazar-Fontana LI, Barr V, Samelson LE, Bierer BE. CD28 engagement promotes actin polymerization through the activation of the small Rho GTPase Cdc42 in human T cells. J Immunol 2003;171:2225-32.

E2. Faure S, Salazar-Fontana LI, Semichon M, Tybulewicz VL, Bismuth G, Trautmann A, et al. ERM proteins regulate cytoskeleton relaxation promoting T cell-APC conjugation. Nat Immunol 2004;5:272-9.

E3. Bal E, Park HS, Belaid-Choucair Z, Kayserili H, Naville M, Madrange M, et al. Mutations in ACTRT1 and its enhancer RNA elements lead to aberrant activation of Hedgehog signaling in inherited and sporadic basal cell carcinomas. Nat Med 2017;23:1226-33.

E4. Poullet P, Carpentier S, Barillot E. myProMS, a web server for management and validation of mass spectrometry-based proteomic data. Proteomics 2007;7:2553-6.

E5. Valot B, Langella O, Nano E, Zivy M. MassChroQ: a versatile tool for mass spectrometry quantification. Proteomics 2011;11:3572-7.

E6. Vizcaino JA, Csordas A, Del-Toro N, Dianes JA, Griss J, Lavidas I, et al. 2016 update of the PRIDE database and its related tools. Nucleic Acids Res 2016;44:11033.

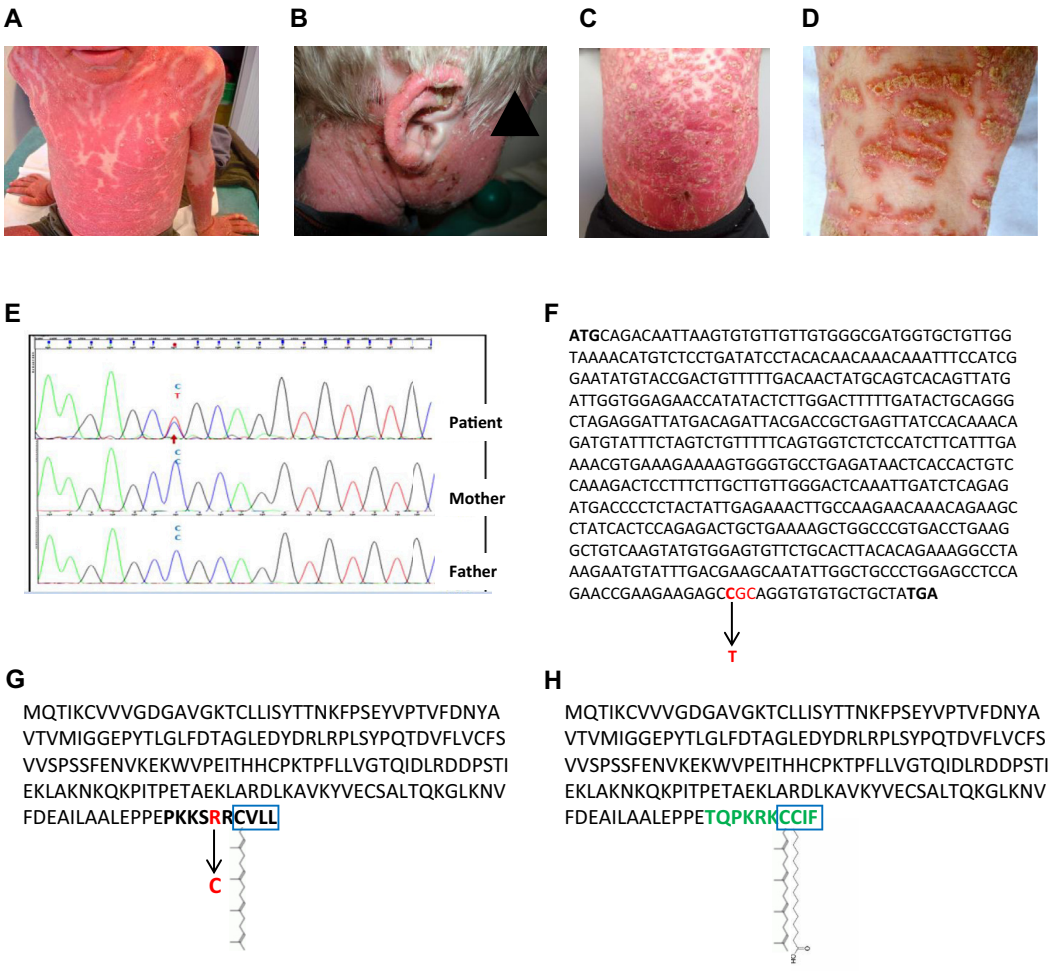

FIG E1. Severe dermatitis (psoriasiform erythroderma) with chronic, crusted lesions and the development of impetigo (**A**). We noted a slight reduction in skin signs with conventional treatments for severe psoriasis (**B**), chronic relapses of pustular psoriasiform lesions, and chronic flares of severe skin inflammation (**C** and **D**). **E,** Electropherogram of the 3′ coding sequence of the *CDC42* gene from the patient (*top*) and his 2 parents (*bottom*). Each peak corresponds to a nucleotide, namely, adenine (A [*green*]), cytosine (C [*blue*]), thymine (T [*red*]), or guanine (G [*black*]). The red arrow indicates the mutation of a cytosine into a thymine on 1 allele. **F,** The nucleotides in the coding sequence for ubiquitous human Cdc42. The 3 nucleotides in red correspond to the codon modified by the C-to-T mutation. The start codon (ATG) and the termination codon (TGA) are shown in bold type. Amino acid sequences of the ubiquitous (**G**) or brain-specific (**H**) isoforms of human Cdc42. The blue box indicates the position of the CAAX sequence containing the geranylgeranylation site. The R186C mutation is shown in red. The end-most amino acids (specific for these isoforms) are shown in bold type.

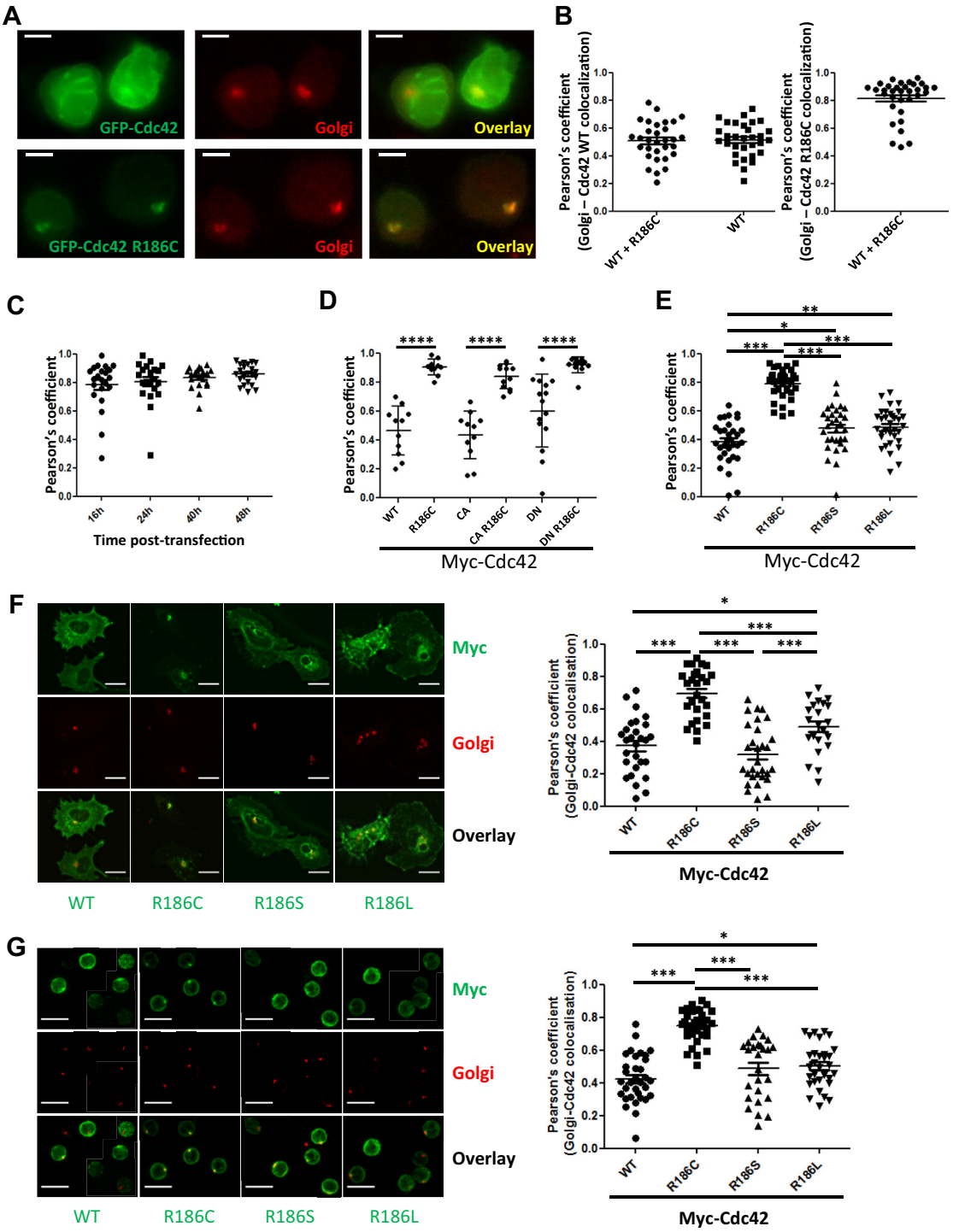

FIG E2. **A,** Staining of the Golgi-resident protein GM130 (red) in CEM cells expressing GFP-Cdc42 (*top*) or GFP-Cdc42 R186C (*bottom*). The overlay of green and red fluorescence is also shown. Scale bars = 5 μm. **B,** HBMECs expressing either Myc-Cdc42 WT plus GFP-Cdc42 R186C or Myc-Cdc42 WT alone were analyzed to determine the degree of colocalization in the Golgi with WT (*left*) or R186C (*right*) Cdc42. **C,** The degree of colocalization between the Golgi apparatus and Myc-Cdc42 R186C, analyzed from 16 to 48 hours after transfection. **D,** Measurement of the Pearson coefficient for the signals from constitutively active (CA) or dominant negative (DN) Cdc42 forms associated (or not) with the R186C substitution. **E,** Quantification of the degree of colocalization between the Golgi and Myc-tagged WT or mutant Cdc42 in CEM cells. The results are representative of at least 3 independent experiments. (*Left*) Microscopy images of HBMECs (**F**) or primary resting human peripheral blood T lymphocytes (**G**) expressing Myc-tagged constructs encoding WT, R186C, R186S, or R186L Cdc42. Staining for Myc (*green*) and Golgi-associated GM130 (*red*) and an overlay of the 2 is shown for each condition. Scale bars = 20 μm (**F**) and 10 μm (**G**). (*Right*) Quantification of the degree of colocalization for each Cdc42 forms and the Golgi apparatus, as quantified by Pearson's coefficient. **P* < .05; ***P* < .01; ****P* < .001; *****P* < .0001.

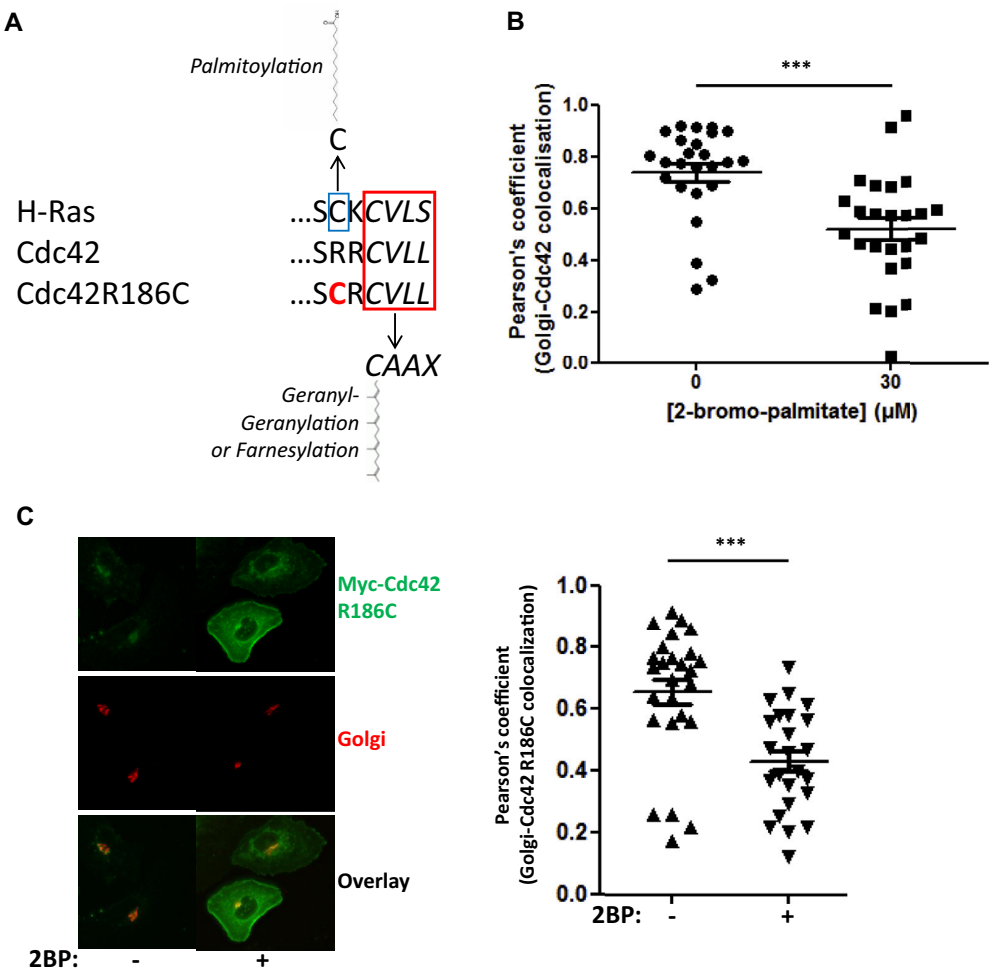

FIG E3. **A,** Alignment of the C-terminal amino acid sequences of Cdc42, Cdc42 R186C, and H-Ras. The cyst residues in the CAAX sequences shown in a red box are geranyl-geranylated in Cdc42 and farnesylated in H-Ras. The H-Ras cyst highlighted in a blue box is palmitoylated. **B,** Quantification of the degree of colocalization between the Golgi apparatus and Myc-Cdc42 R186C in CEM cells treated (or not) with 30 μM 2-bromopalmitate (2BP). **C,** HBMECs expressing Myc-Cdc42 R186C and treated (or not) with 30 μM 2-BP were analyzed in the same way. The respective Pearson coefficients for each condition are shown on the right. Each graph is representative of 3 independent experiments. ***$P < .001$.

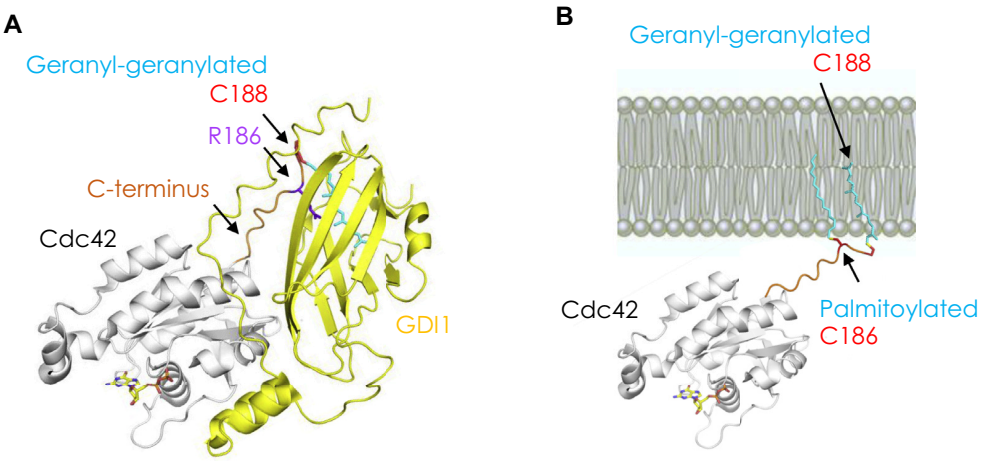

FIG E4. A, Structure of the Cdc42-GDI1 complex. R186 (*in purple*) is buried in a groove of GDI1 (*in yellow*), which regulates the alternation of Cdc42 between the membrane and the cytosol by forming a soluble Cdc42-GDI1 complex. **B,** The R186 to cysteine (C186) mutation allows its modification by a second lipid (palmitate). This second lipid cannot be accommodated by the R186 pocket of GDI1, and it enhances the interaction of Cdc42 R186C with the membrane, impairing the cytosol/membrane alternation.

Article 2 - The Golgi apparatus and cell polarity: Roles of the cytoskeleton, the Golgi matrix, and Golgi membranes

Available online at www.sciencedirect.com

ScienceDirect

Current Opinion in Cell Biology

The Golgi apparatus and cell polarity: Roles of the cytoskeleton, the Golgi matrix, and Golgi membranes

Yamini Ravichandran[1,2,3], Bruno Goud[1,2] and Jean-Baptiste Manneville[1,2]

Abstract

Membrane trafficking plays a crucial role in cell polarity by directing lipids and proteins to specific subcellular locations in the cell and sustaining a polarized state. The Golgi apparatus, the master organizer of membrane trafficking, can be subdivided into three layers that play different mechanical roles: a cytoskeletal layer, the so-called Golgi matrix, and the Golgi membranes. First, the outer regions of the Golgi apparatus interact with cytoskeletal elements, mainly actin and microtubules, which shape, position, and orient the organelle. Closer to the Golgi membranes, a matrix of long coiled–coiled proteins not only selectively captures transport intermediates but also participates in signaling events during polarization of membrane trafficking. Finally, the Golgi membranes themselves serve as active signaling platforms during cell polarity events. We review here the recent findings that link the Golgi apparatus to cell polarity, focusing on the roles of the cytoskeleton, the Golgi matrix, and the Golgi membranes.

Addresses

[1] Institut Curie, PSL Research University, CNRS, UMR 144, 26 rue d'Ulm F-75005, Paris, France

[2] Sorbonne Université, UPMC University Paris 06, CNRS, UMR 144, 26 rue d'Ulm F-75005, Paris, France

[3] Institut Pasteur, CNRS, UMR 3691, 25 rue du Docteur Roux F-75014, Paris, France

Corresponding author: Manneville, Jean-Baptiste (Jean-Baptiste.Manneville@curie.fr)

Current Opinion in Cell Biology 2020, **62**:104–113

This review comes from a themed issue on **Cell architecture**

Edited by **Sandrine Etienne-Manneville** and **Robert Arkowitz**

For a complete overview see the Issue and the Editorial

Available online 18 November 2019

https://doi.org/10.1016/j.ceb.2019.10.003

Keywords

Trafficking, Microtubules, Actin, Signaling, Golgin, Centrosome, Forces, Mechanics, Cell migration.

Introduction

The Golgi apparatus is the transformation and sorting factory of most proteins and plays a pivotal role in membrane trafficking. In the secretory pathway, the Golgi apparatus receives *de novo* synthesized molecules from the endoplasmic reticulum (ER), posttranslationally processes lipids and proteins, and sorts cargoes to their ultimate destination [1,2]. Cell polarity, the process by which a cell defines an oriented axis for instance to migrate, divide, or differentiate, strongly depends on membrane trafficking [3]. Over the past three decades, evidence has accumulated showing that the structure, organization, and positioning of the Golgi apparatus are implicated in maintaining a polarized cell state [2,4–6]. In polarized cells, cellular materials are transported along the polarity axis. This requires polarization of membrane trafficking from the Golgi apparatus. Conversely, the position of the Golgi inside the cell can dictate the directionality of membrane trafficking and the proper localization of polarity cues. This "chicken-and-egg" problem is typical of feedback loops involved in symmetry breaking during establishment of cell polarity. In the case of Golgi-dependent membrane trafficking, the orientation of the Golgi apparatus in the direction of the polarity axis targets transport toward a given region of the cell, for example, toward the leading edge plasma membrane during cell migration (front-rear polarity), in the apical process of neural stem cells (radial polarity), toward the apical compartment of epithelial cells, or toward the immunological synapse (Figure 1). In all these examples and despite intensive research, it is still not clear whether and how external polarity cues are transduced inside the cell to polarize transport from the Golgi apparatus and conversely whether and how the Golgi apparatus could be driving cell polarization. One historical example is given by the small G protein CDC42. CDC42 was identified as an evolutionary conserved polarity protein in several organisms, from yeast to humans [7]. In mammalian cells, beside its functions in cell protrusion formation and cell migration as a plasma membrane–associated protein, CDC42 also operates in intracellular vesicle trafficking [8,9]. Consistently, CDC42 not only localizes at the plasma membrane but also at the Golgi apparatus where it interacts with the Golgi matrix [8], coat proteins [10–12], microtubule motors, and the actin polymerization machinery [11]. However, the precise role of CDC42 at the Golgi apparatus, how the Golgi associated pool of CDC42 interacts with the

Figure 1

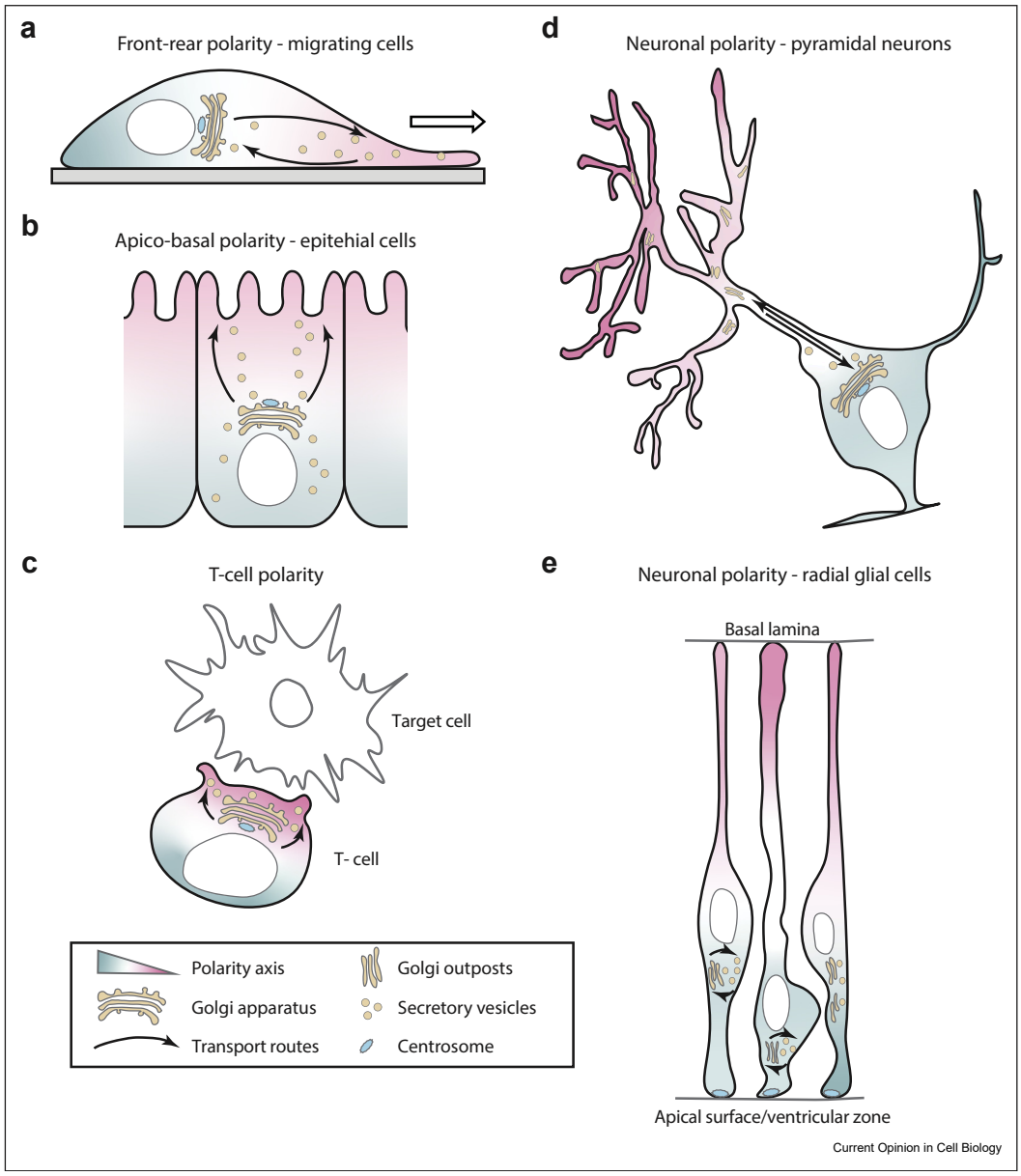

Positioning of the Golgi apparatus in different contexts of cell polarity, (**a**). In most (but not all) migrating cell types, the Golgi apparatus is positioned with the centrosome in front of the nucleus in the direction of migration. Leucocytes are a notable exception. (**b**). Epithelial cells exhibit basolateral polarity which relies on polarized membrane trafficking. In these cells, the Golgi apparatus is located between the nucleus and the apical surface. (**c**). During the formation of an immunological synapse between a T-cell and a target antigen-presenting cell, the T-cell polarizes, and its Golgi apparatus reorients toward the synapse to maintain polarized membrane trafficking toward establishing a target cell-T-cell contact. (**d**). Transport in the axon from the cell body to the growth cone is crucial to maintain the polarized organization of neuronal cells. In pyramidal neurons, the position of the Golgi apparatus in the cell body correlates with the position of the main axon. (**e**). Radial glial cells display a nonpericentrosomal Golgi positioning. The centrosome localizes close to the ventral side, while the Golgi apparatus is shifted toward the basal lamina close to the nucleus. Vesicular trafficking is mostly oriented perpendicular to the polarity axis in these cells.

plasma membrane—associated pool, and whether these interactions impact on cell polarity remain to be determined [8].

We focus here on the machineries localized at the Golgi apparatus which have been shown or hypothesized to participate in establishing directional membrane trafficking during cell polarization in mammalian cells. The Golgi apparatus can be viewed structurally as a three-layered organelle constituted of membrane-enclosed Golgi cisternae, the so-called Golgi matrix and cytoskeletal elements. Because of its organization in *cis*, *median*, and *trans* compartments, the Golgi apparatus possesses an intrinsic polarity. Intra-Golgi trafficking is in itself a polarized process, whether it is described in terms of a vesicular transport or a cisternal maturation model [13]. In mammalian cells, Golgi stacks are tethered laterally to form a Golgi ribbon typically found in tight association with the centrosome. Current models suggest that the assembly of the Golgi ribbon is an actin— and microtubule (MT)—dependent process. Maintenance of the Golgi architecture depends on the cytoskeleton and is coordinated at least in part by Rho and Rab GTPases [14,15]. In the following, we review recent work on the molecular players acting at the Golgi apparatus and relevant for the mechanical aspects of cell polarization, such as the generation of forces involved in Golgi positioning. For clarity, we have separated the description of the molecular mechanisms in three parts each corresponding to one structural component of the Golgi apparatus—the Golgi matrix, the Golgi-associated cytoskeleton, and Golgi membranes—even if these three components are linked and interact with one another.

Golgi matrix proteins and cell polarity

In mammalian cells, Golgi membranes are organized as an interconnected ribbon typically positioned adjacent to the centrosome in the perinuclear region. This proximity is usually disrupted by conditions that perturb Golgi organization. The functional significance of the proximity between the Golgi apparatus and the centrosome is not fully understood. Several studies have linked the spatial connection between the centrosome and the Golgi apparatus with directed protein transport or directional migration [16—18]. In front-rear cell polarity models, such as directed cell migration, centrosomal reorientation toward the leading edge is known to align the Golgi apparatus toward the leading edge (Figure 1**a**).

Strikingly a number of proteins belonging to the Golgi matrix [19,20] are not only critical for maintaining the typical Golgi architecture and its positioning close to the centrosome but also for cell polarity. For instance, Golgi reassembly and stack proteins (GRASPs) link Golgi stacks together. Depletion of GRASP55 or GRASP65 perturbs Golgi organization and function [21], and the phosphorylation of GRASP65 is required for both Golgi and centrosome reorientation during directed cell migration [22]. Depletion of GRASP65 and GRASP55 also reduces the level of α5β1 integrin and consequently decreases adhesion, migration, and invasion of HeLa cells and of the breast cancer cell line MDA-MB-231 [23•].

Similarly, the Golgi matrix protein GM130, a GRASP65 binding partner, has been implicated in cell polarity. GM130 recruits and activates the kinase YSK1 which phosphorylates downstream cell polarity targets [24]. Consistently, expressing inactive YSK1 blocks both Golgi and centrosome reorientation during cell migration [24]. In addition, GM130 may also control cell migration through the activation of both YSK1 and CDC42 [24—26]. More recently, deletion of GM130 in Purkinje neurons has been shown to induce Golgi fragmentation and defects in Golgi positioning [27••]. In contrast, a study carried out in GM130 knock out retinal pigment epithelial (RPE-1) cells shows that the physical proximity between the centrosome and the Golgi apparatus is not necessary for protein transport, cell migration, or ciliogenesis [28•]. While these results further strengthen the proposed role of GM130 in Golgi ribbon formation and in associating the Golgi apparatus to the centrosome by recruiting AKAP450 (A-kinase anchoring protein of 450 kDa, also known as AKAP350, AKAP9, or CG-NAP) [29], they question whether a connection between the Golgi apparatus and the centrosome is required for cell polarity during directed migration (Figure 1**a**) [16].

Golgi-associated cytoskeletal elements

The actin and microtubule network and their associated molecular motors play a key role in maintaining Golgi architecture and positioning during cell polarization by generating forces and mechanical tension [30—32]. In particular, the microtubule minus-end directed motor dynein has been shown both to anchor microtubule plus-ends at the plasma membrane and to concentrate at the Golgi apparatus. During directed cell migration activation of CDC42 at the leading edge plasma membrane recruits and anchors dynein at the cell cortex via the Par polarity complex [33,34]. Dynein in turn pulls on astral microtubules to reorient the centrosome toward the leading edge [33,35—37]. The Golgi apparatus probably reorients via the same mechanism through its mechanical link with the centrosome. Dynein is also found at the cis-Golgi, where it associates with the actin cytoskeleton and coat proteins [11]. Together with results showing the role of the CDC42/COPI interaction in directed intra-Golgi trafficking [10], these observations suggest that Golgi-localized dynein could also participate in redirecting membrane trafficking during establishment of cell polarity. In addition to this physical link

between the dynein motor and the Golgi apparatus, recent studies have mostly focused on the role of Golgi-nucleated microtubules and on actin-generated tension to link the Golgi apparatus with cell polarity.

The Golgi apparatus as a polarized noncentrosomal microtubule organizing center

The Golgi apparatus is a site that can nucleate and stabilize noncentrosomal microtubules [5,31,38,39]. Microtubule nucleating and/or stabilizing factors accumulate at Golgi membranes and act as molecular scaffolds. Golgi-derived microtubule arrays are polarized and can therefore induce cell asymmetry facilitating polarized transport of post-Golgi cargoes in a specific direction [16,40,41] during cell migration and differentiation [42–45]. Recently better characterization of the molecular machineries associated both at the plus and minus-ends of Golgi-derived microtubules involved in their nucleation, dynamics, stabilization, and regulation has led to a model clarifying the role of these microtubules in the polarization of membrane trafficking (Figure 2).

First, the identification of the *cis*-Golgi localized protein AKAP450 as a key player in Golgi-derived microtubule nucleation transformed the field of Golgi-derived microtubules [46,47]. AKAP450 recruits two γ-TuRC-binding homologous proteins namely CEP215 and myomegalin (MMG) which in turn recruit γ-TuRC (Figure 2**a**) [48–51]. Simultaneously several studies showed that recruitment of cytoplasmic linker-associated proteins (CLASPs) to the *trans*-Golgi by the golgin GCC185 was also essential for the nucleation and organization of Golgi-derived microtubules [52,53].

Figure 2

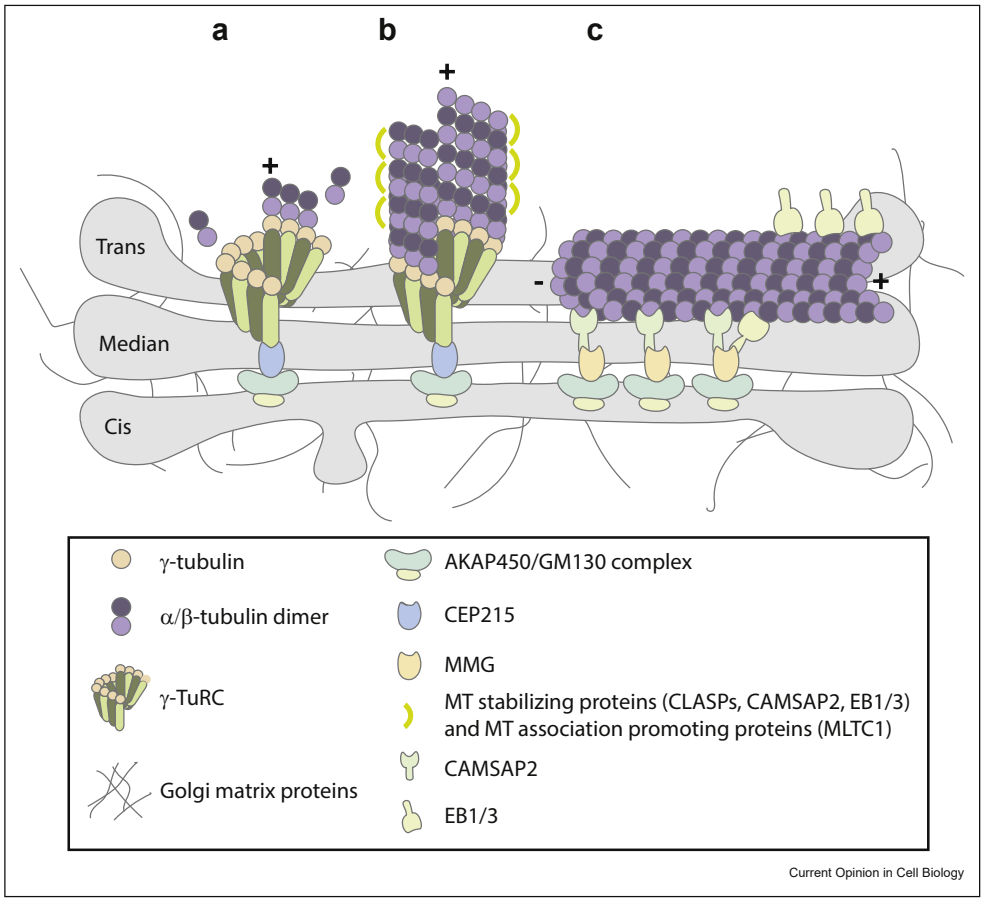

Golgi-associated microtubules, (**a**). The Golgi matrix protein GM130 bound to AKAP450 recruits the γ-TuRC binding proteins CEP215 and myomegalin (MMG). γ–TuRC subsequent binding to CEP215 and MMG induces microtubule nucleation at the surface of the Golgi apparatus. (**b**). The elongation of microtubules is associated with several microtubule-stabilizing proteins such as CLASPs. (**c**). CAMSAP2 and end-binding proteins EB1/3 tether microtubules to the Golgi apparatus therefore regulating Golgi positioning and reorientation during directed cell migration. MT, microtubule.

CLASPs are microtubule plus-end tracking proteins (+TIPs) that stabilize microtubules [54] (Figure 2**b**). Both AKAP450 and CLASPs associate with the microtubule lattice-binding protein MTCL1, which promotes microtubule association with the Golgi apparatus [55]. Therefore, the initial models of Golgi-derived microtubules involved tethering of microtubules regulatory proteins at both *cis*- and *trans*-Golgi compartments. How these differently localized groups of proteins could collaborate in the same pathway to generate polarized microtubule arrays was unclear, especially in the absence of microtubule stabilizing proteins essential for anchoring microtubule minus-ends to Golgi membranes.

Depletion of the calmodulin-regulated spectrin-associated protein CAMSAP2 in mammalian RPE-1 cells leads to the loss of most noncentrosomal microtubules [56], suggesting that CAMSAP2 participates in microtubule stabilization at Golgi membranes. Subsequently, CAMSAP2 was shown to be essential for tethering but not for nucleation of noncentrosomal microtubules at the Golgi apparatus [57••]. AKAP450 is thought to play a dual function by organizing Golgi microtubules at the *cis*-Golgi, initially by anchoring CAMSAP2-bound microtubule minus-ends and then by enhancing microtubule nucleation through γ-TURC recruitment (Figure 2**b** and **c**). Through their roles in organizing Golgi-anchored microtubules, AKAP450 and CAMSAP2 contribute to Golgi reorientation during cell polarization and migration. Interestingly, Golgi-anchored microtubules also appear to participate in Golgi fragmentation during Golgi reorientation, probably by exerting pulling forces on Golgi membranes [57••].

Similar mechanisms may be at play in other polarity models. For instance, noncentrosomal microtubules control cell polarity in endothelial cells migrating in 2D and 3D models and during vessel development in Zebrafish [58•]. Interestingly, another CAMSAP family member, CAMSAP3, has been involved in apico-basal polarity in epithelial cells (Figure 1**b**) [59]. Here CAMSAP3 tethers microtubule minus-ends to the apical cortex, resulting in pulling forces which may orient the microtubule array in the apico-basal direction and lead to the polarized intracellular organization and positioning organelles typical of epithelial cells.

Associated with CAMSAP2, the end binding proteins (EBs) EB1, EB2, and EB3, which form the core components of microtubule plus-end tracking protein (+TIPs) complexes, have been implicated in tethering microtubules to the Golgi apparatus, in Golgi morphology and reorientation during directed cell migration. The current model for EB-dependent polarized organization of microtubules at the Golgi apparatus involves the interaction between AKAP450 and MMG. MMG recruits EBs along microtubules to induce dispersion of Golgi stacks via plus-end tracking. MMG also recruits CAMSAP2 in an EB-dependent manner at microtubule minus-ends to favor Golgi compaction probably via dynein-mediated transport [60•] (Figure 2**c**).

Linking actin and the Golgi apparatus

The Golgi apparatus is a hub for a wide array of actin regulatory proteins. CDC42, WHAMM, WAVE, Arp2/3 complex, cortactin, cofilin, profilin II, and several myosins (II, VI, 18, 1b) localize at the Golgi apparatus and the *trans*-Golgi network [30]. In addition to the evident role of microtubules, the actin cytoskeleton is also emerging as a key factor in the assembly and maintenance of the Golgi architecture, in Golgi mechanics, and in Golgi-dependent membrane trafficking [30,61,62]. Golgi reorientation during cell migration depends on Rho-associated protein kinase, a main regulator of actomyosin contractility [63]. Aside from the Arp2/3 complex which generates branched actin networks, three actin nucleators belonging to the formin family have been linked to the Golgi apparatus, mDia1, INF2, and FMNL1 isoform γ [6,64]. In addition, recent work shows that the formin family members FMNL2 and 3, CDC42 effectors known to regulate cell edge protrusion during migration and invasion, localize, and function at the Golgi apparatus [65••]. Consistent with the role of CDC42 in regulating anterograde transport through the Golgi apparatus via cargo sorting and carrier formation [10], FMNL2/3 depletion also affects anterograde trafficking from the Golgi apparatus to the plasma membrane [65••]. Such a link between FMNL2/3 and the actin-dependent functions of CDC42 could be of particular importance during polarization of membrane trafficking (Figure 3**a**).

Deciphering the link between actin-driven migration and Golgi apparatus reorientation is key to understanding how both processes are coupled in space and time during cell polarization. Golgi phosphoprotein 3 (GOLPH3) is one such pivotal link required for Golgi to plasma membrane trafficking that bridges the Golgi apparatus to the actin cytoskeleton [66–69]. GOLPH3 is known to bind to phosphatidylinositol-4-phosphate (PtdIns(4)P), a lipid enriched in *trans*-Golgi membranes. Most importantly, GOLPH3 binds the unconventional myosin, myosin 18A (MYO18A), which links the Golgi apparatus to F-actin. The GOLPH3/MYO18A/F-actin pathway is thought to exert a tensile force on Golgi cisternae and to participate in Golgi reorientation during cell polarization [70•–72] (Figure 3**b**). However the role of GOLPH3 as one of the main Golgi-associated actor driving polarization of membrane trafficking has been recently questioned by the finding that MYO18A does not display any motor activity [73••].

Figure 3

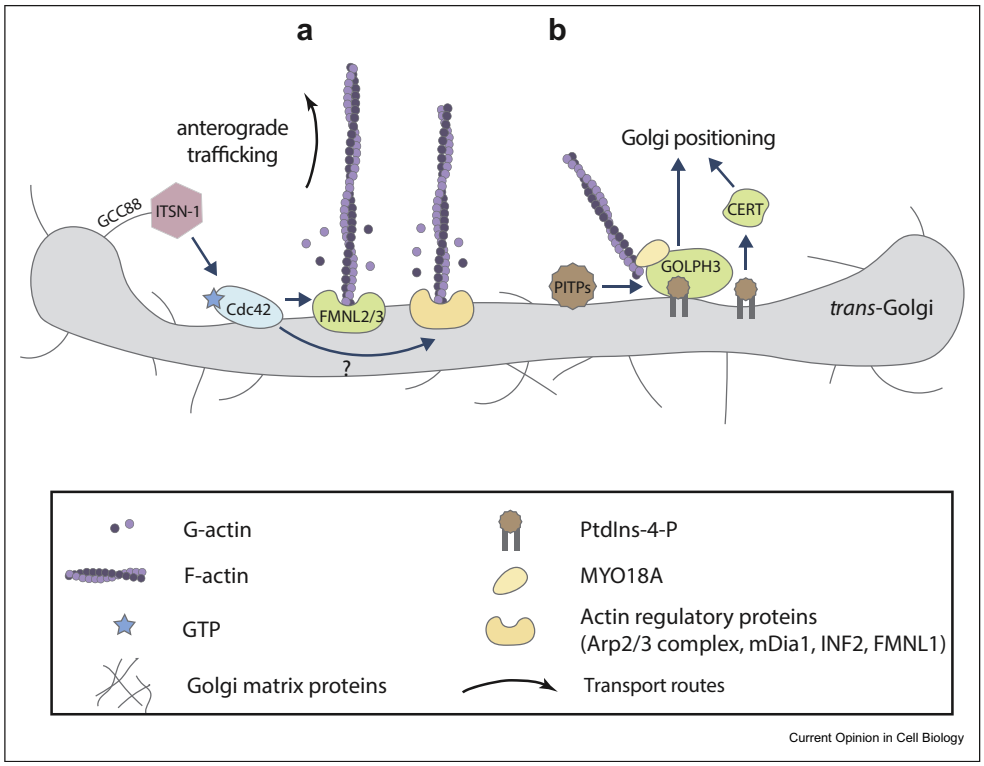

Golgi-associated actin, (**a**). A number of actin regulators have been identified to localize at the Golgi apparatus. Among them, the formin family members FMLNL2/3 are regulated by CDC42, nucleate actin polymerization at the surface of the Golgi apparatus, and participate in cell polarity. (**b**). A main pathway involving Golgi-associated actin in Golgi architecture and in the polarization of membrane trafficking is the GOLPH3/MYO18A/F-actin pathway. Phosphatidylinositol-4-phosphate (PtdIns(4)P) and upstream lipid transfer proteins (PITPs and CERT) regulate this pathway. PITPs, phosphatidylinositol transfer proteins.

Interactions between actin and Golgi-derived microtubules

The actin and microtubule cytoskeletons interactions occur at several subcellular locations, for instance at focal adhesions at the plasma membrane (see Refs. [74,75] for a recent review) or at the nuclear envelope [76]. Not surprisingly, these interactions are also observed at the Golgi apparatus. A distinct connection between Golgi membranes, actin filaments, and Golgi-derived microtubules has been recently proposed. The formin protein FHDC1/IFN1 is thought to coordinate actin and microtubule dynamics during Golgi ribbon formation and to establish intrinsic Golgi polarity [77•].

Golgi membranes

Golgi membranes are located at the crossroads between the anterograde secretory route and the retrograde route. Golgi lipids and membrane proteins are thus ideally situated to be involved in a large number of signaling pathways, among which is signaling involved in cell polarity. Polarity proteins such as CDC42 localize at the Golgi apparatus, although their function there is still not clear. Other Golgi-localized GTPases have been recently shown to mediate trafficking events potentially involved in cell polarization, such as Arf1 in response to cell–matrix adhesion cues [78], Arl5 during amino acids-stimulated retrograde trafficking [79], or Rab6 in targeting secretion to focal adhesions [80]. We focus below on the less studied role of Golgi lipids and lipid metabolism in polarization processes.

Golgi lipids: new roles for PtdIns(4)P

PtdIns(4)P initiates the recruitment of the GOLPH3/MYO18A/F-actin machinery at Golgi membranes to shape the Golgi ribbon during cell polarization. Recently, two studies point to new roles for PtdIns(4)P and GOLPH3 in membrane trafficking and cell polarity. First, elegant *in vitro* experiments with liposomes and purified proteins confirm that PtdIns(4)P is required for GOLPH3 binding to membranes and demonstrate that GOLPH3 binding to PtdIns(4)P-containing membranes induces membrane curvature and tubulation in a PtdIns(4)P-dependent manner [81•]. Second, a developmental biology study has demonstrated a new role for

PtdIns(4)P during neurogenesis [82••]. A lipid signaling pathway involving phosphatidylinositol transfer proteins, PtdIns(4)P, GOLPH3, and ceramide transfer protein (CERT) at the Golgi apparatus appears to regulate apically directed membrane trafficking in neural stem cells during neocortex development in mice. CERT also plays an important role in Golgi positioning in these cells via a PtdIns(4)P-dependent mechanism [82••] (Figure 3**b**).

Lipid metabolism and mechanosensitivity

Cell polarity is often triggered by mechanical cues induced by cell–cell or cell–matrix adhesion. Such mechanical cues have recently been shown to impact on the organization and mechanical properties of the Golgi apparatus [78,]. Mechanotransduction events at the Golgi apparatus may influence cell polarity. For instance, contractile forces induced by adhesion to the extracellular matrix were shown to modulate lipid metabolism through a pathway involving the sterol regulatory element binding protein (SREBP), a regulator of lipogenesis, and the lipin-1 phosphatidate phosphatase that converts phosphatidic acid to diacylglycerol (DAG) [83•]. Since the rigidity of the Golgi apparatus also correlates with the level of actomyosin contractility [61,]], the physical properties of the Golgi apparatus may regulate the binding, and/or activity of some of the components of this metabolic pathway. For instance, the level of DAG could influence membrane curvature [84] and in turn the binding of Arf1 or the activity of lipin-1. Although not demonstrated yet, mechanosensitive pathways such as the lipin-1/DAG/Arf1/SREBP pathway may be involved in polarity events activated by cell–matrix adhesion cues.

Concluding remarks and open questions

The Golgi apparatus plays a pivotal role in polarized cell functions. For instance, Golgi positioning and orientation control polarized membrane transport during cell migration or T-cell immunological synapse formation (Figure 1**a,c**). We have described here the main molecular pathways controlling Golgi-driven polarity, according to which element of the Golgi is involved, Golgi-associated cytoskeleton and motors, the Golgi matrix, or Golgi membranes. As these pathways are likely to interact, understanding how the actors identified so far work in concert and mechanically couple the different constituents of the Golgi apparatus is the main challenge for the coming years. Accordingly, a physical link between the Golgi matrix and the actin cytoskeleton implicating the golgin GCC88 and the CDC42 guanine exchange factor ITSN-1 has recently been identified [85•] (Figure 3**a**). Interesting novel targets could also emerge. For instance, as part of the cytoskeleton, spectrins [86], septins [87,88••], and intermediate filaments [89] may fill some missing links in current models. While they are known to interact with the Golgi apparatus and participate in Golgi organization and membrane trafficking [86,89], it is not known whether their interaction with the Golgi apparatus is directly involved in cell polarity. Technical developments such as optogenetics, FRET-based probes, or laser ablation should be instrumental to better decipher how forces are generated at the Golgi apparatus during cell polarization. It is also tempting to speculate that mechanosensitive properties of the Golgi apparatus are key during establishment of cell polarity.

Finally, because cell polarity is deregulated in cancer, not surprisingly several polarity regulators associated with the Golgi apparatus have been implicated in cancer and invasion. The epithelial-to-mesenchymal transition was recently shown to increase rearward positioning of the Golgi apparatus at the back of the nucleus in migrating breast cancer cells [90]. However, the increased migration of the cells correlates more with a stable positioning of the Golgi apparatus than with its position at the back or at the front of the nucleus [90]. GOLPH3 has been identified as an oncogene [67,91]. By driving Golgi reorientation and polarized trafficking, GOLPH3 enhances cell migration and cellular transformation [70]. Another protein implicated in cancer progression is intraflagellar transport 20, which affects the nucleation of Golgi-derived microtubules and promotes intra-Golgi transport to induce invadopodia and tumor invasion [92]. On the contrary, perturbing Golgi-derived microtubules by depleting CAMSAP2-AKAP450 in highly invasive fibrosarcoma cells diminishes their ability to migrate [57••]. These findings point to polarity pathways associated with the Golgi apparatus as potential targets in cancer therapy.

Conflict of interest statement

Nothing declared.

Acknowledgements

Y.Ravichandran is funded by the Polarnet ITN (Innovative Training Network) part of the European Commission and the Fondation pour la Recherche Médicale. The authors apologize to colleagues whose work they could not cite due to space limitations. The authors declare no conflict of interest.

References

Papers of particular interest, published within the period of review, have been highlighted as:

- • of special interest
- •• of outstanding interest

1. Boncompain G, Weigel AV: **Transport and sorting in the Golgi complex: multiple mechanisms sort diverse cargo**. *Curr Opin Cell Biol* 2018, **50**:94–101.
2. Guo Y, Sirkis DW, Schekman R: **Protein sorting at the trans -golgi network**. *Annu Rev Cell Dev Biol* 2014, **30**:169–206.
3. Bryant DM, Yap AS: **Editorial overview: membrane traffic and cell polarity**. *Traffic* 2016, **17**:1231–1232.
4. Yadav S, Linstedt AD: **Golgi positioning**. *Cold Spring Harb Perspect Biol* 2011, **3**. a005322–a005322.

5. Zhu X, Kaverina I: **Golgi as an MTOC: making microtubules for its own good**. *Histochem Cell Biol* 2013, **140**:361–367.

6. Gurel PS, Hatch AL, Higgs HN: **Connecting the cytoskeleton to the endoplasmic reticulum and Golgi**. *Curr Biol* 2014, **24**: R660–R672.

7. Etienne-Manneville S: **Cdc42 – the centre of polarity**. *J Cell Sci* 2004, **117**:1291–1300.

8. Farhan H, Hsu VW: **Cdc42 and cellular polarity: emerging roles at the golgi**. *Trends Cell Biol* 2016, **26**:241–248.

9. Osmani N, Vitale N, Borg JP, Etienne-Manneville S: **Scrib controls Cdc42 localization and activity to promote cell polarization during astrocyte migration**. *Curr Biol* 2006, **16**: 2395–2405.

10. Park SY, Yang JS, Schmider AB, Soberman RJ, Hsu VW: **Coordinated regulation of bidirectional COPI transport at the Golgi by CDC42**. *Nature* 2015, **521**:529–532.

11. Chen JL, Fucini RV, Lacomis L, Erdjument-Bromage H, Tempst P, Stamnes M: **Coatomer-bound Cdc42 regulates dynein recruitment to COPI vesicles**. *J Cell Biol* 2005, **169**: 383–389.

12. Wu WJ, Erickson JW, Lin R, Cerione RA: **The γ-subunit of the coatomer complex binds Cdc42 to mediate transformation**. *Nature* 2000, **405**:800–804.

13. Glick BS, Luini A: **Models for Golgi traffic: a critical assessment**. *Cold Spring Harb Perspect Biol* 2011, **3**.

14. Goud B, Liu S, Storrie B: **Rab proteins as major determinants of the Golgi complex structure**. *Small GTPases* 2018, **9**:66–75.

15. Phuyal S, Farhan H: **Multifaceted Rho GTPase signaling at the endomembranes**. *Front Cell Dev Biol* 2019, **7**:127.

16. Hurtado L, Caballero C, Gavilan MP, Cardenas J, Bornens M, Rios RM: **Disconnecting the Golgi ribbon from the centrosome prevents directional cell migration and ciliogenesis**. *J Cell Biol* 2011, **193**:917–933.

17. Wu J, Akhmanova A: **Microtubule-organizing centers**. *Annu Rev Cell Dev Biol* 2017, **33**:51–75.

18. Yadav S, Puri S, Linstedt AD: **A primary role for golgi positioning in directed secretion, cell polarity, and wound healing**. *Mol Biol Cell* 2009, **20**:1728–1736.

19. Barinaga-Rementeria Ramirez I, Lowe M: **Golgins and GRASPs: holding the golgi together**. *Semin Cell Dev Biol* 2009, **20**: 770–779.

20. Gillingham AK, Munro S: **Finding the golgi: golgin coiled-coil proteins show the way**. *Trends Cell Biol* 2016, **26**:399–408.

21. Zhang X, Wang Y: **GRASPs in Golgi structure and function**. *Front Cell Dev Biol* 2016, **3**:84.

22. Bisel B, Wang Y, Wei JH, Xiang Y, Tang D, Miron-Mendoza M, Yoshimura SI, Nakamura N, Seemann J: **ERK regulates Golgi and centrosome orientation towards the leading edge through GRASP65**. *J Cell Biol* 2008, **182**:837–843.

23. • Ahat E, Xiang Y, Zhang X, Bekier ME, Wang Y: **GRASP depletion–mediated Golgi destruction decreases cell adhesion and migration via the reduction of α5β1 integrin**. *Mol Biol Cell* 2019, **30**:766–777.

In this paper, depletion of GRASP65 and GRASP 55, which disrupts Golgi morphology and function, is shown to reduce the level of α5β1 integrin and consequently to decrease cell adhesion, cell migration and invasion in HeLa cells and in the breast cancer cell line MDA-MB-231.

24. Preisinger C, Short B, De Corte V, Bruyneel E, Haas A, Kopajtich R, Gettemans J, Barr FA: **YSK1 is activated by the Golgi matrix protein GM130 and plays a role in cell migration through its substrate 14-3-3ζ**. *J Cell Biol* 2004, **164**:1009–1020.

25. Kodani A, Sütterlin C: **A new function for an old organelle: microtubule nucleation at the Golgi apparatus**. *EMBO J* 2009, **28**:995–996.

26. Baschieri F, Confalonieri S, Bertalot G, Di Fiore PP, Dietmaier W, Leist M, Crespo P, MacAra IG, Farhan H: **Spatial control of Cdc42 signalling by a GM130-RasGRF complex regulates polarity and tumorigenesis**. *Nat Commun* 2014, **5**.

27. •• Liu C, Mei M, Li Q, Roboti P, Pang Q, Ying Z, Gao F, Lowe M, Bao S: **Loss of the golgin GM130 causes Golgi disruption, Purkinje neuron loss, and ataxia in mice**. *Proc Natl Acad Sci U S A* 2017, **114**:346–351.

This study shows that loss of GM130 in Purkinje neurons induces loss from the Golgi apparatus of GRASP65 and of AKAP450, a large Golgi and centrosomal protein which links the Golgi apparatus to the centrosome. GM130, although not involved in the initial polarization of Golgi trafficking, plays a central role in maintaining the polarized distribution of the Golgi apparatus in these cells by linking the Golgi apparatus to the centrosome.

28. • Tormanen K, Ton C, Waring BM, Wang K, Sütterlin C: **Function of Golgi-centrosome proximity in RPE-1 cells**. *PLoS One* 2019, **14**.

The authors use stable retinal pigment epithelial (RPE-1) cell lines in which GM130 is knocked out by CRISPR/Cas9 to show that the physical proximity between the centrosome and the Golgi apparatus is not necessary for protein transport, cell migration, or ciliogenesis.

29. Rivero S, Cardenas J, Bornens M, Rios RM: **Microtubule nucleation at the cis-side of the golgi apparatus requires AKAP450 and GM130**. *EMBO J* 2009, **28**:1016–1028.

30. Egea G, Serra-Peinado C, Salcedo-Sicilia L, Gutiérrez-Martínez E: **Actin acting at the golgi**. *Histochem Cell Biol* 2013, **140**:347–360.

31. Sanders AAWM, Kaverina I: **Nucleation and dynamics of Golgi-derived microtubules**. *Front Neurosci* 2015, **9**:431.

32. Allan VJ, Thompson HM, McNiven MA: **Motoring around the golgi**. *Nat Cell Biol* 2002, **4**:E236–E242.

33. Etienne-Manneville S, Hall A: **Integrin-mediated activation of Cdc42 controls cell polarity in migrating astrocytes through PKCζ**. *Cell* 2001, **106**:489–498.

34. Etienne-Manneville S, Hall A: **Cell polarity: Par6, aPKC and cytoskeletal crosstalk**. *Curr Opin Cell Biol* 2003, **15**:67–72.

35. Palazzo AF, Joseph HL, Chen YJ, Dujardin DL, Alberts AS, Pfister KK, Vallee RB, Gundersen GG: **Cdc42, dynein, and dynactin regulate MTOC reorientation independent of Rho-regulated microtubule stabilization**. *Curr Biol* 2001, **11**: 1536–1541.

36. Manneville JB, Jehanno M, Etienne-Manneville S: **Dlg1 binds GKAP to control dynein association with microtubules, centrosome positioning, and cell polarity**. *J Cell Biol* 2010, **191**:585–598.

37. Manneville J-B, Etienne-Manneville S: **Positioning centrosomes and spindle poles: looking at the periphery to find the centre**. *Biol Cell* 2006, **98**:557–565.

38. Chabin-Brion K, Marceiller J, Perez F, Settegrana C, Drechou A, Durand G, Poüs C: **The Golgi complex is a microtubule-organizing organelle**. *Mol Biol Cell* 2001, **12**:2047–2060.

39. Rios RM: **The centrosome – golgi apparatus nexus**. *Philos Trans R Soc B Biol Sci* 2014, **369**.

40. Vinogradova T, Paul R, Grimaldi AD, Loncarek J, Miller PM, Yampolsky D, Magidson V, Khodjakov A, Mogilner A, Kaverina I: **Concerted effort of centrosomal and golgiderived microtubules is required for proper golgi complex assembly but not for maintenance**. *Mol Biol Cell* 2012, **23**:820–833.

41. Vinogradova T, Miller PM, Kaverina I: **Microtubule network asymmetry in motile cells: role of Golgi-derived array**. *Cell Cycle* 2009, **8**:2168–2174.

42. Ori-McKenney KM, Jan LY, Jan YN: **Golgi outposts shape dendrite morphology by functioning as sites of acentrosomal microtubule nucleation in neurons**. *Neuron* 2012, **76**:921–930.

43. Oddoux S, Zaal KJ, Tate V, Kenea A, Nandkeolyar SA, Reid E, Liu W, Ralston E: **Microtubules that form the stationary lattice of muscle fibers are dynamic and nucleated at golgi elements**. *J Cell Biol* 2013, **203**:205–213.

44. Yalgin C, Ebrahimi S, Delandre C, Yoong LF, Akimoto S, Tran H, Amikura R, Spokony R, Torben-Nielsen B, White KP, *et al.*:

Centrosomin represses dendrite branching by orienting microtubule nucleation. *Nat Neurosci* 2015, **18**:1437–1445.

45. Zhu X, Hu R, Brissova M, Stein RW, Powers AC, Gu G, Kaverina I: **Microtubules negatively regulate insulin secretion in pancreatic β cells**. *Dev Cell* 2015, **34**:656–668.

46. Schmidt PH, Dransfield DT, Claudio JO, Hawley RG, Trotter KW, Milgram SL, Goldenring JR: **AKAP350, a multiply spliced protein kinase A-anchoring protein associated with centrosomes**. *J Biol Chem* 1999, **274**:3055–3066.

47. Takahashi M, Shibata H, Shimakawa M, Miyamoto M, Mukai H, Ono Y: **Characterization of a novel giant scaffolding protein, CG-NAP, that anchors multiple signaling enzymes to centrosome and the golgi apparatus**. *J Biol Chem* 1999, **274**:17267–17274.

48. Choi YK, Liu P, Sze SK, Dai C, Qi RZ: **CDK5RAP2 stimulates microtubule nucleation by the γ-tubulin ring complex**. *J Cell Biol* 2010, **191**:1089–1095.

49. Roubin R, Acquaviva C, Chevrier V, Sedjaï F, Zyss D, Birnbaum D, Rosnet O: **Myomegalin is necessary for the formation of centrosomal and Golgi-derived microtubules**. *Biol Open* 2013, **2**:238–250.

50. Wang Z, Wu T, Shi L, Zhang L, Zheng W, Qu JY, Niu R, Qi RZ: **Conserved motif of CDK5RAP2 mediates its localization to centrosomes and the Golgi complex**. *J Biol Chem* 2010, **285**:22658–22665.

51. Wang Z, Zhang C, Qi RZ: **A newly identified myomegalin isoform functions in Golgi microtubule organization and ER-Golgi transport**. *J Cell Sci* 2014, **127**:4904–4917.

52. Miller PM, Folkmann AW, Maia ARR, Efimova N, Efimov A, Kaverina I: **Golgi-derived CLASP-dependent microtubules control Golgi organization and polarized trafficking in motile cells**. *Nat Cell Biol* 2009, **11**:1069–1080.

53. Efimov A, Kharitonov A, Efimova N, Loncarek J, Miller PM, Andreyeva N, Gleeson P, Galjart N, Maia ARR, McLeod IX, *et al.*: **Asymmetric CLASP-dependent nucleation of noncentrosomal microtubules at the trans-golgi network**. *Dev Cell* 2007, **12**:917–930.

54. Mimori-Kiyosue Y, Grigoriev I, Lansbergen G, Sasaki H, Matsui C, Severin F, Galjart N, Grosveld F, Vorobjev I, Tsukita S, *et al.*: **CLASP1 and CLASP2 bind to EB1 and regulate microtubule plus-end dynamics at the cell cortex**. *J Cell Biol* 2005, **168**:141–153.

55. Sato Y, Hayashi K, Amano Y, Takahashi M, Yonemura S, Hayashi I, Hirose H, Ohno S, Suzuki A: **MTCL1 crosslinks and stabilizes non-centrosomal microtubules on the Golgi membrane**. *Nat Commun* 2014, **5**.

56. Jiang K, Hua S, Mohan R, Grigoriev I, Yau KW, Liu Q, Katrukha EA, Altelaar AFM, Heck AJR, Hoogenraad CC, *et al.*: **Microtubule minus-end stabilization by polymerization-driven CAMSAP deposition**. *Dev Cell* 2014, **28**:295–309.

57. •• Wu J, de Heus C, Liu Q, Bouchet BP, Noordstra I, Jiang K, Hua S, Martin M, Yang C, Grigoriev I, *et al.*: **Molecular pathway of microtubule organization at the golgi apparatus**. *Dev Cell* 2016, **39**:44–60.

This study demonstrates how CAMSAP2 organizes the microtubule network at the Golgi apparatus with the help of AKAP450 and myomegalin (MMG). In CAMSAP2 KO RPE-1 cells the localization of CAMSAP2-decorated microtubule stretches at the Golgi apparatus, depends on the AKAP450/MMG complex, ruling out a CLASPs-dependent interaction. The authors use AKAP450, MMG or CAMSAP2 KO cell lines and depletion of centrioles. In cells lacking centrosomes, enhanced interaction of γ-tubulin and microtubules with the Golgi apparatus is driven by AKAP450 and MMG. Cells lacking centrosomes and AKAP450 exhibit intact Golgi stacks and increased number of vesicles surrounding the Golgi apparatus, suggesting that vesicular trafficking, or at least the formation of transport intermediates, requires the presence of abundant Golgi-derived microtubules.

58. • Martin M, Veloso A, Wu J, Katrukha EA, Akhmanova A: **Control of endothelial cell polarity and sprouting angiogenesis by non-centrosomal microtubules**. *Elife* 2018, **7**.

Knockdown experiments in human umbilical vein endothelial cells (HUVECs) show that CAMSAP2 is required for stabilizing a single protrusion for Golgi reorientation and membrane trafficking, which are essential for directed cell migration in 2D and polarization in 3D.

59. Toya M, Kobayashi S, Kawasaki M, Shioi G, Kaneko M, Ishiuchi T, Misaki K, Meng W, Takeichi M: **CAMSAP3 orients the apical-to-basal polarity of microtubule arrays in epithelial cells**. *Proc Natl Acad Sci U S A* 2016, **113**:332–337.

60. • Yang C, Wu J, de Heus C, Grigoriev I, Liv N, Yao Y, Smal I, Meijering E, Klumperman J, Qi RZ, *et al.*: **EB1 and EB3 regulate microtubule minus end organization and Golgi morphology**. *J Cell Biol* 2017, **216**:3179–3198.

The authors show that disruption of end-binding (EB) proteins EB1 and EB3 results in defects in Golgi reorientation during cell migration affecting cell polarity. Depleting EBs induces a decrease in the length of CAMSAP2-decorated stretches along Golgi-anchored microtubules minus-ends, a detachment of Golgi-anchored microtubules from Golgi membranes and Golgi compaction. An EB1/EB3– myomegalin complex tethers microtubules and Golgi membranes and promotes the dispersion of Golgi stacks.

61. Guet D, Mandal K, Pinot M, Hoffmann J, Abidine Y, Sigaut W, Bardin S, Schauer K, Goud B, Manneville JB: **Mechanical role of actin dynamics in the rheology of the Golgi complex and in Golgi-associated trafficking events**. *Curr Biol* 2014, **24**:1700–1711.

62. Lázaro-Diéguez F, Jiménez N, Barth H, Koster AJ, Renau-Piqueras J, Llopis JL, Burger KNJ, Egea G: **Actin filaments are involved in the maintenance of Golgi cisternae morphology and intra-Golgi pH**. *Cell Motil Cytoskelet* 2006, **63**:778–791.

63. Brasch ME, Passucci G, Gulvady AC, Turner CE, Lisa Manning M, Henderson JH: **Nuclear position relative to the Golgi body and nuclear orientation are differentially responsive indicators of cell polarized motility**. *PLoS One* 2019, **14**, e0211408.

64. Zilberman Y, Alieva NO, Miserey-Lenkei S, Lichtenstein A, Kam Z, Sabanay H, Bershadsky A: **Involvement of the Rho-mDia1 pathway in the regulation of Golgi complex architecture and dynamics**. *Mol Biol Cell* 2011, **22**:2900–2911.

65. •• Kage F, Steffen A, Ellinger A, Ranftler C, Gehre C, Brakebusch C, Pavelka M, Stradal T, Rottner K: **FMNL2 and -3 regulate Golgi architecture and anterograde transport downstream of Cdc42**. *Sci Rep* 2017, **7**.

This study demonstrates that perturbing FMNL2/3 formins by siRNA or CRISPR/Cas9-mediated gene deletion induces Golgi fragmentation, enlargement of endosomes as well as defective maturation and/or sorting into late endosomes and lysosomes. The trans-medial Golgi localization of these proteins requires their interaction with Cdc42 and their N-terminal myristoylation, in contrast to their localization in lamellipodia.

66. Farber-Katz SE, Dippold HC, Buschman MD, Peterman MC, Xing M, Noakes CJ, Tat J, Ng MM, Rahajeng J, Cowan DM, *et al.*: **DNA damage triggers golgi dispersal via DNA-PK and GOLPH3**. *Cell* 2014, **156**:413–427.

67. Buschman MD, Rahajeng J, Field SJ: **GOLPH3 links the Golgi, DNA damage, and cancer**. *Cancer Res* 2015, **75**:624–627.

68. Taft MH, Behrmann E, Munske-Weidemann LC, Thiel C, Raunser S, Manstein DJ: **Functional characterization of human myosin-18A and its interaction with F-actin and GOLPH3**. *J Biol Chem* 2013, **288**:30029–30041.

69. Ng MM, Dippold HC, Buschman MD, Noakes CJ, Field SJ: **GOLPH3L antagonizes GOLPH3 to determine Golgi morphology**. *Mol Biol Cell* 2013, **24**:796–808.

70. • Xing M, Peterman MC, Davis RL, Oegema K, Shiau AK, Field SJ: **GOLPH3 drives cell migration by promoting Golgi reorientation and directional trafficking to the leading edge**. *Mol Biol Cell* 2016, **27**:3828–3840.

By overexpressing GOLPH3 in MDA-MB-231 human breast cancer cells, the authors show that GOLPH3 favours directed migration in a wound healing assay by promoting Golgi reorientation and membrane trafficking towards the wound edge through the GOLPH3/MYO18A/actin pathway.

71. Bishé B, Syed GH, Field SJ, Siddiqui A: **Role of phosphatidylinositol 4-phosphate (PI4P) and its binding protein GOLPH3 in hepatitis C virus secretion**. *J Biol Chem* 2012, **287**:27637–27647.

72. Makowski SL, Tran TT, Field SJ: **Emerging themes of regulation at the Golgi**. *Curr Opin Cell Biol* 2017, **45**:17–23.

73. •• Bruun K, Beach JR, Heissler SM, Remmert K, Sellers JR, Hammer JA: **Re-evaluating the roles of myosin 18Aα and F-actin in determining Golgi morphology**. *Cytoskeleton* 2017, **74**: 205–218.
The authors show that the unconventional myosin motor myosin 18A (MYO18A) has no motor activity in the presence of GOLPH3, questioning the GOLPH3/MYO18A/actin model according to which actin-MYO18A contractility stretches the Golgi ribbon. Moreover, MYO18A does not appear to localize on the Golgi apparatus or to impact on Golgi morphology. Disrupting actin induces Golgi lateral compaction and vertical extension which is paralleled by similar morphological changes of the whole cell, suggesting that actin acts indirecly on Golgi morphology.

74. LaFlamme SE, Mathew-Steiner S, Singh N, Colello-Borges D, Nieves B: **Integrin and microtubule crosstalk in the regulation of cellular processes**. *Cell Mol Life Sci* 2018, **75**:4177–4185.

75. Seetharaman S, Etienne-Manneville S: **Microtubules at focal adhesions – a double-edged sword**. *J Cell Sci* 2019, **132**. in press.

76. Mahamid J, Pfeffer S, Schaffer M, Villa E, Danev R, Cuellar LK, Förster F, Hyman AA, Plitzko JM, Baumeister W: **Visualizing the molecular sociology at the HeLa cell nuclear periphery**. *Science* 2016, **351**:969–972.

77. • Copeland SJ, Thurston SF, Copeland JW: **Actin- and microtubule-dependent regulation of Golgi morphology by FHDC1**. *Mol Biol Cell* 2016, **27**:260–276.
Knockdown of the formin protein FHDC1/IFN1 is shown to perturb Golgi assembly in fibroblasts, a phenotype consistent with defects in Golgi-derived microtubules. Conversely, overexpression of FHDC1 induces the dispersion of the Golgi apparatus into functional ministacks. The authors explain these observations by a collaborative effect between the interaction of the microtubule-binding domain of FHDC1 with Golgi-derived microtubules and the interaction between its FH2 domain with the actin cytoskeleton.

78. Singh V, Erady C, Balasubramanian N: **Cell-matrix adhesion controls Golgi organization and function through Arf1 activation in anchorage-dependent cells**. *J Cell Sci* 2018, **131**: jcs215855.

79. Shi M, Chen B, Mahajan D, Boh BK, Zhou Y, Dutta B, Tie HC, Sze SK, Wu G, Lu L: **Amino acids stimulate the endosome-to-Golgi trafficking through Ragulator and small GTPase Arl5**. *Nat Commun* 2018, **9**.

80. Fourriere L, Kasri A, Gareil N, Bardin S, Bousquet H, Pereira D, Perez F, Goud B, Boncompain G, Miserey-Lenkei S: **RAB6 and microtubules restrict protein secretion to focal adhesions**. *J Cell Biol* 2019, **218**:2215–2231.

81. • Rahajeng J, Kuna RS, Makowski SL, Tran TTT, Buschman MD, Li S, Cheng N, Ng MM, Field SJ: **Efficient golgi forward trafficking requires GOLPH3-driven, PI4P-dependent membrane curvature**. *Dev Cell* 2019, https://doi.org/10.1016/j.devcel.2019.05.038.
Following their previous work on GOLPH3, the authors identify PtdIns(4)P as a critical Golgi lipid for anterograde trafficking from the Golgi apparatus to the plasma membrane by allowing GOLPH3 binding to Golgi membranes and subsequent membrane deformation. *In vitro* reconstitution experiments demonstrate that PtdIns(4)P is required for membrane curvature induced by GOLPH3.

82. •• Xie Z, Hur SK, Zhao L, Abrams CS, Bankaitis VA: **A golgi lipid signaling pathway controls apical golgi distribution and cell polarity during neurogenesis**. *Dev Cell* 2018, **44**:725–740.e4.
The authors show that a duo of Phosphatidylinositol transfer proteins (PITPs), PITPNA and PITPNB, drives the PtdIns(4)P-dependent recruitment of GOLPH3 in a redundant manner and also possibly recruits ceramide transfer protein (CERT) to Golgi membranes. The PITP/PtdIns(4)P/GOLPH3/CERT lipid signaling pathway appears to regulate apically directed membrane trafficking rather than bulk membrane trafficking in neural stem cells during neocortex development in mice. Interestingly CERT also plays an important role in Golgi positioning in these cells via a PtdIns(4)P-dependent mechanism. Downregulating CERT by shRNA perturbs both Golgi positioning and radial alignment phenocopying PITPNA/PITPNB or GOLPH3 deficiency phenotypes. However CERT does not operate via the GOLPH3/actin pathway and the downstream effectors of CERT associated with Golgi reorientation and/or polarity proteins remain to be identified.

83. • Romani P, Brian I, Santinon G, Pocaterra A, Audano M, Pedretti S, Mathieu S, Forcato M, Bicciato S, Manneville JB, *et al.*: **Extracellular matrix mechanical cues regulate lipid metabolism through Lipin-1 and SREBP**. *Nat Cell Biol* 2019, **21**: 338–347.
The authors identify a pathway involving the sterol regulatory element binding protein (SREBP), a regulator of lipogenesis, and the Lipin-1 phosphatidate phosphatase that converts phosphatidic acid (PA) to diacylglycerol (DAG) as a key mechanosensitive pathway linking extracellular physical constraints to the Golgi apparatus. High acto-myosin contractility increases Lipin-1 activity and consequently DAG and Arf1 levels on Golgi membranes, preventing SREBP from shuttling from the ER to Golgi apparatus. Interestingly, a force directly applied on the Golgi apparatus using optical tweezers increases the amount of DAG on Golgi membranes mimicking the effects of increased contractility. Conversely, under reduced acto-myosin contractility, Lipin-1 is inhibited, SREBP accumulates in the Golgi apparatus where it is cleaved and then translocates to the nucleus where SREBP transcription factors are activated to promote lipid synthesis.

84. Anitei M, Stange C, Czupalla C, Niehage C, Schuhmann K, Sala P, Czogalla A, Pursche T, Coskun Ü, Shevchenko A, *et al.*: **Spatiotemporal control of lipid conversion, actin-based mechanical forces, and curvature sensors during clathrin/AP-1-coated vesicle biogenesis**. *Cell Rep* 2017, **20**:2087–2099.

85. • Makhoul C, Gosavi P, Duffield R, Delbridge B, Williamson NA, Gleeson PA: **Intersectin-1 interacts with the golgin GCC88 to couple the actin network and Golgi architecture**. *Mol Biol Cell* 2019, **30**:370–386.
The authors show that the TGN golgin GCC88 recruits the CDC42 GEF Intersectin-1 (ITSN-1) to the Golgi apparatus. The GCC88-ITSN-1 pathway is required to maintain the Golgi ribbon organization. This study links the Golgi matrix and the acto-myosin network in the maintenance of Golgi architecture.

86. Beck KA: **Spectrins and the golgi**. *Biochim Biophys Acta Mol Cell Res* 2005, **1744**:374–382.

87. Spiliotis ET, Hunt SJ, Hu Q, Kinoshita M, Nelson WJ: **Epithelial polarity requires septin coupling of vesicle transport to polyglutamylated microtubules**. *J Cell Biol* 2008, **180**:295–303.

88. •• Song K, Gras C, Capin G, Gimber N, Lehmann M, Mohd S, Puchkov D, Rödiger M, Wilhelmi I, Daumke O, *et al.*: **A SEPT1-based scaffold is required for Golgi integrity and function**. *J Cell Sci* 2019, **132**. jcs225557.
This study investigates the potential involvement of septins in the structure and function of the Golgi apparatus. The authors show that septin 1 promotes Golgi positioning and anterograde trafficking by localizing at the cis-Golgi in a GM130-dependent manner, facilitating nucleation of microtubules and recruiting centrosomal proteins at the Golgi surface.

89. Etienne-Manneville S: **Cytoplasmic intermediate filaments in cell biology**. *Annu Rev Cell Dev Biol* 2018, **34**:1–28.

90. Natividad RJ, Lalli ML, Muthuswamy SK, Asthagiri AR: **Golgi stabilization, not its front-rear bias, is associated with EMT-enhanced fibrillar migration**. *Biophys J* 2018, **115**:2067–2077.

91. Kuna RS, Field SJ: **GOLPH3: a Golgi phosphatidylinositol(4) phosphate effector that directs vesicle trafficking and drives cancer**. *J Lipid Res* 2019, **60**:269–275.

92. Nishita M, Park SY, Nishio T, Kamizaki K, Wang Z, Tamada K, Takumi T, Hashimoto R, Otani H, Pazour GJ, *et al.*: **Ror2 Signaling regulates Golgi structure and transport through IFT20 for tumor invasiveness**. *Sci Rep* 2017, **7**.

Résumé

Les mutations sont responsables de diverses pathologies du développement, en particulier chez les patients atteints de maladies rares ou pour lesquels il n'y a pas de diagnostic clinique clair. Cdc42 est une protéine clé pour la polarité cellulaire, une étape cruciale de nombreux processus cellulaires, comme la migration cellulaire, la division cellulaire ou la réponse immunitaire. Les mutations de Cdc42 entrainent une variété de pathologies, par exemple des dérégulations de la croissance ou de la morphologie faciale ainsi que des anomalies immunologiques, hématologiques et du développement neuronal. Les fonctions de Cdc42 reposent en grande partie sur la localisation de cette protéine dans la cellule. La comparaison des différentes formes de Cdc42 et de certaines formes mutantes montrent que les derniers acides aminés de la protéine jouent un rôle clé dans sa localisation et donc dans sa fonction. Nous avons centré notre étude sur l'identification : 1) des acides aminés essentiels à la localisation de la protéine ; et 2) de nouveaux mécanismes de régulation de Cdc42 responsables de sa localisation intracellulaire. Nous avons aussi montré que les deux isoformes jouent des rôles différents au cours de la migration cellulaire. Ce travail devrait nous permettre de mieux comprendre les pathologies liées aux mutations de Cdc42.

Summary

Mutations in proteins are responsible for diverse developmental disorders, particularly for individuals with rare clinical conditions or for whom a unifying clinical diagnosis is unknown. Cdc42 is one such protein; vital for establishing cell polarity, a crucial step in many biological processes such as cell migration, cell division and cell immune responses. Not surprisingly, mutations in Cdc42 cause a range of diseases such as growth dysregulation, facial dysmorphism and neurodevelopmental, immunological, and hematological abnormalities. In vertebrates there are two isoforms of Cdc42. The first isoform, known as the ubiquitous isoform, has almost exclusively been studied and the role of the second isoform, known as the brain isoform, is largely unknown. We have shown that the two isoforms are localized differently in cells. While the ubiquitous isoform is mostly found in the cell cytoplasm and at the plasma membrane, the Brain isoform localizes at the Golgi apparatus and on intracellular vesicles. We have also shown that the two isoforms carry out different functions during cell migration, suggesting that the differences between these two isoforms which only differs by the last 10 amino acids are responsible for their distinct localisation and function. Interestingly, a mutation in the C-ter sequence of Cdc42 ubiquitous isoform alters Cdc42 localisation and is linked to a generalized pustular psoriasis disease. Two main objectives have been studied in this project 1) the impact of the last amino acids of the protein in Cdc42 localization; and 2) new regulatory mechanisms of Cdc42 responsible for its intracellular localization. These findings will bring a better understanding of pathologies related to Cdc42 mutations.